Natural Resources Canada | Ressources naturelles Canada

GEOLOGICAL SURVEY OF CANADA
OPEN FILE 6692

Overpressure detection from geophysical, drilling and well-testing data for petroleum exploration wells in the Beaufort–Mackenzie Basin, Yukon and Northwest Territories

K. Hu, D.R. Issler, and Z. Chen

2021

Canada

GEOLOGICAL SURVEY OF CANADA
OPEN FILE 6692

Overpressure detection from geophysical, drilling and well-testing data for petroleum exploration wells in the Beaufort–Mackenzie Basin, Yukon and Northwest Territories

K. Hu, D.R. Issler, and Z. Chen

2021

Permanent link: https://doi.org/10.4095/327948

This publication is available for free download through GEOSCAN (https://geoscan.nrcan.gc.ca/).

Recommended citation

Hu, K., Issler, D.R., and Chen, Z., 2021. Overpressure detection from geophysical, drilling and well-testing data for petroleum exploration wells in the Beaufort–Mackenzie Basin, Yukon and Northwest Territories; Geological Survey of Canada, Open File 6692, 1 .zip file. https://doi.org/10.4095/327948

Publications in this series have not been edited; they are released as submitted by the author.

TABLE OF CONTENTS

ABSTRACT

A comprehensive database consisting of geophysical data, drilling mud weights, and subsurface temperature, and formation pressure measurements was compiled and utilized to detect the depth to top of overpressure for the petroleum exploration wells in the Beaufort-Mackenzie Basin. One hundred and fifty-two depths to the top of overpressure were determined for 112 wells by using geophysical methods, supplemented with drilling and geothermal data. The majority of overpressure picks were confirmed using measured pore fluid pressure data. An additional 36 wells are believed to be too shallow to have penetrated an underlying overpressured zone. Composite plots for each well are presented graphically with wireline logs, well seismic velocities, mud weights, and borehole temperatures to illustrate the geophysical, drilling and geothermal responses and their correlations with well testing data, thus providing multi-parameter evidence for an integrated interpretation of overpressure distribution.

Overpressure interpretations were ranked based on the availability and quality of the various types of data, as well as the reliability of the different methods used. Among the geophysical data that are good indicators of overpressure occurrences, shale sonic transit-time (and transformed porosity) and continuous sonic velocity are preferred because of the abundance of these data and the sensitivity of rock acoustic properties to porosity and stress. Mud weights provide an upper estimate of in situ pore pressure because of the need to approximately balance formation pressures during drilling; interpretations based on mud weights are mostly consistent with the results from geophysical data and measured fluid pressures from well tests. The interpreted depth to the top of overpressure varies from <1000 to over 4500 m (GL/SL) and is largely confined to undercompacted sediments in the central-northern delta and offshore areas. Overpressure occurs predominantly within the Paleogene Aklak, Taglu, Richards, and Kugmallit sequences, but can reach the base of the Plio-Pleistocene Iperk Sequence in wells on the outer shelf in the deep-water region of the Beaufort Sea. Our refined interpretations of overpressure occurrence in exploration wells provide key control points for more detailed mapping and modelling of overpressures in the basin.

1. INTRODUCTION

Overpressure is a term used to describe pore fluid pressure that exceeds normal hydrostatic pressure. Reliable detection of overpressure is vital to avoid and mitigate potential drilling and safety hazards, and it is a fundamental component of well design. The cause of overpressure has been attributed to numerous stress and temperature dependent mechanisms that alter pore fluid and rock matrix properties with increasing burial depth (e.g. Osborne and Swarbrick, 1997; Zhao et al., 2018) and it is likely that multiple factors contribute to overpressure development in dynamically evolving sedimentary basins. The Beaufort-Mackenzie Basin (BMB) is a late Cretaceous-Cenozoic post-rift basin that is composed of a series of normally pressured and overpressured, folded and faulted deltaic complexes. It extends from the outer edge of Mackenzie Delta in the Beaufort Sea to the southern basin margin between 128°W and 141°W in northern Canada where about 290 wells have been drilled between 1962 and 2009 (Fig. 1). Overpressure in the BMB is associated with rapid sediment accumulation, undercompacted shale, shale diapirism, and major fault systems (Hitchon et al., 1990; Issler, 1992; Issler et al., 2002; Chen et al., 2010a). The abundance of publicly available well data and samples make the BMB a natural laboratory for studying the dynamics of shale compaction and overpressure generation.

Cenozoic shale (Fig. 2) of the BMB is relatively homogeneous in mineral composition (Youn, 1974; Bloch and Issler, 1996) and organic carbon content (Snowdon, 1990; Snowdon et al., 2010) and therefore displays consistent geophysical properties (Issler, 1992; Issler and Jessop, 2011) that enable good correlations between core petrophysical and well log measurements. Accordingly, Issler (1992) established a relation between shale sonic log transit-time and core porosity and used it to define five major shale compaction zones with distinct overpressure trends. Follow up studies by the GSC (Katsube and Issler, 1993; Issler and Katsube, 1994; Katsube et al., 1995, 1996, 2011; Issler et al., 2002) confirmed the strong association between overpressure and the shale porosity trends within Cenozoic strata (Fig. 2) that are detectable using multiple well logs. This culminated in a map showing overpressure distribution for the BMB (Issler et al., 2011) based on using compiled shale log data and fluid pressure data to detect the overpressure zone (OPZ) at different borehole locations.

The main purpose of this study is to provide detailed documentation of the large comprehensive datasets and the overpressure detection methods used to map the distribution of overpressure at well locations in the BMB (Issler et al., 2011). This includes the following key steps: 1) to compile and examine multiple data sets consisting of well log data and calculated porosities for identified shales, formation pressure measurements from well testing and drilling mud weight, velocities from sonic log and well seismic surveys, and borehole temperatures for studied wells; 2) to interpret the top of the OPZ for individual wells by using composite plots that integrate multiple parameters; and 3) to display the picks for the depth to top of the OPZ with supporting evidence and a reliability assessment. This study includes the most up-to-date picks for the top of the OPZ to ensure the most accurate mapping of overpressure for the BMB. Unless otherwise indicated, the datum used for downhole depths in this report is either one of Ground Level "GL" for onshore wells or Sea Level "SL" for offshore wells; other depth datums are specified when used, such as Kelly Bushing "KB" and Sea Floor "SF".

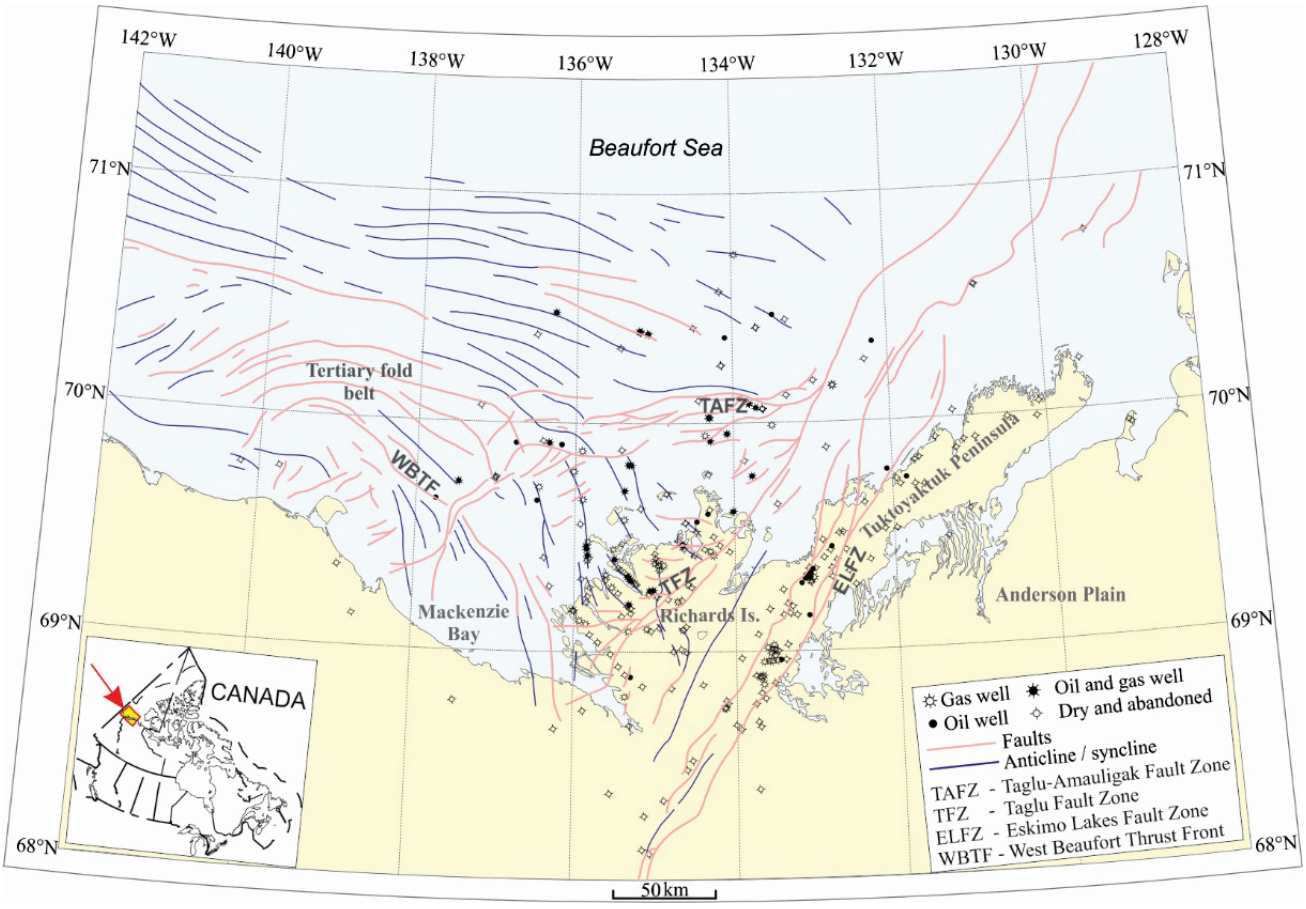

Figure 1. Map showing the study area and wells drilled in the Beaufort-Mackenzie Basin, Arctic Canada.

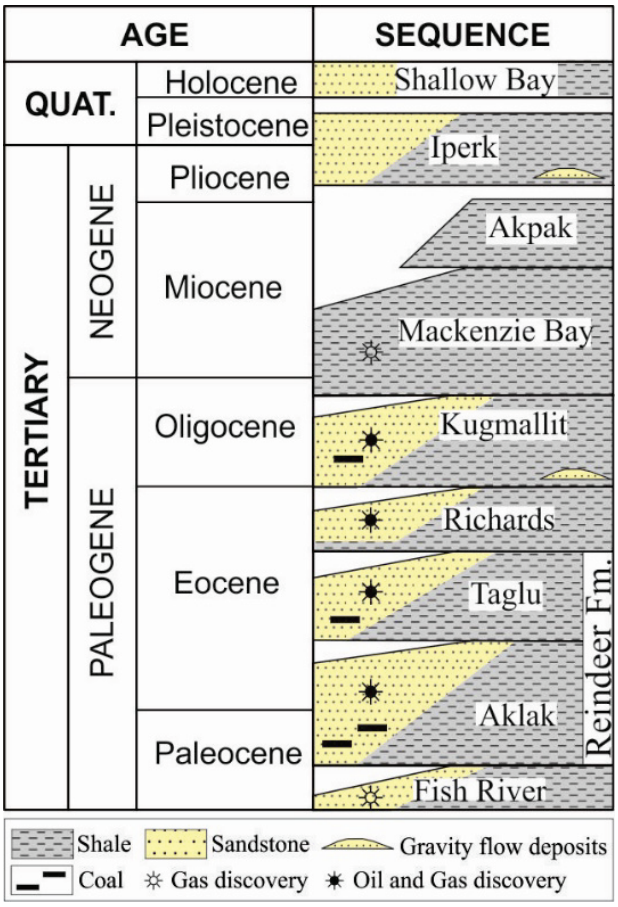

Figure 2. Scheme showing the stratigraphic units for Cenozoic strata in the Beaufort-Mackenzie Basin (modified from Dixon et al., 1996, 2007, 2019).

2. DATA SOURCES

A large volume of technical information and data are available for overpressure detection. Data sources include engineering data from well testing, drilling data such as mud weight, and borehole geophysical data consisting of well logs (and associated temperatures) and well seismic velocity.

2.1. Well testing data

Well tests are performed by measuring flow rates and pressure with a downhole gauge to evaluate well productivity and reservoir performance over a large scale of investigation, such as fluid properties, reservoir pressure, drawdown pressure, permeability, formation damage, productivity index and much more. For the BMB, the pore fluid pressure measurements from

well testing include drill stem test (DST), repeat formation test (RFT), modular formation dynamics tester (MDT), and formation interval tester (FIT).

Among the well tests, DST is the most common method in the study area. DST provides reliable pressure data if sufficient time elapses during the test for the higher formation pressure to equilibrate with the lower borehole pressure, but it may not be reliable if the tool is not shut in long enough for pressure to stabilize at final reservoir pressure. Thus, DSTs contain two types of data; corrected (extrapolated pressure), and uncorrected (original initial or final shut-in pressure). Corrected DST pressure data are more reliable and assigned quality "a" (DST-a) whereas uncorrected DST data are less accurate and assigned quality "b" (DST-b). Reliable pressures can be difficult to obtain in low-permeability reservoirs with DSTs due to insufficient pressure buildup following shut in. However, even if the true pressure is underestimated, it may still provide evidence for overpressure.

The repeat formation tester (RFT) tool was designed to measure formation pressure quickly and accurately. It measures pressure at specific points on the borehole wall. An RFT is well suited for thick and permeable clastic formations and has several important advantages for pressure measurement in comparison to a DST. Some of these include: a shorter time to take a single measurement, more samples per run, and a lower cost per test. However, the tool can be more susceptible to skin damage around the borehole and sometimes it can be hard to get a good seat for pressure measurement. Furthermore, RFT data are not reliable for difficult conditions such as fractured reservoirs, thin and laminated formations.

Modular Formation Dynamics Tester (MDT) is a new technique to measure formation pressure and is developed to overcome the difficulties with RFT. This method has been applied successfully to a fractured reservoir, a thinly bedded reservoir and a formation with very low permeability.

A formation interval tester (FIT) is a method to test strength of formation and shoe by increasing bottom hole pressure (BHP) to designed pressure. FIT is normally conducted to ensure that formation below a casing shoe will not fracture while drilling the next section with higher BHP or circulating gas influx in a well control situation.

For this study, the digital fluid pressure data were compiled for over 260 wells and used to make fluid pressure vs depth profiles. Figure 3 shows all compiled formation pressure measurements from the wells located mainly on Richards Island and in the offshore region.

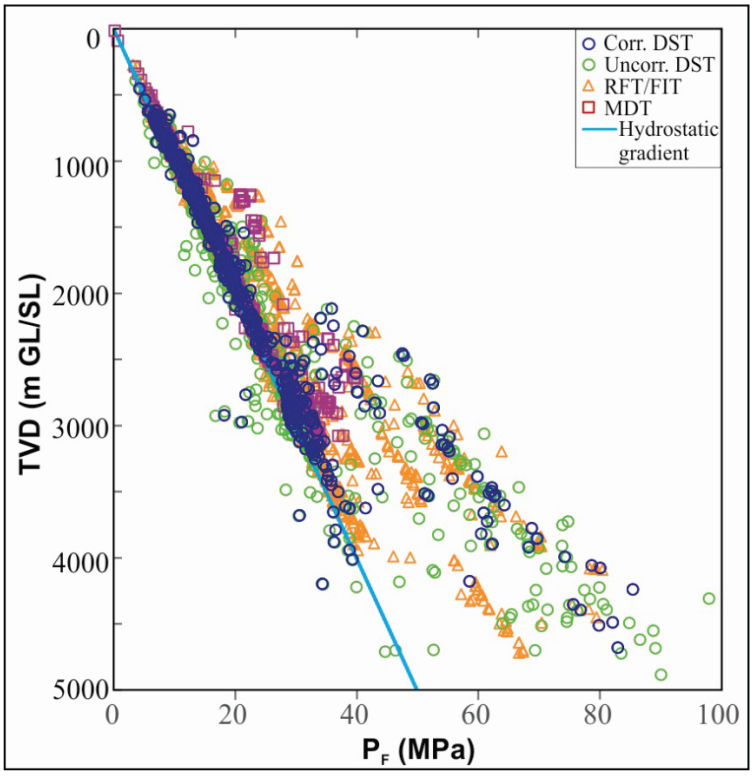

Figure 3. Pore fluid pressure-depth profiles from most available well testing for all the drilled wells in the Beaufort-Mackenzie Basin. The normal hydrostatic pressure is approximately 10.5/km (the solid light blue line).

2.2. Drilling mud weight

To drill safely and efficiently, drillers generally maintain the smallest possible positive differential pressure between mud and formation fluids. Mud weight is monitored and is typically adjusted so that pressure in the well is slightly higher than that in the formation. The fluid pressure can be calculated from drilling mud weight and true vertical depth as follows:

$$P_{mud}=\rho_m\, g\, Z \qquad (1)$$

where P_{mud} is fluid pressure from mud weight in Pa; ρ_m is mud density in kg/m^3 or ppg (1ppg=119.8394 kg/m^3); Z is the formation depth (true vertical depth) below sea level or the land surface in metres; g is acceleration of gravity (9.8 m/s^2).

In the study area, mud weight data were compiled for over 270 wells in the BMB, and fluid pressures from mud weight are calculated using Eq. (1) above. Figure 4 shows a plot of fluid pressure from mud weight versus depth for all the wells.

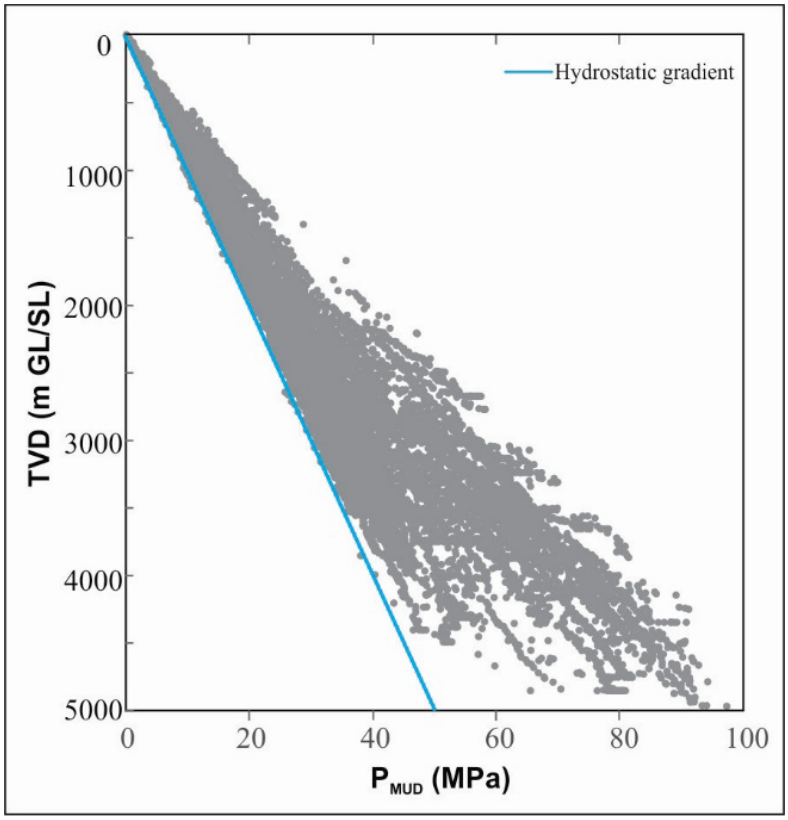

Figure 4. Calculated fluid pressure from drilling mud weight for the wells in the Beaufort-Mackenzie Basin. The normal hydrostatic pressure is approximately 10.5/km (the solid light blue line).

2.3. Identification and log data extraction of shale sections

Shales are the preferred lithology for pore pressure interpretation because they are more responsive to overpressure than most other rock types and their compaction behavior is relatively consistent due to their fine grain size. In addition, selecting the purest shales minimizes the effects of mineral variation, fluid composition and distribution, leaving only porosity as the major variable within shale sections.

For this study, reasonably thick homogeneous (avoiding sand or lime stringers) shale intervals were selected to ensure valid log responses and they were identified using typical shale indicators such as the (spectral) gamma ray - (S)GR, spontaneous potential (SP) base line, and neutron log (usually neutron porosity NPHI). Three types of well logs are used for overpressure

detection in the identified shale intervals including sonic transit time (Δt or DT), bulk density (ρ_b or RHOB) and deep resistivity (R). Commonly the caliper log shows a higher value than the bit size within shale intervals and this affects all the log data, particularly the density response. Sonic and density data quality are assessed based on the difference between the caliper log reading and bit size as a measure of borehole enlargement.

2.3.1. Sonic log and porosity for shale sections

Sonic log quality

Sonic transit time data are extracted for identified shale sections in which enlarged boreholes commonly occur. Compensated logs can mitigate some of the problems with over gauge boreholes provided they are not too wide. The degree of borehole enlargement is used to assign sonic data to one of two groups, "a" (good) and "b" (fair), based on data quality:

Quality a: sonic log reading for the shale interval where the difference between sonic caliper log reading and bit size is less than 15 mm,

Quality b: sonic log reading for the shale interval where the difference between sonic caliper log reading and bit size is greater than 15 mm.

Shale sonic porosity (ϕ_S)

Sonic porosity for identified shale can be calculated using the equation (Issler, 1992; adapted from Chapman, 1981, p. 223 and Raiga-Clemenceau et al., 1988):

$$\phi_S = 1 - (\Delta t_{ma} / \Delta t_{log})^{1/x} \quad (2)$$

where ϕ_S is the shale sonic porosity (expressed as a fraction), Δt_{ma} is sonic transit time for the rock matrix of shale (μs/m), usually being 220 μs/m for Tertiary shale in the Beaufort-Mackenzie Basin. Δt_{log} is the shale sonic log reading (μs/m), and x is the acoustic formation-factor exponent (2.19 for the study area).

2.3.2. Density log and porosity in shale sections

Density log quality

The density log value is related to the density of the rock matrix, its pore space, and the density of the fluids filling the pores. In many shale formations, when enlarged boreholes or washouts occur, the density tool often loses contact with the borehole wall, resulting in log readings that are adversely affected by the borehole fluid. Hence, poor density logging conditions are commonly associated with enlarged boreholes as indicated by the caliper log. Therefore,

density log data are categorized into four groups with corresponding quality rankings, which are defined in terms of borehole condition: "a", "b", "c" and "d". The quality letter grades are "a" (best) to "d" (worst), as listed in Table 1.

Table 1. Quality ranking definitions for density log data (RHOB) for identified shale formations

Quality of RHOB value	Difference between density caliper diameter and bit size
a	<10 mm
b	10 – 20 mm
c	20 – 30 mm
d	>30 mm

Shale density porosity (ϕ_D)

Based on the bulk volume model for a shale formation that consists of grains/matrix with an average log value (ρ_{ma}), and porosity (ϕ, fractional) filled by a fluid with an average log value (ρ_f), the total bulk density log reading (ρ_{log}), and shale density porosity (ϕ_D) (adapted from Schlumberger, 1989) are given by:

$$\rho_{log} = \phi\, \rho_f + (1 - \phi)\, \rho_{ma} \quad (3a)$$

$$\phi_D = (\rho_{log} - \rho_{ma}) / (\rho_f - \rho_{ma}) \quad (3b)$$

where ρ_{ma} is the shale matrix density in kg/m^3, ρ_{log} is the reading on the density log in kg/m^3 for the shale formation, and ρ_f is the fluid density. For the study area, ρ_{ma} is 2670 kg/m^3 for the shale in Kugmallit Sequence, and 2700 kg/m^3 for the shale from other sequences.

2.3.3. Resistivity log for shale intervals

The deep resistivity curve is used for overpressure detection because it minimizes the detrimental influence of enlarged boreholes (common in shale formations) on log readings. The deep resistivity values of shale sections are obtained from the high-resolution deep array laterolog or deep array induction log for newly drilled wells, and the deep induction log or deep laterolog for most of the older wells. In addition, the long normal 64" log was used for some of the older wells.

2.3.4. Shale log data used for overpressure detection

Over 9000 shale sections are identified and accordingly their average well log readings are extracted for about 280 wells in the basin. Furthermore, profiles of log-depth and porosity-depth are plotted for the shales from each well. Figure 5 shows the well log data from the wells

mainly located in Richards Island and offshore area of the basin, illustrating shale sonic transit time (Δt_{SH}), density (ρ_{SH}) and resistivity (R_{SH}) responses to the identified shales mainly in Neogene (Miocene and Pliocene) (Fig. 5a), and Paleogene (Paleocene, Eocene and Oligocene) (Fig. 5b) strata. Data analysis indicates that the average sonic transit time values range from 300 to 700 µs/m and 220 to 600 µs/m for the Neogene and Paleogene shales, respectively, with corresponding sonic porosity values of 15 - 44% and 5 - 35%. The average density values range mainly from 2000 to 2450 kg/m^3 and 2050 to 2700 kg/m^3, with corresponding density porosity values in the range of 15 - 45% and 5 - 40% for the Neogene and Paleogene shales, respectively. The deep resistivity values from the Neogene and Paleogene shales fluctuate dominantly within 1 - 4 ohmm and 1.5 - 20 ohmm, respectively.

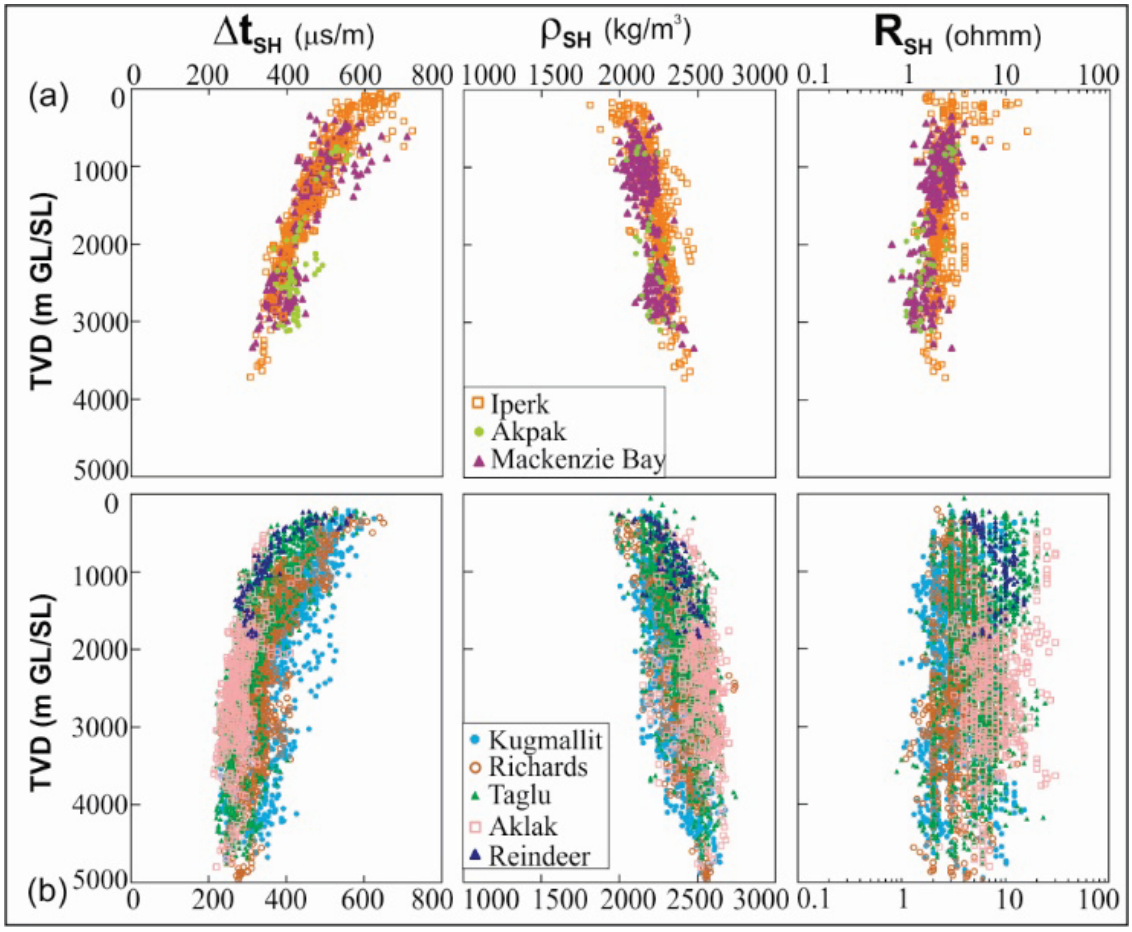

Figure 5. Plots showing extracted well log data for identified shale sections from wells in the Beaufort-Mackenzie delta and offshore area, including sonic transit time (Δt_{SH}), bulk density (ρ_{SH}), and deep resistivity (R_{SH}) for the Neogene Iperk, Akpak, and Mackenzie Bay sequences (a), and for the Paleogene Kugmallit, Richards, Taglu, and Aklak sequences (b).

2.4. Velocity from well seismic survey and sonic log

2.4.1. Well seismic survey

Well seismic velocity survey data compiled in this study include check shot, vertical seismic profile (VSP), and crystal cable surveys. The check shot survey is a type of well seismic survey designed to measure the seismic travel time from the ground surface to a downhole geophone at a given depth. VSP is a technique of simultaneously recording the up-going and down-going acoustic wave trains. The crystal cable velocity survey is designed for determination of the shallow (<1000 m) seismic velocity distribution and it has a higher resolution than conventional check-shot surveys due to a closer spacing of downhole geophones. All the survey methods define a unique relationship between time and depth that can be converted easily to velocity as a function of depth. Average interval velocities can be calculated and the travel times corrected to a reference datum (Hu et al., 2015). Figure 6 shows well seismic survey profiles from the wells mainly located in the delta and offshore area of the BMB.

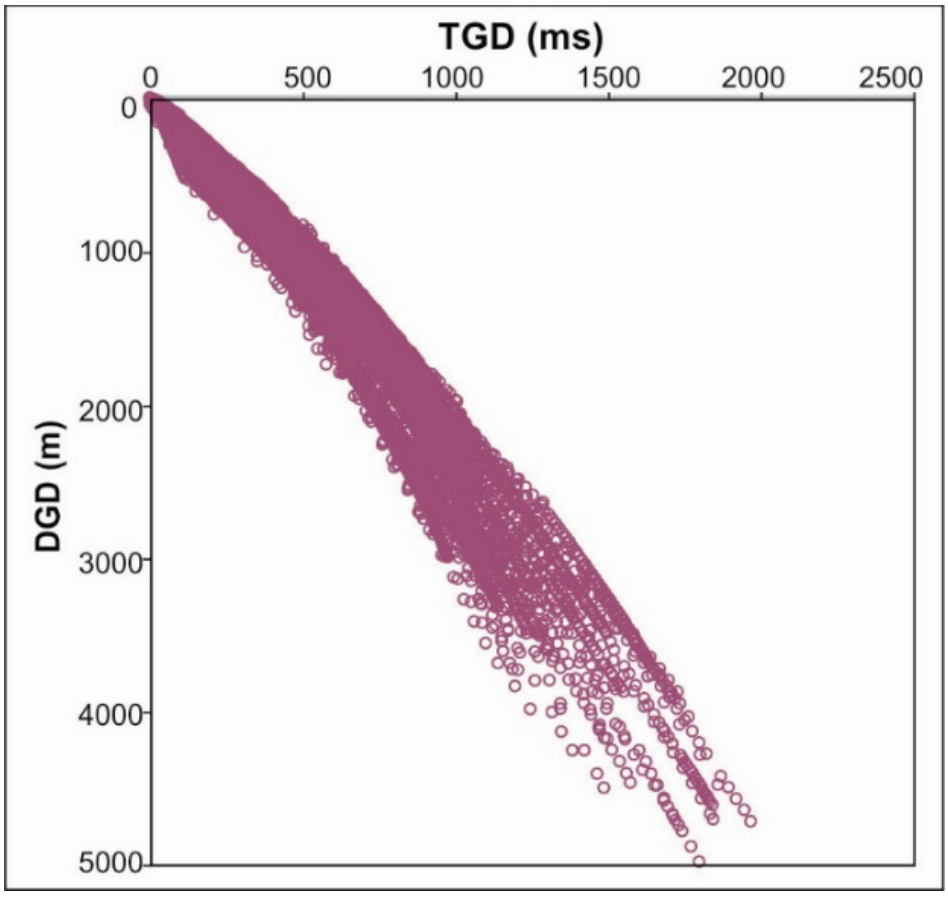

Figure 6. Well seismic survey profiles consisting of check-shot, VSP and crystal cable from all the wells located in the delta and offshore area in the Beaufort-Mackenzie Basin. DGD – Vertical depth below datum (m), TGD – vertical travel time from datum in milliseconds.

2.4.2. Continuous sonic velocity log (V_{DT})

The sonic logging tool measures the acoustic velocity through rocks over a fixed interval. Sonic velocity is simply calculated as the inverse of transit time from the sonic log ($V_{DT} = 10^6/DT$) and results are presented as a continuous sonic velocity log. If there is no sonic transit time log available then sonic velocity is estimated using the density log.

Velocity-depth profiles were generated for each well in the study area using calculated average interval velocities (V_{INT}) from available well seismic surveys and continuous sonic velocity logs (V_{DT}). Figure 7 shows an example of velocity versus (true vertical) depth for an offshore well, displaying the changes of continuous sonic velocity and well seismic velocity along the whole borehole interval.

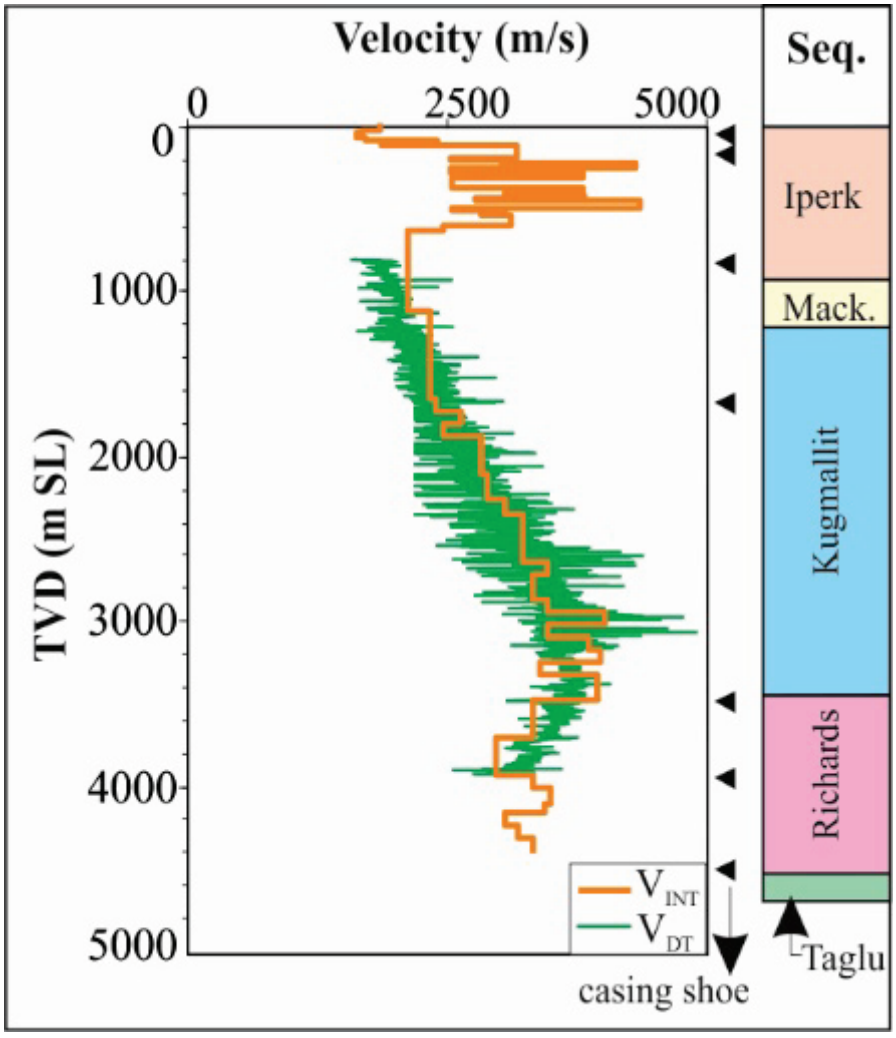

Figure 7. Velocity profile from sonic log and well seismic survey for an offshore well in the study area. V_{INT} – interval well seismic velocity; V_{DT} – velocity from sonic log; Mack. – Mackenzie Bay.

2.5. Formation temperature data

Subsurface temperature data were compiled for 280 exploration wells in the BMB (modified from Hu et al., 2010), consisting of all the formation temperature data from well testing and log-derived bottomhole temperature measurements. Bottomhole temperature data were corrected for drilling disturbances where possible (see Hu et al., 2010). Figure 8 illustrates the temperature-depth profiles from the wells in the BMB.

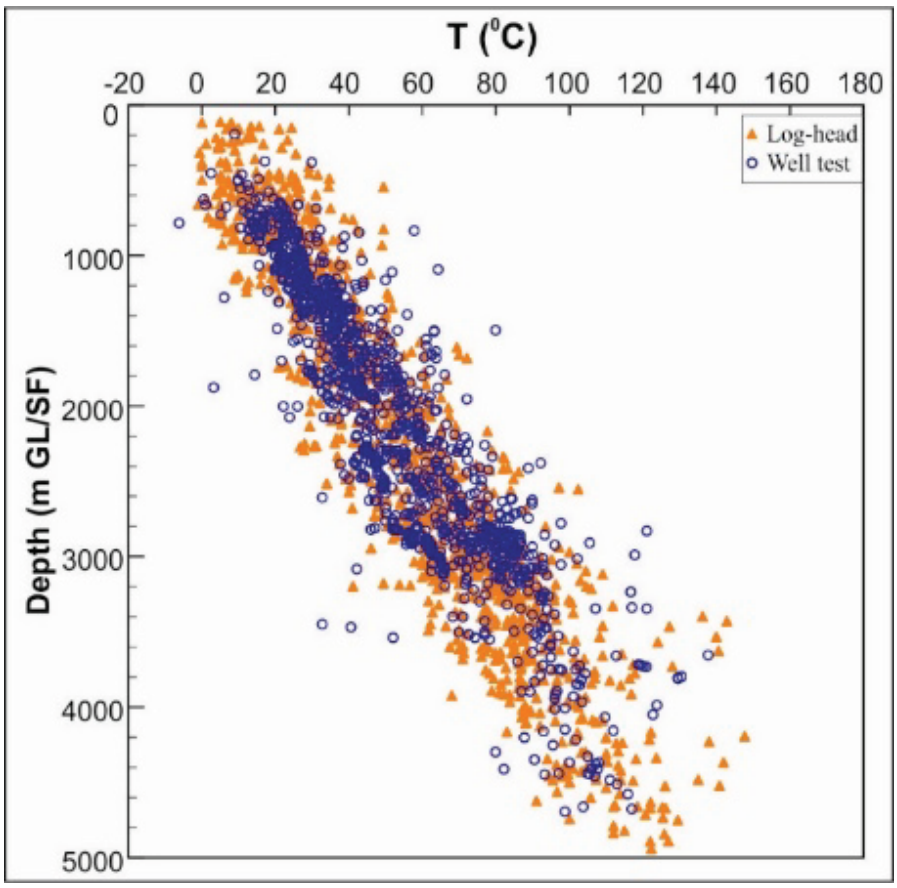

Figure 8. Borehole temperature (T) vs depth from well test and log-header information from wells located mainly in the delta and offshore area of the Beaufort-Mackenzie Basin. GL – ground elevation, SF – sea floor.

3. OVERPRESSURE INTERPRETATION

3.1. Overpressure detection at petroleum well locations

3.1.1. Pore fluid pressure measurements

Overburden pressure is a function of the sum of the weight of the rock matrix and its pore-filling constituents in an overlying column of rock. The pore pressure of a formation refers to that portion of the overburden pressure that is supported by the fluids within its pore spaces.

Generally, well tests provide the most reliable pore pressure measurements that give direct indications of abnormal pressures. Normal or hydrostatic pore fluid pressure (P_H) for the BMB is calculated for a water column with a hydrostatic pressure gradient of approximately 10.5 MPa/km (solid blue line in Figs. 3, 4 and 9). Overpressure can be identified readily on pressure-depth profiles because the measured pressure exceeds the hydrostatic pressure. As shown in Figure 3, the largest excess pore fluid pressures occur mainly at depths between 2080 and 4880 m whereas milder overpressure occurs at shallower depths of 840 to 2080 m. Only a small number of data points plot below the hydrostatic line.

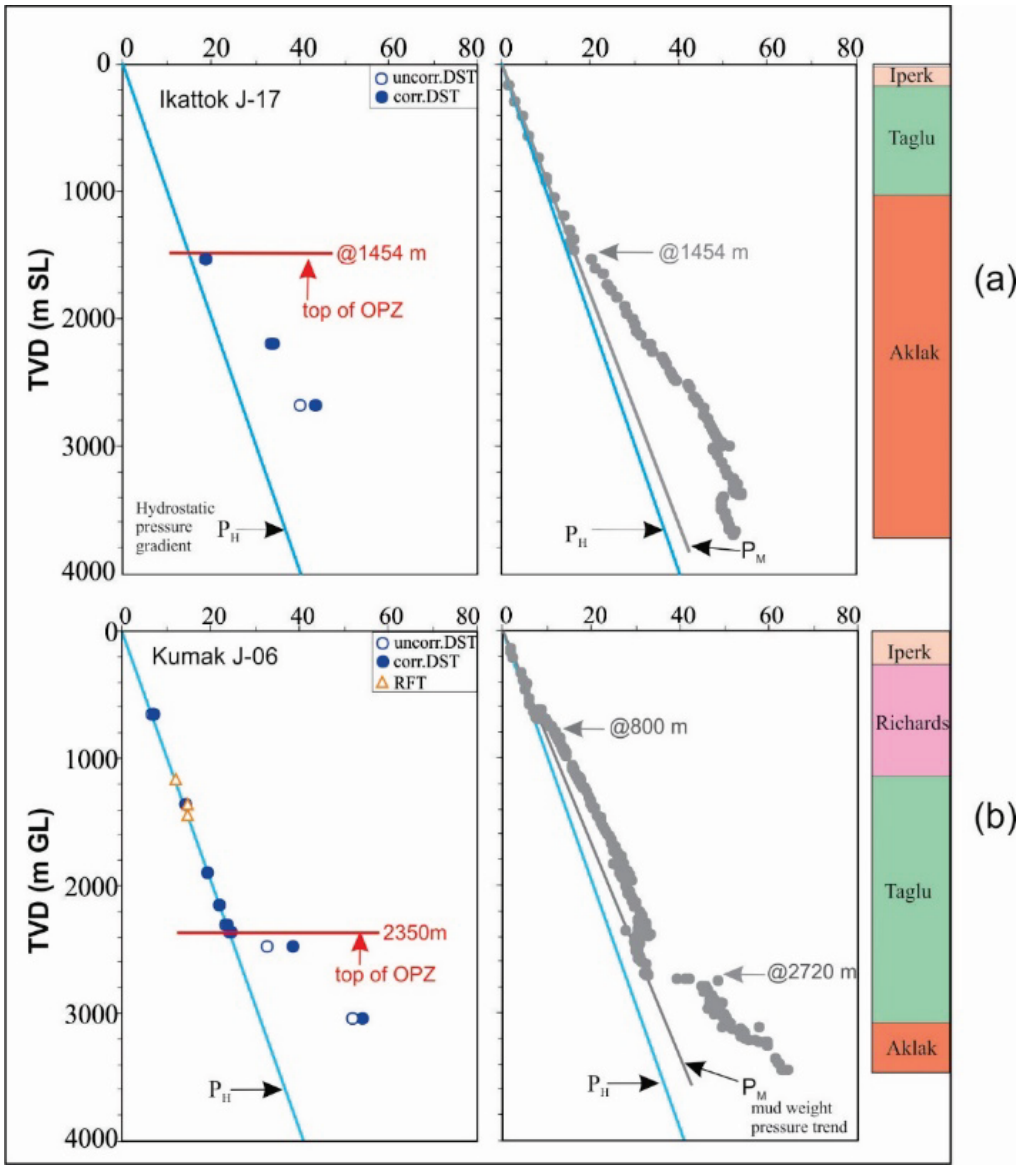

Figure 9. Examples showing overpressure identified by fluid pressure from well testing and drilling mud weight for the wells Ikattok J-17 (a) and Kumak J-06 (b) in the Beaufort-Mackenzie Basin.

In Figure 9, the top of overpressure is estimated using pointwise pore fluid pressure data in two wells (left panels in Fig. 9). For the offshore well Ikattok J-17, corrected DST pressure data show the top of the OPZ within the Aklak Sequence at 1454 m depth (left panel; Fig. 9a). In the Kumak J-06 well on Richards Island, DST and RFT pressure data show the top of the OPZ in the Taglu Sequence at a depth of 2350 m (left panel; Fig. 9b).

3.1.2. Equivalent fluid pressure calculated from mud weight

Drilling mud weight is a conventional proxy measurement for pore pressure that is used for overpressure detection. Generally, mud pressures tend to be higher than formation pressures for safety reasons and therefore a separate mud weight trend line can be drawn as a baseline (gray colored line in right panels; Fig. 9). Overpressure may be indicated where mud pressures increase significantly relative to this baseline. As an example, calculated mud pressure in the Ikattok J-17 well shows an abrupt increase below 1454 m, consistent with DST data indicating the onset of overpressure (Fig. 9a). In some cases, mud pressure data do not accurately reflect formation pressure trends. For example, mud pressures are significantly higher than hydrostatic formation pressures in the Kumak J-06 well between 800 m and 2350 m (right panel; Fig. 9b). It appears that the well was drilled overbalanced over this interval and then mud weight was reduced within the upper part of the OPZ before being substantially increased at 2720 m. If only mud weight data were available, the top of overpressure would be picked at 2720 m whereas the true top is closer to 2350 m based on DST pressure measurements. This example shows the value of integrating multiple pressure indicators to arrive at the best possible interpretation.

3.1.3. Geophysical methods

Well log and interval seismic velocity are the geophysical data used for overpressure detection in this study. Log and acoustic properties are affected by the rock matrix, pore space and pore-filling fluids. Overpressure detection is based on the premise that fluid pressure affects rock geophysical properties such as sonic velocity, density, and resistivity. Porosity can be viewed as consisting of storage space (the main porosity volume within the rock matrix) and connecting pores (pore throats and/or fracture porosity linking the storage pores). Density logs are sensitive to total porosity (connecting and storage pores) whereas sonic (and interval seismic velocity)

and resistivity logs are especially sensitive to connecting porosity. Microcrack porosity can have a significant effect on reducing acoustic velocity and resistivity near to top of the OPZ.

The compaction trend is the trend of a property of clastic sediments (resistivity, sonic travel time, density, velocity, etc.) undergoing compaction due to increased burial. Changes in compaction trends with depth will appear in log signatures and velocity-depth trends. In offshore regions of the BMB, pore pressure is correlated with porosity-depth trends in undercompacted shale but, even in more compacted shale, overpressure is still strongly correlated with changes in compaction trends.

Sedimentary strata of the BMB are composed predominantly of sand and shale, especially for the Cenozoic succession. As these sediments compact under normal pressure conditions, porosity reduction with depth follows a normal compaction trend (NCT). Similarly, density, resistivity and velocity increase with depth (sonic transit time decreases) and NCT lines within shale formations can be established for each log and velocity-depth profile (Fig. 10). Overpressure can be identified where log and velocity values deviate from the NCT. Sonic and density log data (and velocity data) show the most consistent compaction related trends. Resistivity logs are included as an aid to interpretation but they can exhibit behaviour that is more variable because they are sensitive to the chemistry of the drilling mud and formation fluid and the contrast between them. In general, formation fluids in the BMB have relatively low salinity (mostly < 20,000 mg/l; Grasby et al., 2009). It should be noted that neutron logs were not used for overpressure evaluation because the enlarged borehole conditions that commonly occur in shales substantially degrade the accuracy and reliability of the neutron data.

Figure 10 illustrates an example in which two overpressure zones are detected clearly using geophysical methods for the Uviluk P-66 well that is located in the deep-water shelf area of the Beaufort Sea. Three profiles of log data from shale intervals (Fig. 10a-c) and velocity data (from sonic log and well seismic surveys) (Fig. 10d) versus depth are shown with respect to NCT lines established for each type of data. The tops of two stacked overpressure zones are estimated at 2120 m (base of Iperk Sequence) and 3486 m (near base of Kugmallit Sequence) depth based on consistent deviations of log (sonic, density and resistivity) and velocity data from the NCT (Figs. 10a-d) and this is confirmed by RFT and DST pressure measurements (Fig. 10e). The high sonic and density porosity values within the OPZs (Fig. 10a and b) indicate

that the sediments are undercompacted as a result of rapid burial by the overlying Iperk Sequence and there is a distinct shift to low resistivity at the top of both OPZs (Fig. 10c).

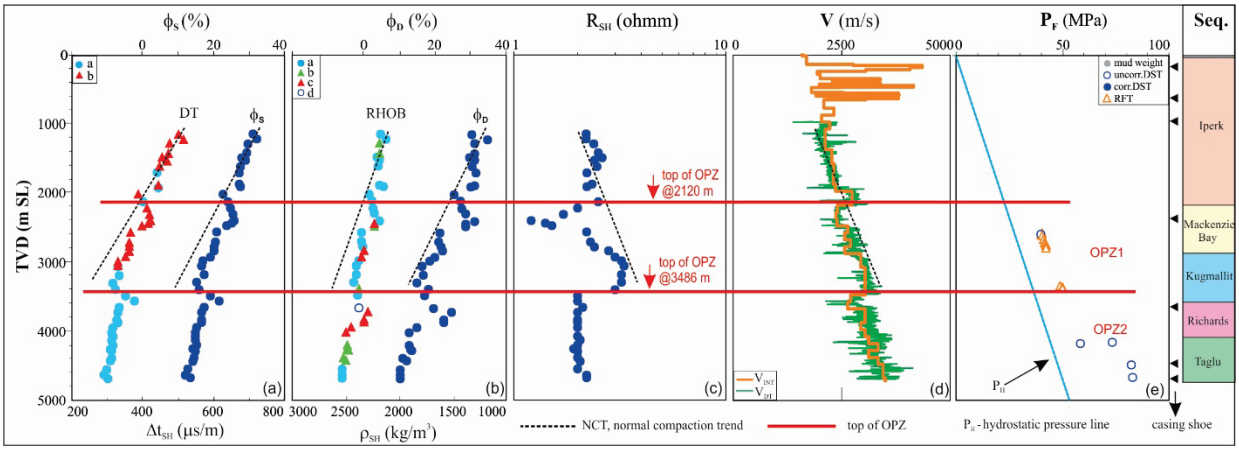

Figure 10. Illustration exemplifying overpressure detection using geophysical methods in the offshore Uviluk P-66 well in the Beaufort-Mackenzie Basin. (a) Shale sonic log (Δt_{SH}) and porosity (ϕ_S); (b) shale density (ρ_{SH}) and porosity (ϕ_D); (c) shale resistivity (R_{SH}); (d) velocity versus depth from sonic log (V_{DT}) and well seismic survey (V_{INT}); and (e) pore fluid pressure from well testing.

3.1.4. Geothermal gradients

Abnormally high temperature gradients have been observed in association with overpressured zones. Lewis and Rose (1970) suggested that undercompacted, overpressured rocks act as thermal insulators that increase temperatures due to the low thermal conductivity of water compared with the rock matrix. To investigate a possible relationship between temperature and overpressure, bottomhole temperature (BHT) and well test (mainly DST) temperature data were plotted with respect to depth for the wells with interpreted OPZs. The plotted data are quality-ranked according to the scheme of Hu et al. (2010): a (excellent), b (good), c (fair) and (d) poor for BHT data, and a (successful test) and b (unsuccessful test) for DST data. BHT data quality depends on whether there is sufficient data to correct the data for drilling disturbances and reliably extrapolate the temperatures to equilibrium conditions.

It is difficult to infer a relationship between overpressure and temperature for the BMB due to the sparse, pointwise nature of the temperature data. Although some data suggests that geothermal gradients may be higher in the overpressure zone, it is unclear whether this is due to overpressuring. Rapid deposition of late Pliocene-Pleistocene Iperk Sequence (McNeil et al., 2001; ~1 km/Myr on the outer shelf) and deep permafrost (Hu et al., 2013; Taylor et al., 2013) have suppressed temperature and heat flow in the upper part of the sedimentary section. The

BMB is in a transient thermal state (e.g. Majorowicz et al., 2008a) and it is heating up from its base. Therefore, temperature gradients may be expected to increase with depth in areas of rapid burial and thick permafrost (Chen et al., 2010b). Chen et al. (2008) and Hu et al. (2014) provide a more detailed discussion of the temperature regime of the BMB and factors influencing the temperature measurements.

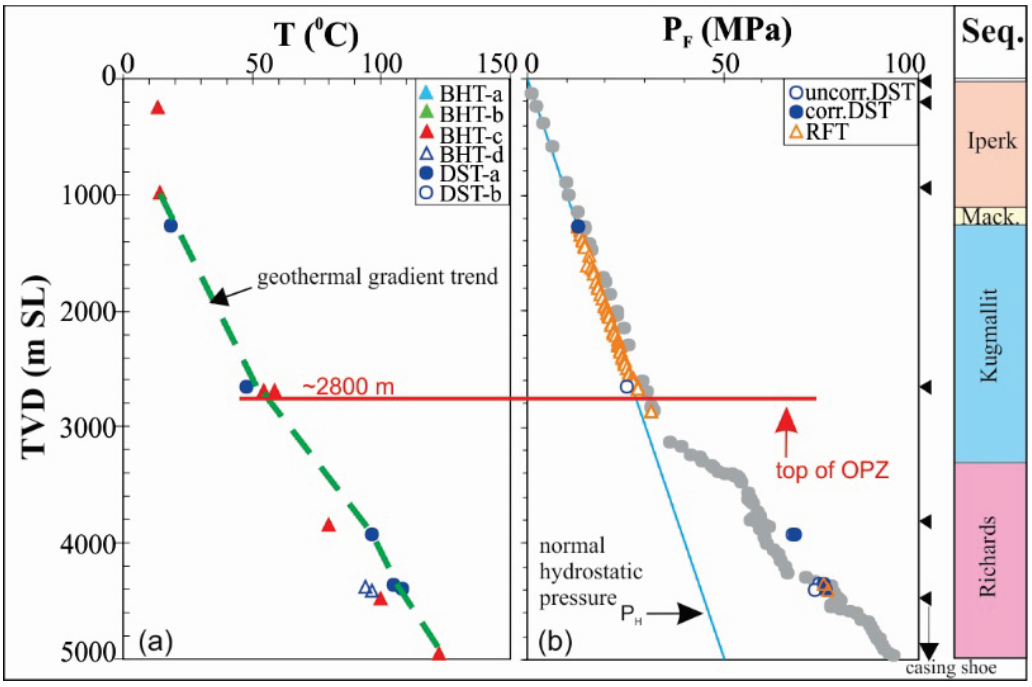

Figure 11. A comparison of temperature (a) and pore pressure (b) versus depth for the Amerk O-09 well. Overpressure below 2800 m is confirmed by pore fluid pressure measurements from well tests and mud weights (gray dots). Mack. – Mackenzie Bay Sequence.

Figure 11a shows a plot of temperature versus depth for the Amerk O-09 well, located in the deep-water region of the Beaufort Sea shelf. The dashed green line shows an interpreted temperature trend that was drawn to emphasize a possible increase in geothermal gradient in the OPZ (Fig. 11b) assuming that the DST temperature data are the most reliable. However, given the uncertainties with individual temperature measurements, geothermal gradient can also be approximated to first order using a single linear trend (see Fig. 34 of Hu et al., 2014).

3.1.5. Overpressure detection using integrated methods

The borehole geophysical, drilling and engineering data that are used to detect and interpret overpressure zones are displayed in six panels in a composite plot for the Koakoak O-22 well located in the deep-water region of the outer shelf in the Beaufort Sea (Fig. 12). Similar plots

for other wells used in the study are included in Appendix A to C. Figures 12a-d illustrate extracted geophysical data profiles especially for shale intervals (Figure 12a-c), Figure 12e illustrates fluid pressure from well tests and drilling mud weights, and Figure 12f shows borehole temperatures. Additionally, the casing shoe depth and penetrated stratigraphy are displayed on the right side of both upper and lower panels, providing additional context for overpressure interpretation.

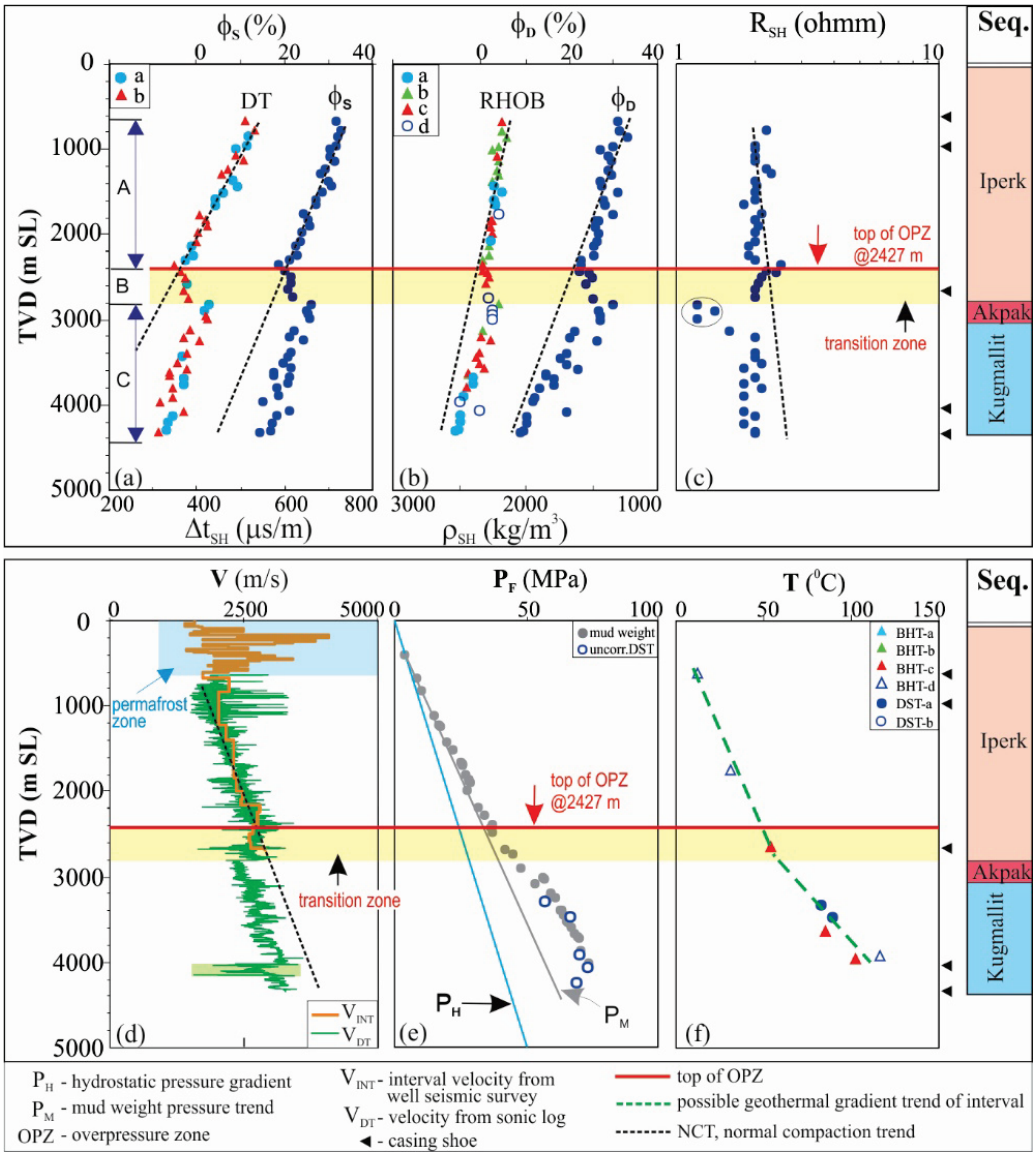

Figure 12. An example composite plot from the Koakoak O-22 well demonstrating the integrated approach of overpressure interpretation. The upper panel illustrates profiles of well log data versus depth for identified shale formations, (a) sonic transit time (Δt_{SH}) and sonic porosity (ϕ_S), (b) bulk density (ρ_{SH}) and density porosity (ϕ_D), and (c) deep resistivity (R_{SH}). The lower panel shows continuous sonic velocity (V_{DT}) and average interval velocity (V_{INT}) from well seismic survey (d), pore fluid pressure (P_F) from well test and drilling mud weight (e), and borehole temperature (T) versus depth (f).

The Koakoak O-22 well penetrated nearly 2800 m of Iperk Sequence, greater than 1000 m of Kugmallit Sequence, and a thin (~240 m) intervening Akpak Sequence (Fig. 12). There is a complete set of conventional well logs and 53 shale sections were identified using GR and neutron porosity logs, and corresponding values of sonic transit time (Δt_{SH}), bulk density (ρ_{SH}), and resistivity data (R_{SH}) were obtained (Fig. 12a-c). The quality of the sonic and density data was assessed and corresponding porosity values, ϕ_S and ϕ_D, were calculated, respectively. The velocity profile from the well seismic survey (V_{INT}) shows good agreement with velocity values calculated from the sonic log (V_{DT}; Fig. 12d). A fluid pressure profile (P_F - depth) is plotted using measured pressure (DST) and calculated fluid pressure from drilling mud weight and an approximate hydrostatic pressure line (P_H, the solid blue line in Fig. 12e) and mud pressure trend line (P_M, the solid grey line in Fig. 12e) are shown. Finally, a temperature-depth trend is estimated using variable quality BHT and DST temperature data (Fig. 12f).

Three zones, A, B and C, are identified from top to bottom in the Koakoak O-22 well on the basis of geophysical attributes and pore pressure trends (Fig. 12). Zone A is interpreted as a normally compacted zone with a NCT (dashed black lines in Figs. 12a-d) that exhibits typical geophysical features: shale sonic transit time and its porosity decrease with depth; shale density and resistivity increase but density porosity decreases with depth; both sonic velocity (V_{DT}) and well seismic interval velocity (V_{INT}) increase with increasing depth. An uppermost interval above Zone A with anomalous interval velocity is interpreted as a permafrost zone (Fig. 12d; Hu et al., 2013).

The top of Zone B (the yellow coloured region in Fig. 12) starts at 2427 m where data begin to depart from the NCT line and it occurs near the base of the Iperk Sequence. It is interpreted as an overpressure transition zone (~400 m thick) that is characterized by a reversal in geophysical trends with depth: shale sonic transit time and its porosity increase, shale density and resistivity decrease while density porosity increases (Fig. 12a-c), and sonic and interval seismic velocity decrease (Fig. 12d). These changes coincide with higher calculated mud pressure values that depart from the normal mud pressure trend (Fig. 12e).

Zone C is entirely overpressured as verified by measured high fluid pressures from uncorrected DST and mud weight data (Fig. 12e). Most of the geophysical parameters in Zone C show approximate parallel but offset trends with respect to the NCT. The patterns suggest that

compaction within Zone C is in disequilibrium due to the very high deposition rate of the Iperk Sequence. Limited temperature data suggest that the geothermal gradient is higher within Zone C (Fig. 12f). However, as mentioned above, this may have more to do with transient thermal conditions related to rapid burial than the presence of overpressure. The abnormally low resistivity values (circled points) in Figure 12c are associated an enlarged borehole due to caving of laminated claystone. The anomalously low sonic velocity values (light green colored area in Fig. 12d) are associated with changes of log runs near the casing shoe.

3.1.6. Quality assessment of overpressure detection

Pore fluid pressure measurements from well tests give direct estimates of the magnitude of overpressure and provide confirmation of overpressure interpretations derived from other methods. However, these pointwise measurements are generally only available for relatively few depth points. Continuous measurements are needed for better characterization of overpressure zones and the direct pressure measurements can be used as calibration points for geophysically-based pressure estimates. Mud weight is a more continuous proxy measurement that generally provides an upper limit on formation fluid pressure due to overbalanced drilling but it can be affected by the presence of hydrocarbons. Therefore, interpretations of overpressure based on mud weight need to be confirmed using other methods.

Shale log data (sonic, density and resistivity) are the most common indicators of overpressure in the study area but each log can be influenced by different factors. The shale sonic log can be affected by hydrocarbons; especially the presence of gas but it is less affected by enlarged borehole that can substantially reduce density log readings. Shale resistivity values can be influenced by many factors such as salinity, mineral composition, hydrocarbon saturation and temperature. Overall, among the three well logs, the sonic log is the best indicator for overpressure in the study area. Continuous sonic velocity logs are especially useful for detecting overpressured sand bodies where shales are interbedded with thin sand intervals. Well seismic velocity surveys are mostly limited to shallow depth intervals and have lower vertical resolution compared to well logs. They are affected by lithology changes and major stratigraphic boundaries because interval velocity is calculated based on average travel time and distance without distinguishing lithology. Although pointwise temperature data suggest increased geothermal gradient in the overpressured zone in some wells, this may be associated

with the transient thermal effects in the rapid burial deltaic sequences where overpressure develops.

The overpressure detection from the integrated approach is not always straightforward because of limitations of the method and missing part of the log datasets in some wells. Therefore, the quality of overpressure detection depends on the availability and quality of the different parameters, the robustness of the responses of these parameters to overpressure, and whether measured fluid pressure data are available to confirm interpretations. These factors are considered in defining quality-ranking criteria for interpreted depths to the top of the overpressured zone.

a – **high reliability**:

The key criteria are the overall consistency in the picks of depth to top of overpressure for most of the data sets and direct pore pressure measurements to confirm the presence of an OPZ. For example, Figure 12 shows a complete suite of data where all geophysical parameters and mud weight data show a consistent top of overpressure at 2427 m near the base of the Iperk Sequence and DST pressures are consistent with mud weight data. Figure 13 is another example illustrating an "a" quality overpressure determination. Although the density log data are of poor quality above and within the OPZ (Fig. 13b), other geophysical and mud weight parameters show a consistent depth to the OPZ at 3353 m near the base of the Kugmallit sequence. The pore pressure data are more variable but they overlap with the mud weight data and confirm that overpressure exists (Fig. 13e). Both examples show an apparent increase in geothermal gradient within the OPZ.

b – **medium reliability**:

Medium reliability interpretations show some key geophysical signatures for overpressure but the data are incomplete. They lack direct pore pressure measurements to confirm if overpressure exists in all identified zones, there may show gaps in geophysical data, and/or some parameters may give conflicting information. In such cases, interpretations are based on the weight of evidence, using parameters that give the most consistent results. Figure 14 is an example where geophysical data suggest that the top of overpressure occurs within the Taglu Sequence at 2717 m but mud weight data show a sharp increase at 3000 m. Sparse DST data confirm that overpressure exists at 3000 m (Fig. 14d). Given the coherence of the

geophysical data, the preferred interpretation is that overpressure begins at the shallower depth.

Figure 15 is a second example of "b" quality data where there is a good correspondence between geophysical determinations of top of overpressure at 1952 m within the Kugmallit Sequence and mud weight data. Mud pressure shows a sharp increase below the interpreted top of overpressure but there are no direct fluid pressure measurements to confirm interpretations (Fig. 15e). Figure 16 is a third example where there are two inferred OPZs. The top of the upper OPZ is picked at 2092 m at the base of the Iperk Sequence based on log and velocity data but there are no direct pore pressure measurements to confirm the interpretation. The top of the lower OPZ is picked at 3350 m near the top of the Kugmallit Sequence using seismic velocity data. A single DST measurement indicates that this lower zone is overpressured (Fig. 16e). This well appears to have been drilled overbalanced so mud weight data only provide weak support for overpressure. Only the Arluk E-90 well shows compelling evidence for an increase in geothermal gradient within the deeper OPZ (Fig. 16f).

c – **low reliability**:

Low reliability interpretations are based on ambiguous data with subtle geophysical signatures and no pore pressure measurements in the possible overpressure zone. The ambiguity may arise from low resolution data, wells that are too shallow, and/or logs that were not run deep enough. Under such circumstances, mud pressure data may have a stronger influence on interpretations. Overpressure may be suspected for some of these wells with "c" quality data because they are near other wells with confirmed overpressure.

Figure 17 shows an example of a "c" quality interpretation related to well depth and data resolution. The top of overpressure is inferred to occur at 2780 m in the Taglu Sequence at the depth of the casing shoe near the bottom of the well. There are few log points to provide much resolution and the interpretation is based mainly on velocity data (Fig. 17d) and a subtle increase in mud pressure (Fig. 17d). Figure 18 is a similar example of a possible OPZ below approximately 1273 m near the base of the well in the Reindeer Formation that the internal sequences have not been identified. The interpretation is based on subtle reversals in sonic velocity log estimated from density log and velocity trends. The well appears to be drilled overbalanced so mud pressure data are not diagnostic (Fig. 18e). Figure 19 is a third

example of a low reliability interpretation where the top of overpressure is picked at approximately 3315 m in the Richards Sequence based on the sharp increase in mud pressure (Figure 19e). All the geophysical data terminate above the inferred top of ovepressure. Temperature data are too sparse or too shallow to show any relation with the inferred OPZ for all three examples.

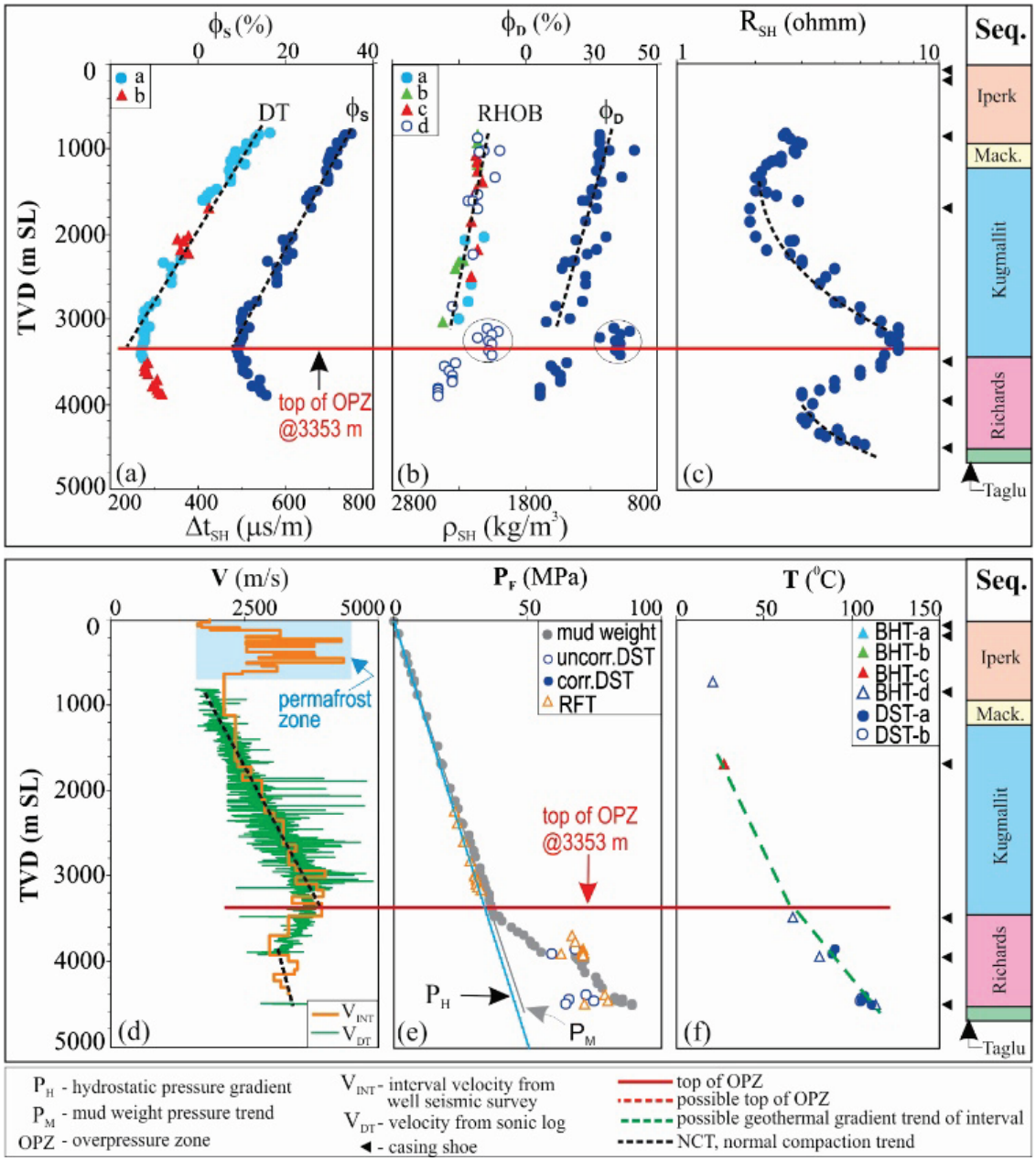

Figure 13. Example showing an "a" quality overpressure interpretation for the offshore Arnak L-30 well in the BMB. (a) Shale sonic transit time (Δt_{SH}) and sonic porosity (ϕ_S), (b) shale bulk density (ρ_{SH}) and density porosity (ϕ_D), and (c) shale deep resistivity (R_{SH}). (d) Continuous sonic velocity (V_{DT}) and average interval seismic velocity (V_{INT}), (e) pore fluid pressure (P_F) from well test and drilling mud weight, and (f) borehole temperature (T). Mack. – Mackenzie Bay Sequence.

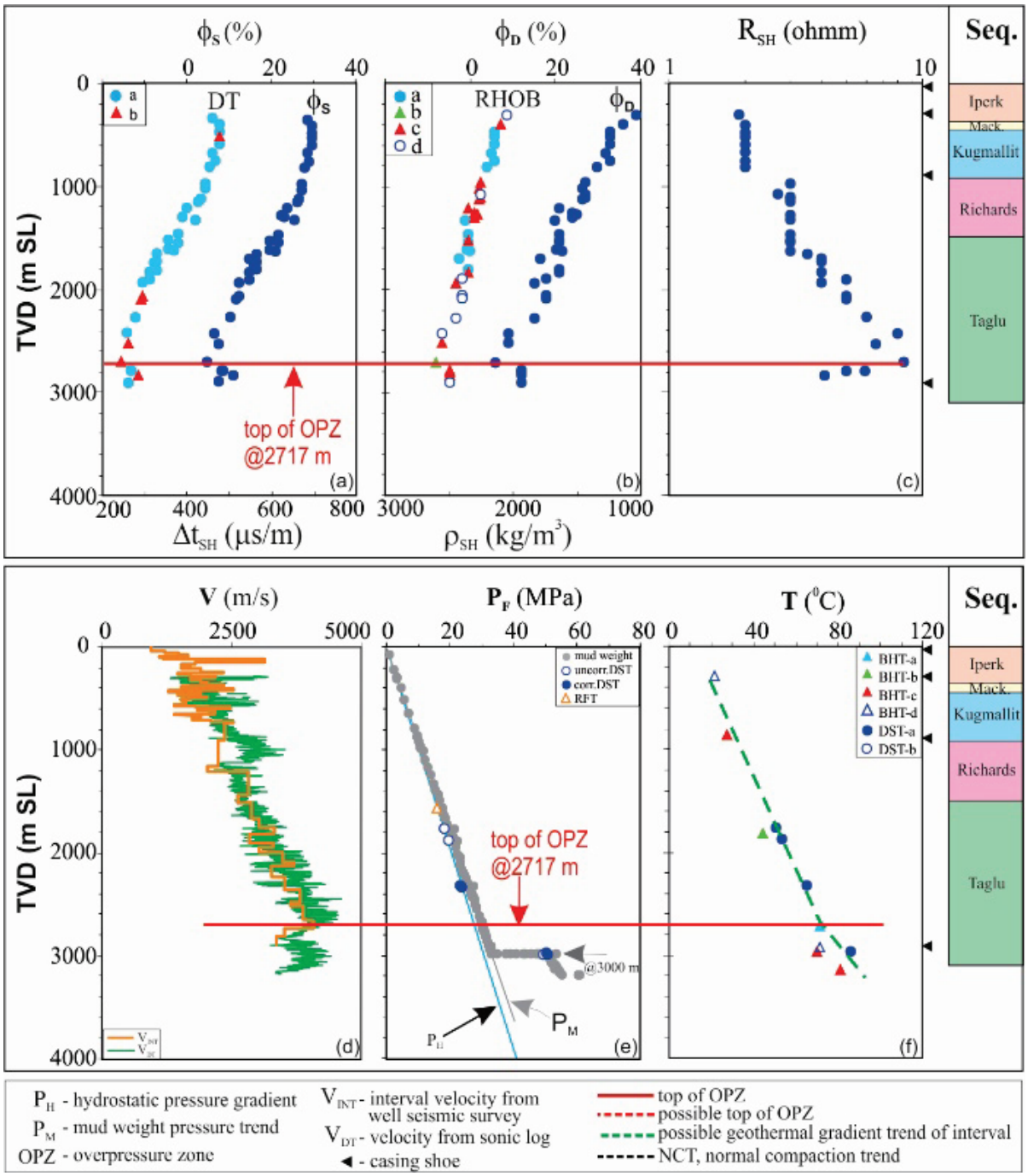

Figure 14. Example showing "b" quality overpressure interpretation for the offshore Adgo C-15 well in the BMB. (a) Shale sonic transit time (Δt_{SH}) and sonic porosity (ϕ_S), (b) shale bulk density (ρ_{SH}) and density porosity (ϕ_D), and (c) shale deep resistivity (R_{SH}). (d) Continuous sonic velocity (V_{DT}) and average interval seismic velocity (V_{INT}), (e) pore fluid pressure (P_F) from well test and drilling mud weight, and (f) borehole temperature (T). Mack. – Mackenzie Bay.

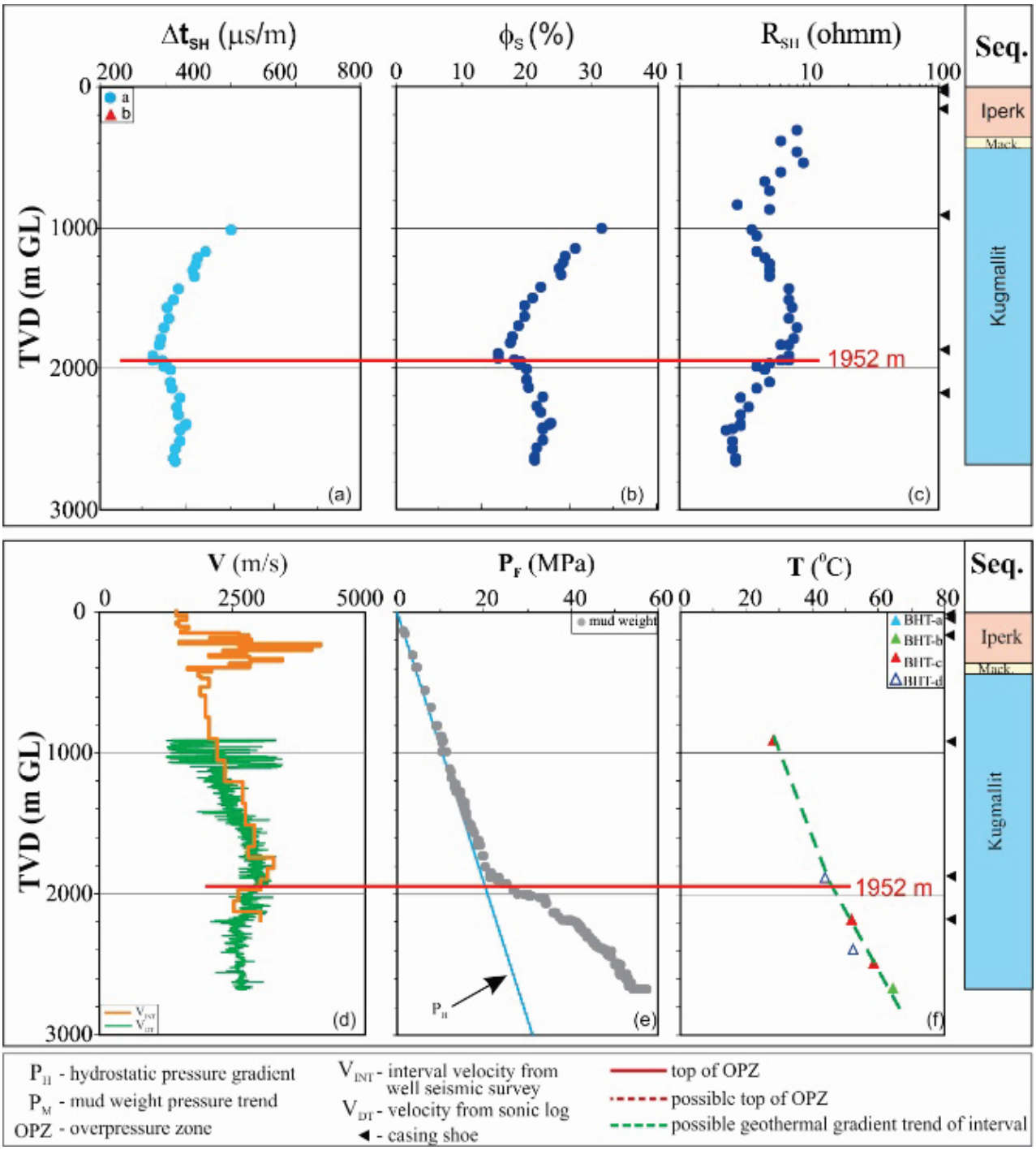

Figure 15. Example showing that an overpressure zone is detected using geophysical and drilling methods for the onshore Immerk B-48 well in the BMB, which is considered as "b" quality because there are no pore fluid pressure measurements for verification. (a) shale sonic log, (b) shale sonic porosity, (c) shale resistivity log, (d) velocity from sonic log (V_{DT}) and average interval seismic velocity (V_{INT}), (e) estimated fluid pressure from drilling mud weight, and (f) borehole temperature. Mack. – Mackenzie Bay.

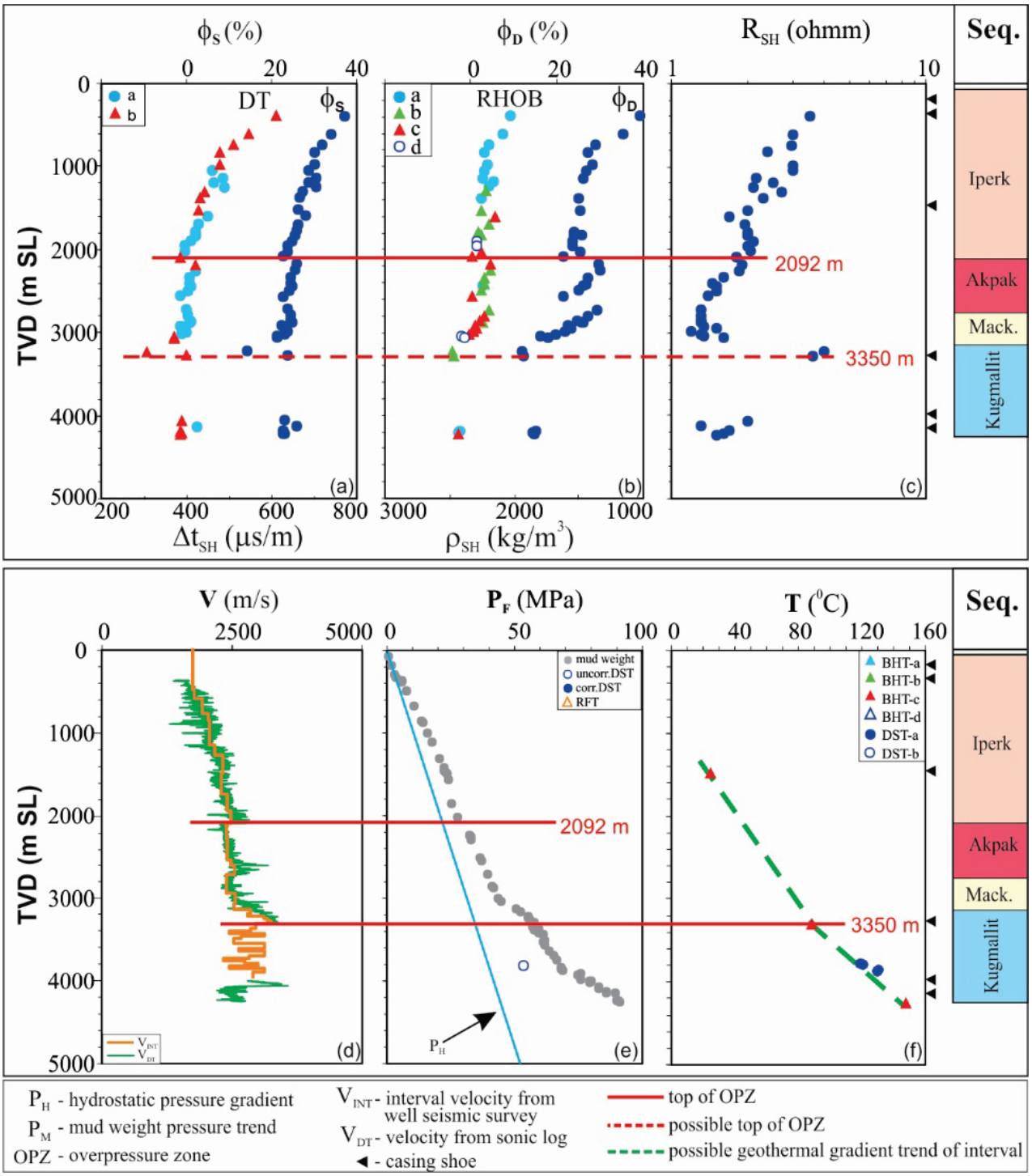

Figure 16. Two overpressure zones are detected using integrated analysis for the Arluk E-90 well in the BMB, interpretation is considered as "b" quality because well testing is absent for the shallow OPZ detection and there is no clear evidence from well logs for the deeper OPZ interpretation. (a) Shale sonic transit time (Δt_{SH}) and sonic porosity (ϕ_S), (b) shale bulk density (ρ_{SH}) and density porosity (ϕ_D), and (c) shale deep resistivity (R_{SH}). (d) Continuous sonic velocity (V_{DT}) and average interval seismic velocity (V_{INT}), (e) pore fluid pressure (P_F) from well test and drilling mud weight, and (f) borehole temperature. Mack. – Mackenzie Bay.

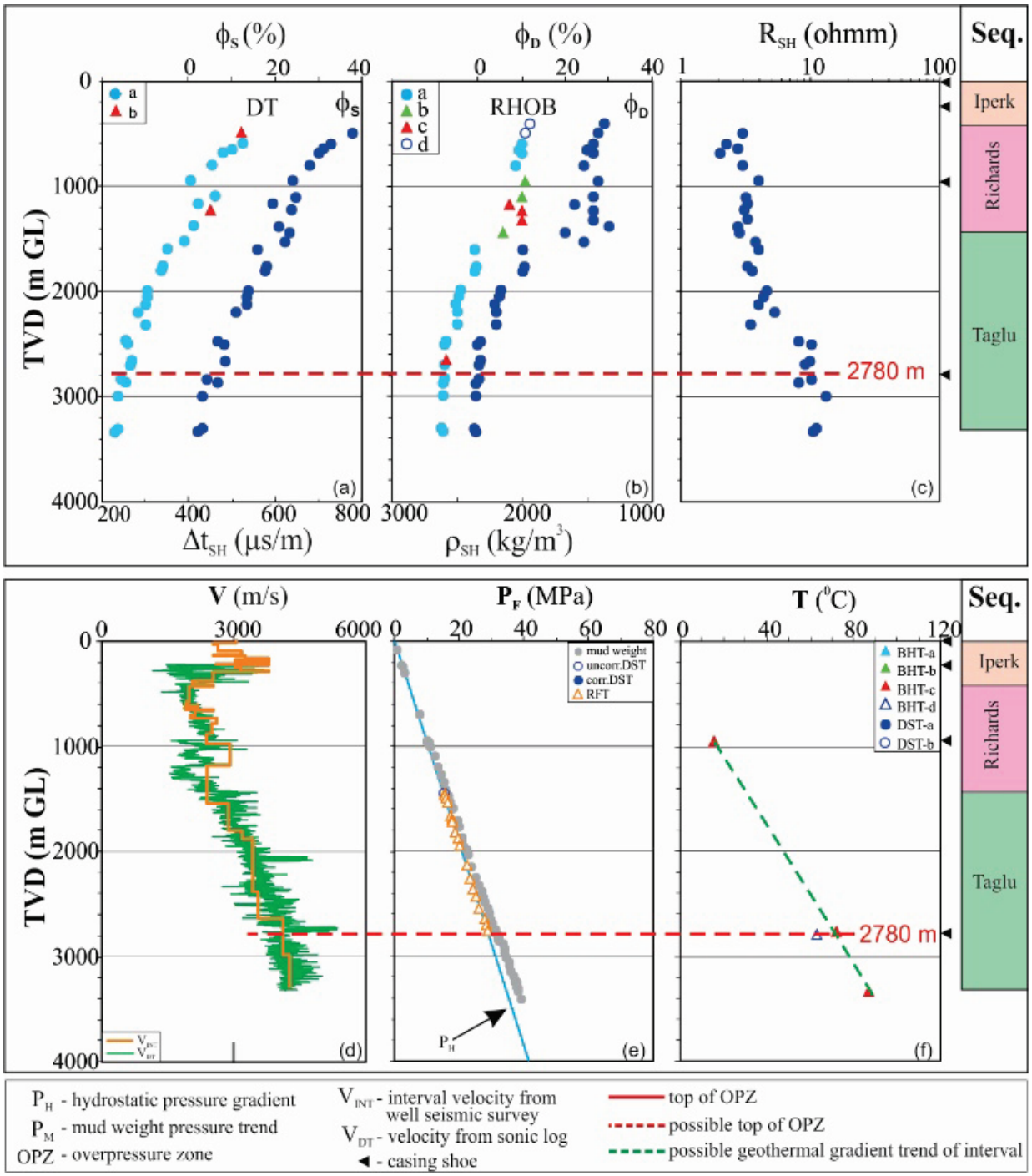

Figure 17. An uncertain "c" quality interpretation for the top of overpressure zone is shown based on integrated analysis of multiparameter data for the onshore Upluk L-42 well in the BMB. (a) shale sonic transit time (Δt_{SH}) and sonic porosity (ϕ_S), (b) shale bulk density (ρ_{SH}) and density porosity (ϕ_D), (c) shale deep resistivity (R_{SH}), (d) continuous sonic velocity (V_{DT}) and average interval seismic velocity (V_{INT}), (e) pore fluid pressure (P_F) from well test and drilling mud weight, and (f) borehole temperature.

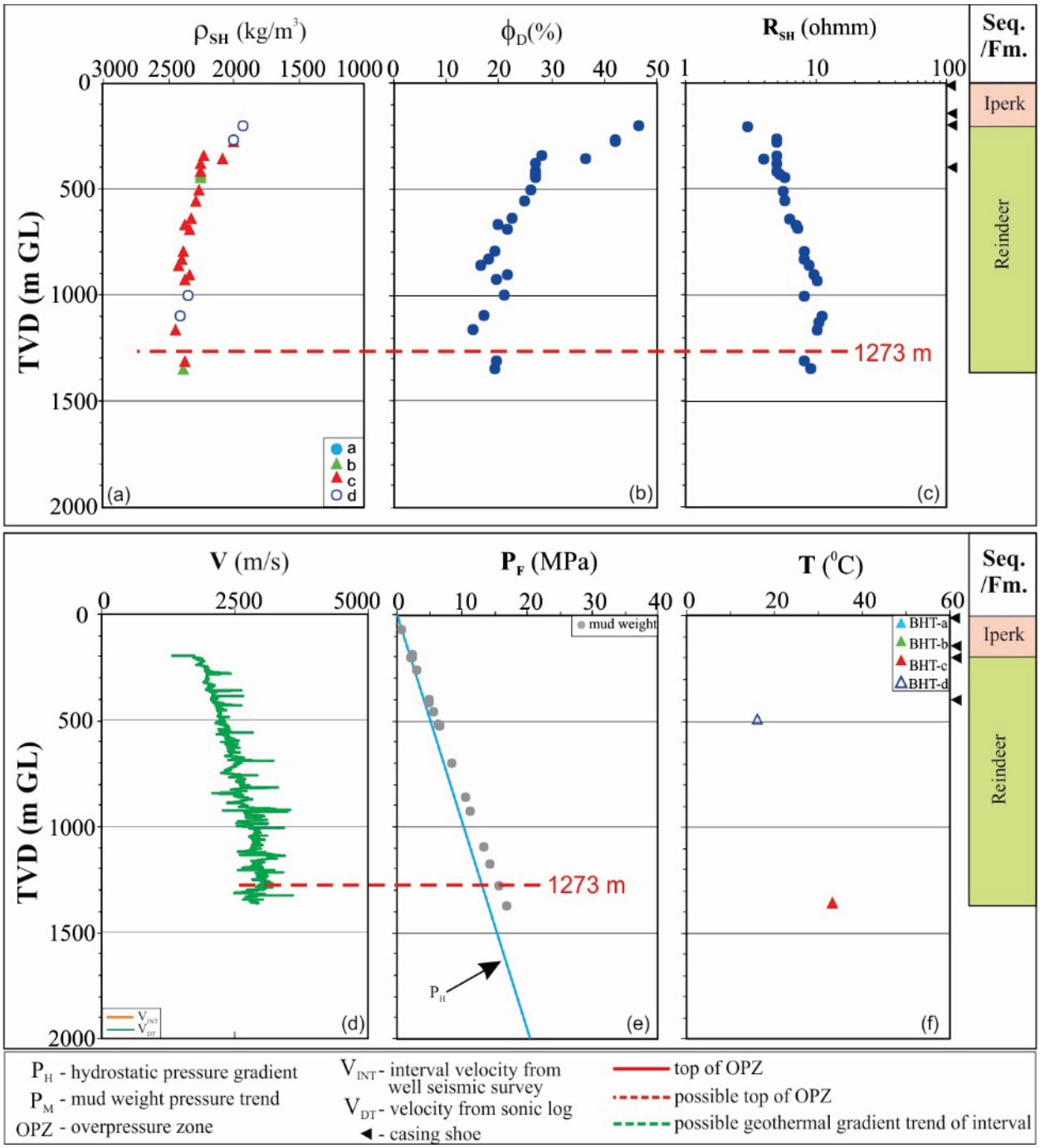

Figure 18. A "c" quality interpretation for a possible top of overpressure zone near the bottom of the well Shavilig J-20 well in the BMB based on using geophysical methods. (a) Shale bulk density (ρ_{SH}), (b) shale density porosity (ϕ_D), (c) shale deep resistivity (R_{SH}), (d) estimated sonic velocity (V_{DT}) from density log, (e) estimated fluid pressure (P_F) from drilling mud weight, and (f) borehole temperature.

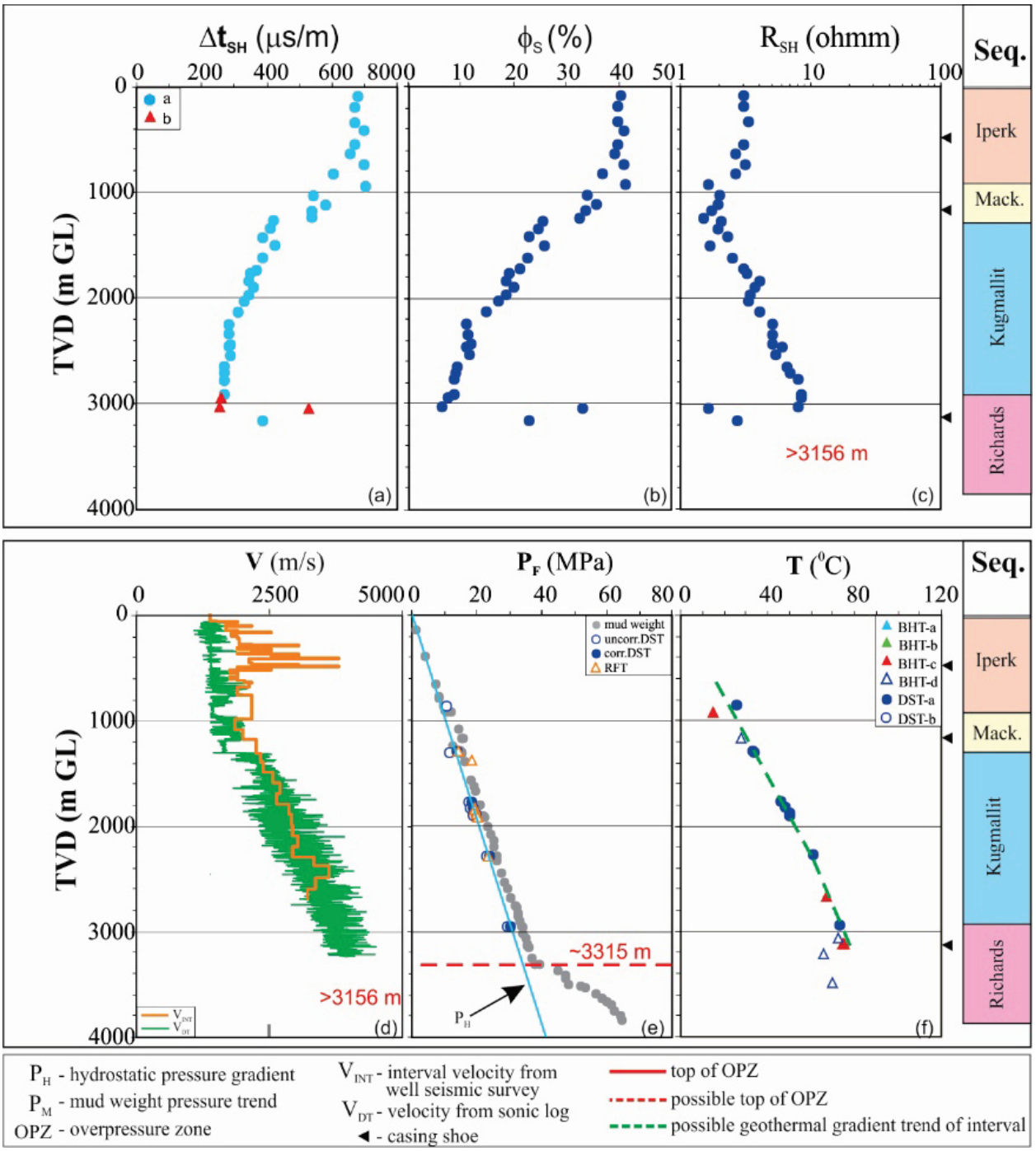

Figure 19. A "c" quality interpretation for the top of overpressure for the Nipterk L-19 well in the BMB based on using only drilling mud pressure because geophysical data are too shallow. (a) Shale sonic log, (b) shale sonic porosity, (c) shale resistivity log, (d) velocity from sonic log (V_{DT}) and average interval seismic velocity (V_{INT}), (e) estimated fluid pressure from drilling mud weight vs. depth, and (f) borehole temperature. Mack. – Mackenzie Bay.

3.2. Overpressure distribution

The depth to the top of overpressure has been determined and quality-assessed for 112 exploration wells in the BMB using an integrated analysis of multiparameter well data (red dots in Fig. 20). Table 2 lists relevant details for the wells with interpreted overpressure and includes the well UWI, well name, the inferred depth to overpressure, the quality rank for the interpretation, and the stratigraphic unit in which the top of overpressure occurs. There are 152 top of overpressure determinations in Table 2 because 36 of the 112 boreholes encountered two or three OPZs. Approximately 91% of the OPZ determinations are "a" (59 picks in 48 wells) or "b" (79 picks in 65 wells) quality whereas 14 picks in 13 wells have "c" quality values. An additional 36 wells (green dots in Fig. 20) are believed to be too shallow to have penetrated an overpressured zone based regional geological trends. The majority of wells with overpressure are located northwest of the TFZ (Taglu Fault Zone) and northeast of the WBTF (West Beaufort Thrust Front) on Richard Islands and in the offshore delta area (Fig. 20).

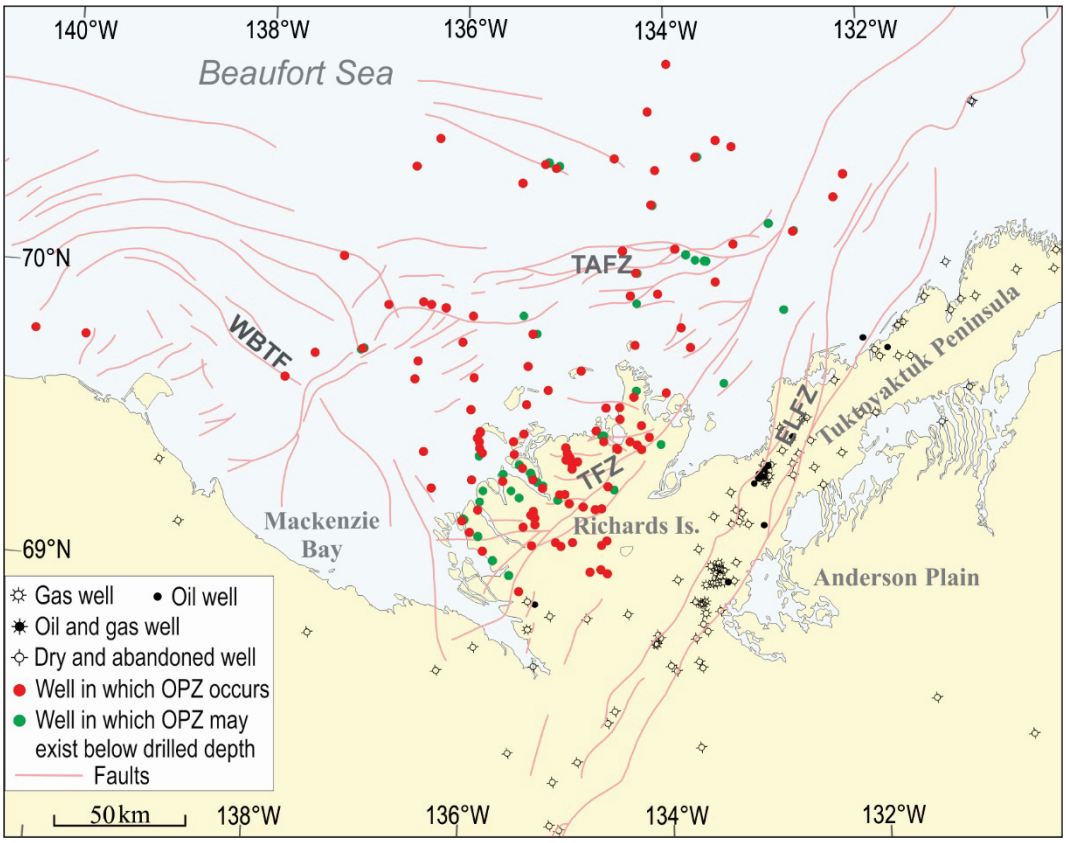

Figure 20. Map showing the wells with overpressure detected and the wells that did not reach the overpressure zone in the Beaufort-Mackenzie Basin.

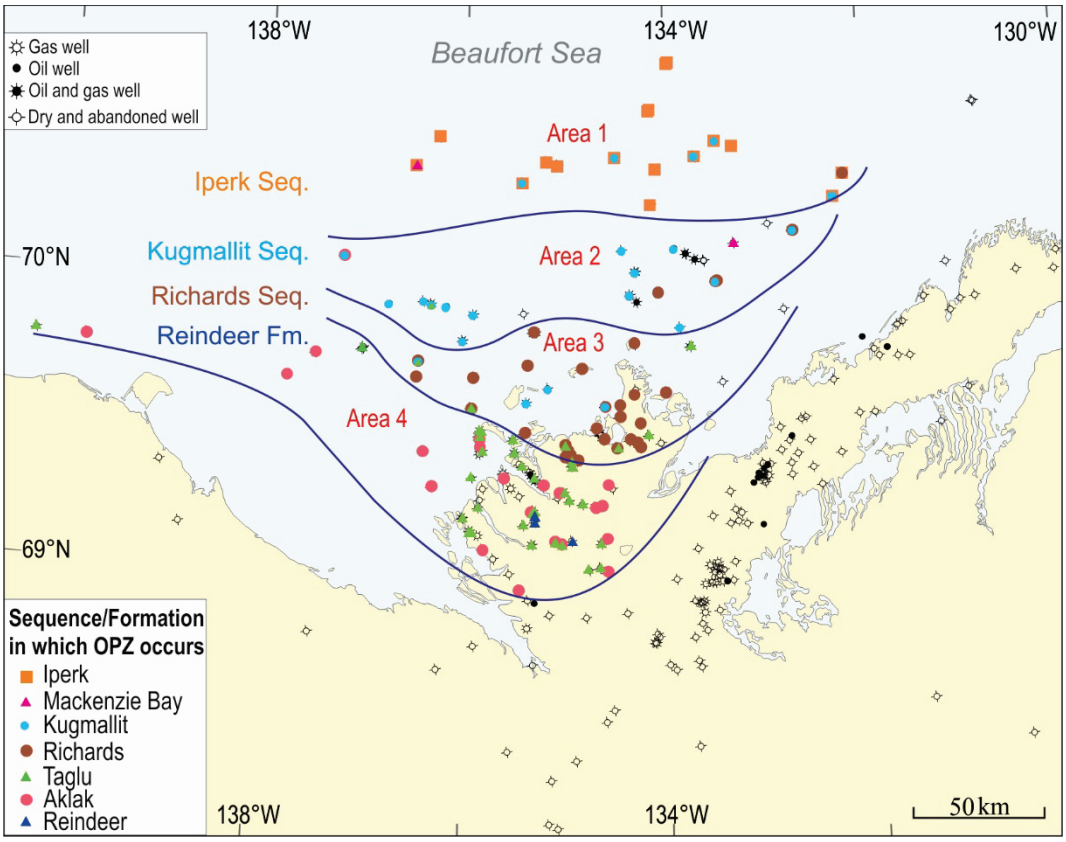

Figure 21. Map showing the stratigraphic distribution of detected overpressure zones in the Beaufort-Mackenzie Basin.

The depth to top of overpressure is mainly within four stratigraphic units (Fig. 21; Table 2): 66 tops of OPZ are identified within the Reindeer Formation (Taglu and Aklak sequences), 38 in Richards Sequence, 30 in Kugmallit Sequence, and 16 in Iperk Sequence. Wells locations in Figure 21 are colour-coded according to the stratigraphic unit in which the top of overpressure occurs. In the case of multiple OPZs within a well, more than one colour is shown. The stratigraphic interval of overpressured zone becomes progressively younger from onshore in Richards Island to Beaufort Sea. Mainly north of TAFZ (Tarsiut-Amauligak Falut Zone; Fig. 20) in the deep-water region of the Beaufort Sea (Area 1 in Fig. 21), the top surface of the OPZ fluctuates within the Iperk Sequence in 15 wells and the depth varies from 1341 to 3780 m. The depth to overpressure varies from 870 to 4358 m within the Kugmallit Sequence at 30 locations (mainly in Area 2 and Area 1; Fig. 21) and from 1140 m and 4594 m within the Richards Sequence at 36 well locations (predominantly in Area 3; Fig. 21). Among the 66 detected overpressure zones in Reindeer Formation, 37 and 25 overpressures occur in the Taglu and

Aklak sequences, respectively, with corresponding tops ranging from 1136 m to 4289 m, and 1025 m to 3579 m (primarily in Area 4; Fig. 21; Table 2).

Appendix A includes detailed composite plots showing the multiparameter data used to determine the top of overpressure for 48 wells (ordered alphabetically by well name) with "a" quality interpretations (at least one in the case of multiple overpressure picks). Appendix B has similar composite plots for 57 alphabetically listed wells with at least one "b" quality overpressure determination. Appendix C contains composite plots showing possible depths to top of overpressure for seven wells with "c" quality interpretations.

4. CONCLUSIONS

This study uses geophysical, engineering and drilling data from petroleum exploration wells to determine the depth to the top of overpressured formations in the Beaufort-Mackenzie Basin. All together, 152 depths to the top of overpressure are determined for 112 wells, and the reliability of each pick is ranked according to a quality assessment scheme. Most of the 152 overpressure zones detected using geophysical methods are confirmed by formation pressure tests. Overpressure is interpreted to occur below drilled depths for an additional 36 shallower wells based on geological trends.

Overall, well logs and log-derived formation properties in shale sections are good indicators of overpressure. However, the most reliable and consistent geophysical parameter for detecting overpressure is shale sonic transit-time (and its porosity) because it is least affected by poor borehole conditions. In general, mud pressure trends calculated from drilling mud weight data are consistent with overpressure interpretations from well logs and measured fluid pressure data. However, for some wells, mud weight data predict that overpressure starts at a greater depth than indicated by other methods. Some wells show an increase in geothermal gradient within the overpressured zone but the temperature data are too discontinuous and variable to establish any clear correlations.

Overpressure occurs within Cenozoic strata on Richards Island and in the offshore shelf region in the Beaufort Sea. The top of overpressure is restricted to the Paleocene-Eocene Aklak, Taglu and Richards sequences on Richards Island and overpressure may extend into underlying Cretaceous rocks based on observations in a few wells. The top of overpressure becomes

progressively younger northward in offshore to the outer shelf. In the central shelf region, the top of overpressure is mainly within the Richards and Kugmallit sequences but, in the outer shelf area, it rises above the base of the thick Pliocene-Pleistocene Iperk Sequence.

ACKNOWLEDGEMENTS

The authors would like to thank Dr. Glen Stockmal for providing a comprehensive review of this report. We are thankful to Dr. Jim Dixon for confirmations about formation tops. We also thank Dr. Jackson Yang for his technical assistance in the first revision of the well plots. Our research was greatly facilitated by available well history reports and image well logs curated by the National Energy Board (NEB) of Canada from which large datasets were compiled. We would like to thank IHS Energy Ltd. (current name is IHS Markit Ltd.) and Divestco Incorporated for their generous donations of digital log data. Earlier phases of this work were supported by former members of the Beaufort-Mackenzie consortium (Anadarko Canada Corporation, BP Canada Energy Company, Burlington Resources, Chevron Canada Limited, ConocoPhillips Canada Resources Corporation, Devon Canada Corporation, EnCana Corporation, Imperial Oil Resources Ventures Limited, MGM Energy Corporation, Petro-Canada, Shell Canada Limited, and Shell Exploration and Production Company), the Program on Energy Research and Development (PERD), and the Earth Sciences Sector of Natural Resources Canada through the Northern Resources Development, Secure Canadian Energy Supply and GEM Energy programs. Our special thanks go to Dr. Rob MacNaughton, leader of the GEM I Mackenzie Delta and Corridor project, and Dr. Keith Dewing and Jim Dietrich, leaders of the GNES Frontier Basin Analysis project for their support.

REFERENCES

Bloch, J.D. and Issler, D.R. 1996. Petrographic and geochemical analyses of Beaufort-Mackenzie Basin shales. Geological Survey of Canada, Open File 3220, 71p.

Chapman, R.E. 1981. Geology and Water - An Introduction to Fluid Mechanics for Geologists. Martinus Nijhof/Dr. W. Junk, The Hague, 228 p.

Chen, Z., Osadetz, K.G., Issler, D.R. and Grasby, S.E. 2008. Hydrocarbon migration detected by regional temperature field variations, Beaufort-Mackenzie Basin, Canada. AAPG Bulletin, v. 92, no. 12, p. 1639-1653.

Chen, Z., Osadetz, K.G., Issler, D.R. and Grasby, S.E. 2010a. Fluid pressure patterns in Tertiary successions and hydrodynamic implications, Beaufort-Mackenzie Basin, Canada. Bulletin of Canadian Petroleum Geology, v. 58, no. 1, p. 3-16.

Chen, Z., Issler, D.R. and Hu, K. 2010b. A non-linear fit to formation temperature profiles from petroleum exploration wells in the Beaufort-Mackenzie Basin, Canada. Geological Survey of Canada, Open File 6216, 16 p., https://doi.org/10.4095/262721

Dixon, J., Morrow, D.W. and MacLean, B.C. 2007. A guide to the hydrocarbon potential of the northern mainland of Canada. Geological Survey of Canada, Open File 5641.

Dixon, J. (Editor), 1996. Geological Atlas of the Beaufort-Mackenzie Area. Geological Survey of Canada Miscellaneous Report 59.

Dixon, J., Lane, L.S, Dietrich, J.R., McNeil, D.H. and Chen, Z. 2019. The Sedimentary Basins of United States and Canada, Chapter 17 - Geological History of the Late Cretaceous to Cenozoic Beaufort-Mackenzie Basin, Arctic Canada. p. 695-717. https://doi.org/10.1016/B978-0-444-63895-3.00017-6

Grasby, S.E., Chen, Z., Issler, D.R. and Stasiuk, L. 2009. Evidence for deep anaerobic biodegradation associated with rapid sedimentation and burial in the Beaufort-Mackenzie basin, Canada. Applied Geochemistry, v. 24, p. 536-542.

Hitchon, B., Underschultz, J.R., Bachu, S. and Sauveplane, C.M. 1990. Hydrogeology, Geopressures and Hydrocarbon Occurrences, Beaufort-Mackenzie Basin. Bulletin of Canadian Petroleum Geology, v. 38, no. 2, p. 215-235.

Hu, K., Issler, D.R. and Jessop, A. 2010. Well temperature data compilation, correction and quality assessment for the Beaufort-Mackenzie Basin. Geological Survey of Canada, Open File 6057, 17 p. (1 CD-ROM), https://doi.org/10.4095/262755

Hu, K., Issler, D.R., Chen, Z. and Brent, T.A. 2013. Permafrost investigation by well logs, and seismic velocity and repeated shallow temperature surveys, Beaufort-Mackenzie Basin. Geological Survey of Canada. Geological Survey of Canada, Open File 6956, 33 p., 246 figures, and 3 tables. https://doi.org/10.4095/293120

Hu, K., Chen, Z. and Issler, D.R. 2014. Determination of geothermal gradient from borehole temperature and permafrost base for exploration wells in the Beaufort-Mackenzie Basin. Geological Survey of Canada, Open File 6957, 23 p. plus figures and table. https://doi.org/10.4095/293872

Hu, K., Brent, T.A., Issler, D.R. and Chen, Z. 2015. Synthetic seismograms from borehole seismic data and well logs, Beaufort-Mackenzie Basin. Geological Survey of Canada, Open File 6056, 228 p., https://doi.org/10.4095/296213

Issler, D.R., Hu, K., Lane, L.S. and Dietrich, J.R. 2011. GIS Compilations of Overpressure, Permafrost Distribution, Geothermal Gradient, and Geology, Beaufort-Mackenzie Region, Northern Canada. Geological Survey of Canada, Open File 5689 (1 CD-ROM), https://doi.org/10.4095/289113

Issler, D.R., Katsube, T.J., Bloch, J.D. and McNeil, D.H. 2002. Shale compaction and overpressure in the Beaufort-Mackenzie Basin of northern Canada. Geological Survey of Canada, Open File 4192, 10 p. (1 diskette) https://doi.org/10.4095/213052

Issler, D.R. 1992. A new approach to shale compaction and stratigraphic restoration, Beaufort-Mackenzie Basin and Mackenzie Corridor, northern Canada. AAPG Bulletin, v. 76, p. 1170-1189.

Issler, D.R. and Jessop, A.M. 2011. Thermal conductivity analysis of Cenozoic, Mesozoic and Paleozoic core samples, Beaufort-Mackenzie Basin, northern Canada. Geological Survey of Canada, Open File 6734, 128 p., https://doi.org/10.4095/288026

Issler, D.R. and Katsube, T.J. 1994. Effective porosity of shale samples from the Beaufort-Mackenzie Basin. In: Current Research, 1994-B, Geological Survey of Canada, p. 19-26. https://doi.org/10.4095/193649

Katsube, T.J., Issler, D.R. and Connell-Madore, S. 2011. Porosity characteristics of shale samples for varied compaction zones in the Beaufort-Mackenzie Basin, Northwest Territories. Geological Survey of Canada, Current Research (Online) no. 2011-12, 14 p. https://doi.org/10.4095/289040

Katsube, T.J., Issler, D.R. and Coyner, K. 1996. Petrophysical characteristics of shale from the Beaufort-Mackenzie Basin, northern Canada: permeability, formation factor and porosity vs. pressure. In: Current Research 1996-B; Geological Survey of Canada, p. 45-50. https://doi.org/10.4095/207430

Katsube, T.J., Bloch, J.D. and Issler, D.R. 1995. Shale pore-structure evolution under variable sedimentation rates in the Beaufort-Mackenzie Basin. In: Bell, J.S., Bird, T.D., Hillier, T.L. and Greener, P.L. (eds.), Proceedings of the Oil and Gas Forum '95 - Energy from Sediments, Geological Survey of Canada Open File 3058, p. 211-215. https://doi.org/10.4095/203623

Katsube, T.J. and Issler, D.R. 1993. Pore-size distributions of shales from the Beaufort-Mackenzie Basin, northern Canada. In: Current Research, Part E, Geological Survey of Canada, Paper 93-1E, p. 123-132. https://doi.org/10.4095/184104

Lewis, C.R. and Rose., S.C. 1970. A theory relating high temperatures and overpressures. Journal of Petroleum Technology, v. 22, no. 1, p. 11-16.

Majorowicz, J.A., Osadetz, K.G., and Safanda, J. 2008a. Modeling temperature profiles considering the latent heat of physical-chemical reactions in permafrost and gas hydrates – the Mackenzie Delta terrestrial case. In: Permafrost on a Warming Planet: Implications for Ecosystems, Infrastructure and Climate. D.L. Kane and K.M. Hinkel (eds.). Proceedings of the 9th International Conference on Permafrost; University of Fairbanks Alaska, June 29–July 3, 2008, v. 2, p. 1113–1118.

McNeil, D.H., Duk-Rodkin, A., Dixon, J., Dietrich, J.R., White, J.M., Miller, K.G., and Issler, D.R. 2001. Sequence stratigraphy, biotic change, $^{87}Sr/^{86}Sr$ record, paleoclimatic history, and sedimentation rate change across a regional late Cenozoic unconformity in Arctic Canada. Canadian Journal of Earth Sciences, v. 38, p. 309-331.

Osborne, M.J. and Swarbrick, R.E. 1997. Mechanisms for generating overpressure in sedimentary basins: a reevaluation. AAPG Bulletin, v. 81, no. 6, p. 1023-1041.

Raiga-Clemenceau, J., Martin, J. P. and Nicoletis, S. 1988. The concept of acoustic formation factor for more accurate porosity determination from sonic transit time data. The Log Analyst, v. 29, no. 1, p. 54-60.

Schlumberger 1989. Log Interpretation Principles/Application. p. 5.12.

Snowdon, L.R. 1990. Rock-Eval/TOC results from 29 Beaufort-Mackenzie wells. Geological Survey of Canada, Open File 2192, 210 p. https://doi.org/10.4095/130813

Snowdon, L.R., Obermajer, M. and Issler, D.R. 2010. Rock-Eval/TOC data for thirty wells from Beaufort-Mackenzie Basin, Northwest Territories. Geological Survey of Canada, Open File 6682, 7 p. (1 CD-ROM), https://doi.org/10.4095/287138

Taylor, A.E., Dallimore, S.R., Hill, P.R., Issler, D.R., Blasco, S. and Wright, F. 2013. Numerical model of the geothermal regime on the Beaufort Shelf, arctic Canada since the Last Interglacial. Journal of Geophysical Research: Earth Surface, v. 118, p. 2365-2379, doi:10.1002/2013JF00285

Youn, S.H. 1974. Comparison of porosity and density values of shale from cores and well logs. Master's thesis, University of Tulsa, Tulsa, Oklahoma, 62 p.

Zhao, J., Li, J. and Xu, Z. 2018. Advances in the origin of overpressures in sedimentary basins. Petroleum Research, v. 3, p. 1-24. https://doi.org/10.1016/j.ptlrs.2018.03.007

TABLE 2

APPENDICES

Appendix A (Figs. A-1 to A-48)

Appendix B (Figs. B-1 to B-57)

Appendix C (Figs. C-1 to C-7)

Table 2. Detected top of overpressure for 112 petroleum exploration wells in the Baufort-Mackenzie Basin

UWI	Well name	Top of overpressure zone				Comments
		m SL	m GL	Quality	OPZ@Seq. / Fm.	Plots @
300E566950136450	Aagnerk E-56	870		b	Kugmallit	Appendix B
300C156930135450	Adgo C-15	2717		b	Taglu	Appendix B
300F286930135450	Adgo F-28	2525		b	Taglu	Appendix B
300H296930135450	Adgo H-29	3087		b	Taglu	Appendix B
300J276930135450	Adgo J-27	2585		a	Aklak	Appendix A
300P256930135450	Adgo P-25	2140		b	Aklak	Appendix B
300P096940137450	Adlartok P-09	1760		a	Aklak	Appendix A
302I457030133300	Aiverk 2I-45	2732		b	Iperk	Appendix A
302I457030133300	Aiverk 2I-45	3913		a	Kugmallit	Appendix A
302I457030133302	Akpak 2P-35	2170		a	Iperk	Appendix A
300O867010133300	Amauligak O-86	3658		b	Kugmallit	Appendix B
300O097000133300	Amerk O-09	2830		b	Kugmallit	Appendix A
300O097000133300	Amerk O-09	3870		b	Richards	Appendix A
300O097000133300	Amerk O-09	4400		a	Richards	Appendix A
300E907020135000	Arluk E-90	2092		b	Iperk	Appendix B
300E907020135000	Arluk E-90	3350		b	Kugmallit	Appendix B
300K066950133450	Arnak K-06	3700		b	Taglu	Appendix B
300L306950133450	Arnak L-30	3353		a	Kugmallit	Appendix A
300N447000136000	E. Tarsiut N-44	2050		b	Kugmallit	Appendix B
300N447000136000	E. Tarsiut N-44	3068		c	Richards	Appendix B
300N447000136001	E. Tarsiut N-44A	2106		b	Kugmallit	Appendix B
300M566950140000	Edlok M-56 (N-56)	2281		c	Taglu	Appendix C
300I486910135450	Ellice I-48		1227	c	Richards	Appendix B
300I486910135450	Ellice I-48		2270	b	Taglu	Appendix B
300I486910135450	Ellice I-48		3064	b	Taglu	Appendix B
300O146910135450	Ellice O-14		2647	b	Aklak	Appendix B
300G076930135300	Garry G-07		3091	b	Richards	Appendix B
300P046930135300	Garry P-04		2720	b	Taglu	Appendix B
300G076940134000	Hansen G-07		3081	b	Richards	Appendix B
300B417030132000	Havik B-41	2218		a	Iperk	Appendix A
300B417030132000	Havik B-41	3632		a	Richards	Appendix A
300J176920136150	Ikattok J-17	1454		a	Aklak	Appendix A
300J176920136150	Ikattok J-17	3656		b	Aklak	Appendix A
300B486940135000	Immerk B-48	1952		b	Kugmallit	Appendix B
300A066950137000	Immiugak A-06	1600		c	Richards	Appendix B
300A066950137000	Immiugak A-06	3040		b	Taglu	Appendix B
300B357040134000	Irkaluk B-35	3541		a	Iperk	Appendix A
300E277000134150	Isserk E-27	3877		b	Kugmallit	Appendix B
302O617010134000	Issungnak 2O-61	3456		b	Kugmallit	Appendix B
300I277000134000	Itiyok I-27	3300		b	Kugmallit	Appendix B
300C526940134150	Ivik C-52		2015	b	Richards	Appendix B
300J266940134150	Ivik J-26		3190	b	Richards	Appendix B
300K546940134150	Ivik K-54		2600	b	Richards	Appendix B
300O076950136000	Kadluk O-07	2445		a	Kugmallit	Appendix A
300J947050133300	Kenalooak J-94	3780		b	Iperk	Appendix B
300A437000135450	Kiggavik A-43	2562		a	Kugmallit	Appendix A
300N466910134450	Kikoralok N-46		1471	b	Reindeer	Appendix B
300F486930134000	Kilagmiotak F-48		3262	a	Taglu	Appendix A
300F486930134000	Kilagmiotak F-48		4005	b	Taglu	Appendix A
300J546950137150	Kingark J-54	1025		b	Aklak	Appendix B

UWI	Well name	Top of overpressure zone				Comments
		m SL	m GL	Quality	OPZ@Seq. / Fm.	Plots @
300J546950137150	Kingark J-54	1713		b	Aklak	Appendix B
300O206850134450	Koakoak O-22	2427		a	Iperk	Appendix A
300N677010133000	Kogyuk N-67	2450		a	Mackenzie Bay	Appendix A
300N677010133000	Kogyuk N-67	3706		b	Kugmallit	Appendix A
302I447030135000	Kopanoar 2I-44	2473		a	Iperk	Appendix A
302I447030135000	Kopanoar 2I-44	3858		c	Kugmallit	Appendix A
300M137030135000	Kopanoar M-13	2438		a	Iperk	Appendix A
300M137030135000	Kopanoar M-13	4071		b	Kugmallit	Appendix A
300L466900135150	Kugpik L-46		1376	a	Aklak	Appendix A
300C586920135000	Kumak C-58		3148	b	Aklak	Appendix B
300J066920135000	Kumak J-06		2350	a	Taglu	Appendix A
300K166920135000	Kumak K-16		2893	a	Aklak	Appendix A
300M156910135150	Kurk M-15		1972	a	Taglu	Appendix A
300M396910135150	Kurk M-39	2304		c	Taglu	Appendix C
300M396910135150	Kurk M-39	2780		c	Aklak	Appendix C
300E296920135300	Langley E-29		3112	b	Aklak	Appendix B
300A066930134300	Mallik A-06		2330	a	Richards	Appendix A
300A066930134300	Mallik A-06		3231	a	Taglu	Appendix A
300J376930134300	Mallik J-37		1926	a	Richards	Appendix A
300L386930134300	Mallik L-38		2288	c	Richards	Appendix C
300P596930134300	Mallik P-59		2146	b	Richards	Appendix B
300I536950136150	Minuk I-53	1445		a	Kugmallit	Appendix A
300I536950136150	Minuk I-53	2057		a	Richards	Appendix A
300I536950136150	Minuk I-53	2873		a	Taglu	Appendix A
300J236920135450	N. Ellice J-23		1674	b	Taglu	Appendix B
300J236920135450	N. Ellice J-23		2923	b	Taglu	Appendix B
300L396920135450	N. Ellice L-39		1556	a	Taglu	Appendix A
300L867010134000	N. Issungnak L-86	3753		a	Kugmallit	Appendix A
300O447010137000	Natiak O-44	2309		b	Kugmallit	Appendix B
300O447010137000	Natiak O-44	3920		b	Aklak	Appendix B
300E566950139300	Natsek E-56	2560		c	Aklak	Appendix C
300K597030136000	Nektoralik K-59	1341		b	Iperk	Appendix A
300K597030136000	Nektoralik K-59	2095		a	Iperk	Appendix A
300J677030133000	Nerlerk J-67	3024		b	Iperk	Appendix B
300M987030133000	Nerlerk M-98	2777		a	Iperk	Appendix A
300M987030133000	Nerlerk M-98	4350		a	Kugmallit	Appendix A
300B446940135450	Netserk B-44	2243		a	Richards	Appendix A
300B446940135450	Netserk B-44	3120		a	Richards	Appendix A
300F406940135450	Netserk F-40	2395		b	Kugmallit	Appendix A
300F406940135450	Netserk F-40	3566		a	Richards	Appendix A
300M196920135150	Niglintgak M-19		2779	b	Taglu	Appendix B
300L196950135150	Nipterk L-19	3315		c	Richards	Appendix C
300P326950135150	Nipterk P-32	1828		a	Richards	Appendix A
300C226950134450	Nuktak C-22		2431	b	Richards	Appendix B
300H016920136000	Olivier H-01		2757	b	Taglu	Appendix B
300O037030136300	Orvilruk O-03	2050		b	Iperk	Appendix B
300O037030136300	Orvilruk O-03	2803		b	Mackenzie Bay	Appendix B
300C606940136150	Paktoa C-60	1140		a	Richards	Appendix A
300B356940135150	Pelly B-35	2435		b	Kugmallit	Appendix B
300A057000136450	Pitsiulak A-05	1640		b	Kugmallit	Appendix B
300E176950134150	Pullen E-17	3498		a	Richards	Appendix A
300A416910134300	Reindeer A-41		1336	b	Taglu	Appendix B

UWI	Well name	Top of overpressure zone				Comments
		m SL	m GL	Quality	OPZ@Seq. / Fm.	Plots @
300D276910134300	Reindeer D-27		2045	a	Aklak	Appendix A
300C366910134300	Reindeer F-36 (C-36)		1457	b	Taglu	Appendix B
300B356930136150	Sarpik B-35	2530		a	Aklak	Appendix A
300J206910135150	Shavilig J-20		1273	c	Reindeer	Appendix C
300I057030134300	Siulik I-05	2928		b	Iperk	Appendix B
300I057030134300	Siulik I-05	4232		b	Kugmallit	Appendix B
300C426930134450	Taglu C-42		3381	a	Taglu	Appendix A
300C426930134450	Taglu C-42		4289	b	Taglu	Appendix A
300D436930134450	Taglu D-43		2086	b	Richards	Appendix A
300D436930134450	Taglu D-43		3957	a	Taglu	Appendix A
300D556930134450	Taglu D-55		2400	b	Richards	Appendix A
300D556930134450	Taglu D-55		2970	a	Richards	Appendix A
300G336930134450	Taglu G-33		2300	a	Richards	Appendix A
300H546930134450	Taglu H-54		2092	b	Richards	Appendix B
300H066930135000	Taglu West H-06		2535	a	Richards	Appendix A
300H066930135000	Taglu West H-06		3985	a	Taglu	Appendix A
300P036930135000	Taglu West P-03		2168	b	Richards	Appendix B
300A257000136150	Tarsiut A-25	2077		a	Kugmallit	Appendix A
300A257000136150	Tarsiut A-25	3470		a	Taglu	Appendix A
300K266910135000	Titalik K-26		2920	a	Aklak	Appendix A
300K266910135000	Titalik K-26		1861	a	Taglu	Appendix A
300O156910135000	Titalik O-15		2502	b	Aklak	Appendix B
300O156910135000	Titalik O-15		1694	b	Taglu	Appendix B
300H246920134450	Toapolok H-24		2340	b	Taglu	Appendix B
300O546920134450	Toapolok O-54		2426	a	Taglu	Appendix A
300F306900134300	Tununuk F-30		2160	a	Aklak	Appendix A
300K106900134450	Tununuk K-10		1150	b	Aklak	Appendix B
300K106900134450	Tununuk K-10		1757	c	Taglu	Appendix B
302C507010132300	Ukalerk 2C-50	2874		b	Kugmallit	Appendix B
302C507010132300	Ukalerk 2C-50	4594		b	Richards	Appendix B
300J376930134150	Umiak J-37		2338	b	Richards	Appendix B
300N056930134150	Umiak N-05		2549	b	Richards	Appendix B
300N106930134150	Umiak N-10		2970	b	Richards	Appendix B
300N166930134150	Umiak N-16		2561	b	Richards	Appendix B
300L246940134300	Unark L-24	2794		a	Richards	Appendix A
302L246940134300	Unark L-24A	2831		b	Kugmallit	Appendix B
300B126920135150	Unipkat B-12	680	680	c	Reindeer	Appendix B
300B126920135150	Unipkat B-12		1120	b	Reindeer	Appendix B
300I226920135150	Unipkat I-22		3088	a	Aklak	Appendix A
300I226920135150	Unipkat I-22		1790	a	Taglu	Appendix A
300N126920135150	Unipkat N-12		1136	b	Taglu	Appendix B
300N126920135150	Unipkat N-12		1403	b	Taglu	Appendix B
300L426930135150	Upluk L-42		2780	c	Taglu	Appendix C
300M386930135150	Upluk M-38		2402	a	Richards	Appendix A
300P667020132000	Uviluk P-66	2120		a	Iperk	Appendix A
300P667020132000	Uviluk P-66	3486		a	Kugmallit	Appendix A
300P457000136150	W.Tarsiut P-45	1650		b	Kugmallit	Appendix B
300A286920134300	Ya Ya A-28		3579	a	Aklak	Appendix A
300M336920134300	Ya Ya M-33		2570	b	Aklak	Appendix B
300P536920134300	Ya Ya P-53		2446	b	Aklak	Appendix B

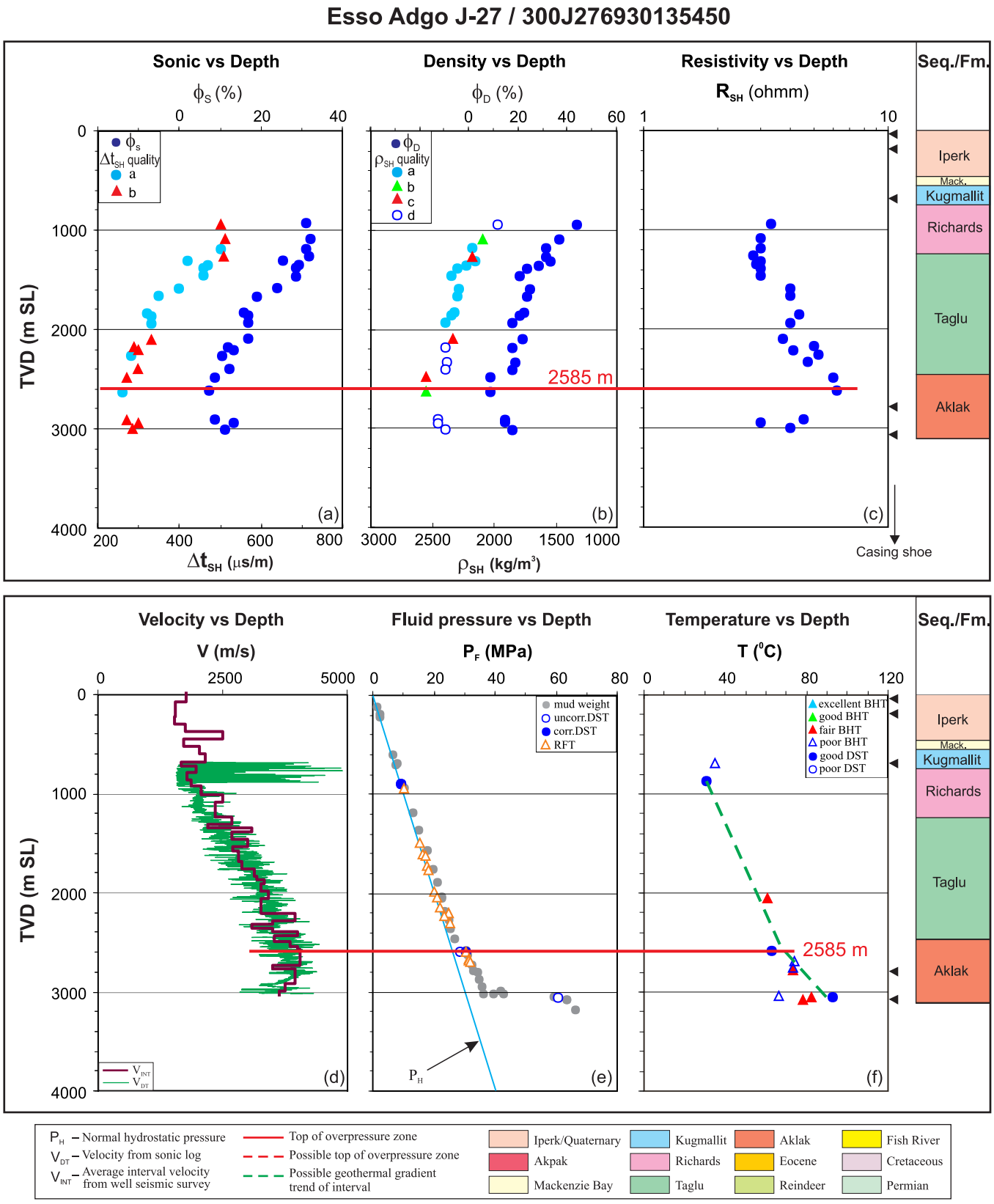

Figure A-1. Top of overpressure zone is detected at 2585 m with quality "a" by using the integrated analysis for the Adgo J-27 well in the Beaufort-Mackenzie Basin. (a) shale sonic transit time (Δt_{SH}) and sonic porosity (ϕ_S) vs. depth; (b) shale bulk density (ρ_{SH}) and density porosity (ϕ_D) vs depth; (c) shale deep resistivity (R_{SH}) vs. depth; (d) continuous sonic velocity (V_{DT}) and average interval seismic velocity (V_{INT}) vs. depth; (e) fluid pressure (P_F) from well test and drilling mud weight vs. depth; and (f) borehole temperature vs. depth. Mack. - Mackenzie Bay.

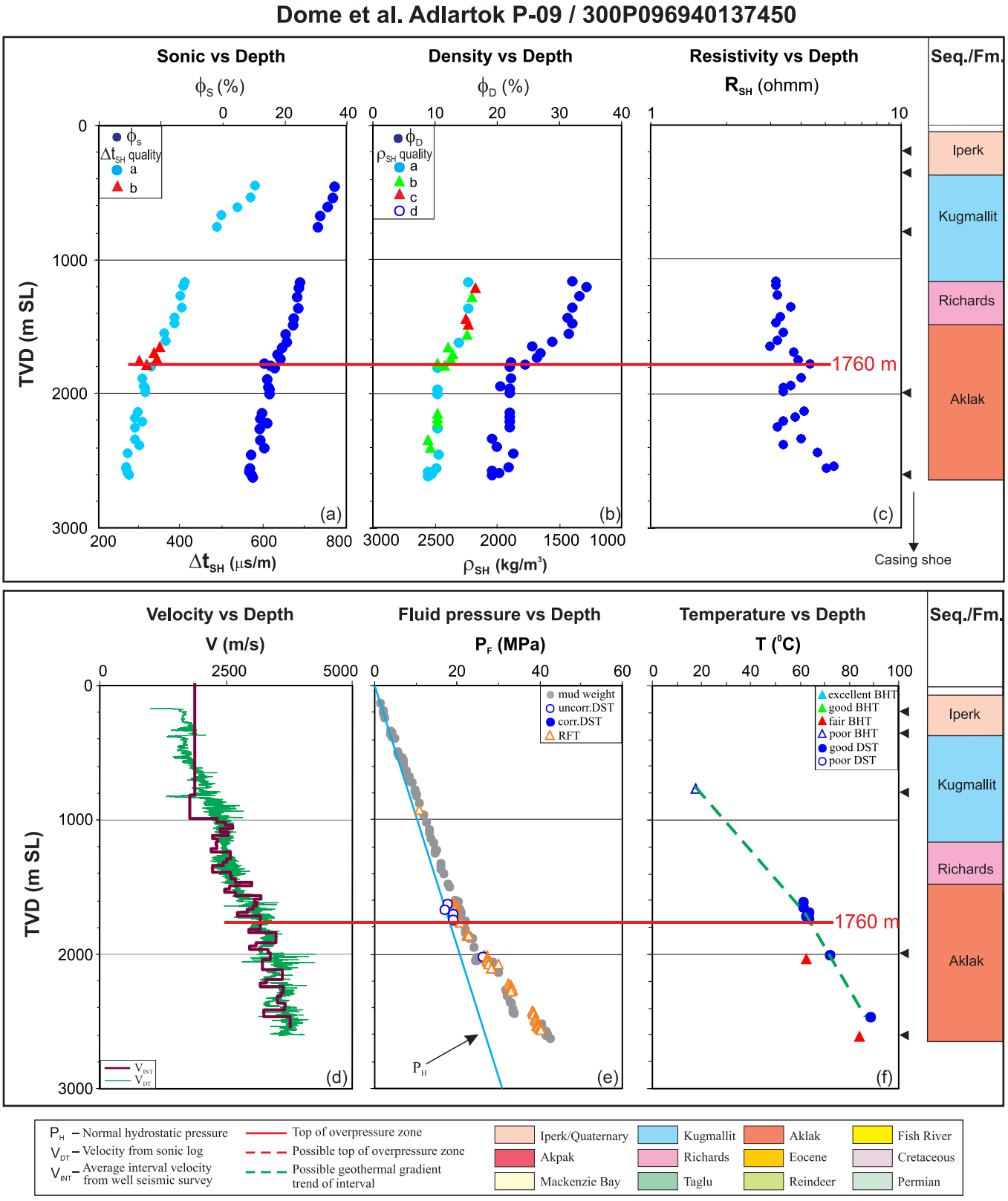

Figure A-2. Top of overpressure zone is detected at 1760 m with quality "a" by using the integrated analysis for the Adlartok P-09 well in the Beaufort-Mackenzie Basin. (a) shale sonic transit time (Δt_{SH}) and sonic porosity (ϕ_S) vs. depth; (b) shale bulk density (ρ_{SH}) and density porosity (ϕ_D) vs depth; (c) shale deep resistivity (R_{SH}) vs. depth; (d) continuous sonic velocity (V_{DT}) and average interval seismic velocity (V_{INT}) vs. depth; (e) fluid pressure (P_F) from well test and drilling mud weight vs. depth; and (f) borehole temperature vs. depth.

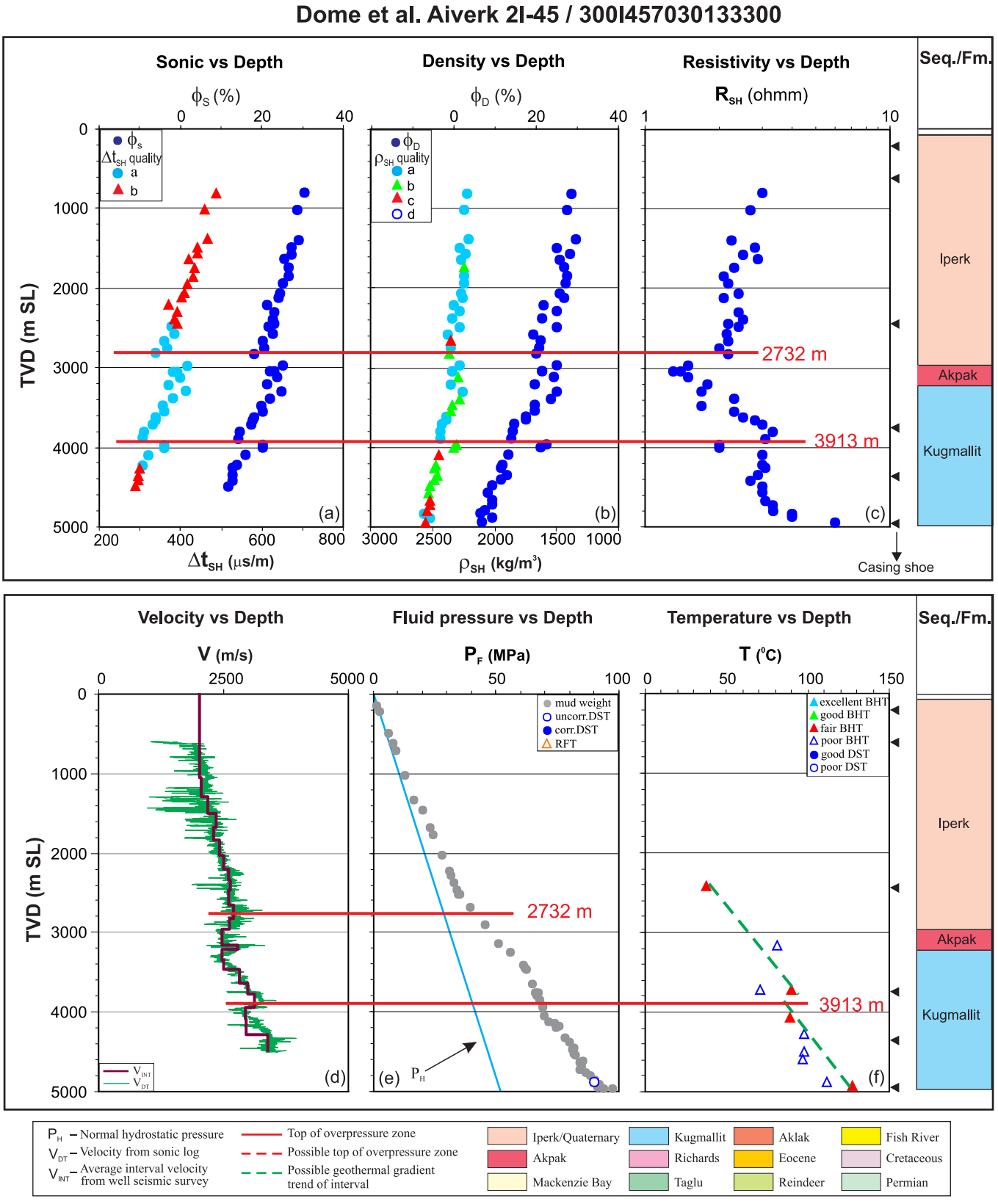

Figure A-3. Overpressure zones are detected with tops of OPZ at 2732 m (quality "b") and 3913 m (quality "a") by using the integrated analysis for the Aiverk 2I-45 well in the Beaufort-Mackenzie Basin. (a) shale sonic transit time (Δt_{SH}) and sonic porosity (ϕ_S) vs. depth; (b) shale bulk density (ρ_{SH}) and density porosity (ϕ_D) vs depth; (c) shale deep resistivity (R_{SH}) vs. depth; (d) continuous sonic velocity (V_{DT}) and average interval seismic velocity (V_{INT}) vs. depth; (e) fluid pressure (P_F) from well test and drilling mud weight vs. depth; and (f) borehole temperature vs. depth.

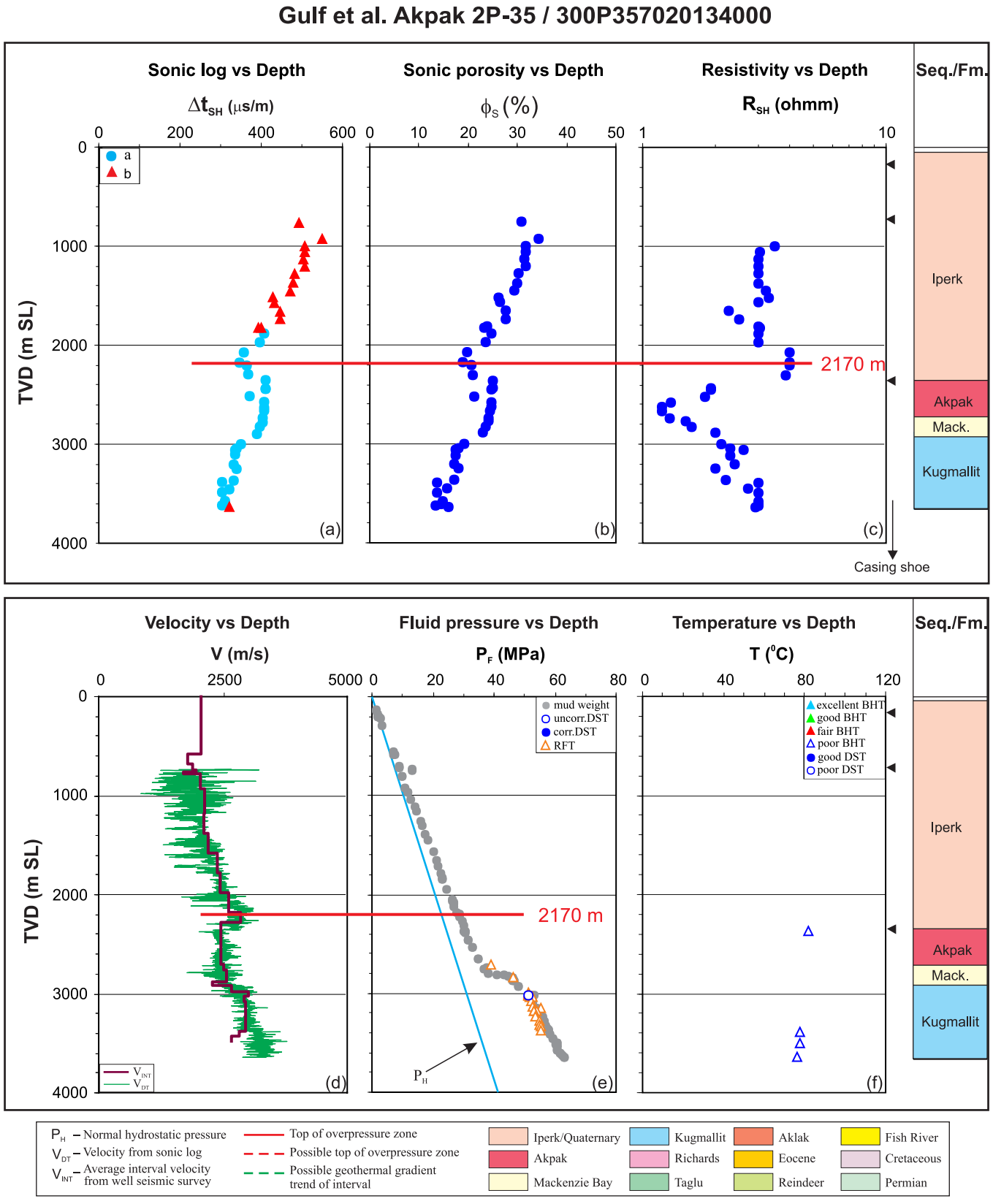

Figure A-4. Top of overpressure zone is detected at 2170 m with quality "a" by using the integrated analysis for the Akpak 2P-35 well in the Beaufort-Mackenzie Basin. (a) shale sonic transit time (Δt_{SH}) vs. depth; (b) shale sonic porosity (ϕ_S) vs. depth; (c) shale deep resistivity (R_{SH}) vs. depth; (d) continuous sonic velocity (V_{DT}) and average interval seismic velocity (V_{INT}) vs. depth; (e) fluid pressure (P_F) from well test and drilling mud weight vs. depth; and (f) borehole temperature vs. depth. Mack. - Mackenzie Bay.

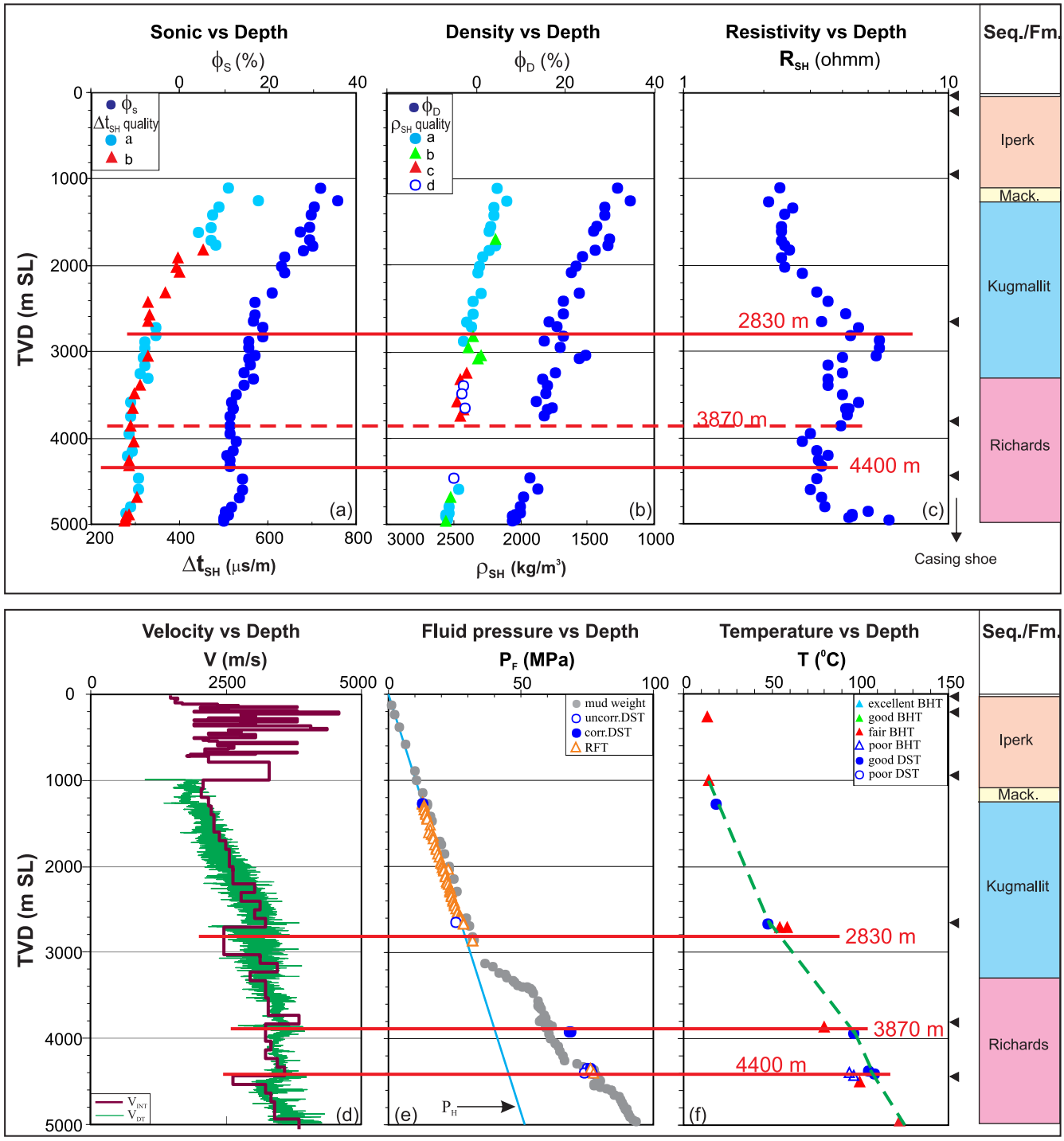

Figure A-5. Overpressure zones are detected with tops of OPZ at 2830 m (quality "a"), 3870 m (quality "b") and 4400 m (quality "a") by using the integrated analysis for the Amerk O-09 well in the Beaufort-Mackenzie Basin. (a) shale sonic transit time (Δt_{SH}) and sonic porosity (ϕ_S) vs. depth; (b) shale bulk density (ρ_{SH}) and density porosity (ϕ_D) vs depth; (c) shale deep resistivity (R_{SH}) vs. depth; (d) continuous sonic velocity (V_{DT}) and average interval seismic velocity (V_{INT}) vs. depth; (e) fluid pressure (P_F) from well test and drilling mud weight vs. depth; and (f) borehole temperature vs. depth. Mack. - Mackenzie Bay.

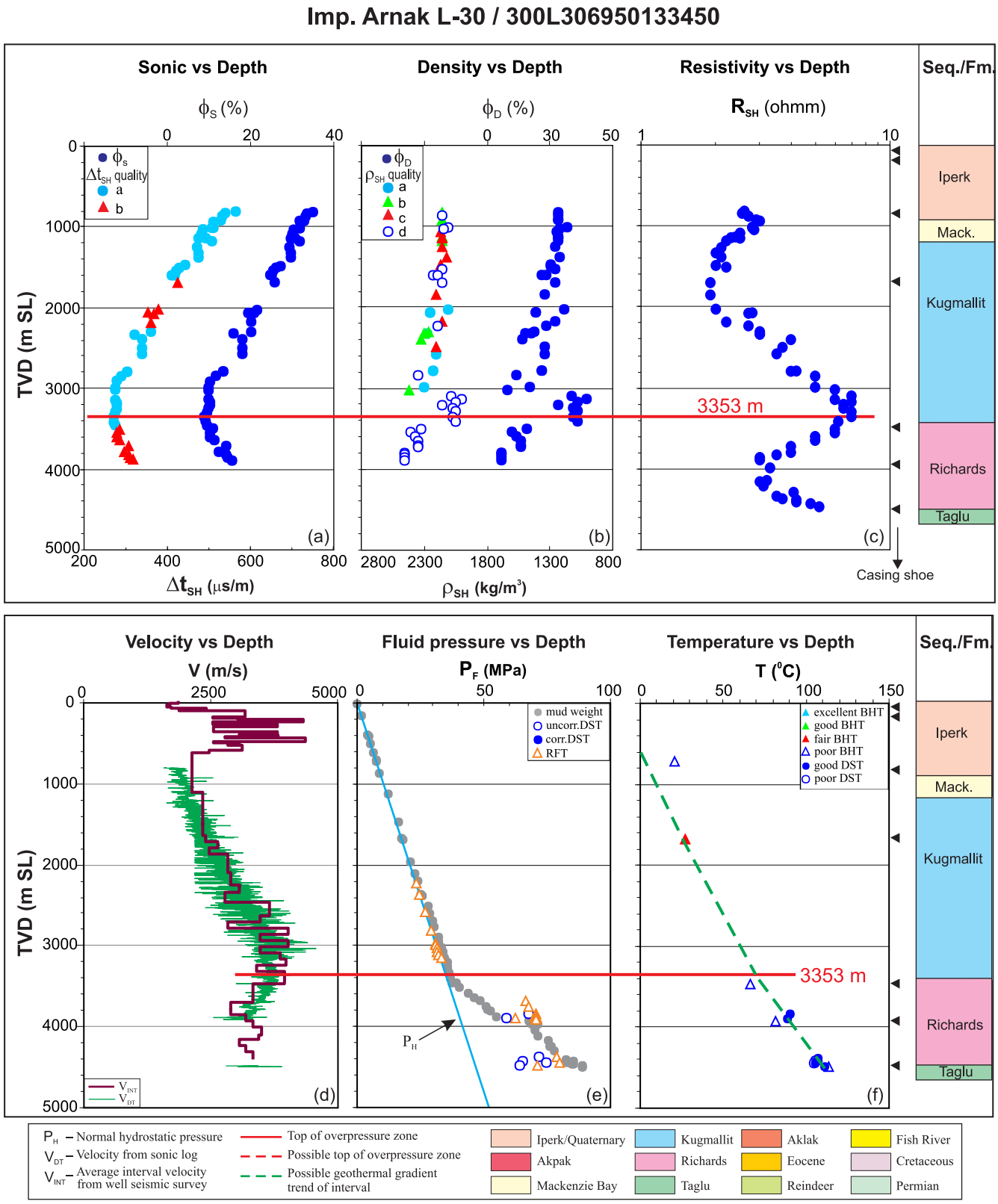

Figure A-6. Top of overpressure zone is detected at 3353 m with quality "a" by using the integrated analysis for the Arnak L-30 well in the Beaufort-Mackenzie Basin. (a) shale sonic transit time (Δt_{SH}) and sonic porosity (ϕ_S) vs. depth; (b) shale bulk density (ρ_{SH}) and density porosity (ϕ_D) vs depth; (c) shale deep resistivity (R_{SH}) vs. depth; (d) continuous sonic velocity (V_{DT}) and average interval seismic velocity (V_{INT}) vs. depth; (e) fluid pressure (P_F) from well test and drilling mud weight vs. depth; and (f) borehole temperature vs. depth. Mack. - Mackenzie Bay.

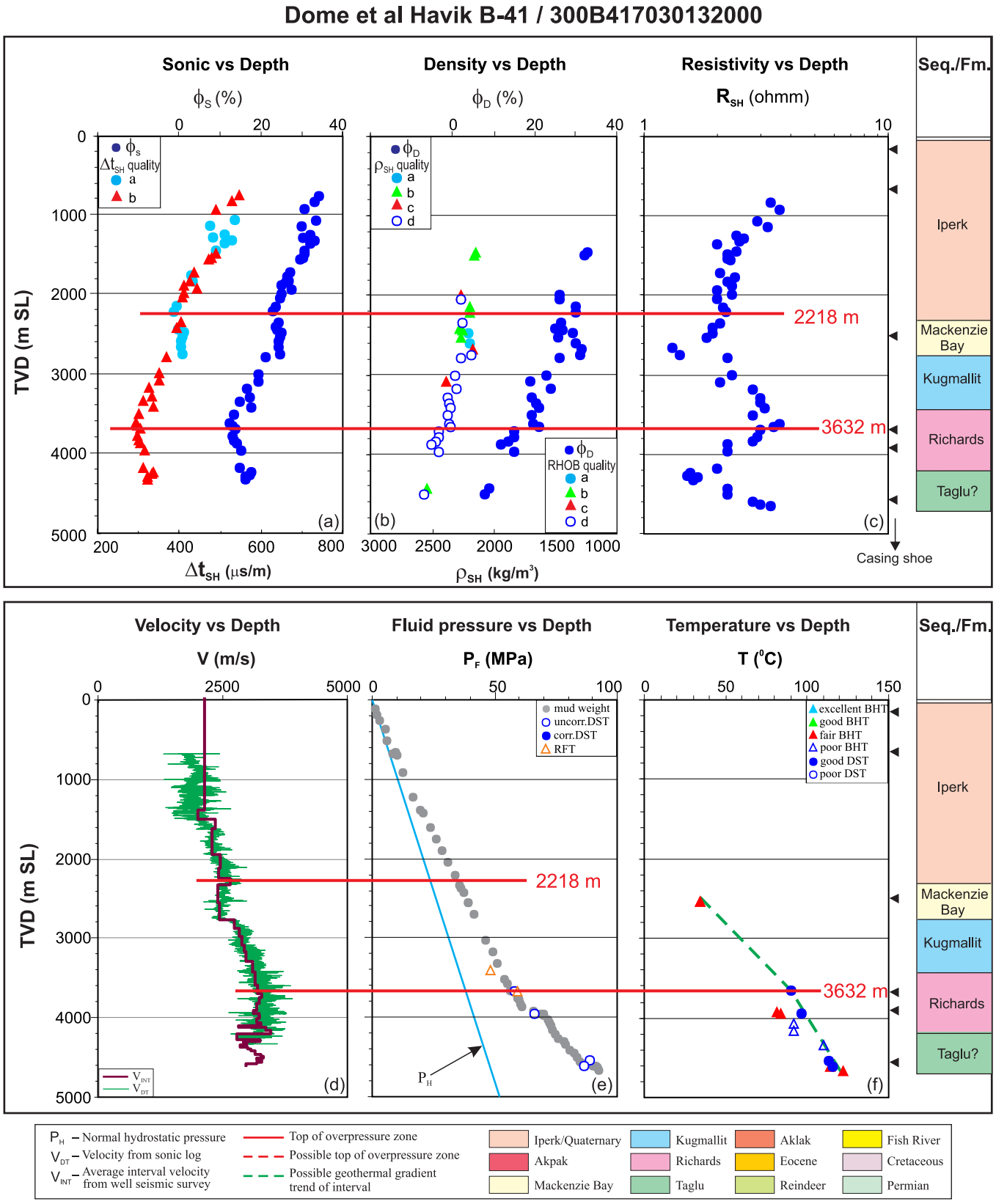

Figure A-7. Overpressure zones are detected with tops of OPZ at 2218 m and 3632 m with quality "a by using the integrated analysis for the Havik B-41 well in the Beaufort-Mackenzie Basin. (a) shale sonic transit time (Δt_{SH}) and sonic porosity (ϕ_S) vs. depth; (b) shale bulk density (ρ_{SH}) and density porosity (ϕ_D) vs depth; (c) shale deep resistivity (R_{SH}) vs. depth; (d) continuous sonic velocity (V_{DT}) and average interval seismic velocity (V_{INT}) vs. depth; (e) fluid pressure (P_F) from well test and drilling mud weight vs. depth; and (f) borehole temperature vs. depth.

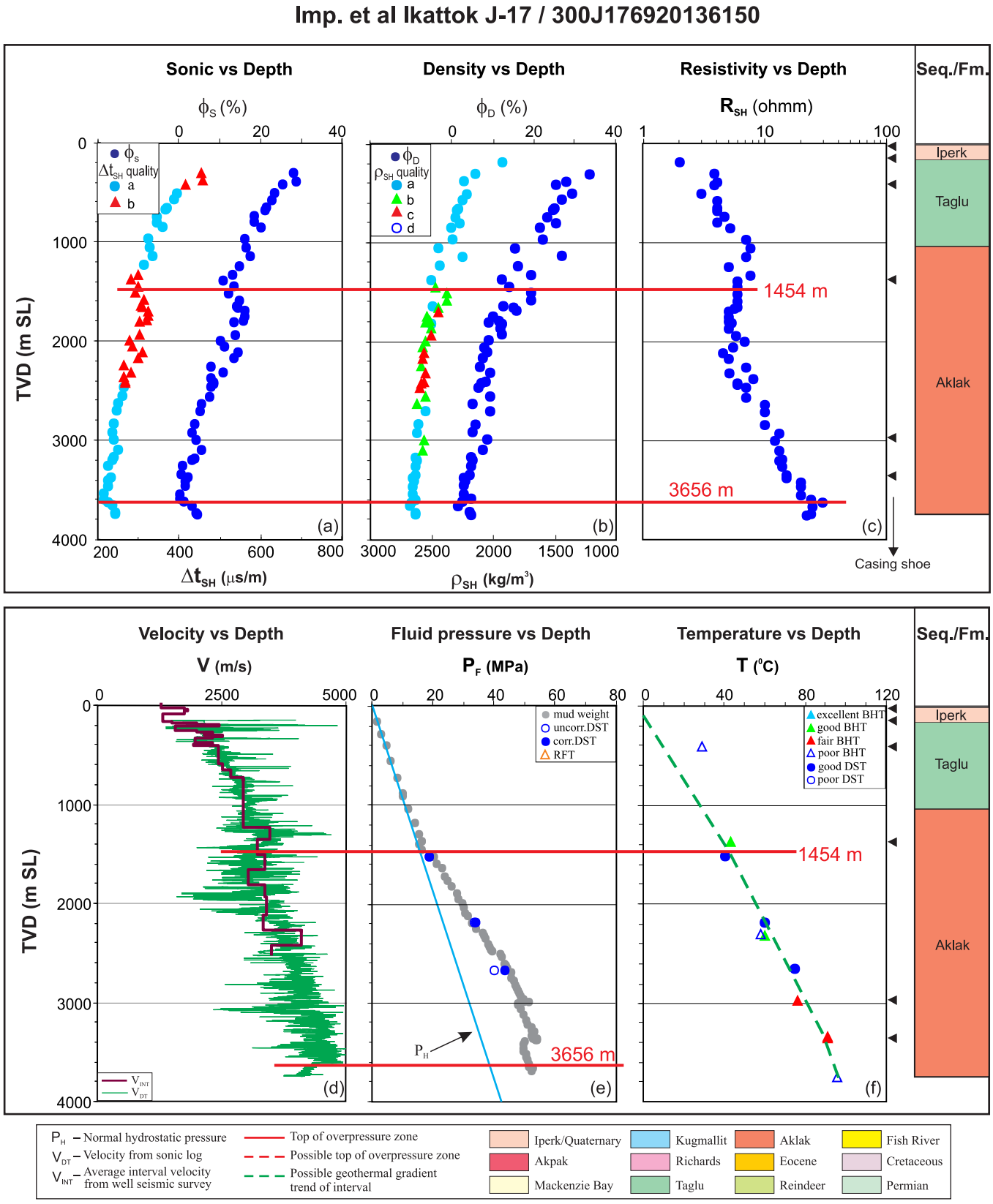

Figure A-8. Overpressure zones are detected with tops of OPZ at 1454 m (quality "a") and at 3656 m (quality "b") by using the integrated analysis for the Ikattok J-17 well in the Beaufort-Mackenzie Basin. (a) shale sonic transit time (Δt_{SH}) and sonic porosity (ϕ_S) vs. depth; (b) shale bulk density (ρ_{SH}) and density porosity (ϕ_D) vs depth; (c) shale deep resistivity (R_{SH}) vs. depth; (d) continuous sonic velocity (V_{DT}) and average interval seismic velocity (V_{INT}) vs. depth; (e) fluid pressure (P_F) from well test and drilling mud weight vs. depth; and (f) borehole temperature vs. depth.

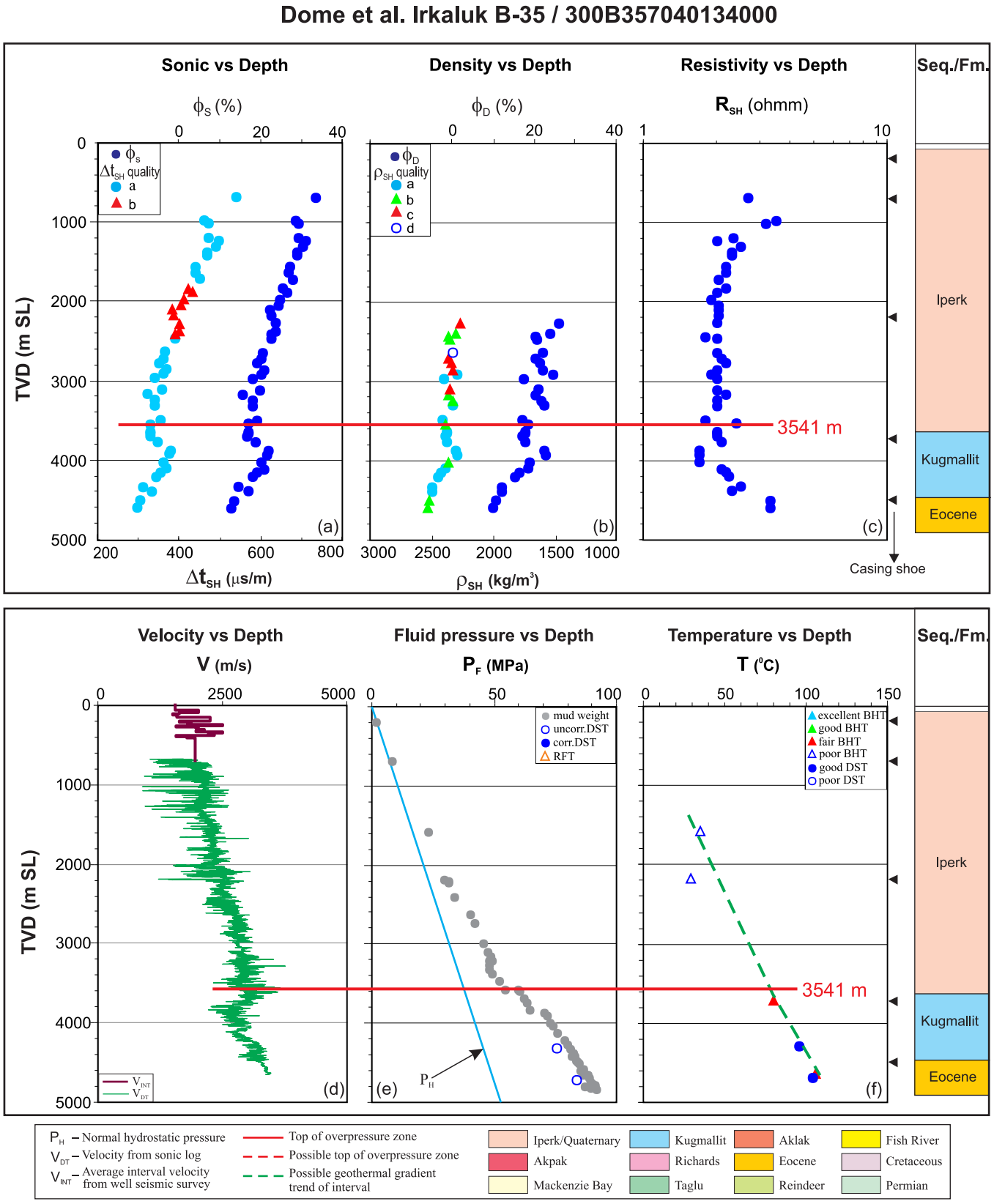

Figure A-9. Top of overpressure zone is detected at 3541 m with quality "a" by using the integrated analysis for the Irkaluk B-35 well in the Beaufort-Mackenzie Basin. (a) shale sonic transit time (Δt_{SH}) and sonic porosity (ϕ_S) vs. depth; (b) shale bulk density (ρ_{SH}) and density porosity (ϕ_D) vs depth; (c) shale deep resistivity (R_{SH}) vs. depth; (d) continuous sonic velocity (V_{DT}) and average interval seismic velocity (V_{INT}) vs. depth; (e) fluid pressure (P_F) from well test and drilling mud weight vs. depth; and (f) borehole temperature vs. depth.

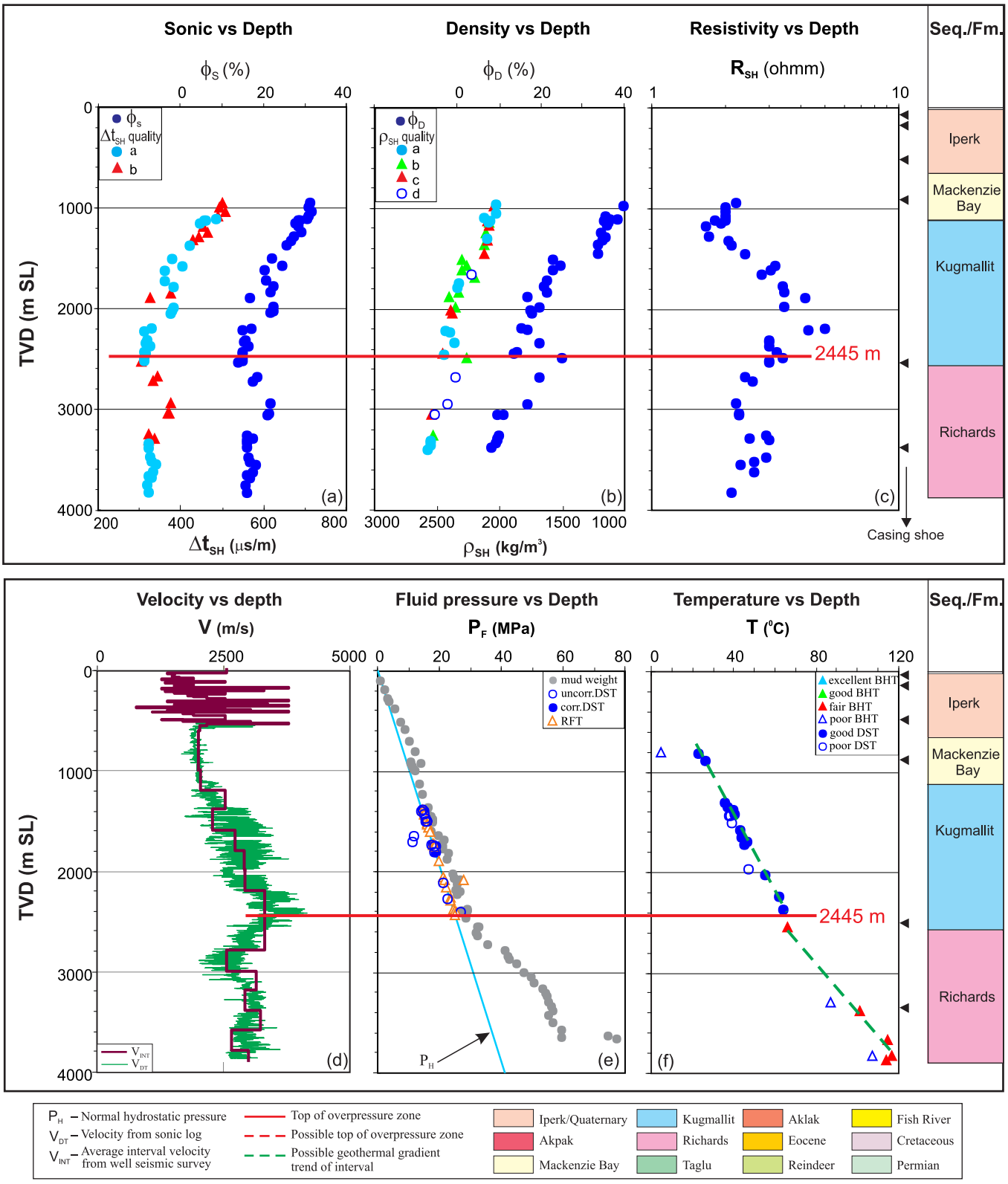

Figure A-10. Top of overpressure zone is detected at 2445 m with quality "a" by using the integrated analysis for the Kadluk O-07 well in the Beaufort-Mackenzie Basin. (a) shale sonic transit time (Δt_{SH}) and sonic porosity (ϕ_S) vs. depth; (b) shale bulk density (ρ_{SH}) and density porosity (ϕ_D) vs depth; (c) shale deep resistivity (R_{SH}) vs. depth; (d) continuous sonic velocity (V_{DT}) and average interval seismic velocity (V_{INT}) vs. depth; (e) fluid pressure (P_F) from well test and drilling mud weight vs. depth; and (f) borehole temperature vs. depth.

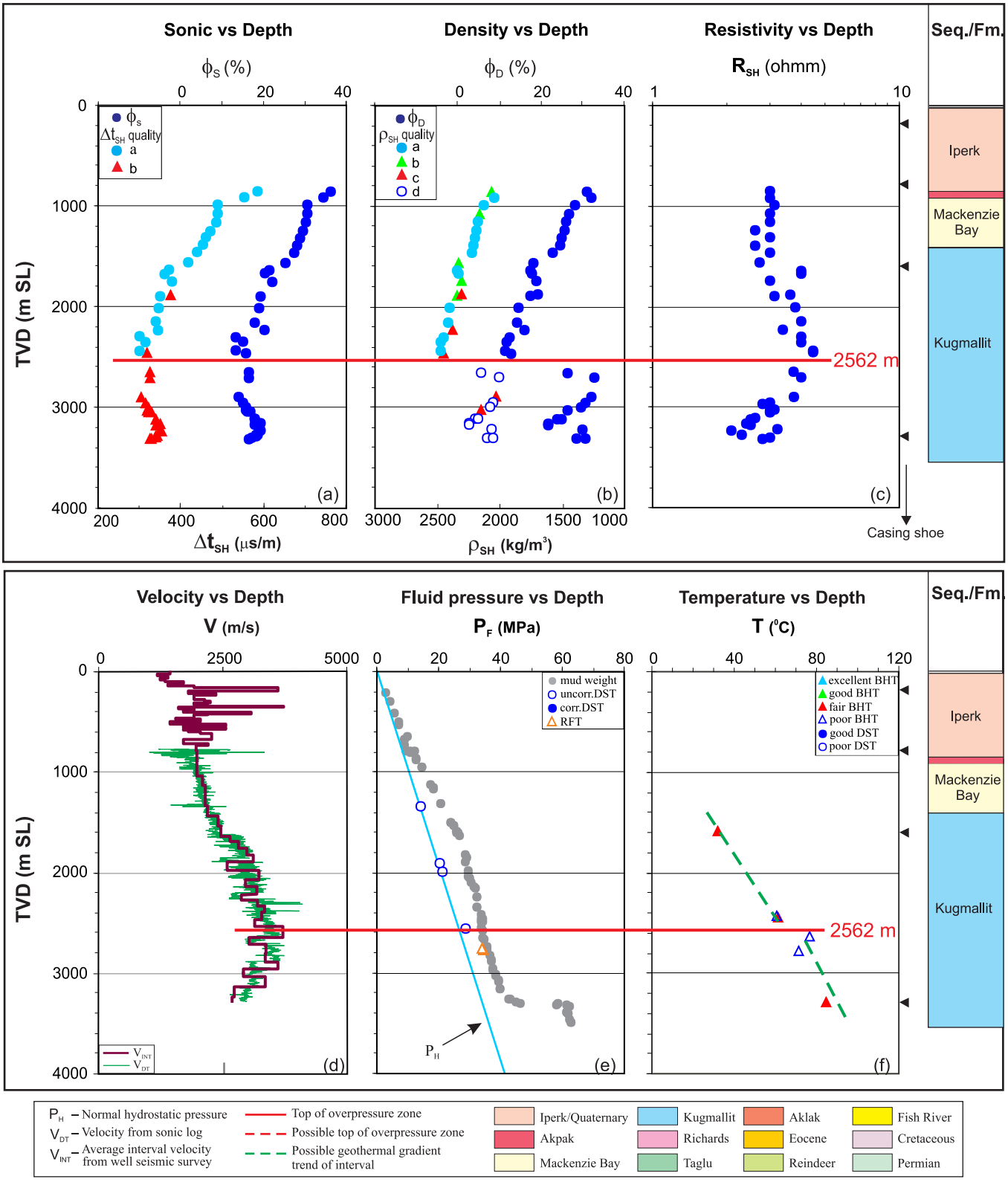

Figure A-11. Top of overpressure zone is detected at 2562 m with quality "a" by using the integrated analysis for the Kiggavik A-43 well in the Beaufort-Mackenzie Basin. (a) shale sonic transit time (Δt_{SH}) and sonic porosity (ϕ_S) vs. depth; (b) shale bulk density (ρ_{SH}) and density porosity (ϕ_D) vs depth; (c) shale deep resistivity (R_{SH}) vs. depth; (d) continuous sonic velocity (V_{DT}) and average interval seismic velocity (V_{INT}) vs. depth; (e) fluid pressure (P_F) from well test and drilling mud weight vs. depth; and (f) borehole temperature vs. depth.

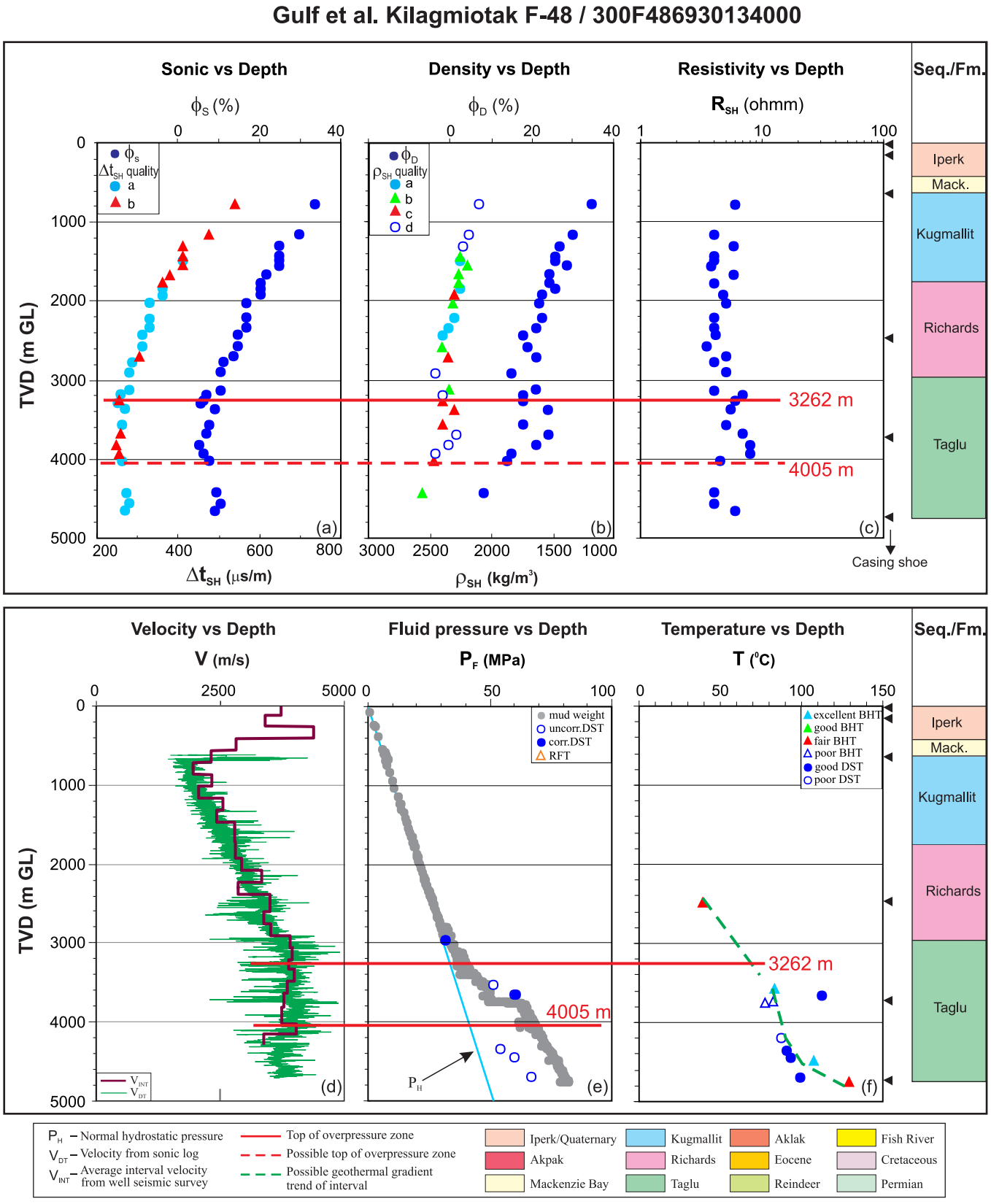

Figure A-12. Overpressure zones are detected with tops of OPZ at 3262 m (quality "a") and at 4005 m (quality "b") by using the integrated analysis for the Kilagmiotak F-48 well in the Beaufort-Mackenzie Basin. (a) shale sonic transit time (Δt_{SH}) and sonic porosity (ϕ_S) vs. depth; (b) shale bulk density (ρ_{SH}) and density porosity (ϕ_D) vs depth; (c) shale deep resistivity (R_{SH}) vs. depth; (d) continuous sonic velocity (V_{DT}) and average interval seismic velocity (V_{INT}) vs. depth; (e) fluid pressure (P_F) from well test and drilling mud weight vs. depth; and (f) borehole temperature vs. depth. Mack. - Mackenzie Bay.

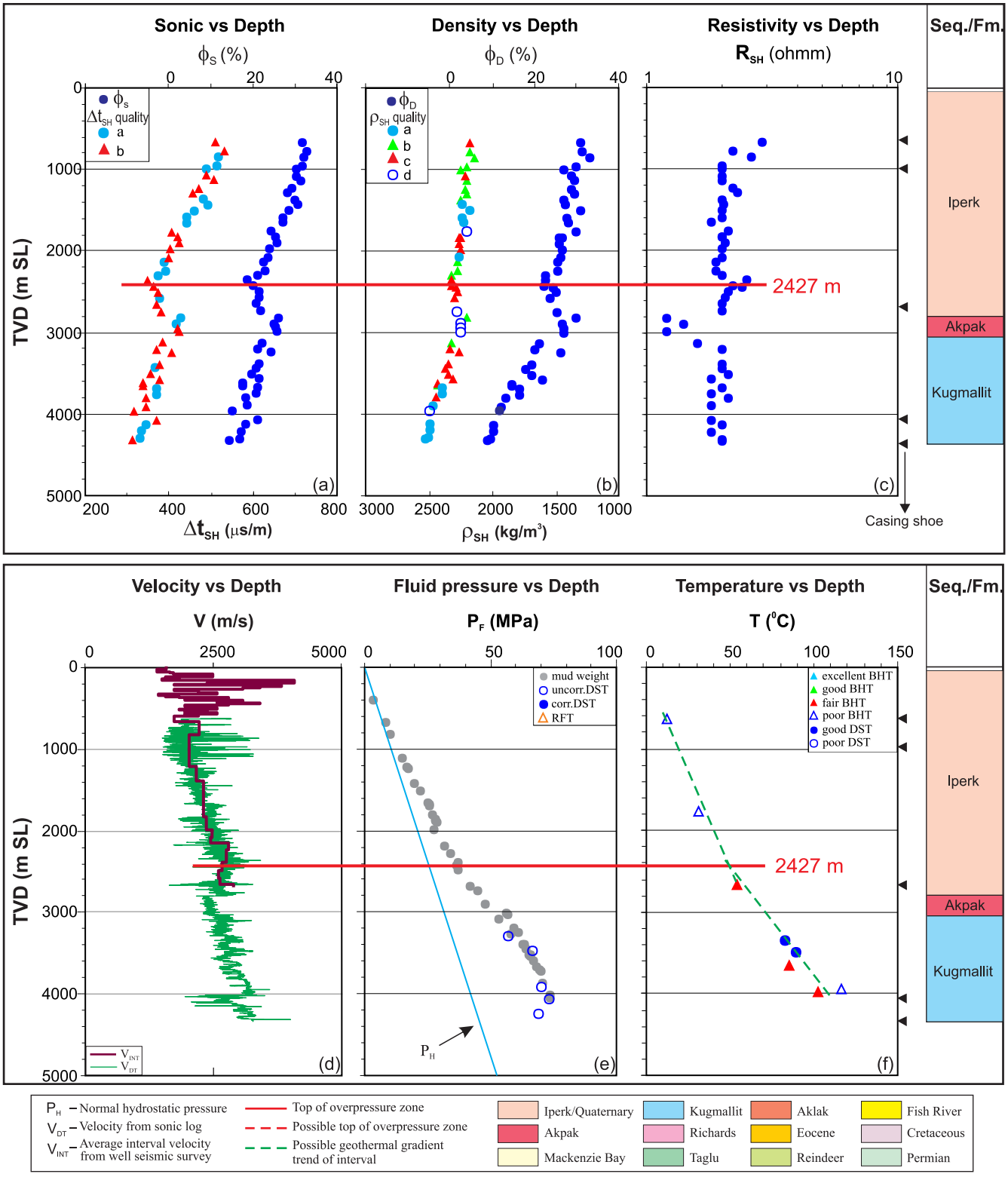

Figure A-13. Top of overpressure zone is detected at 2427 m with quality "a" by using the integrated analysis for the Koakoak O-22 well in the Beaufort-Mackenzie Basin. (a) shale sonic transit time (Δt_{SH}) and sonic porosity (ϕ_S) vs. depth; (b) shale bulk density (ρ_{SH}) and density porosity (ϕ_D) vs depth; (c) shale deep resistivity (R_{SH}) vs. depth; (d) continuous sonic velocity (V_{DT}) and average interval seismic velocity (V_{INT}) vs. depth; (e) fluid pressure (P_F) from well test and drilling mud weight vs. depth; and (f) borehole temperature vs. depth.

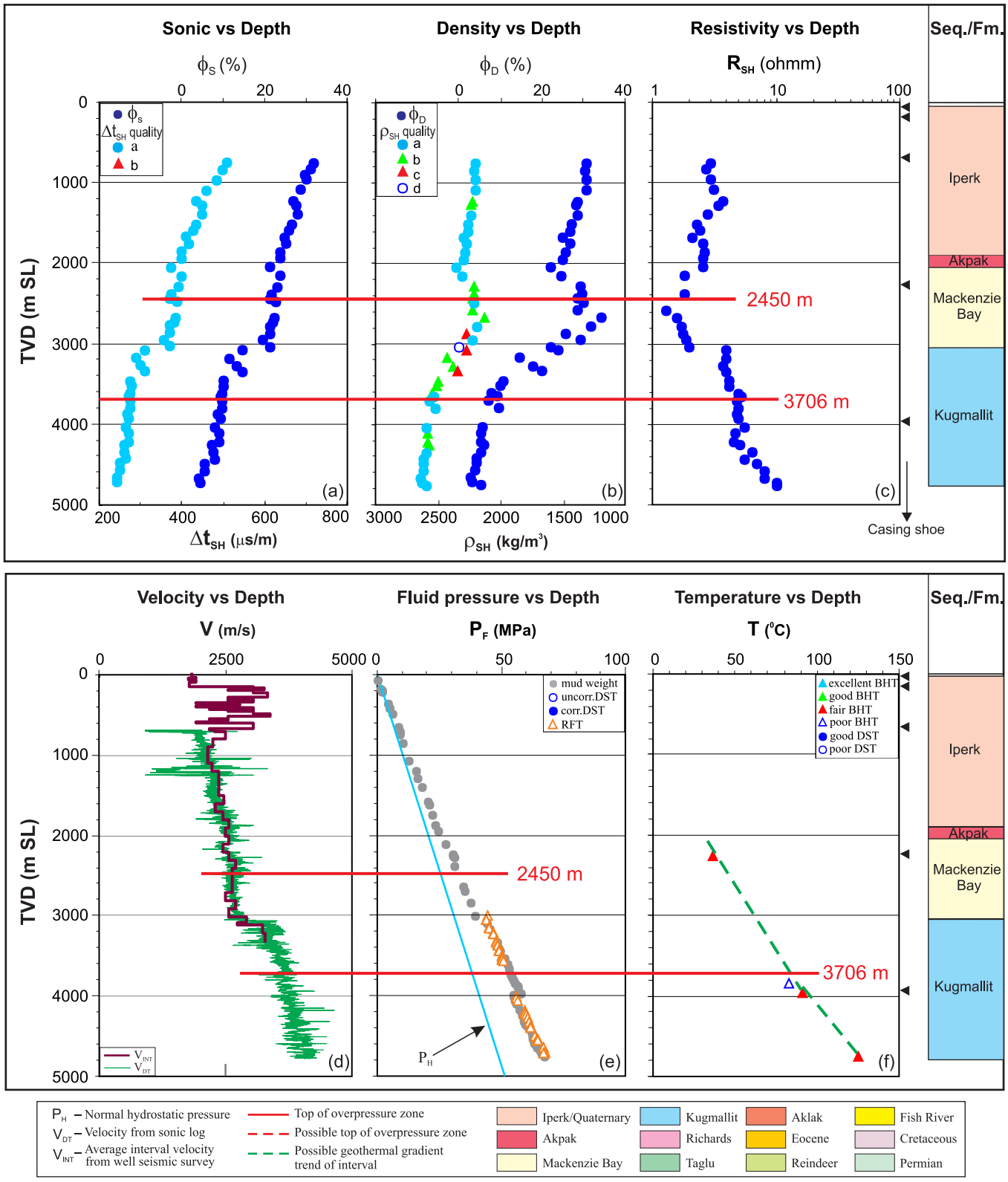

Figure A-14. Overpressure zones are detected with tops of OPZ at 2450 m (quality "a") and at 3706 m (quality "b") by using the integrated analysis for the Kogyuk N-67 well in the Beaufort-Mackenzie Basin. (a) shale sonic transit time (Δt_{SH}) and sonic porosity (ϕ_S) vs. depth; (b) shale bulk density (ρ_{SH}) and density porosity (ϕ_D) vs depth; (c) shale deep resistivity (R_{SH}) vs. depth; (d) continuous sonic velocity (V_{DT}) and average interval seismic velocity (V_{INT}) vs. depth; (e) fluid pressure (P_F) from well test and drilling mud weight vs. depth; and (f) borehole temperature vs. depth.

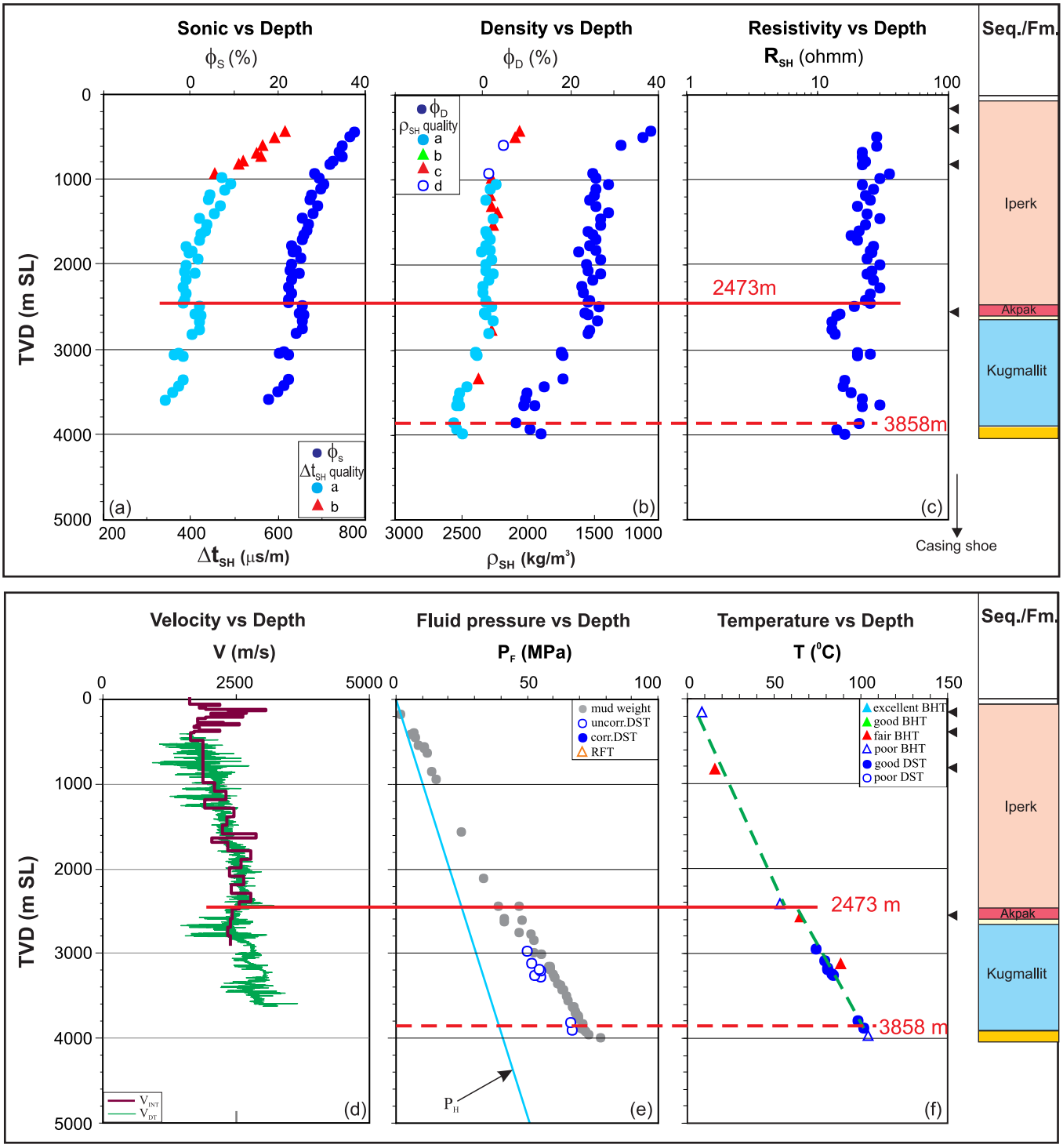

Figure A-15. Top of overpressure zone at 2473 m with quality "a" and a possible top of overpressure at 3858 m with quality "c" are detected by using the integrated analysis for the Kopanoar 2I-44 well in the Beaufort-Mackenzie Basin. (a) shale sonic transit time (Δt_{SH}) and sonic porosity (ϕ_S) vs. depth; (b) shale bulk density (ρ_{SH}) and density porosity (ϕ_D) vs depth; (c) shale deep resistivity (R_{SH}) vs. depth; (d) continuous sonic velocity (V_{DT}) and average interval seismic velocity (V_{INT}) vs. depth; (e) fluid pressure (P_F) from well test and drilling mud weight vs. depth; and (f) borehole temperature vs. depth.

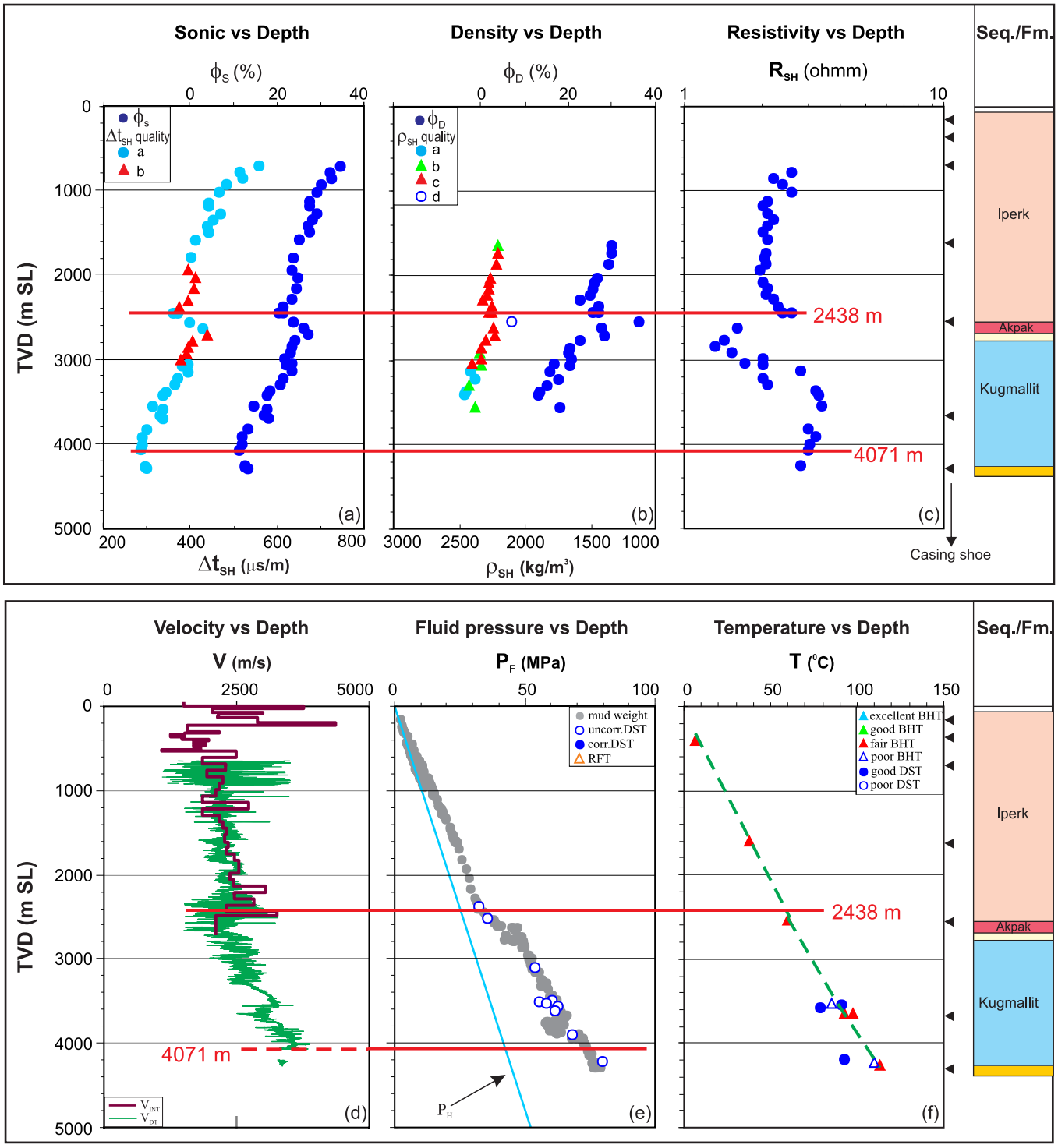

Figure A-16. Overpressure zones are detected with tops of OPZ at 2438 m (quality "a") and at 4071 m (quality "b") by using the integrated analysis for the Kopanoar M-13 well in the Beaufort-Mackenzie Basin. (a) shale sonic transit time (Δt_{SH}) and sonic porosity (ϕ_S) vs. depth; (b) shale bulk density (ρ_{SH}) and density porosity (ϕ_D) vs depth; (c) shale deep resistivity (R_{SH}) vs. depth; (d) continuous sonic velocity (V_{DT}) and average interval seismic velocity (V_{INT}) vs. depth; (e) fluid pressure (P_F) from well test and drilling mud weight vs. depth; and (f) borehole temperature vs. depth.

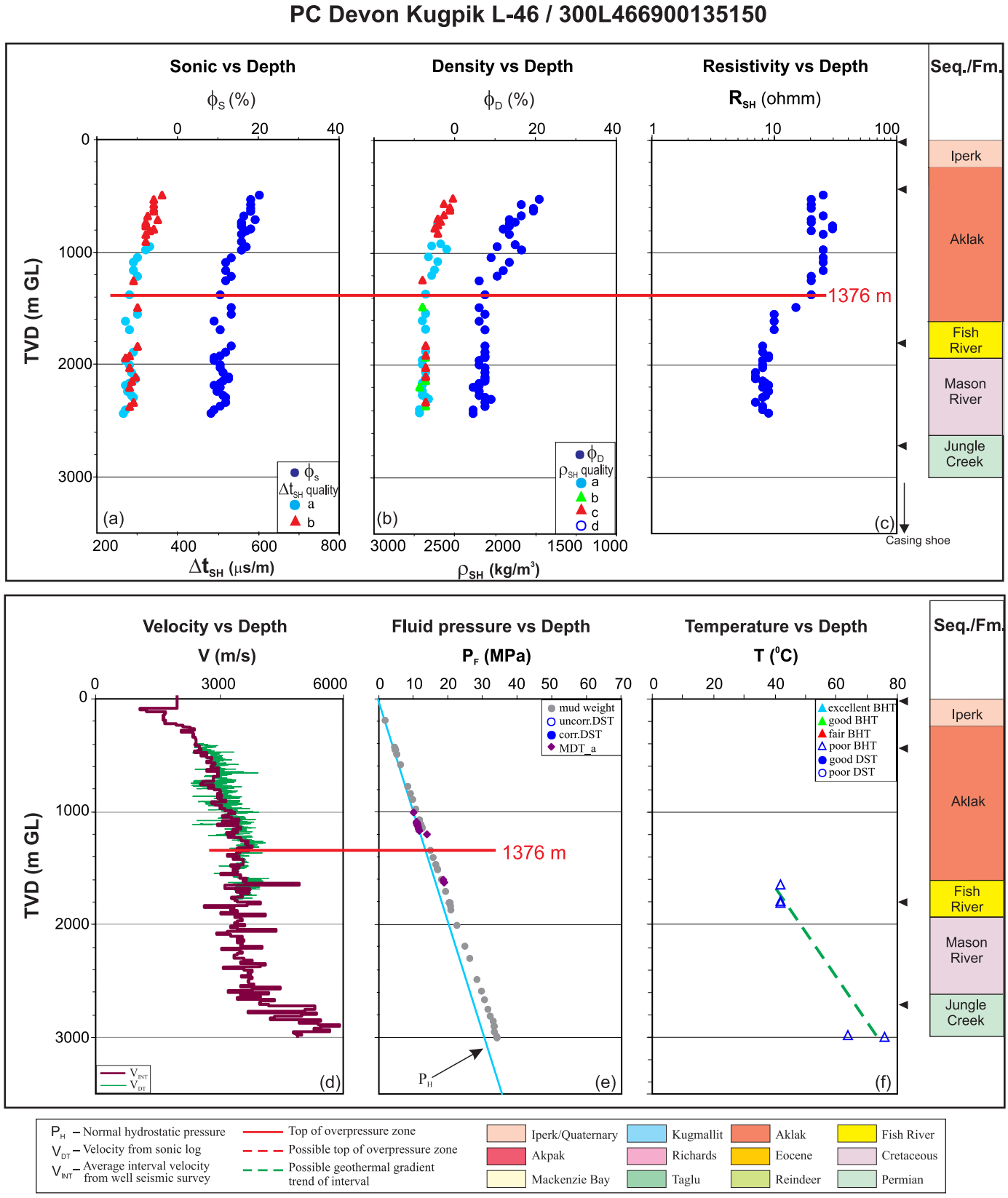

Figure A-17. Top of overpressure zone is detected at 1376 m with quality "a" by using the integrated analysis for the Kugpik L-46 well in the Beaufort-Mackenzie Basin. (a) shale sonic transit time (Δt_{SH}) and sonic porosity (ϕ_S) vs. depth; (b) shale bulk density (ρ_{SH}) and density porosity (ϕ_D) vs depth; (c) shale deep resistivity (R_{SH}) vs. depth; (d) continuous sonic velocity (V_{DT}) and average interval seismic velocity (V_{INT}) vs. depth; (e) fluid pressure (P_F) from well test and drilling mud weight vs. depth; and (f) borehole temperature vs. depth.

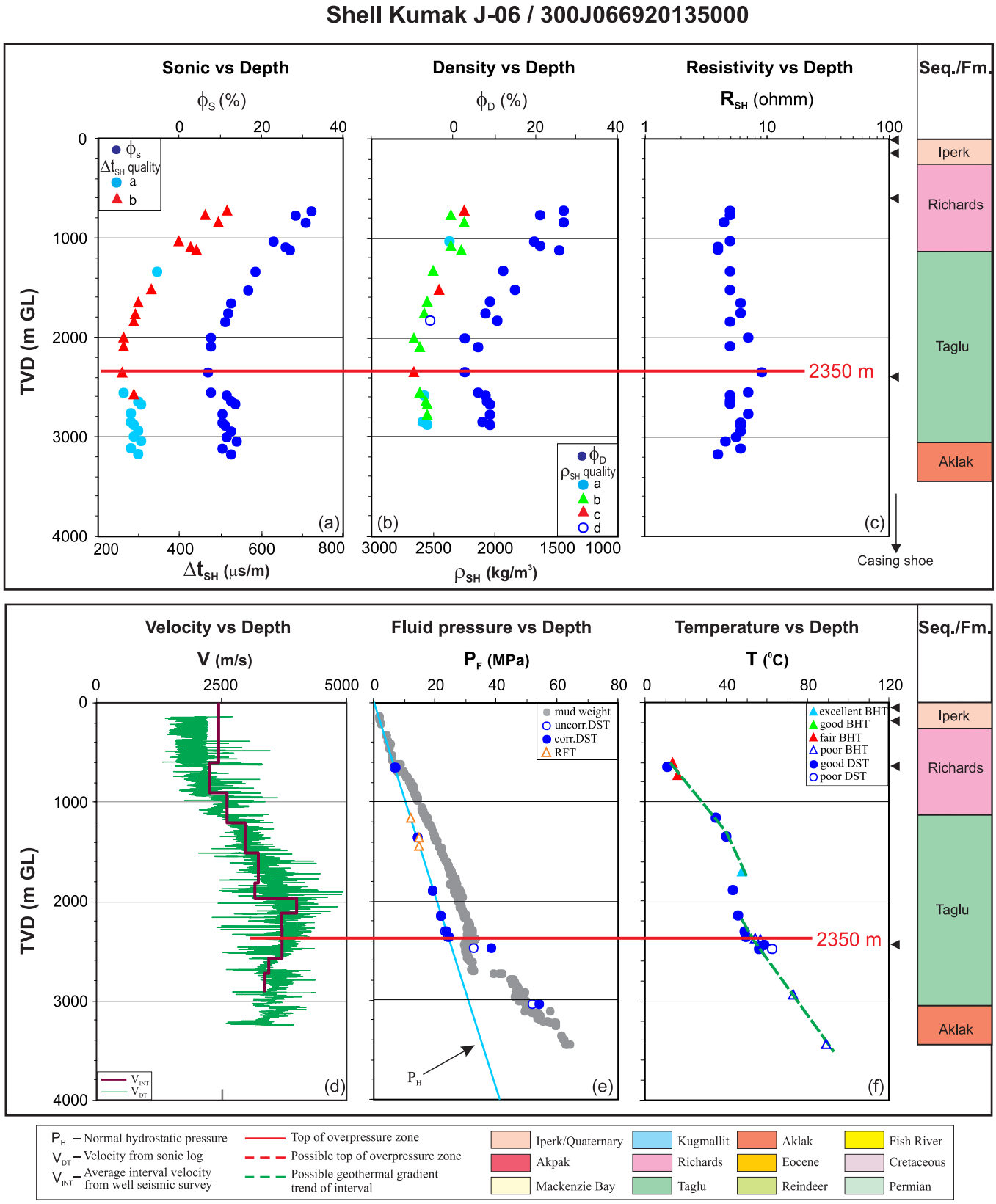

Figure A-18. Top of overpressure zone is detected at 2350 m with quality "a" by using the integrated analysis for the Kumak J-06 well in the Beaufort-Mackenzie Basin. (a) shale sonic transit time (Δt_{SH}) and sonic porosity (ϕ_S) vs. depth; (b) shale bulk density (ρ_{SH}) and density porosity (ϕ_D) vs depth; (c) shale deep resistivity (R_{SH}) vs. depth; (d) continuous sonic velocity (V_{DT}) and average interval seismic velocity (V_{INT}) vs. depth; (e) fluid pressure (P_F) from well test and drilling mud weight vs. depth; and (f) borehole temperature vs. depth.

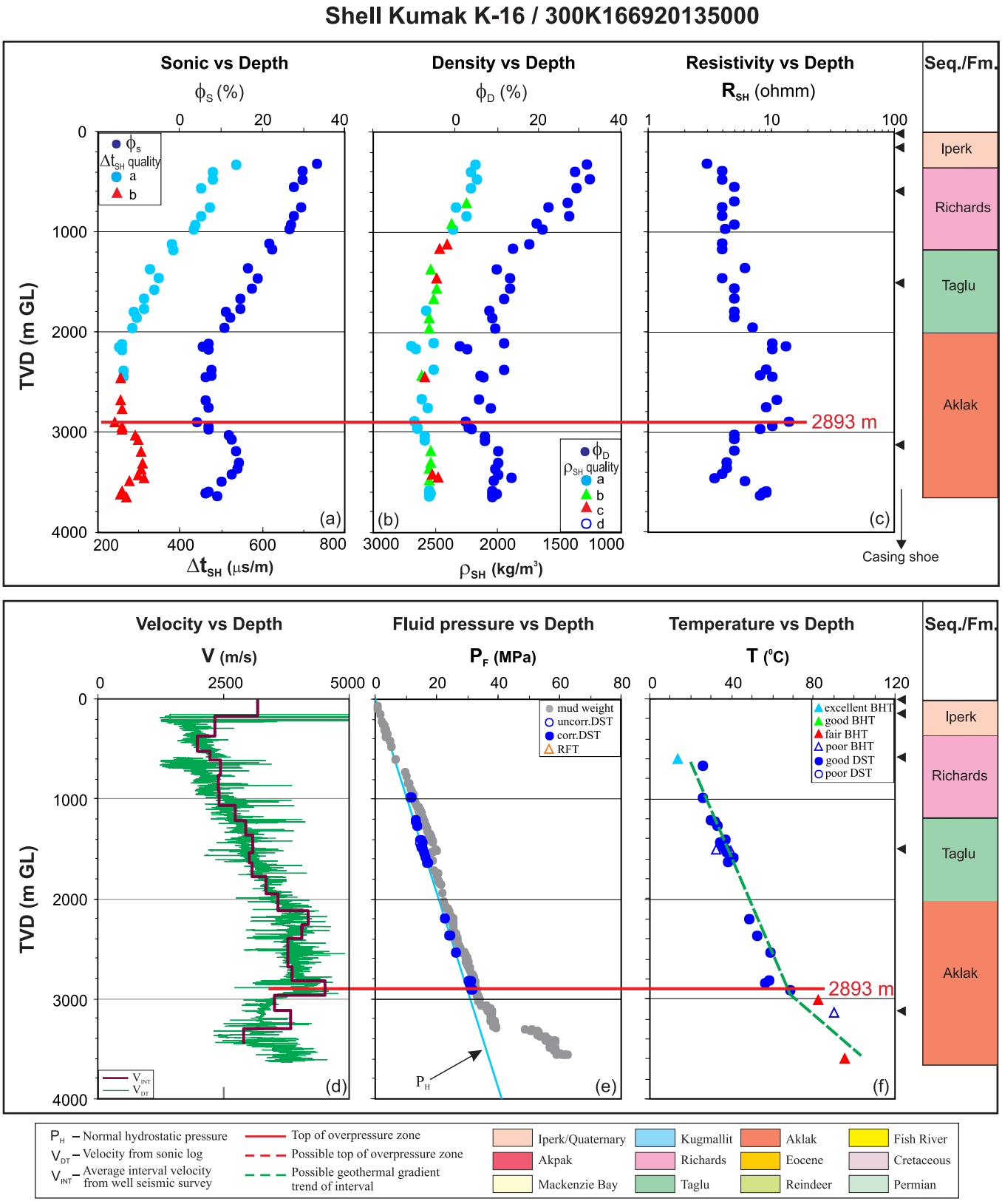

Figure A-19. Top of overpressure zone is detected at 2893 m with quality "a" by using the integrated analysis for the Kumak K-16 well in the Beaufort-Mackenzie Basin. (a) shale sonic transit time (Δt_{SH}) and sonic porosity (ϕ_S) vs. depth; (b) shale bulk density (ρ_{SH}) and density porosity (ϕ_D) vs depth; (c) shale deep resistivity (R_{SH}) vs. depth; (d) continuous sonic velocity (V_{DT}) and average interval seismic velocity (V_{INT}) vs. depth; (e) fluid pressure (P_F) from well test and drilling mud weight vs. depth; and (f) borehole temperature vs. depth.

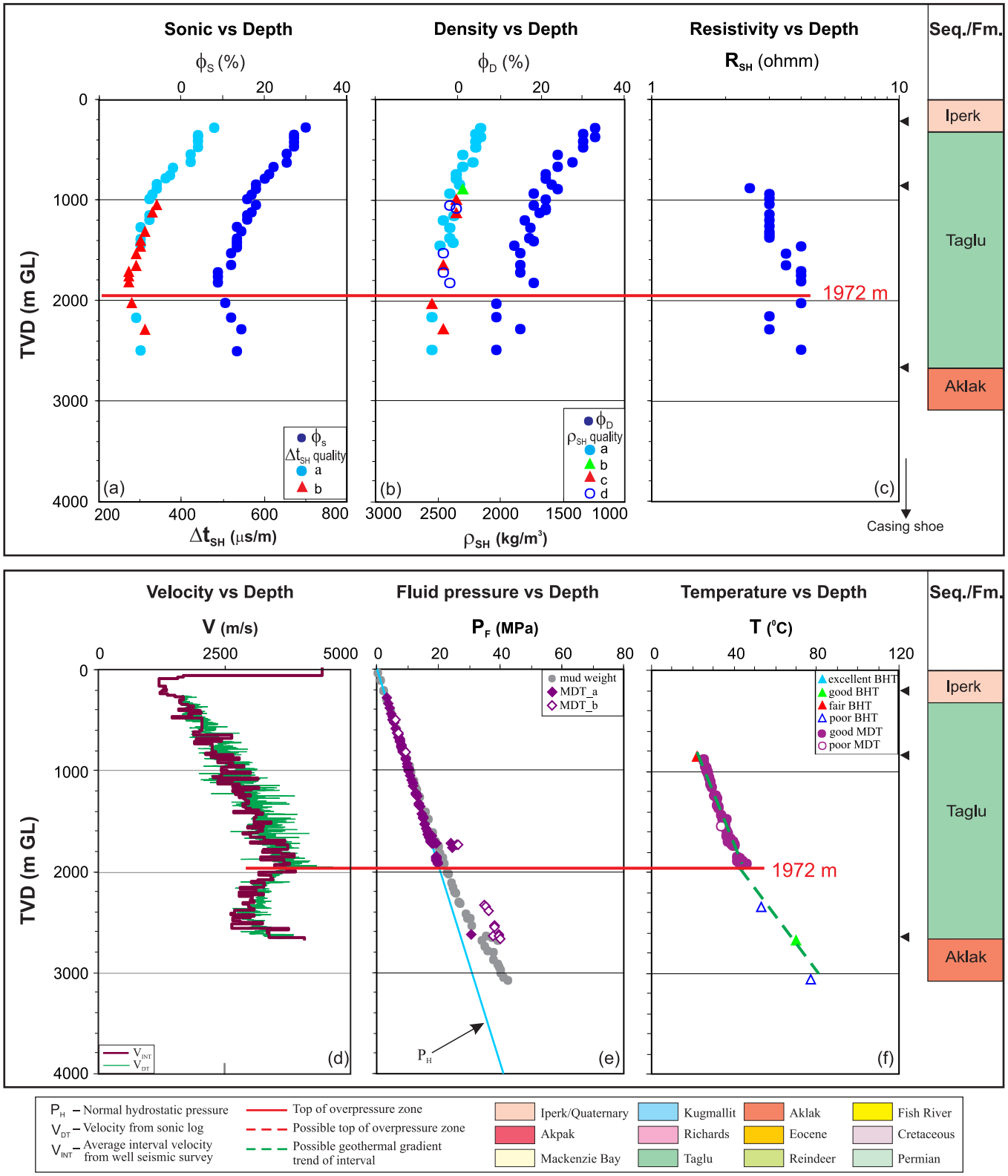

Figure A-20. Top of overpressure zone is detected at 1972 m with quality "a" by using the integrated analysis for the Kurk M-15 well in the Beaufort-Mackenzie Basin. (a) shale sonic transit time (Δt_{SH}) and sonic porosity (ϕ_S) vs. depth; (b) shale bulk density (ρ_{SH}) and density porosity (ϕ_D) vs depth; (c) shale deep resistivity (R_{SH}) vs. depth; (d) continuous sonic velocity (V_{DT}) and average interval seismic velocity (V_{INT}) vs. depth; (e) fluid pressure (P_F) from well test and drilling mud weight vs. depth; and (f) borehole temperature vs. depth.

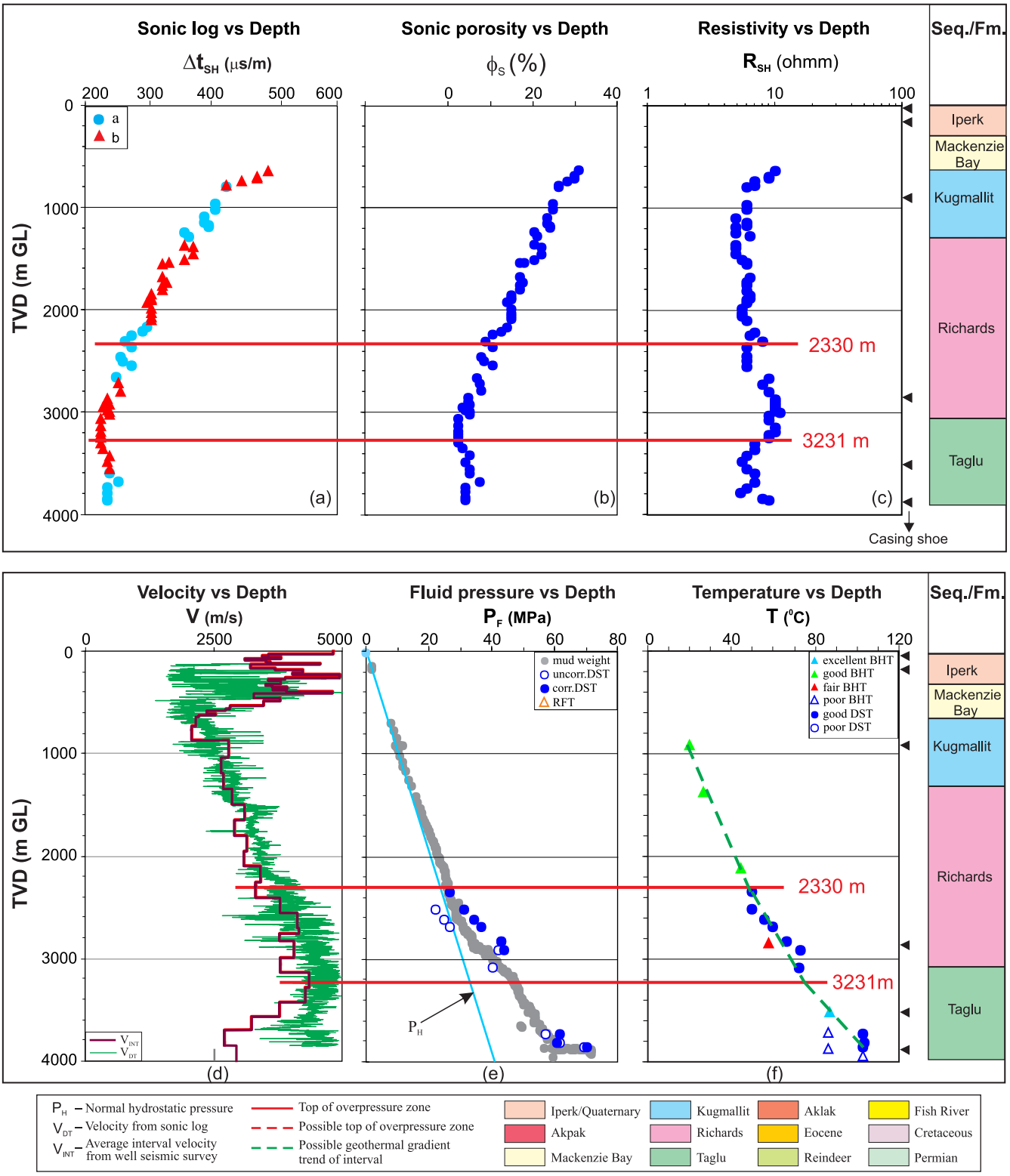

Figure A-21. Overpressure zones are detected with tops of OPZ at 2330 m (quality "a") and 3231 m (quality "a") by using the integrated analysis for the Mallik A-06 well in the Beaufort-Mackenzie Basin. (a) shale sonic transit time (Δt_{SH}) vs. depth; (b) shale sonic porosity (ϕ_S) vs. depth; (c) shale deep resistivity (R_{SH}) vs. depth; (d) continuous sonic velocity (V_{DT}) and average interval seismic velocity (V_{INT}) vs. depth; (e) fluid pressure (P_F) from well test and drilling mud weight vs. depth; and (f) borehole temperature vs. depth.

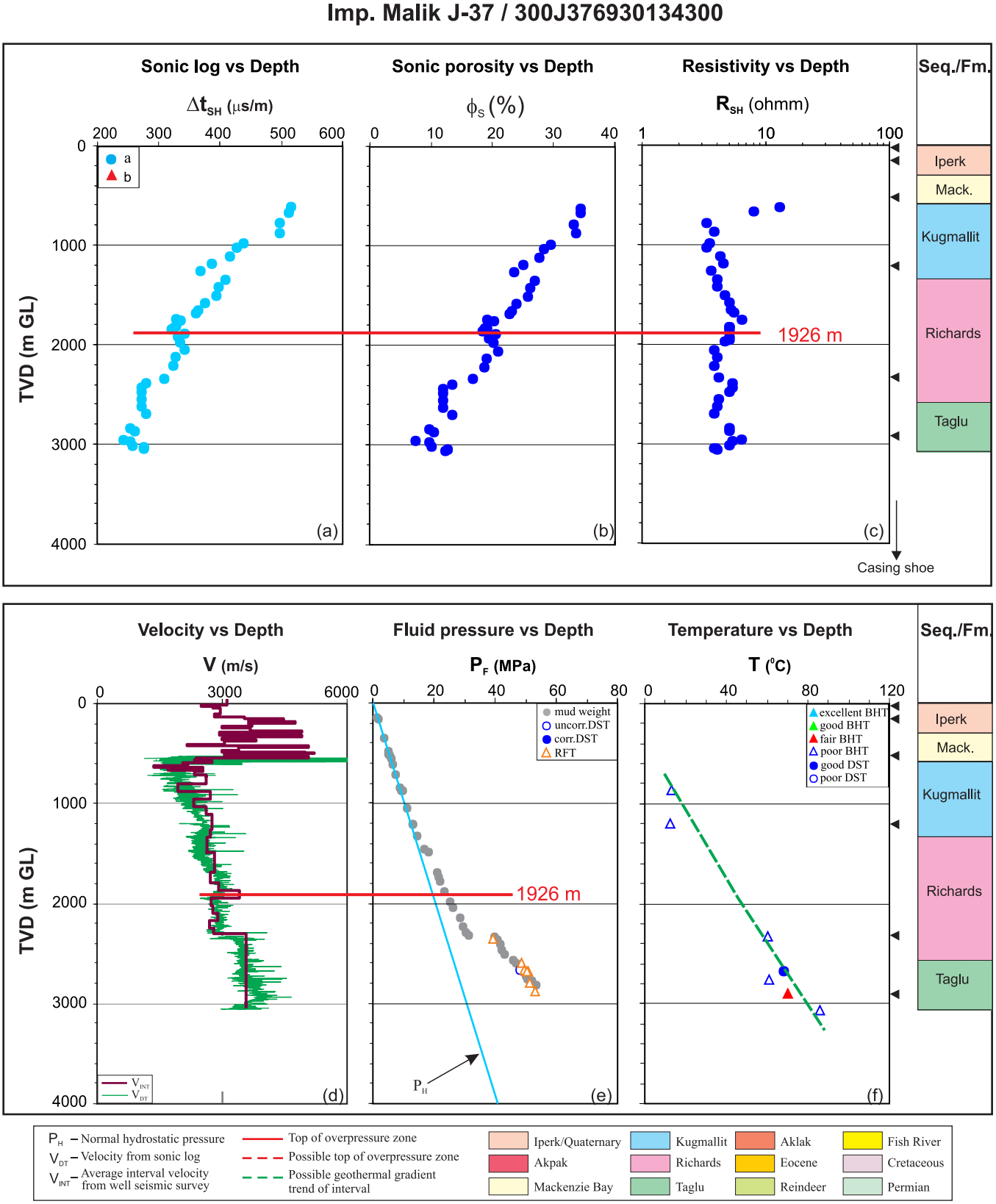

Figure A-22. Top of overpressure zone is detected at 1926 m with quality "a" by using the integrated analysis for the Mallik J-37 well in the Beaufort-Mackenzie Basin. (a) shale sonic transit time (Δt_{SH}) vs. depth; (b) shale sonic porosity (ϕ_S) vs. depth; (c) shale deep resistivity (R_{SH}) vs. depth; (d) continuous sonic velocity (V_{DT}) and average interval seismic velocity (V_{INT}) vs. depth; (e) fluid pressure (P_F) from well test and drilling mud weight vs. depth; and (f) borehole temperature vs. depth. Mack. - Mackenzie Bay.

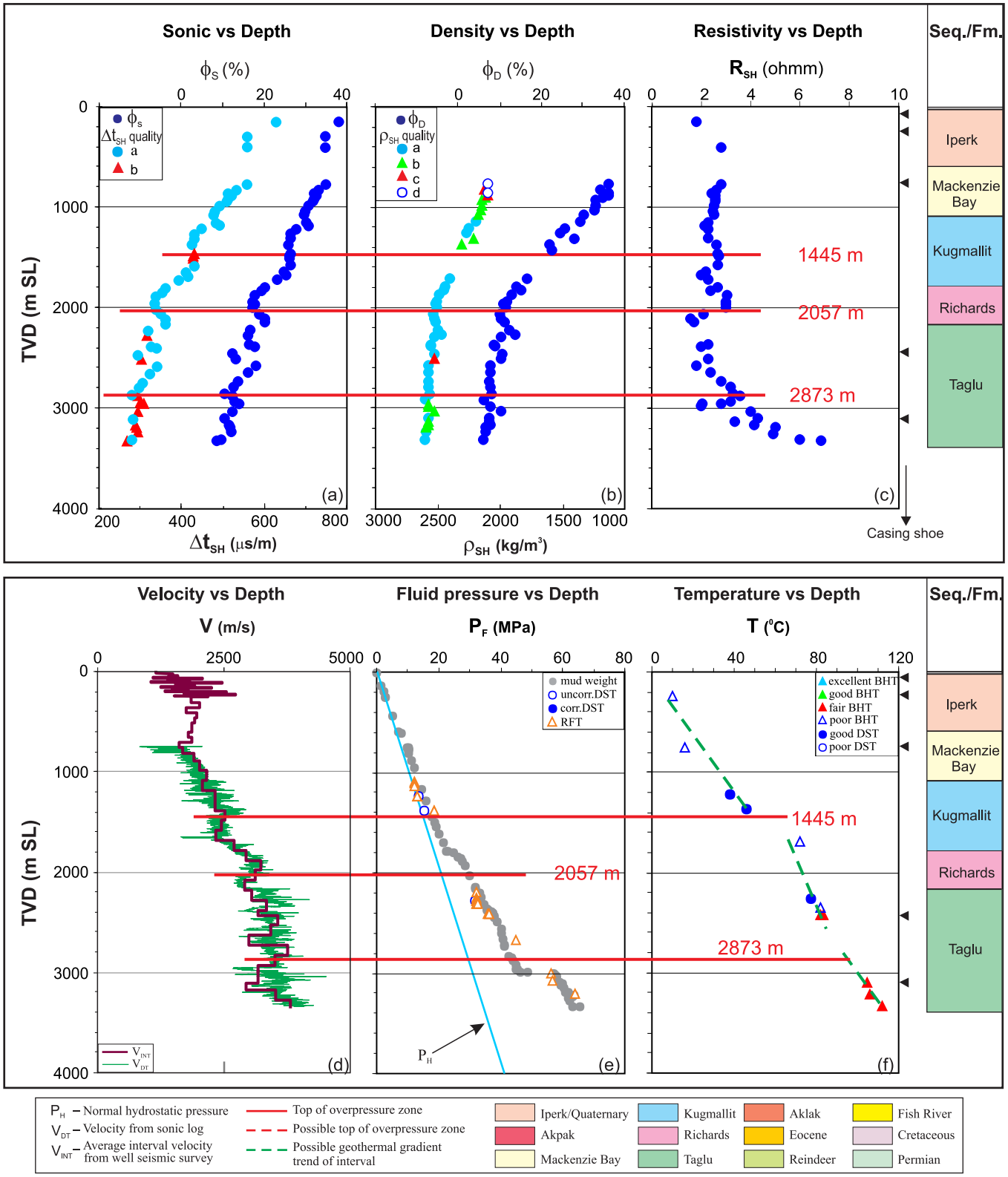

Figure A-23. Overpressure zones are detected with tops of OPZ at 1445 m, 2057 m and 2873 m with quality "a" by using the integrated analysis for the Minuk I-53 well in the Beaufort-Mackenzie Basin. (a) shale sonic transit time (Δt_{SH}) and sonic porosity (ϕ_S) vs. depth; (b) shale bulk density (ρ_{SH}) and density porosity (ϕ_D) vs depth; (c) shale deep resistivity (R_{SH}) vs. depth; (d) continuous sonic velocity (V_{DT}) and average interval seismic velocity (V_{INT}) vs. depth; (e) fluid pressure (P_F) from well test and drilling mud weight vs. depth; and (f) borehole temperature vs. depth.

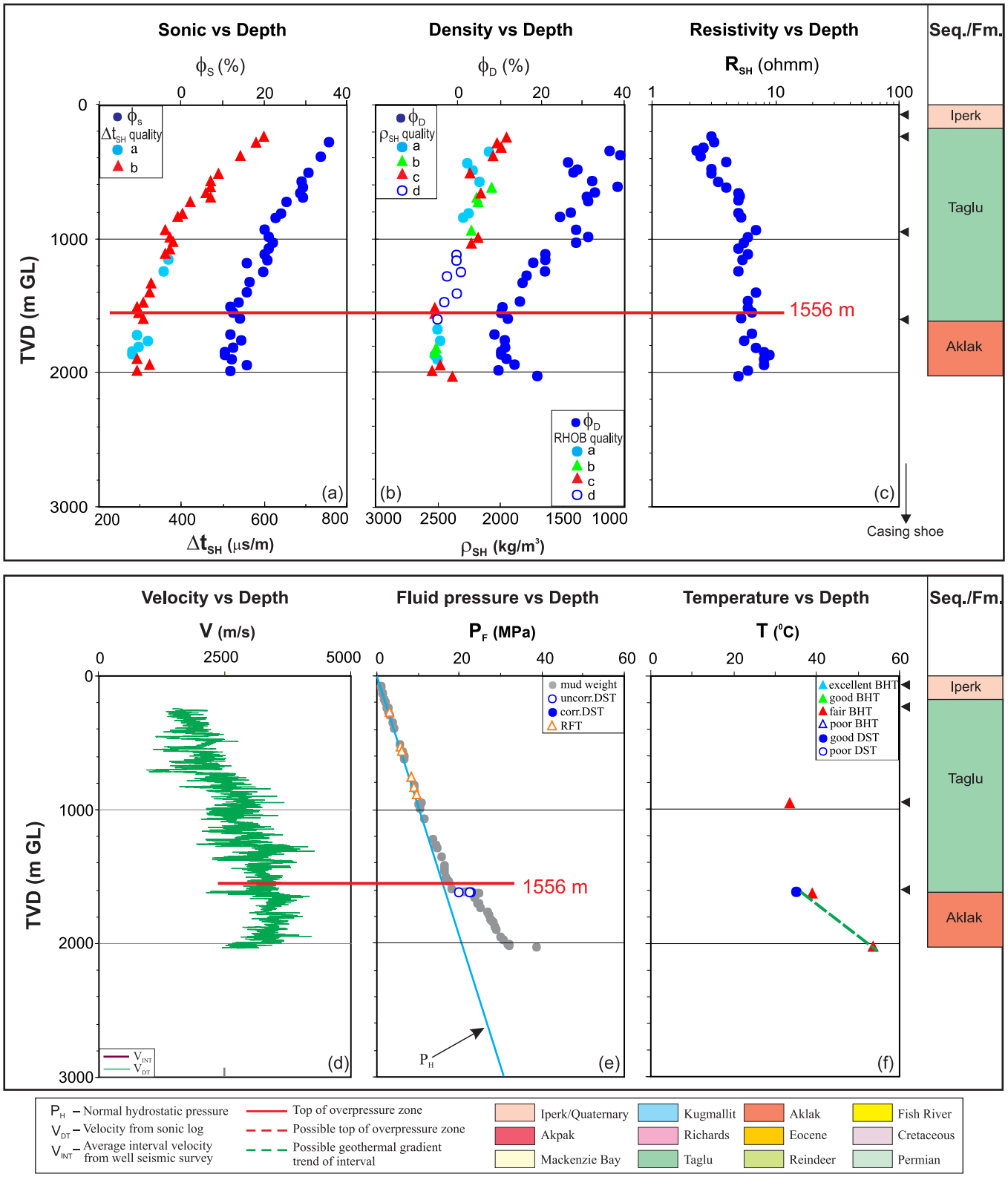

Figure A-24. Top of overpressure zone is detected at 1556 m with quality "a" by using the integrated analysis for the North Ellice L-39 well in the Beaufort-Mackenzie Basin. (a) shale sonic transit time (Δt_{SH}) and sonic porosity (ϕ_S) vs. depth; (b) shale bulk density (ρ_{SH}) and density porosity (ϕ_D) vs depth; (c) shale deep resistivity (R_{SH}) vs. depth; (d) continuous sonic velocity (V_{DT}) vs. depth; (e) fluid pressure (P_F) from well test and drilling mud weight vs. depth; and (f) borehole temperature vs. depth.

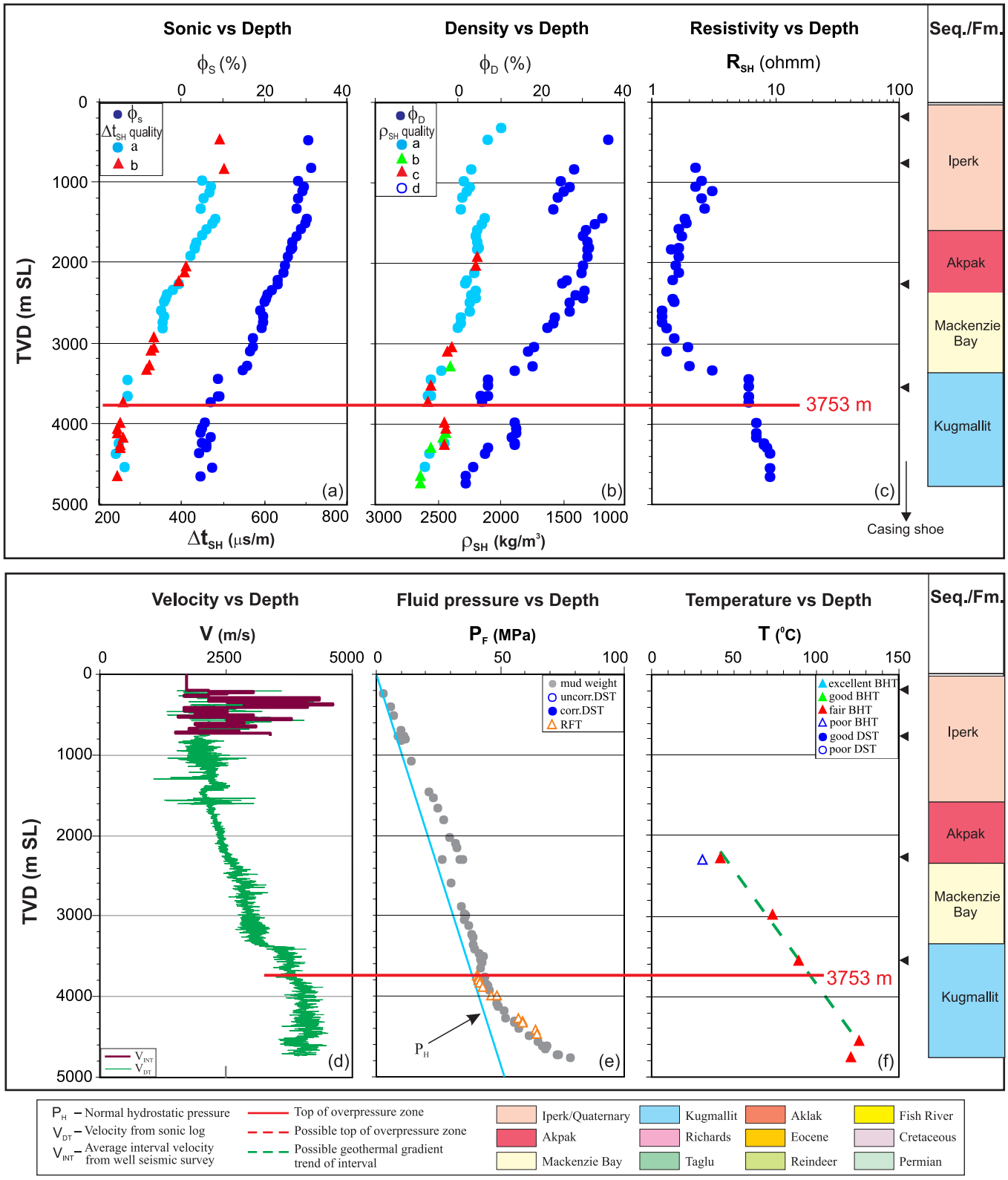

Figure A-25. Top of overpressure zone is detected at 3753 m with quality "a" by using the integrated analysis for the North Issungnak L-86 well in the Beaufort-Mackenzie Basin. (a) shale sonic transit time (Δt_{SH}) and sonic porosity (ϕ_S) vs. depth; (b) shale bulk density (ρ_{SH}) and density porosity (ϕ_D) vs depth; (c) shale deep resistivity (R_{SH}) vs. depth; (d) continuous sonic velocity (V_{DT}) and average interval seismic velocity (V_{INT}) vs. depth; (e) fluid pressure (P_F) from well test and drilling mud weight vs. depth; and (f) borehole temperature vs. depth.

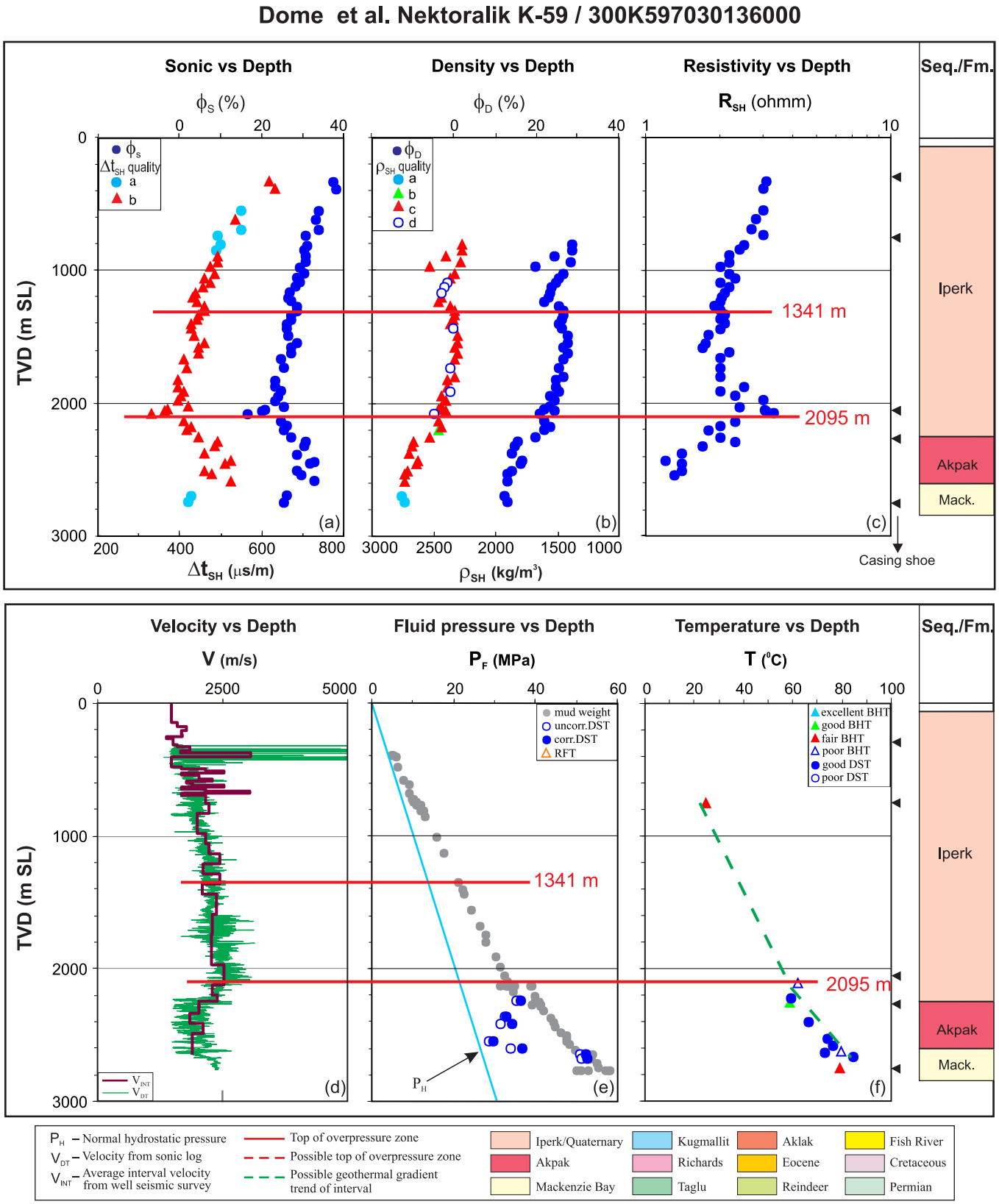

Figure A-26. Overpressure zones are detected with tops at 1341 m (quality "b") and 2095 m (quality "a") by using the integrated analysis for the Nektoralik K-59 well in the Beaufort-Mackenzie Basin. (a) shale sonic transit time (Δt_{SH}) and sonic porosity (ϕ_S) vs. depth; (b) shale bulk density (ρ_{SH}) and density porosity (ϕ_D) vs depth; (c) shale deep resistivity (R_{SH}) vs. depth; (d) continuous sonic velocity (V_{DT}) and average interval seismic velocity (V_{INT}) vs. depth; (e) fluid pressure (P_F) from well test and drilling mud weight vs. depth; and (f) borehole temperature vs. depth. Mack. - Mackenzie Bay.

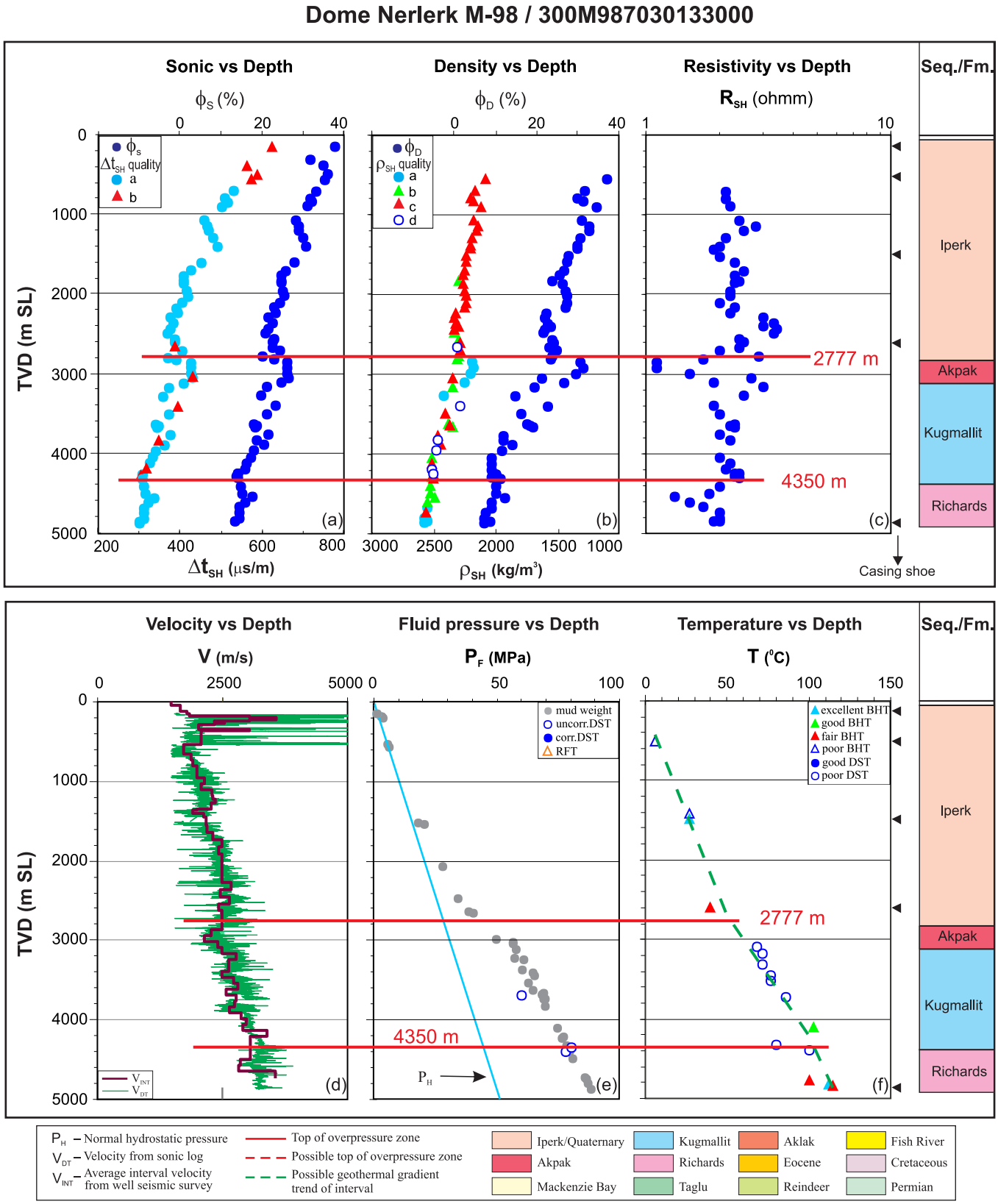

Figure A-27. Overpressure zones are detected with tops at 2777 m and 4350 m (quality "a") by using the integrated analysis for the Nerlerk M-98 well in the Beaufort-Mackenzie Basin. (a) shale sonic transit time (Δt_{SH}) and sonic porosity (ϕ_S) vs. depth; (b) shale bulk density (ρ_{SH}) and density porosity (ϕ_D) vs depth; (c) shale deep resistivity (R_{SH}) vs. depth; (d) continuous sonic velocity (V_{DT}) and average interval seismic velocity (V_{INT}) vs. depth; (e) fluid pressure (P_F) from well test and drilling mud weight vs. depth; and (f) borehole temperature vs. depth.

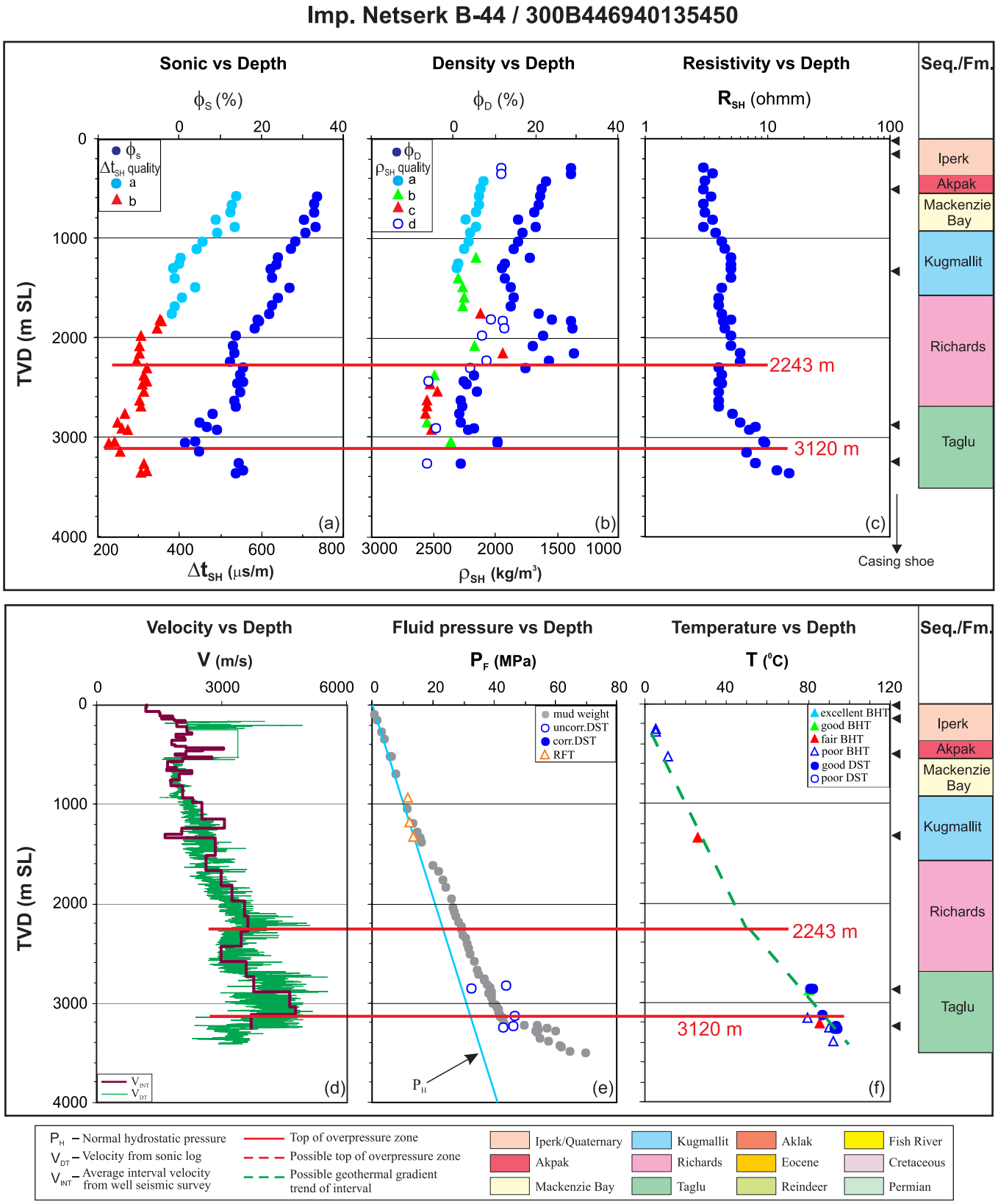

Figure A-28. Overpressure zones are detected with tops at 2243 m and 3120 m (quality "a") by using the integrated analysis for the Netserk B-44 well in the Beaufort-Mackenzie Basin. (a) shale sonic transit time (Δt_{SH}) and sonic porosity (ϕ_S) vs. depth; (b) shale bulk density (ρ_{SH}) and density porosity (ϕ_D) vs depth; (c) shale deep resistivity (R_{SH}) vs. depth; (d) continuous sonic velocity (V_{DT}) and average interval seismic velocity (V_{INT}) vs. depth; (e) fluid pressure (P_F) from well test and drilling mud weight vs. depth; and (f) borehole temperature vs. depth.

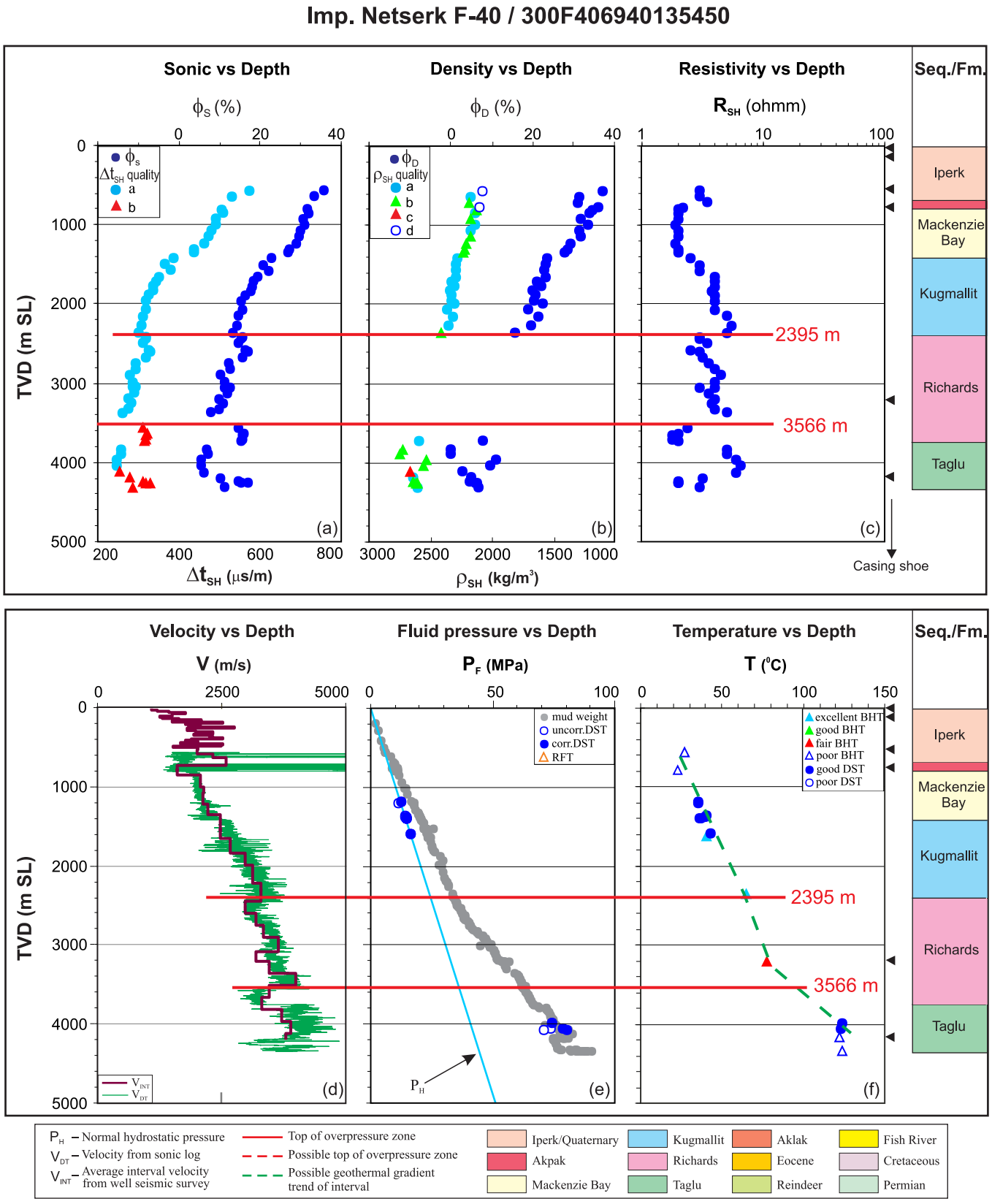

Figure A-29. Overpressure zones are detected with tops at 2395 m (quality "b") and 3566 m (quality "a") by using the integrated analysis for the Netserk F-40 well in the Beaufort-Mackenzie Basin. (a) shale sonic transit time (Δt_{SH}) and sonic porosity (ϕ_S) vs. depth; (b) shale bulk density (ρ_{SH}) and density porosity (ϕ_D) vs depth; (c) shale deep resistivity (R_{SH}) vs. depth; (d) continuous sonic velocity (V_{DT}) and average interval seismic velocity (V_{INT}) vs. depth; (e) fluid pressure (P_F) from well test and drilling mud weight vs. depth; and (f) borehole temperature vs. depth.

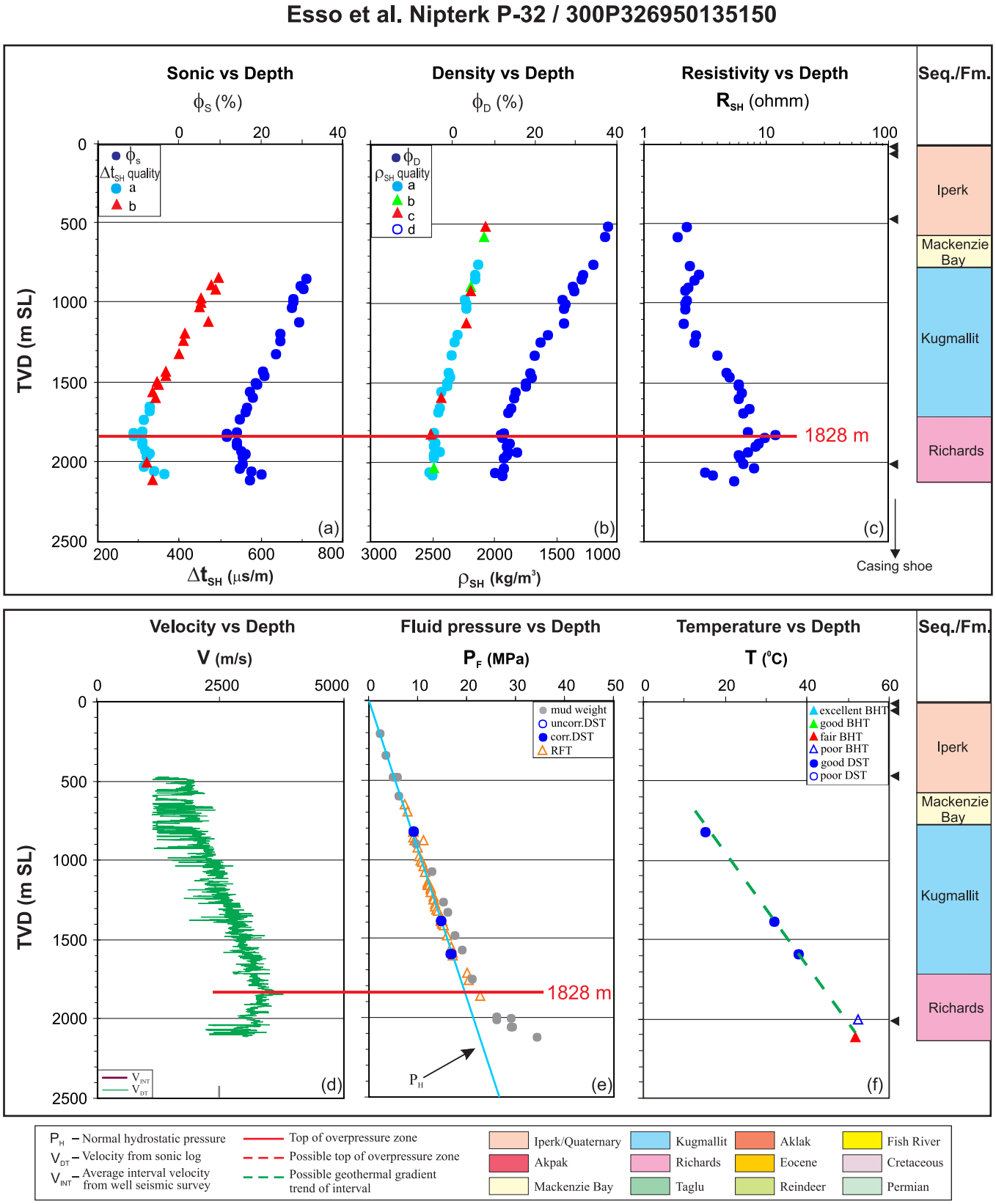

Figure A-30. Top of overpressure zone is detected at 1828 m with quality "a" by using the integrated analysis for the Nipterk P-32 well in the Beaufort-Mackenzie Basin. (a) shale sonic transit time (Δt_{SH}) and sonic porosity (ϕ_S) vs. depth; (b) shale bulk density (ρ_{SH}) and density porosity (ϕ_D) vs depth; (c) shale deep resistivity (R_{SH}) vs. depth; (d) continuous sonic velocity (V_{DT}) vs. depth; (e) fluid pressure (P_F) from well test and drilling mud weight vs. depth; and (f) borehole temperature vs. depth.

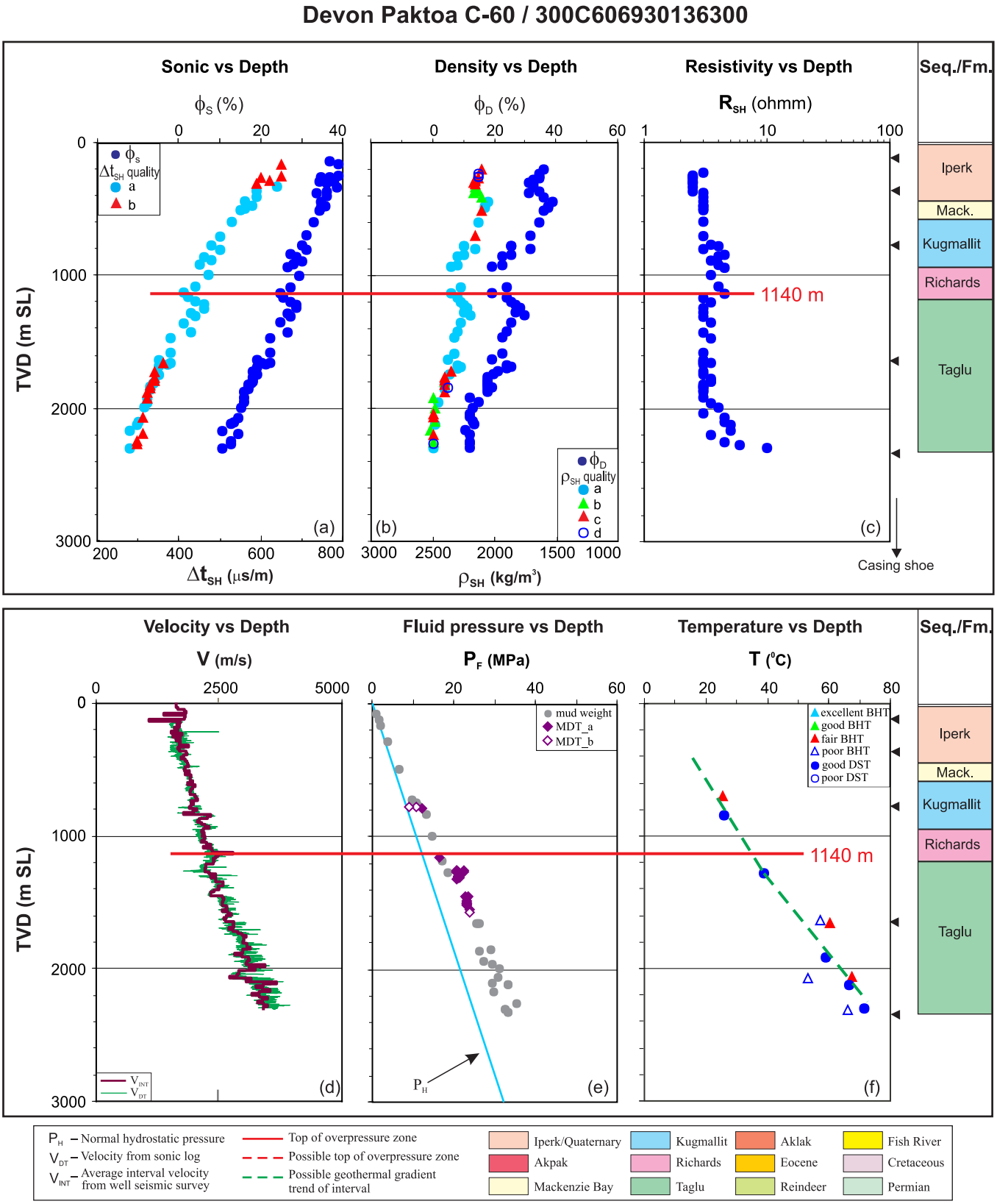

Figure A-31. Top of overpressure zone is detected at 1140 m with quality "a" by using the integrated analysis for the Paktoa C-60 well in the Beaufort-Mackenzie Basin. (a) shale sonic transit time (Δt_{SH}) and sonic porosity (ϕ_S) vs. depth; (b) shale bulk density (ρ_{SH}) and density porosity (ϕ_D) vs depth; (c) shale deep resistivity (R_{SH}) vs. depth; (d) continuous sonic velocity (V_{DT}) and average interval seismic velocity (V_{INT}) vs. depth; (e) fluid pressure (P_F) from well test and drilling mud weight vs. depth; and (f) borehole temperature vs. depth. Mack. - Mackenzie Bay.

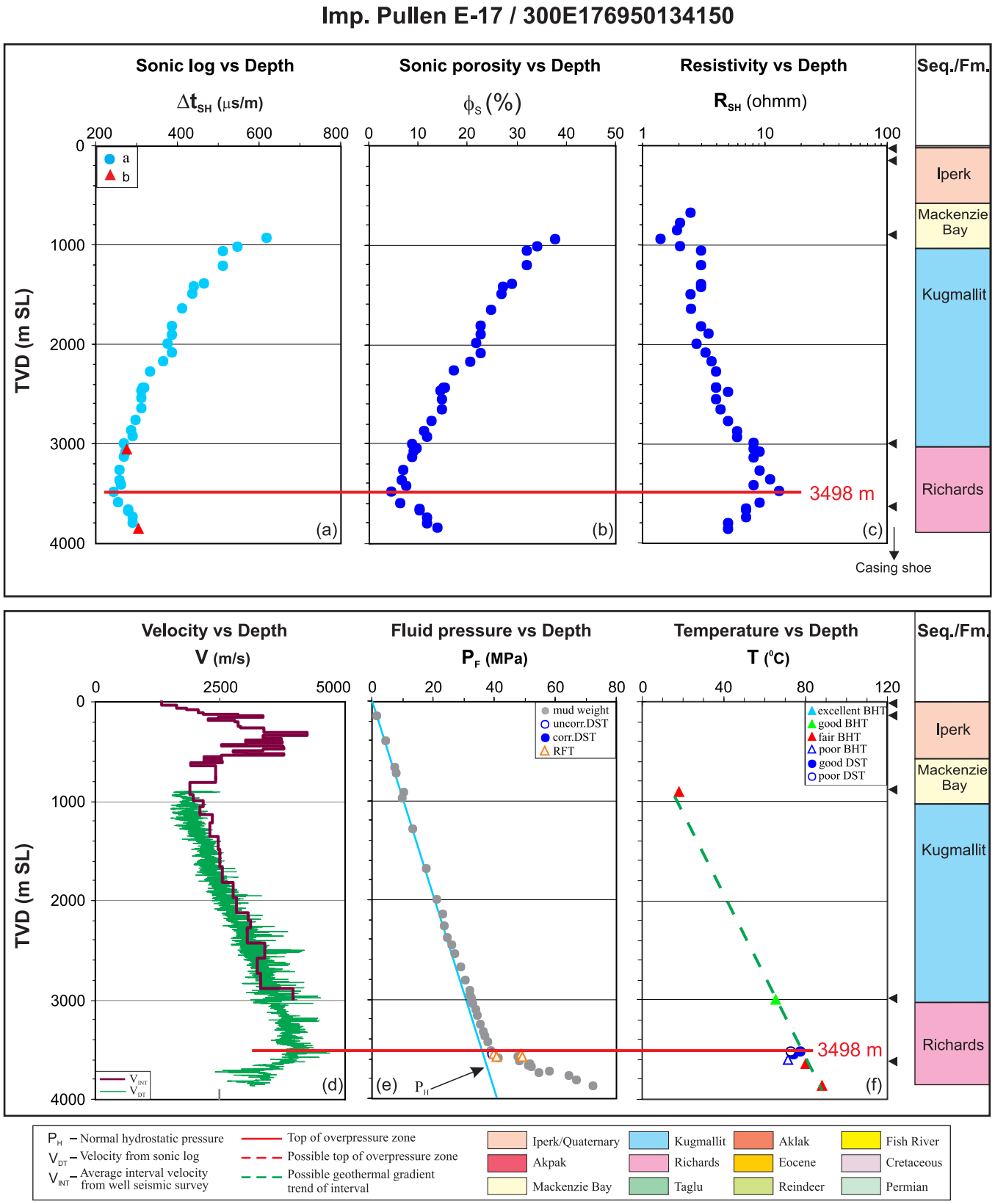

Figure A-32. Top of overpressure zone is detected at 3498 m with quality "a" by using the integrated analysis for the Pullen E-17 well in the Beaufort-Mackenzie Basin. (a) shale sonic transit time (Δt_{SH}) vs. depth; (b) shale sonic porosity (ϕ_S) vs. depth; (c) shale deep resistivity (R_{SH}) vs. depth; (d) continuous sonic velocity (V_{DT}) and average interval seismic velocity (V_{INT}) vs. depth; (e) fluid pressure (P_F) from well test and drilling mud weight vs. depth; and (f) borehole temperature vs. depth.

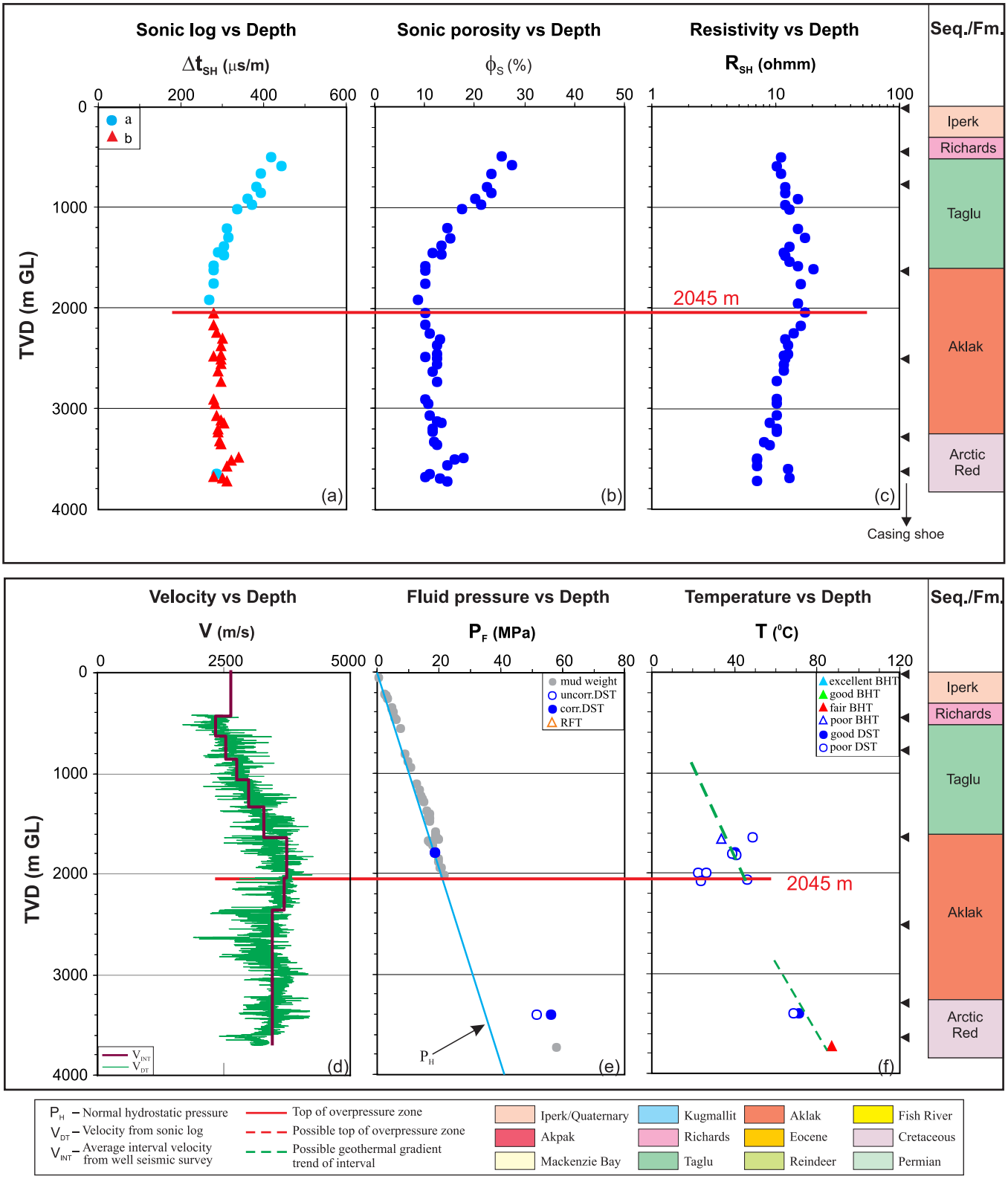

Figure A-33. Top of overpressure zone is detected at 2045 m with quality "a" by using the integrated analysis for the Reindeer D-27 well in the Beaufort-Mackenzie Basin. (a) shale sonic transit time (Δt_{SH}) vs. depth; (b) shale sonic porosity (ϕ_S) vs. depth; (c) shale deep resistivity (R_{SH}) vs. depth; (d) continuous sonic velocity (V_{DT}) and average interval seismic velocity (V_{INT}) vs. depth; (e) fluid pressure (P_F) from well test and drilling mud weight vs. depth; and (f) borehole temperature vs. depth.

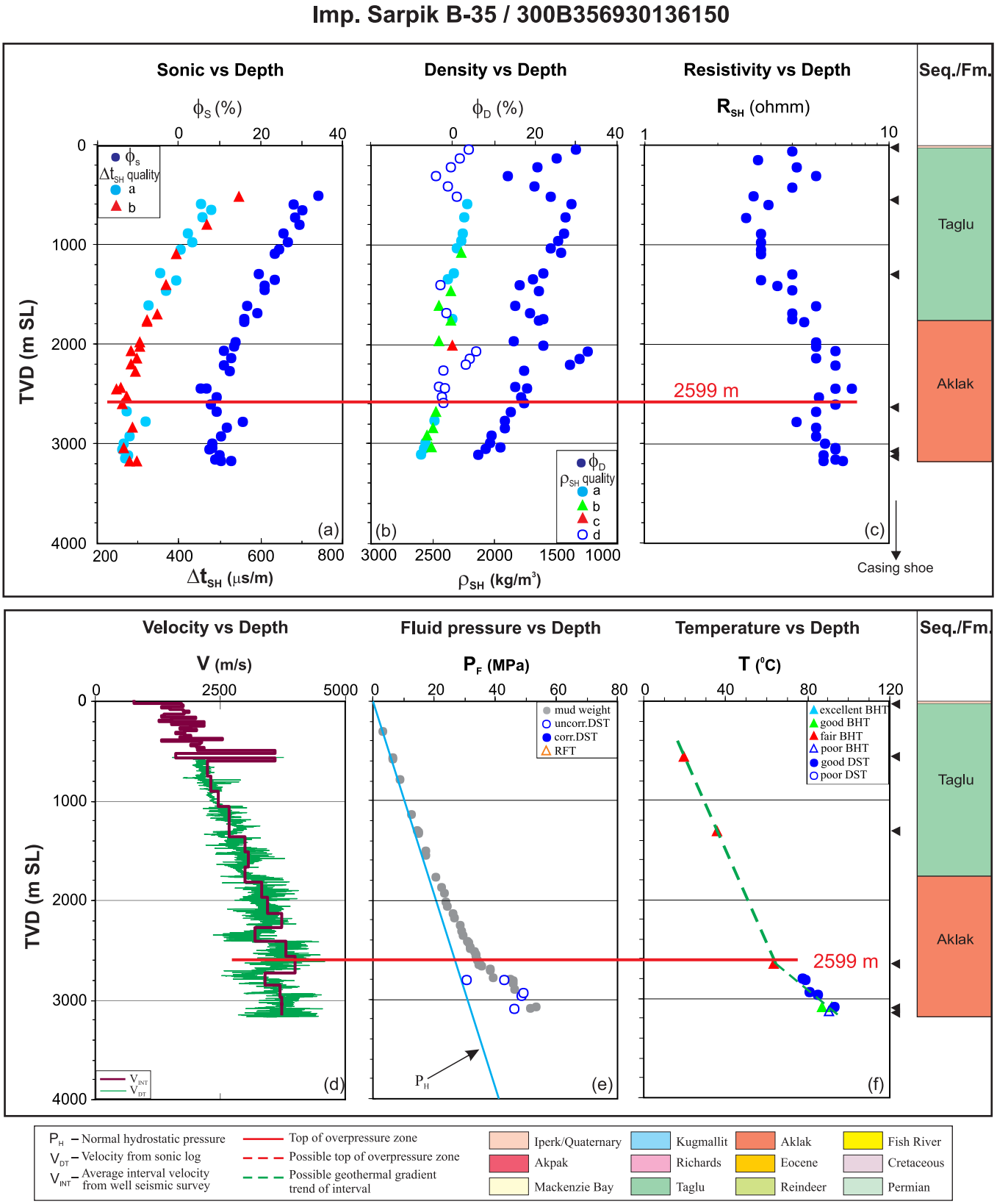

Figure A-34. Top of overpressure zone is detected at 2599 m with quality "a" by using the integrated analysis for the Sarpik B-35 well in the Beaufort-Mackenzie Basin. (a) shale sonic transit time (Δt_{SH}) and sonic porosity (ϕ_S) vs. depth; (b) shale bulk density (ρ_{SH}) and density porosity (ϕ_D) vs depth; (c) shale deep resistivity (R_{SH}) vs. depth; (d) continuous sonic velocity (V_{DT}) and average interval seismic velocity (V_{INT}) vs. depth; (e) fluid pressure (P_F) from well test and drilling mud weight vs. depth; and (f) borehole temperature vs. depth.

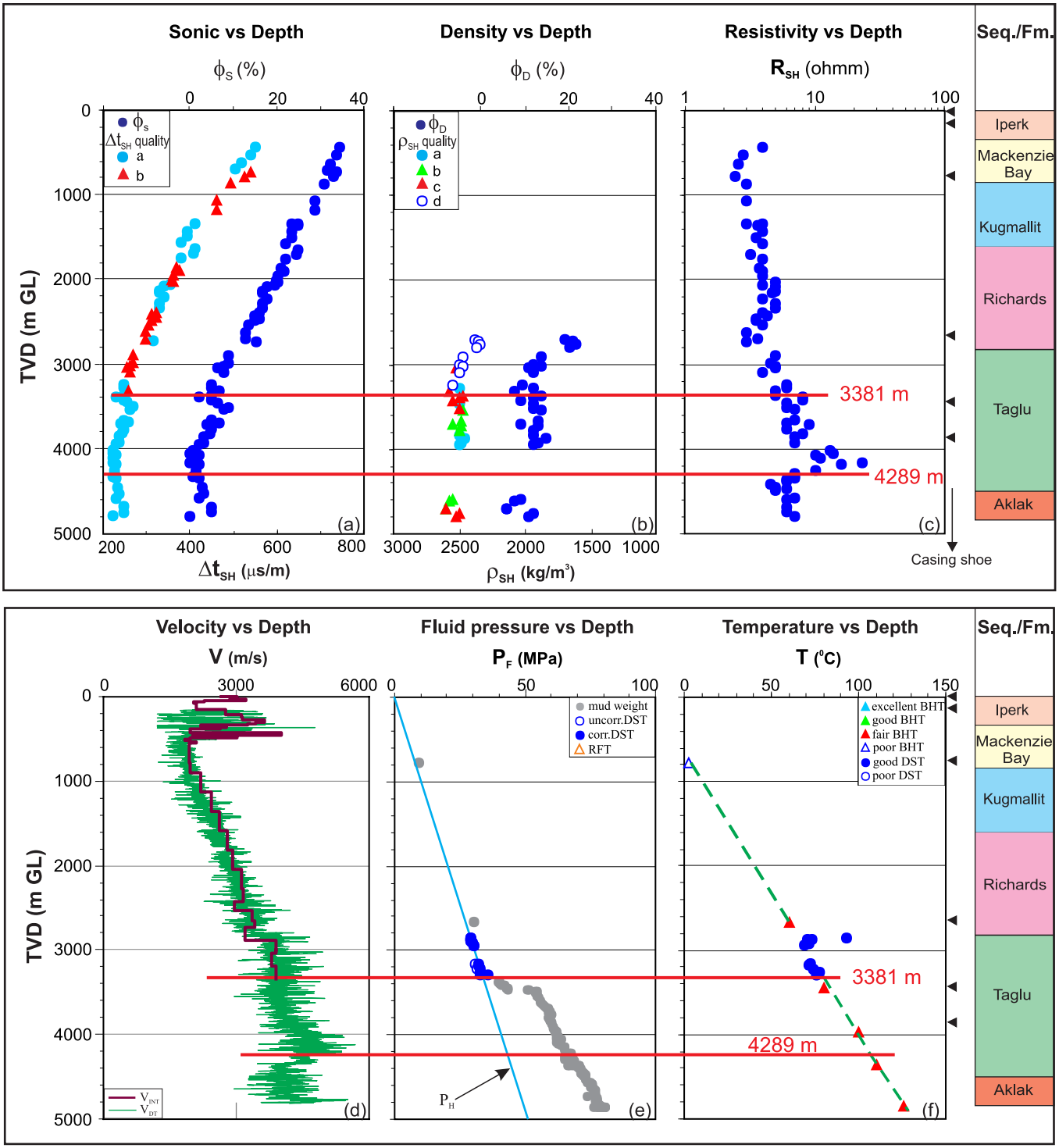

Figure A-35. Overpressure zones are detected with tops at 3381 m (quality "a") and 4289 m (quality "b") by using the integrated analysis for the Taglu C-42 well in the Beaufort-Mackenzie Basin. (a) shale sonic transit time (Δt_{SH}) and sonic porosity (ϕ_S) vs. depth; (b) shale bulk density (ρ_{SH}) and density porosity (ϕ_D) vs depth; (c) shale deep resistivity (R_{SH}) vs. depth; (d) continuous sonic velocity (V_{DT}) and average interval seismic velocity (V_{INT}) vs. depth; (e) fluid pressure (P_F) from well test and drilling mud weight vs. depth; and (f) borehole temperature vs. depth.

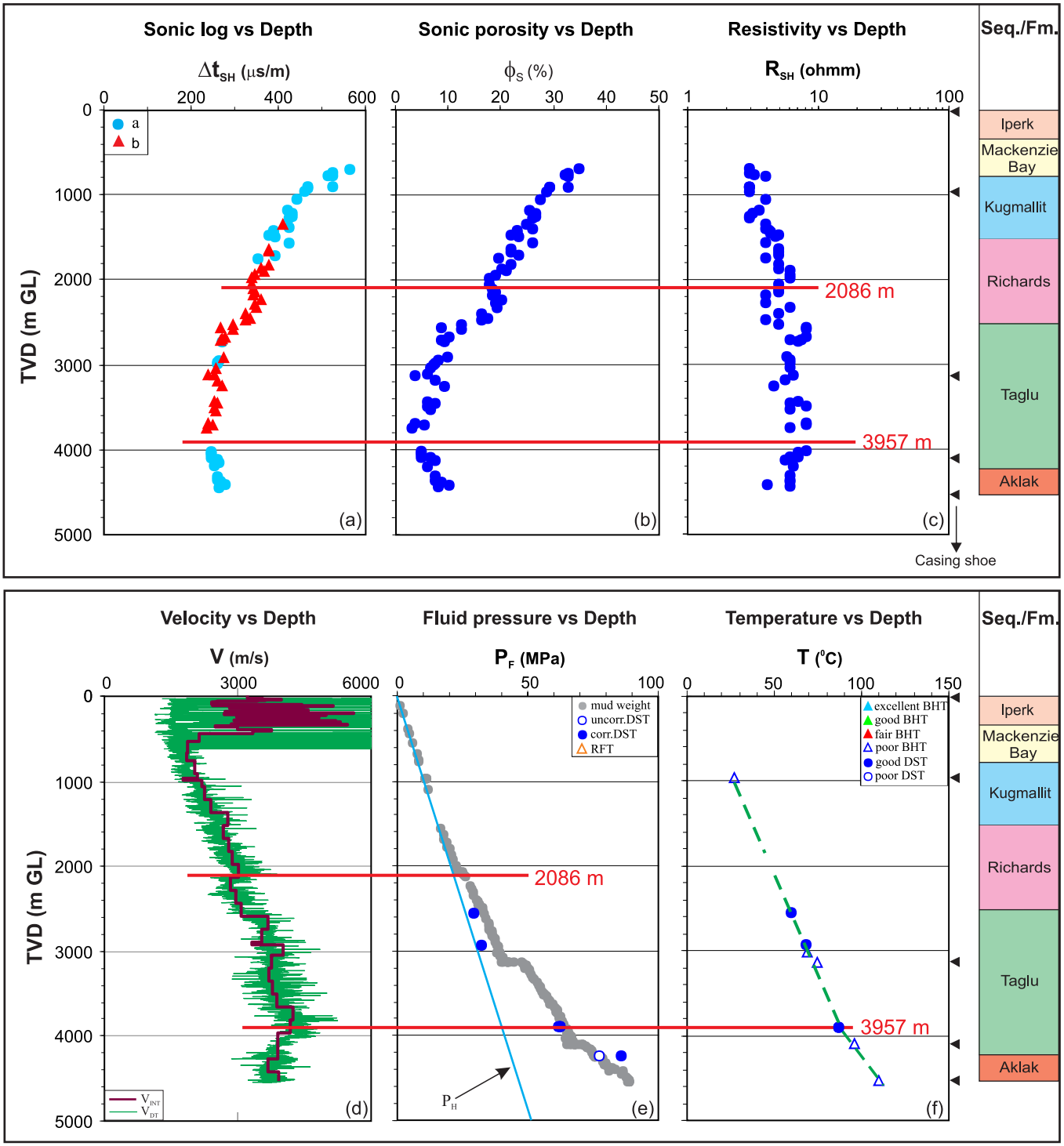

Figure A-36. Overpressure zones are detected with tops at 2086 m (quality "b") and 3957 m (quality "a") by using the integrated analysis for the Taglu D-43 well in the Beaufort-Mackenzie Basin. (a) shale sonic transit time (Δt_{SH}) vs. depth; (b) shale sonic porosity (ϕ_S) vs. depth; (c) shale deep resistivity (R_{SH}) vs. depth; (d) continuous sonic velocity (V_{DT}) and average interval seismic velocity (V_{INT}) vs. depth; (e) fluid pressure (P_F) from well test and drilling mud weight vs. depth; and (f) borehole temperature vs. depth.

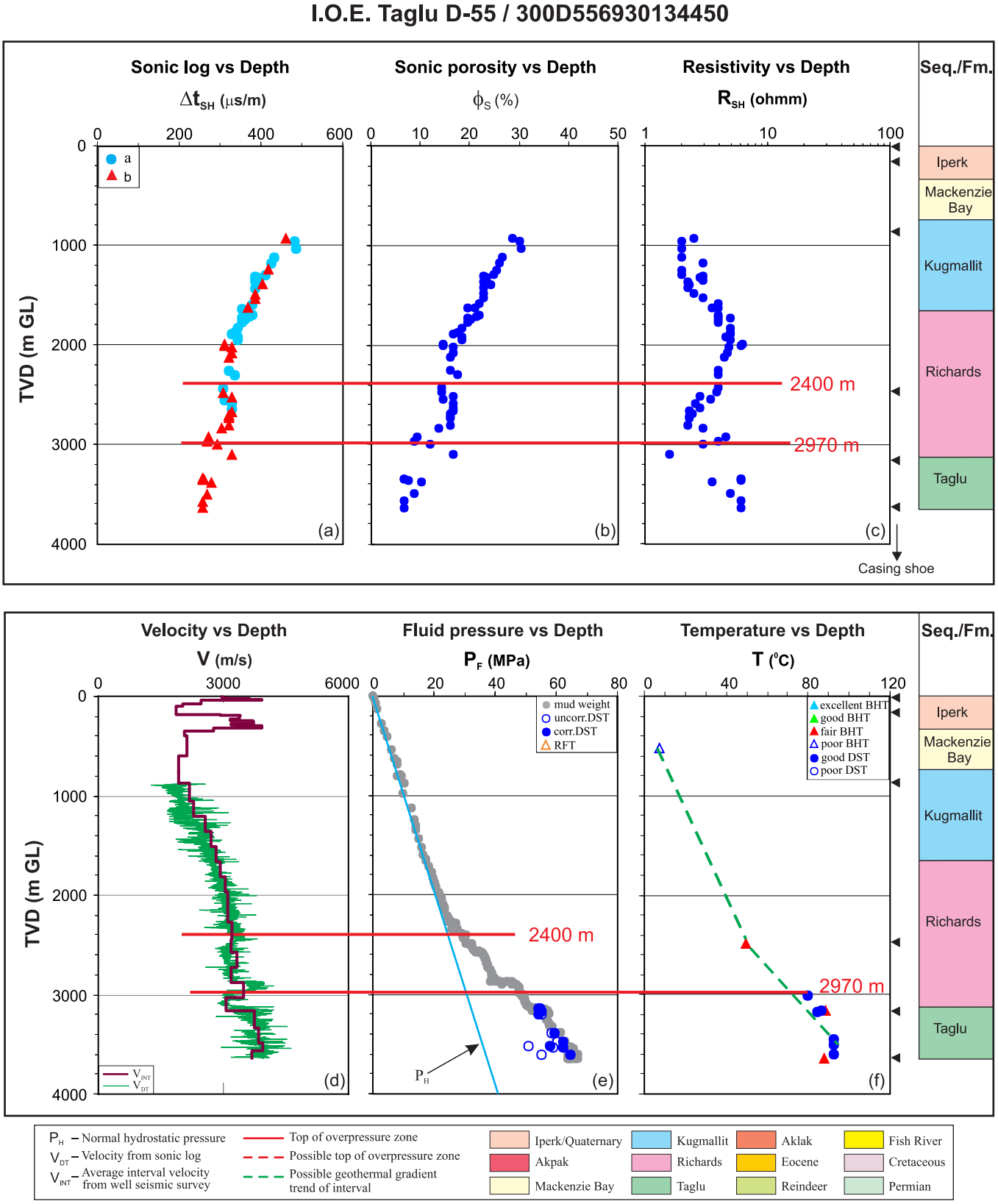

Figure A-37. Overpressure zones are detected with tops of OPZ at 2400 m (quality "b") and 2970 m (quality "a") by using the integrated analysis for the Taglu D-55 well in the Beaufort-Mackenzie Basin. (a) shale sonic transit time (Δt_{SH}) vs. depth; (b) shale sonic porosity (ϕ_S) vs. depth; (c) shale deep resistivity (R_{SH}) vs. depth; (d) continuous sonic velocity (V_{DT}) and average interval seismic velocity (V_{INT}) vs. depth; (e) fluid pressure (P_F) from well test and drilling mud weight vs. depth; and (f) borehole temperature vs. depth.

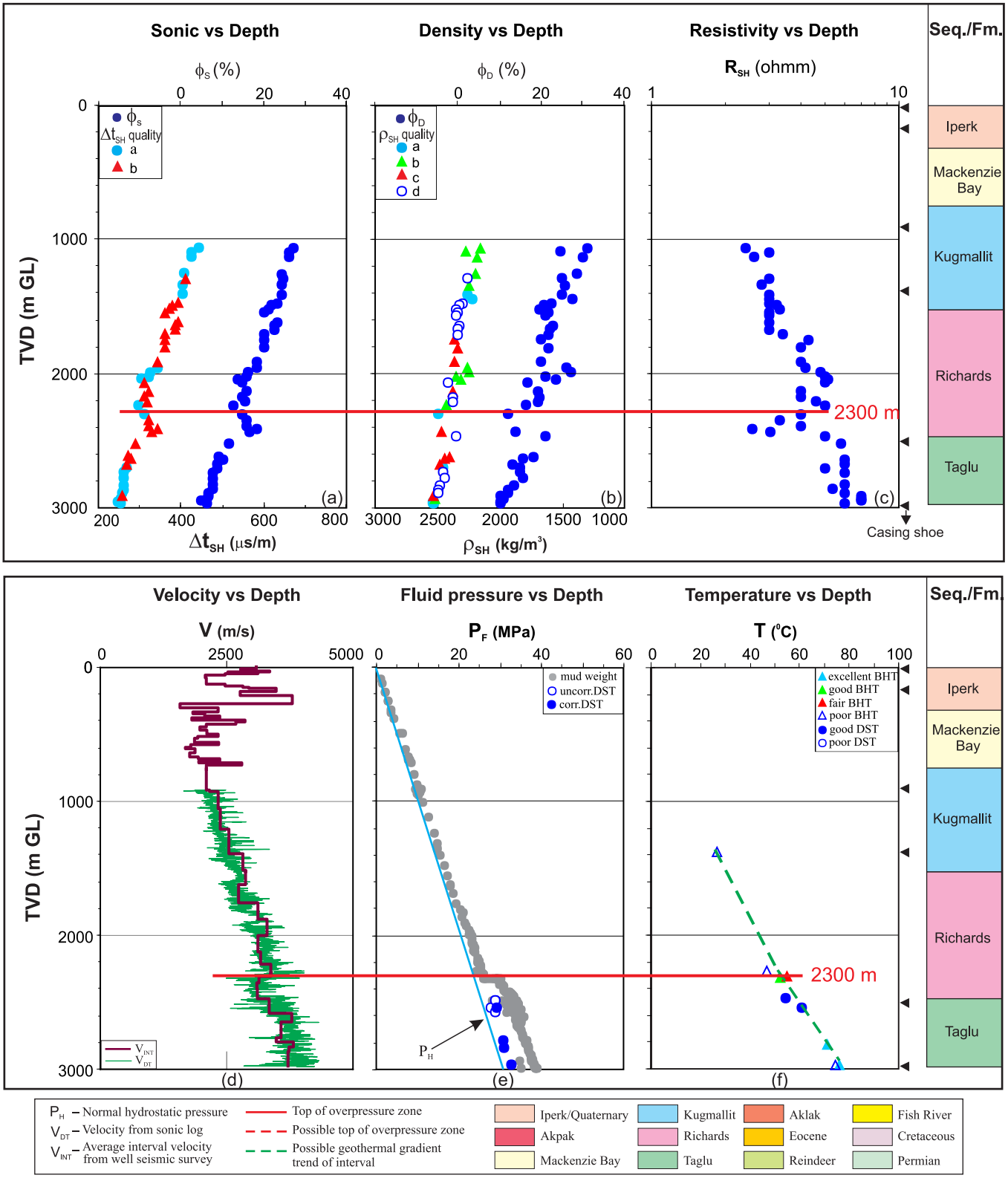

Figure A-38. Top of overpressure zone is detected at 2300 with quality "a" by using the integrated analysis for the Taglu G-33 well in the Beaufort-Mackenzie Basin. (a) shale sonic transit time (Δt_{SH}) and sonic porosity (ϕ_S) vs. depth; (b) shale bulk density (ρ_{SH}) and density porosity (ϕ_D) vs depth; (c) shale deep resistivity (R_{SH}) vs. depth; (d) continuous sonic velocity (V_{DT}) and average interval seismic velocity (V_{INT}) vs. depth; (e) fluid pressure (P_F) from well test and drilling mud weight vs. depth; and (f) borehole temperature vs. depth.

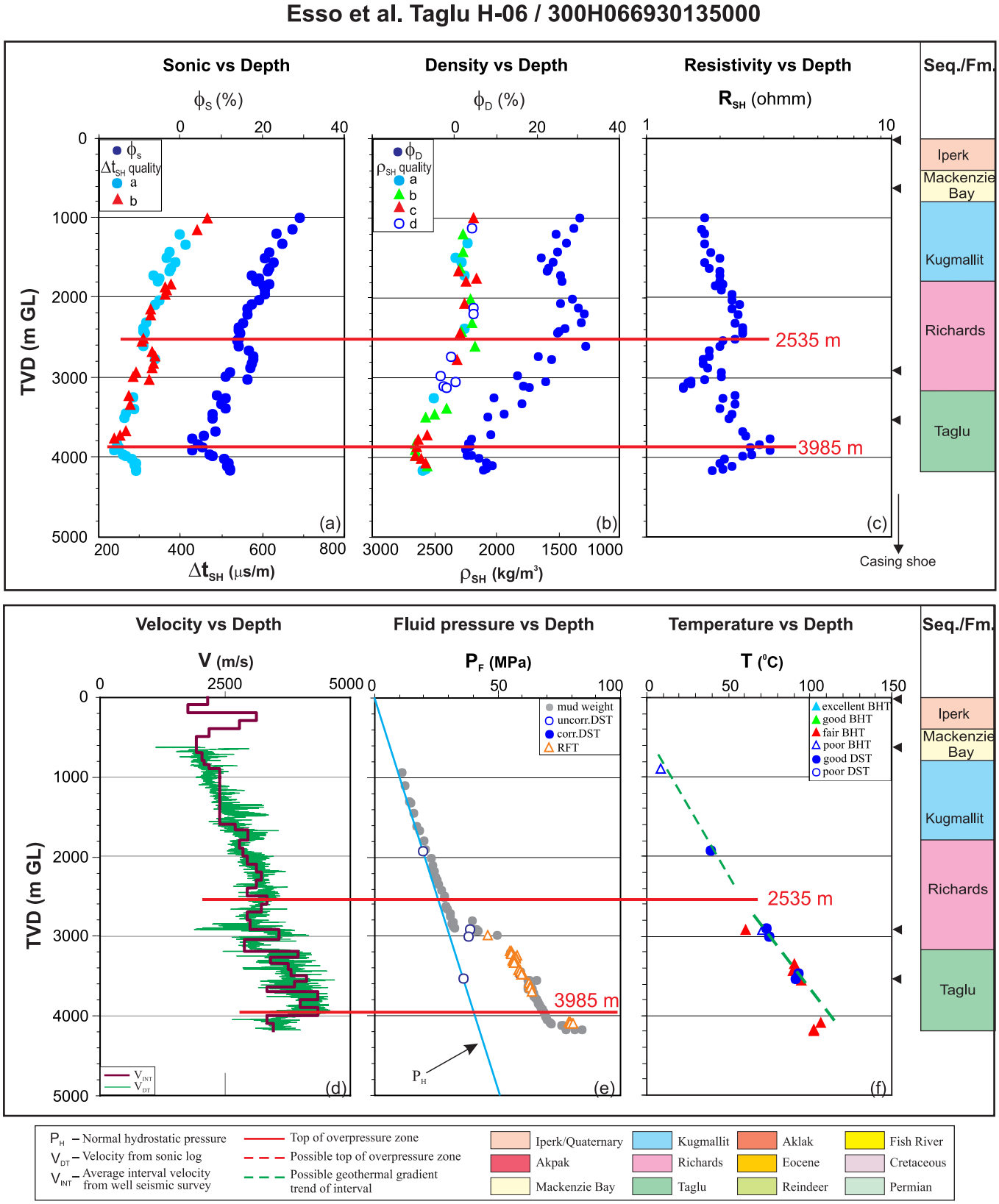

Figure A-39. Overpressure zones are detected with tops of OPZ at 2535 m (quality "a") and 3985 m (quality "a") by using the integrated analysis for the Taglu W. H-06 well in the Beaufort-Mackenzie Basin. (a) shale sonic transit time (Δt_{SH}) and sonic porosity (ϕ_S) vs. depth; (b) shale bulk density (ρ_{SH}) and density porosity (ϕ_D) vs depth; (c) shale deep resistivity (R_{SH}) vs. depth; (d) continuous sonic velocity (V_{DT}) and average interval seismic velocity (V_{INT}) vs. depth; (e) fluid pressure (P_F) from well test and drilling mud weight vs. depth; and (f) borehole temperature vs. depth.

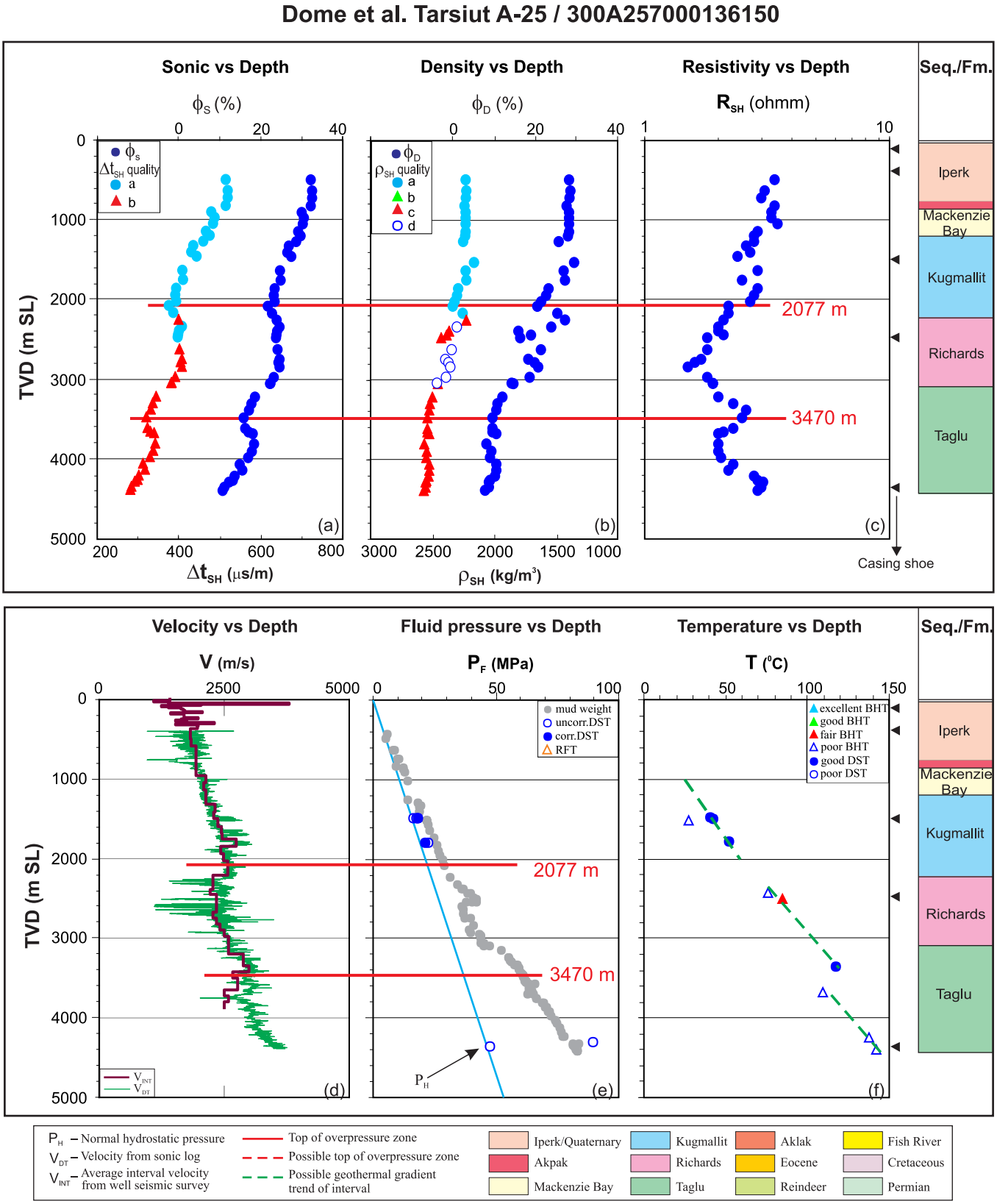

Figure A-40. Overpressure zones are detected with tops of OPZ at 2077 m (quality "a") and 3470 m (quality "a") by using the integrated analysis for the Tarsiut A-25 well in the Beaufort-Mackenzie Basin. (a) shale sonic transit time (Δt_{SH}) and sonic porosity (ϕ_S) vs. depth; (b) shale bulk density (ρ_{SH}) and density porosity (ϕ_D) vs depth; (c) shale deep resistivity (R_{SH}) vs. depth; (d) continuous sonic velocity (V_{DT}) and average interval seismic velocity (V_{INT}) vs. depth; (e) fluid pressure (P_F) from well test and drilling mud weight vs. depth; and (f) borehole temperature vs. depth.

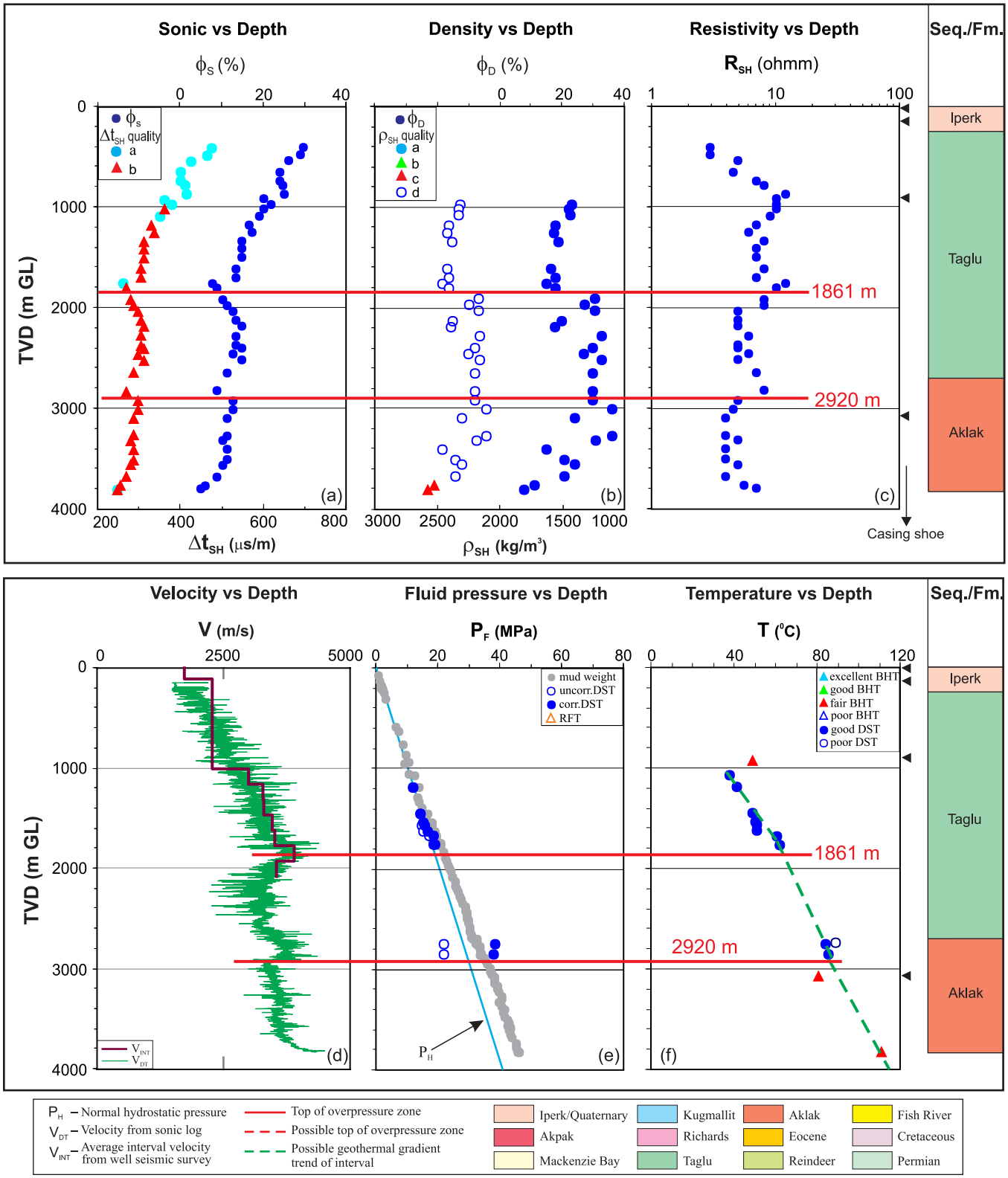

Figure A-41. Overpressure zones are detected with tops of OPZ at 1861 m (quality "a") and at 2920 m (quality "a") by using the integrated analysis for the Titalik K-26 well in the Beaufort-Mackenzie Basin. (a) shale sonic transit time (Δt_{SH}) and sonic porosity (ϕ_S) vs. depth; (b) shale bulk density (ρ_{SH}) and density porosity (ϕ_D) vs depth; (c) shale deep resistivity (R_{SH}) vs. depth; (d) continuous sonic velocity (V_{DT}) and average interval seismic velocity (V_{INT}) vs. depth; (e) fluid pressure (P_F) from well test and drilling mud weight vs. depth; and (f) borehole temperature vs. depth.

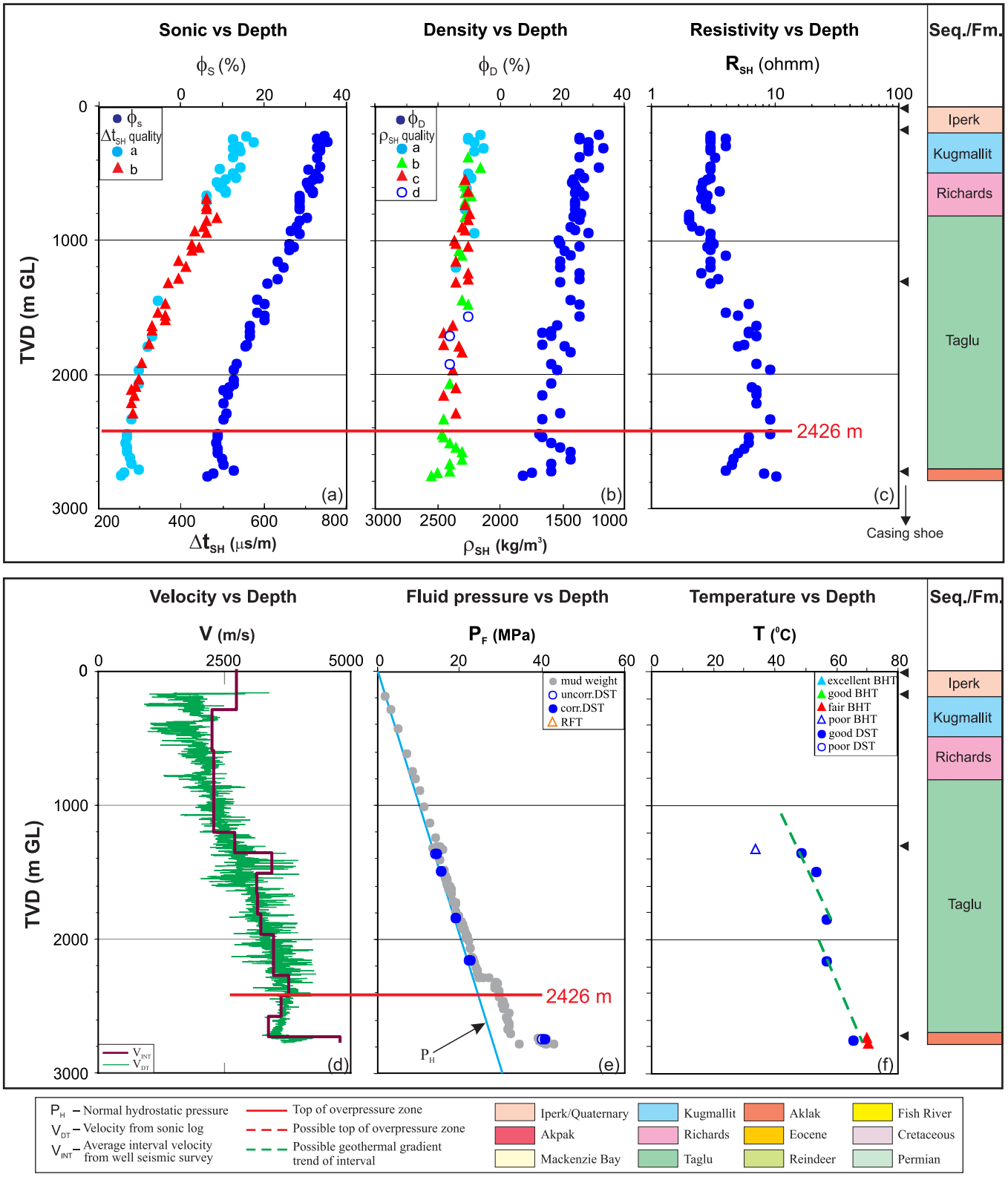

Figure A-42. Top of overpressure zone is detected at 2426 m with quality "a" by using the integrated analysis for the Toapolok O-54 well in the Beaufort-Mackenzie Basin. (a) shale sonic transit time (Δt_{SH}) and sonic porosity (ϕ_S) vs. depth; (b) shale bulk density (ρ_{SH}) and density porosity (ϕ_D) vs depth; (c) shale deep resistivity (R_{SH}) vs. depth; (d) continuous sonic velocity (V_{DT}) and average interval seismic velocity (V_{INT}) vs. depth; (e) fluid pressure (P_F) from well test and drilling mud weight vs. depth; and (f) borehole temperature vs. depth.

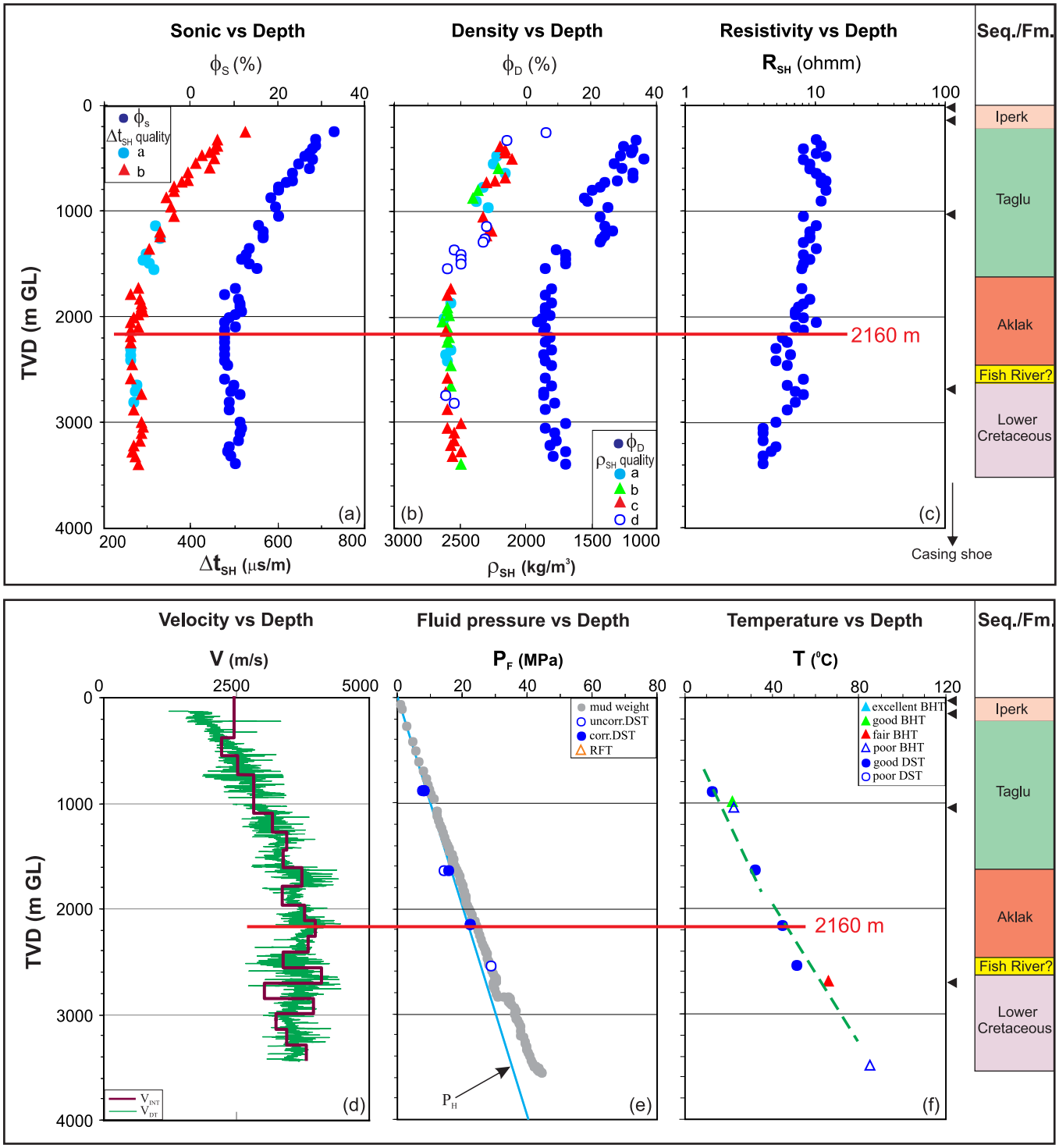

Figure A-43. Top of overpressure zone is detected at 2160 m with quality "a" by using the integrated analysis for the Tununuk F-30 well in the Beaufort-Mackenzie Basin. (a) shale sonic transit time (Δt_{SH}) and sonic porosity (ϕ_S) vs. depth; (b) shale bulk density (ρ_{SH}) and density porosity (ϕ_D) vs depth; (c) shale deep resistivity (R_{SH}) vs. depth; (d) continuous sonic velocity (V_{DT}) and average interval seismic velocity (V_{INT}) vs. depth; (e) fluid pressure (P_F) from well test and drilling mud weight vs. depth; and (f) borehole temperature vs. depth.

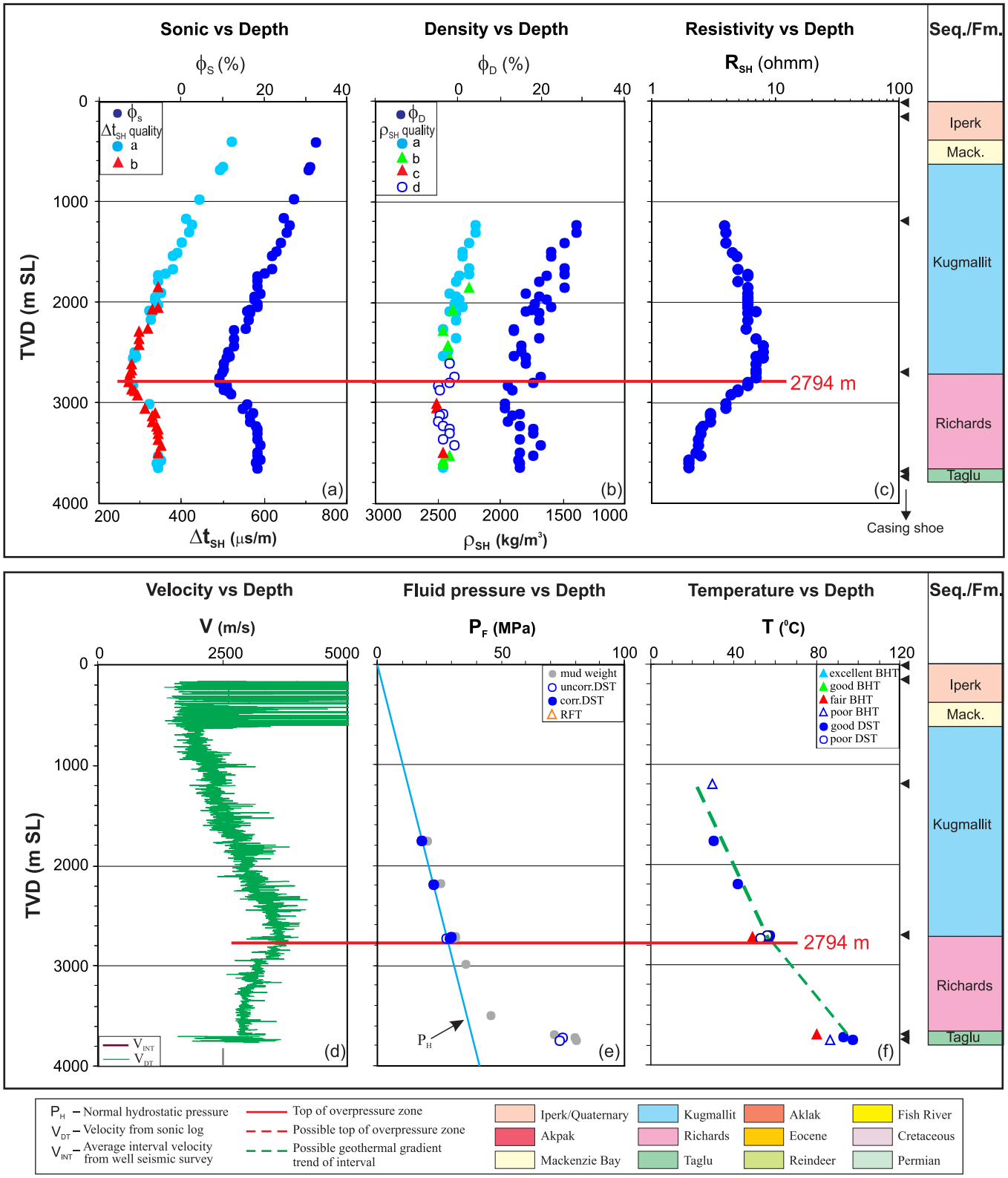

Figure A-44. Top of overpressure zone is detected at 2794 m with quality "a" by using the integrated analysis for the Unark L-24 well in the Beaufort-Mackenzie Basin. (a) shale sonic transit time (Δt_{SH}) and sonic porosity (ϕ_S) vs. depth; (b) shale bulk density (ρ_{SH}) and density porosity (ϕ_D) vs depth; (c) shale deep resistivity (R_{SH}) vs. depth; (d) continuous sonic velocity (V_{DT}) and average interval seismic velocity (V_{INT}) vs. depth; (e) fluid pressure (P_F) from well test and drilling mud weight vs. depth; and (f) borehole temperature vs. depth. Mack. - Mackenzie Bay.

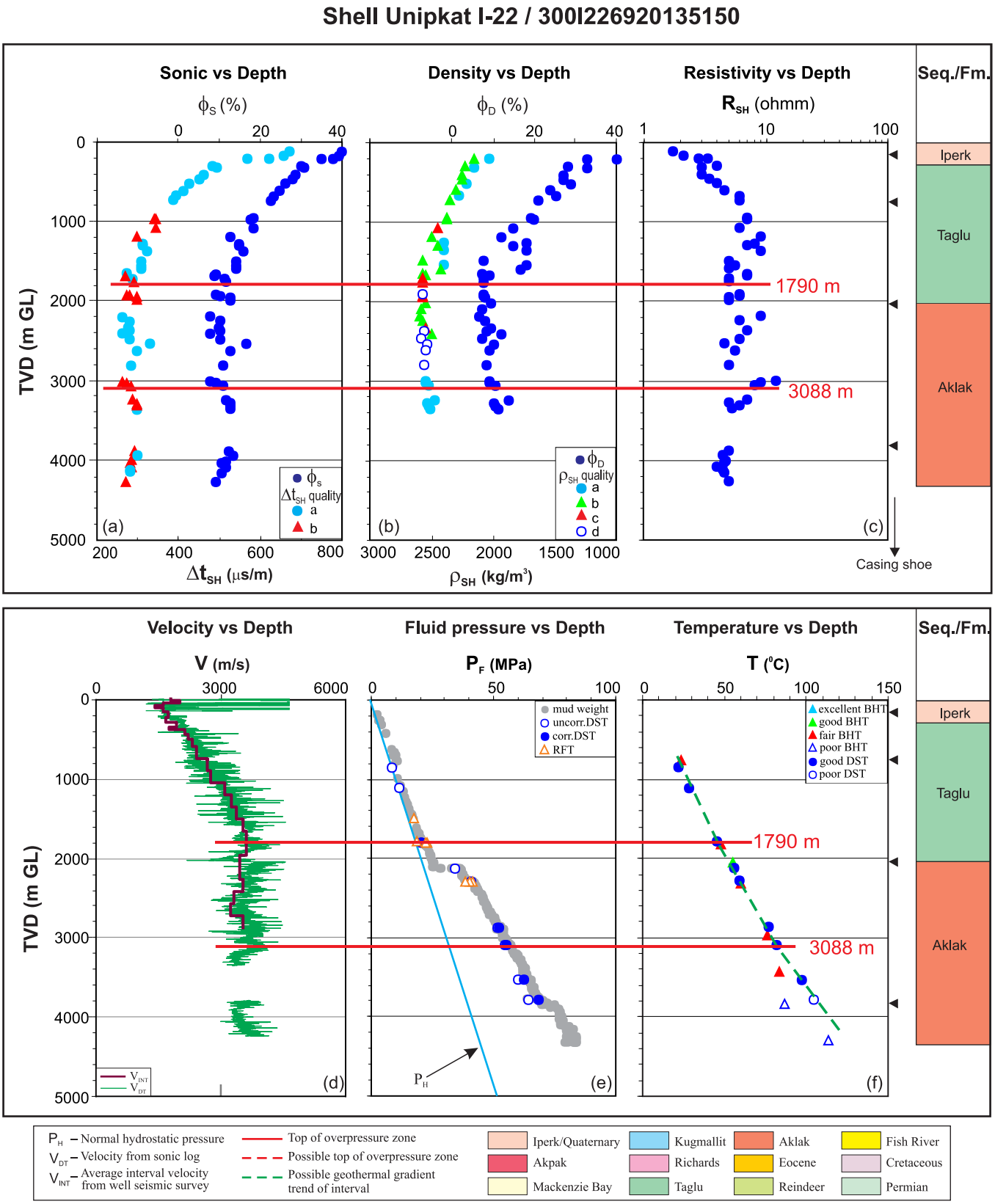

Figure A-45. Overpressure zones are detected with tops of OPZ at 1790 m (quality "a") and 3088 m (quality "a") by using the integrated analysis for the Unipkat I-22 well in the Beaufort-Mackenzie Basin. (a) shale sonic transit time (Δt_{SH}) and sonic porosity (ϕ_S) vs. depth; (b) shale bulk density (ρ_{SH}) and density porosity (ϕ_D) vs depth; (c) shale deep resistivity (R_{SH}) vs. depth; (d) continuous sonic velocity (V_{DT}) and average interval seismic velocity (V_{INT}) vs. depth; (e) fluid pressure (P_F) from well test and drilling mud weight vs. depth; and (f) borehole temperature vs. depth.

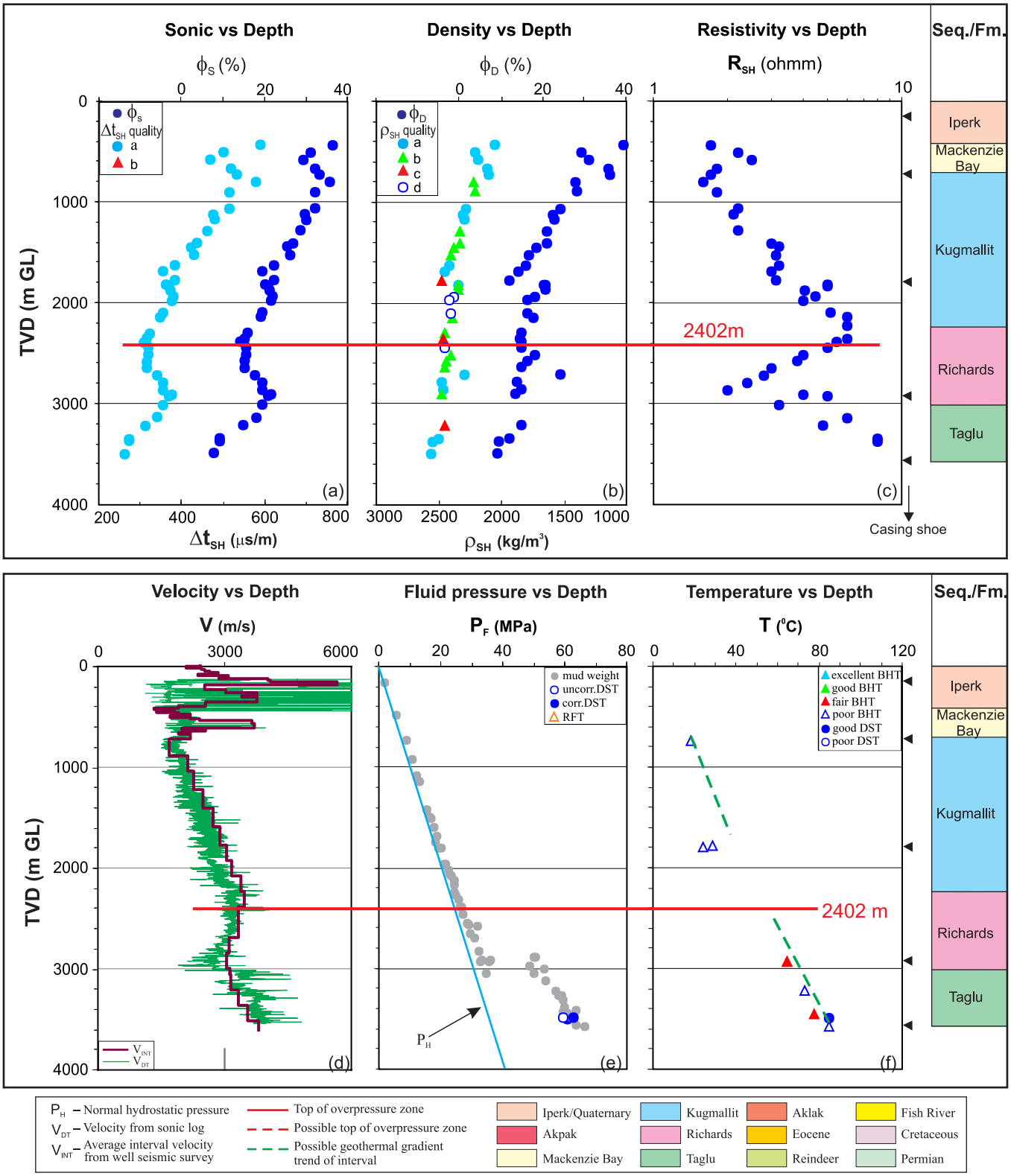

Figure A-46. Top of overpressure zone is detected at 2402 m with quality "a" by using the integrated analysis for the Upluk M-38 well in the Beaufort-Mackenzie Basin. (a) shale sonic transit time (Δt_{SH}) and sonic porosity (ϕ_S) vs. depth; (b) shale bulk density (ρ_{SH}) and density porosity (ϕ_D) vs depth; (c) shale deep resistivity (R_{SH}) vs. depth; (d) continuous sonic velocity (V_{DT}) and average interval seismic velocity (V_{INT}) vs. depth; (e) fluid pressure (P_F) from well test and drilling mud weight vs. depth; and (f) borehole temperature vs. depth.

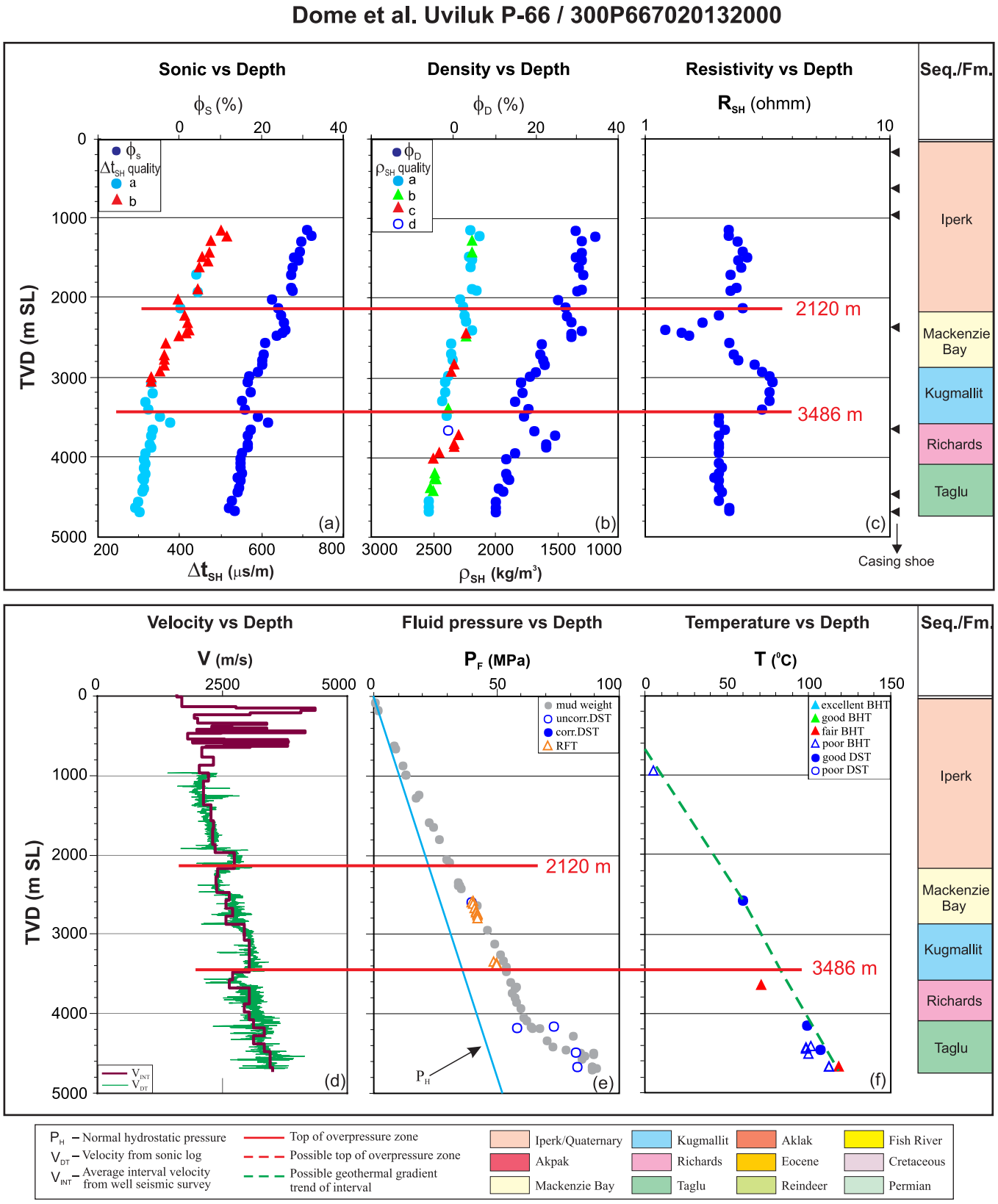

Figure A-47. Overpressure zones are detected with tops of OPZ at 2120 m (quality "a") and 3486 m (quality "a") by using the integrated analysis for the Uviluk P-66 well in the Beaufort-Mackenzie Basin. (a) shale sonic transit time (Δt_{SH}) and sonic porosity (ϕ_S) vs. depth; (b) shale bulk density (ρ_{SH}) and density porosity (ϕ_D) vs depth; (c) shale deep resistivity (R_{SH}) vs. depth; (d) continuous sonic velocity (V_{DT}) and average interval seismic velocity (V_{INT}) vs. depth; (e) fluid pressure (P_F) from well test and drilling mud weight vs. depth; and (f) borehole temperature vs. depth.

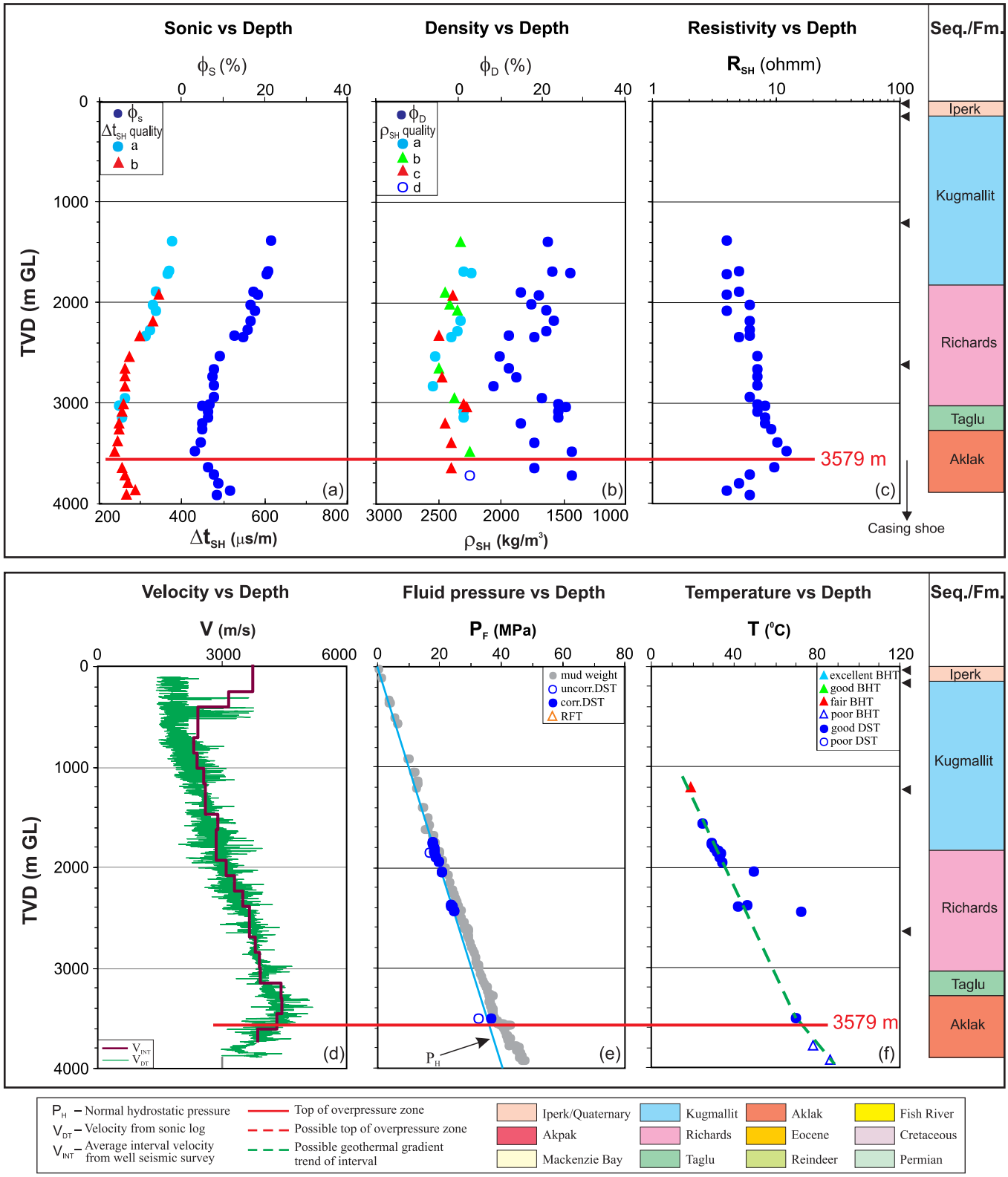

Figure A-48. Top of overpressure zone is detected at 3579 m with quality "a" by using the integrated analysis for the Ya Ya A-28 well in the Beaufort-Mackenzie Basin. (a) shale sonic transit time (Δt_{SH}) and sonic porosity (ϕ_S) vs. depth; (b) shale bulk density (ρ_{SH}) and density porosity (ϕ_D) vs depth; (c) shale deep resistivity (R_{SH}) vs. depth; (d) continuous sonic velocity (V_{DT}) and average interval seismic velocity (V_{INT}) vs. depth; (e) fluid pressure (P_F) from well test and drilling mud weight vs. depth; and (f) borehole temperature vs. depth.

Gulf et al. Aagnerk E-56 / 300E566950136450

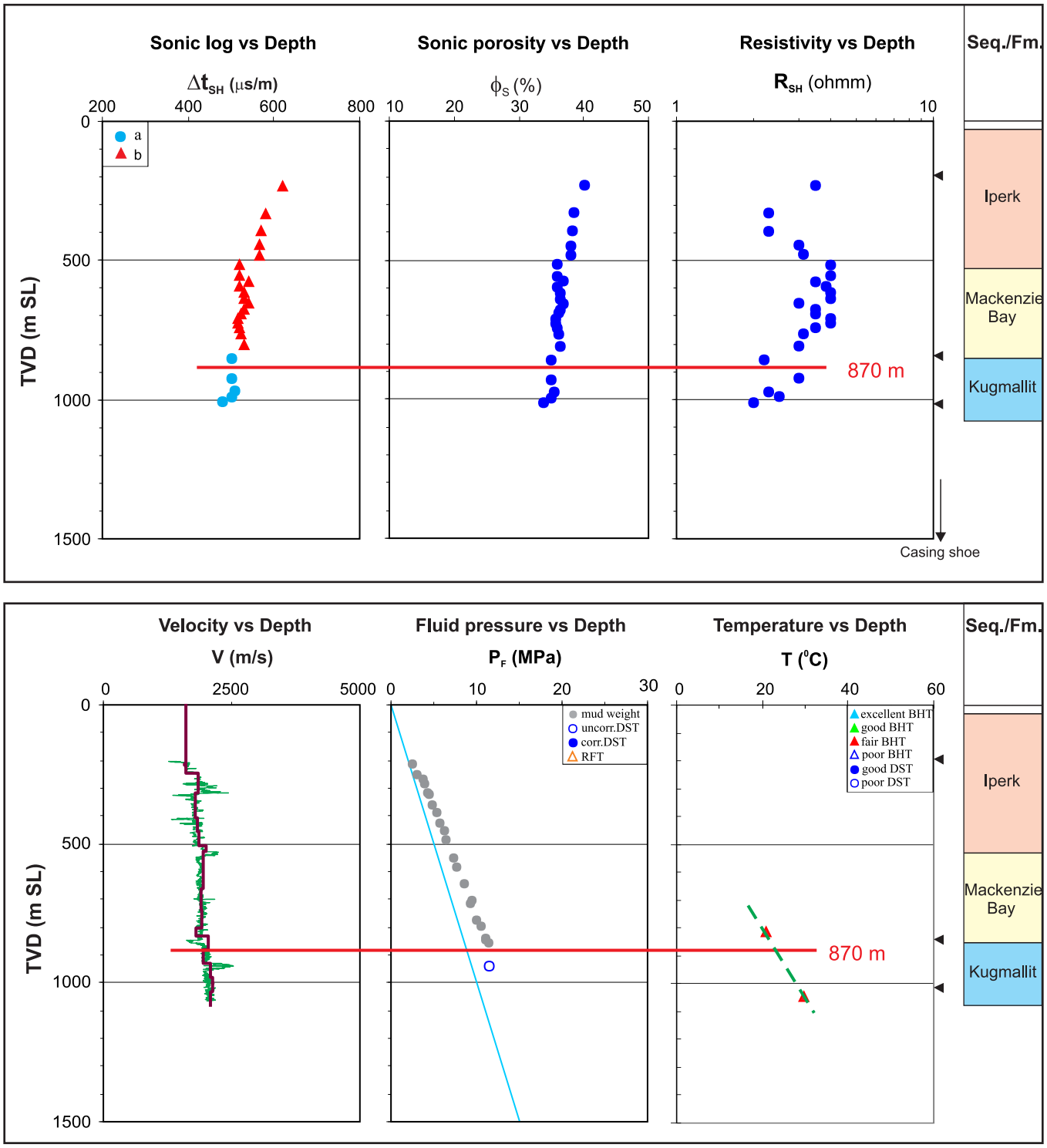

Figure B-1. Top of overpressure zone is marked at 870 m with quality "b" by using the integrated analysis for the Aagnerk E-56 well in the Beaufort-Mackenzie Basin. (a) shale sonic transit time (Δt_{SH}) vs. depth; (b) shale sonic porosity (ϕ_S) vs. depth; (c) shale deep resistivity (R_{SH}) vs. depth; (d) continuous sonic velocity (V_{DT}) and average interval seismic velocity (V_{INT}) vs. depth; (e) fluid pressure (P_F) from well test and drilling mud weight vs. depth; and (f) borehole temperature vs. depth.

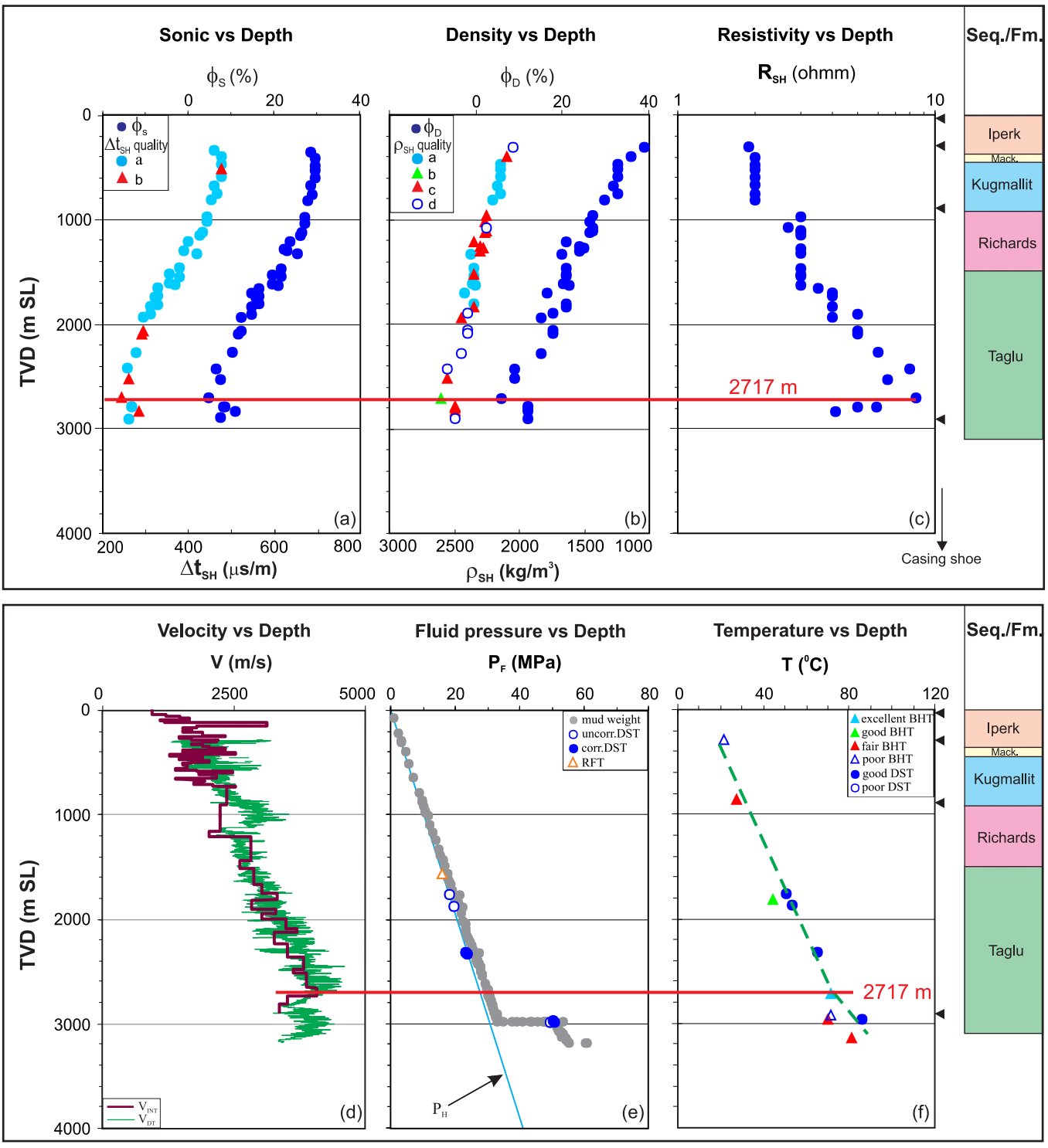

Figure B-2. Top of overpressure zone is detected at 2717 m with quality "b" by using the integrated analysis for the Adgo C-15 well in the Beaufort-Mackenzie Basin. (a) shale sonic transit time (Δt_{SH}) and sonic porosity (ϕ_S) vs. depth; (b) shale bulk density (ρ_{SH}) and density porosity (ϕ_D) vs depth; (c) shale deep resistivity (R_{SH}) vs. depth; (d) continuous sonic velocity (V_{DT}) and average interval seismic velocity (V_{INT}) vs. depth; (e) fluid pressure (P_F) from well test and drilling mud weight vs. depth; and (f) borehole temperature vs. depth. Mack. - Mackenzie Bay.

Imp. Adgo F-28 / 300F286930135450

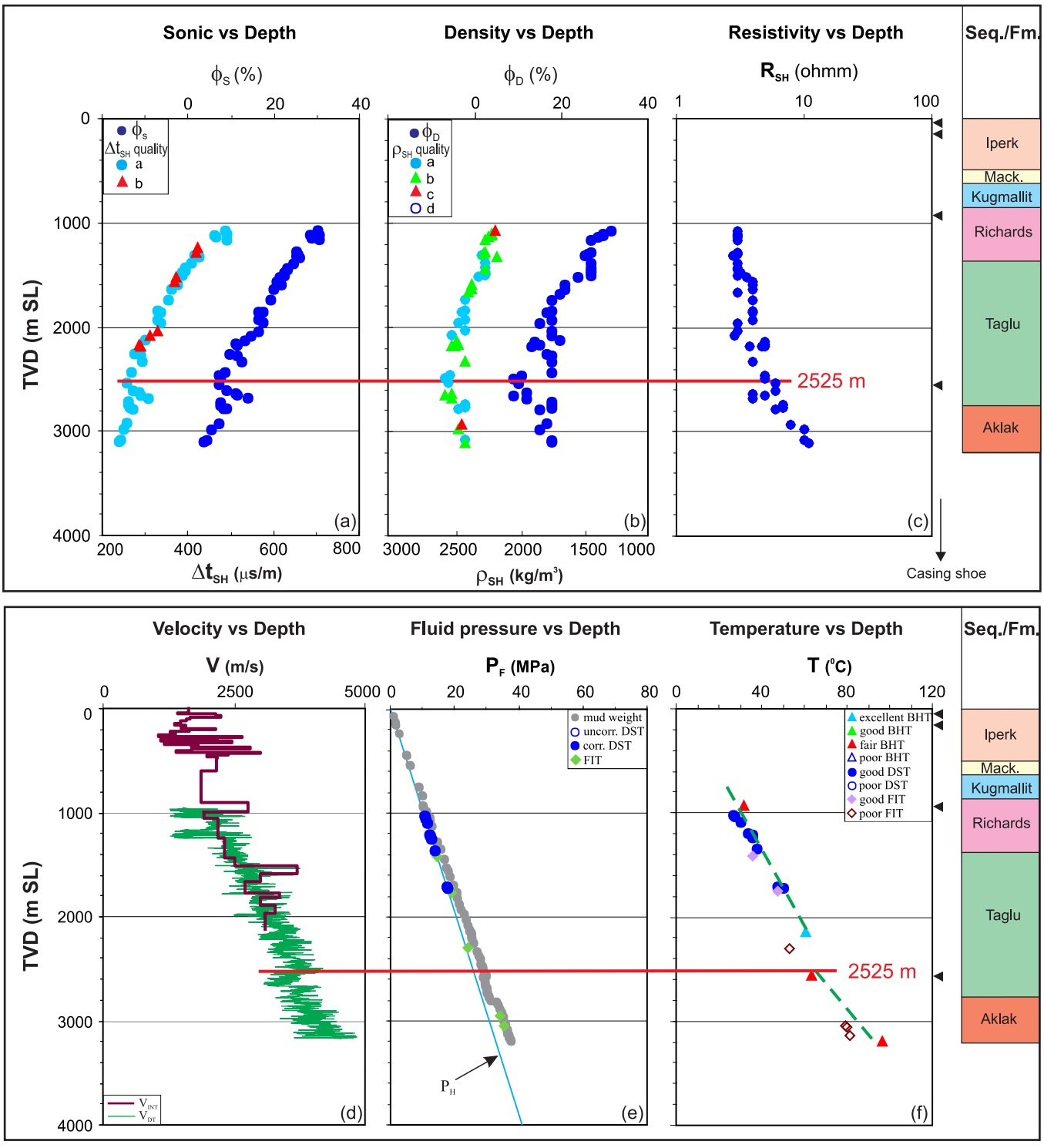

Figure B-3. Top of overpressure zone is detected at 2525 m with quality "b" by using the integrated analysis for the Adgo F-28 well in the Beaufort-Mackenzie Basin. (a) shale sonic transit time (Δt_{SH}) and sonic porosity (ϕ_S) vs. depth; (b) shale bulk density (ρ_{SH}) and density porosity (ϕ_D) vs depth; (c) shale deep resistivity (R_{SH}) vs. depth; (d) continuous sonic velocity (V_{DT}) and average interval seismic velocity (V_{INT}) vs. depth; (e) fluid pressure (P_F) from well test and drilling mud weight vs. depth; and (f) borehole temperature vs. depth. Mack. - Mackenzie Bay.

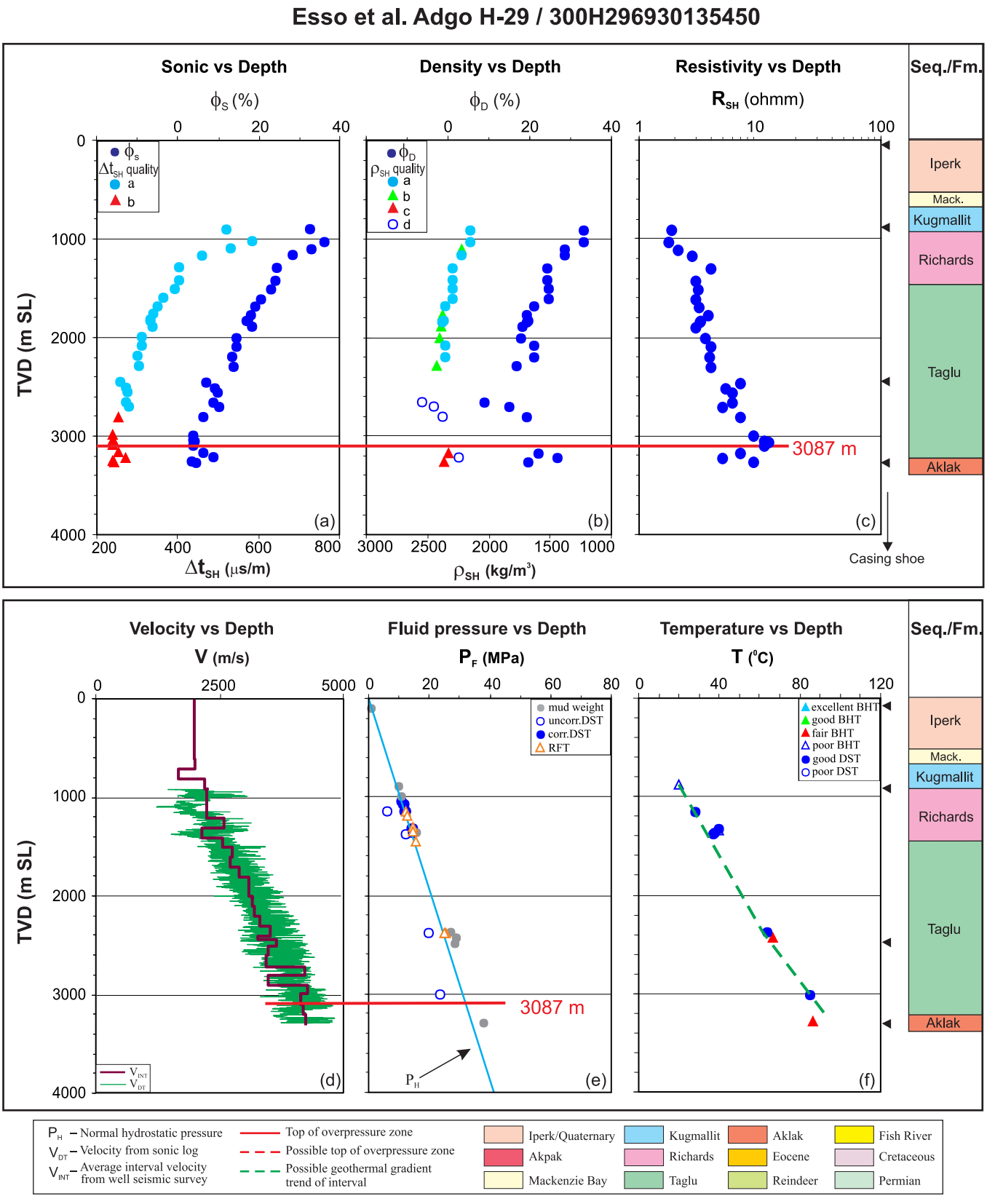

Figure B-4. Top of overpressure is detected at 3087 m with quality "b" by using the integrated analysis for the Adgo H-29 well in the Beaufort-Mackenzie Basin. (a) shale sonic transit time (Δt_{SH}) and sonic porosity (ϕ_S) vs. depth; (b) shale bulk density (ρ_{SH}) and density porosity (ϕ_D) vs depth; (c) shale deep resistivity (R_{SH}) vs. depth; (d) continuous sonic velocity (V_{DT}) and average interval seismic velocity (V_{INT}) vs. depth; (e) fluid pressure (P_F) from well test and drilling mud weight vs. depth; and (f) borehole temperature vs. depth. Mack. - Mackenzie Bay.

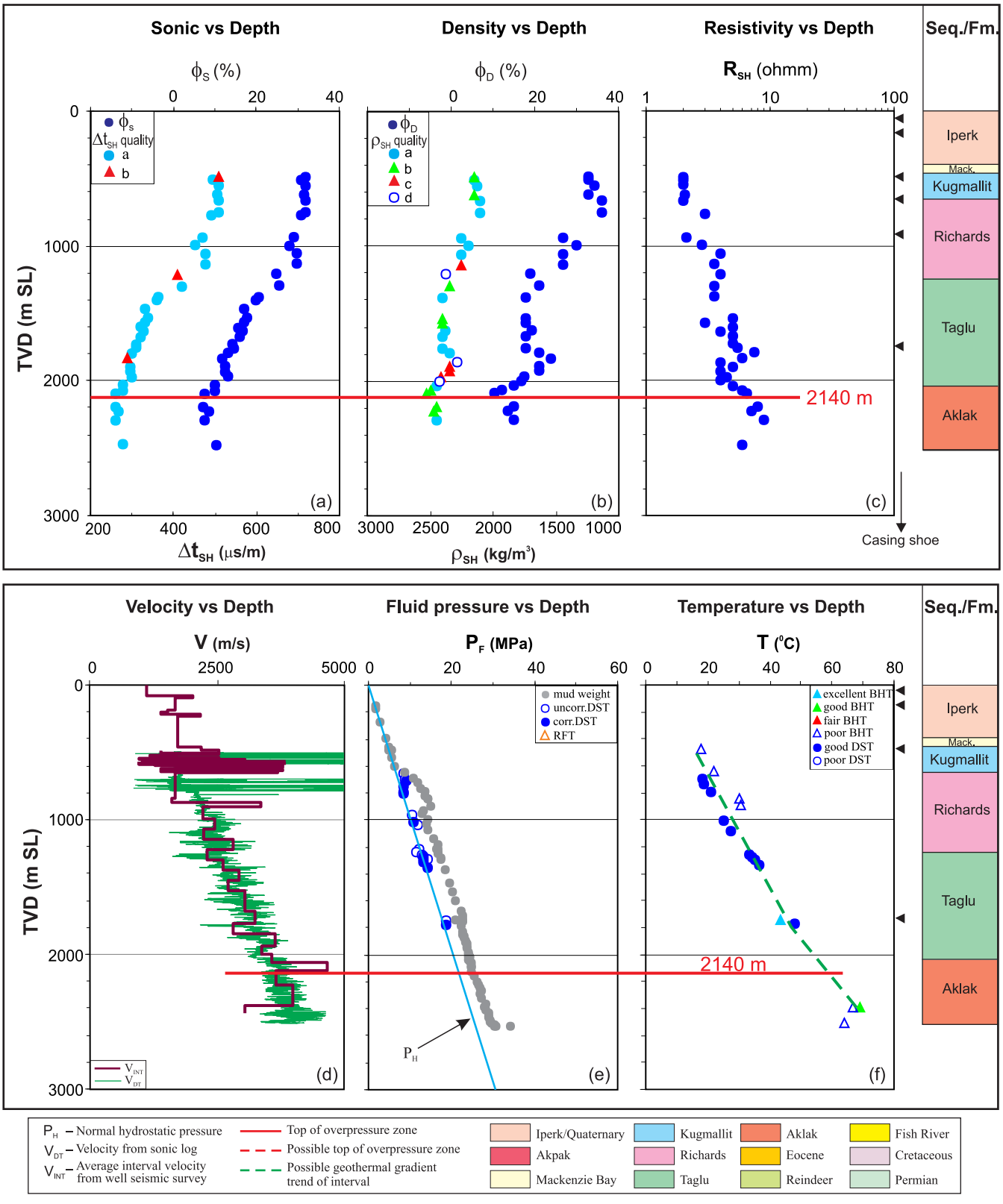

Figure B-5. Top of overpressure zone is detected at 2140 m with quality "b" for the Adgo P-25 well in the Beaufort-Mackenzie Basin. (a) shale sonic transit time (Δt_{SH}) and sonic porosity (ϕ_S) vs. depth; (b) shale bulk density (ρ_{SH}) and density porosity (ϕ_D) vs depth; (c) shale deep resistivity (R_{SH}) vs. depth; (d) continuous sonic velocity (V_{DT}) and average interval seismic velocity (V_{INT}) vs. depth; (e) fluid pressure (P_F) from well test and drilling mud weight vs. depth; and (f) borehole temperature vs. depth. Mack. - Mackenzie Bay.

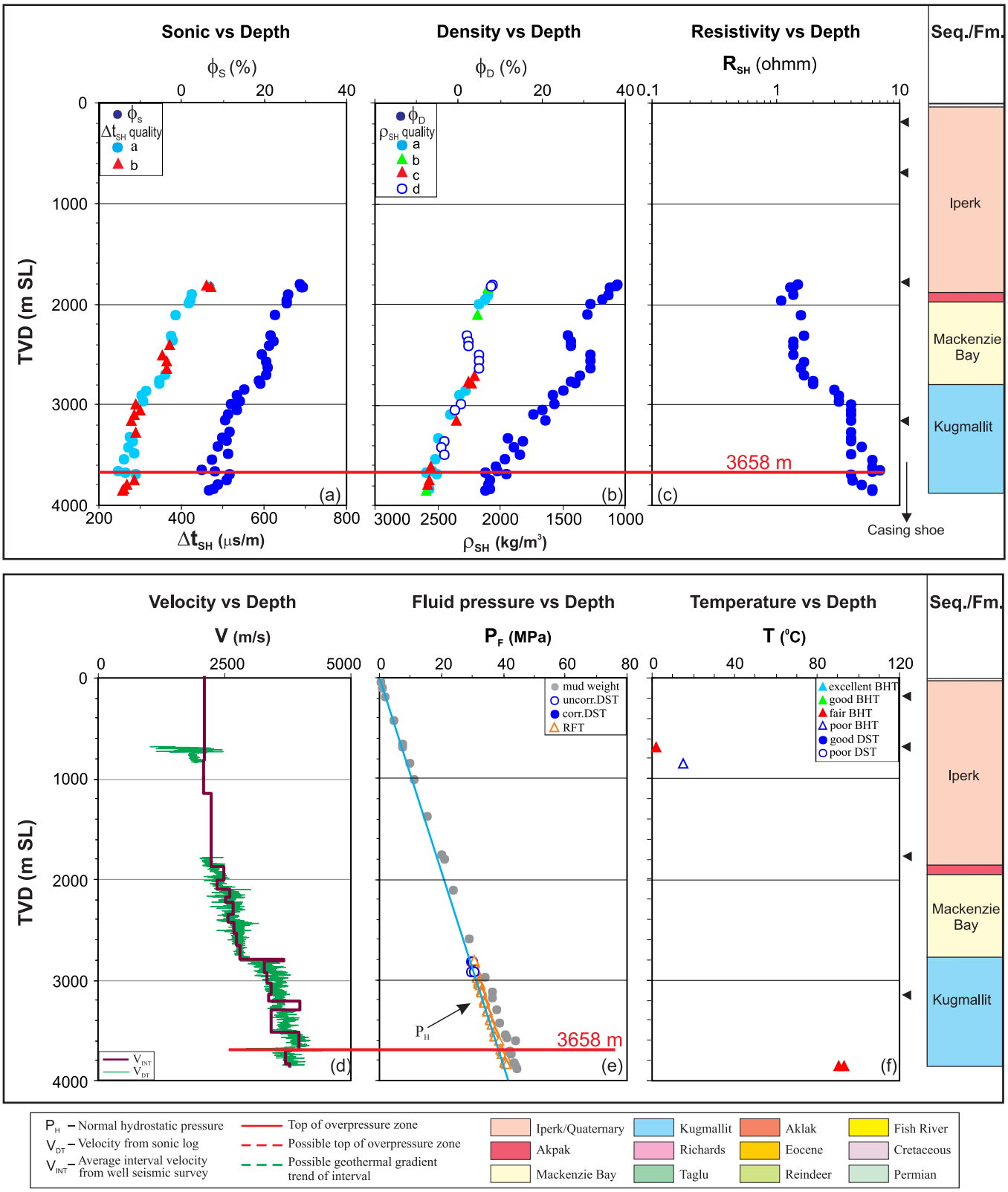

Figure B-6. Top of overpressure is detected at 3658 m with quality "b" by using the integrated analysis for the Amauligak O-86 well in the Beaufort-Mackenzie Basin. (a) shale sonic transit time (Δt_{SH}) and sonic porosity (ϕ_S) vs. depth; (b) shale bulk density (ρ_{SH}) and density porosity (ϕ_D) vs depth; (c) shale deep resistivity (R_{SH}) vs. depth; (d) continuous sonic velocity (V_{DT}) and average interval seismic velocity (V_{INT}) vs. depth; (e) fluid pressure (P_F) from well test and drilling mud weight vs. depth; and (f) borehole temperature vs. depth.

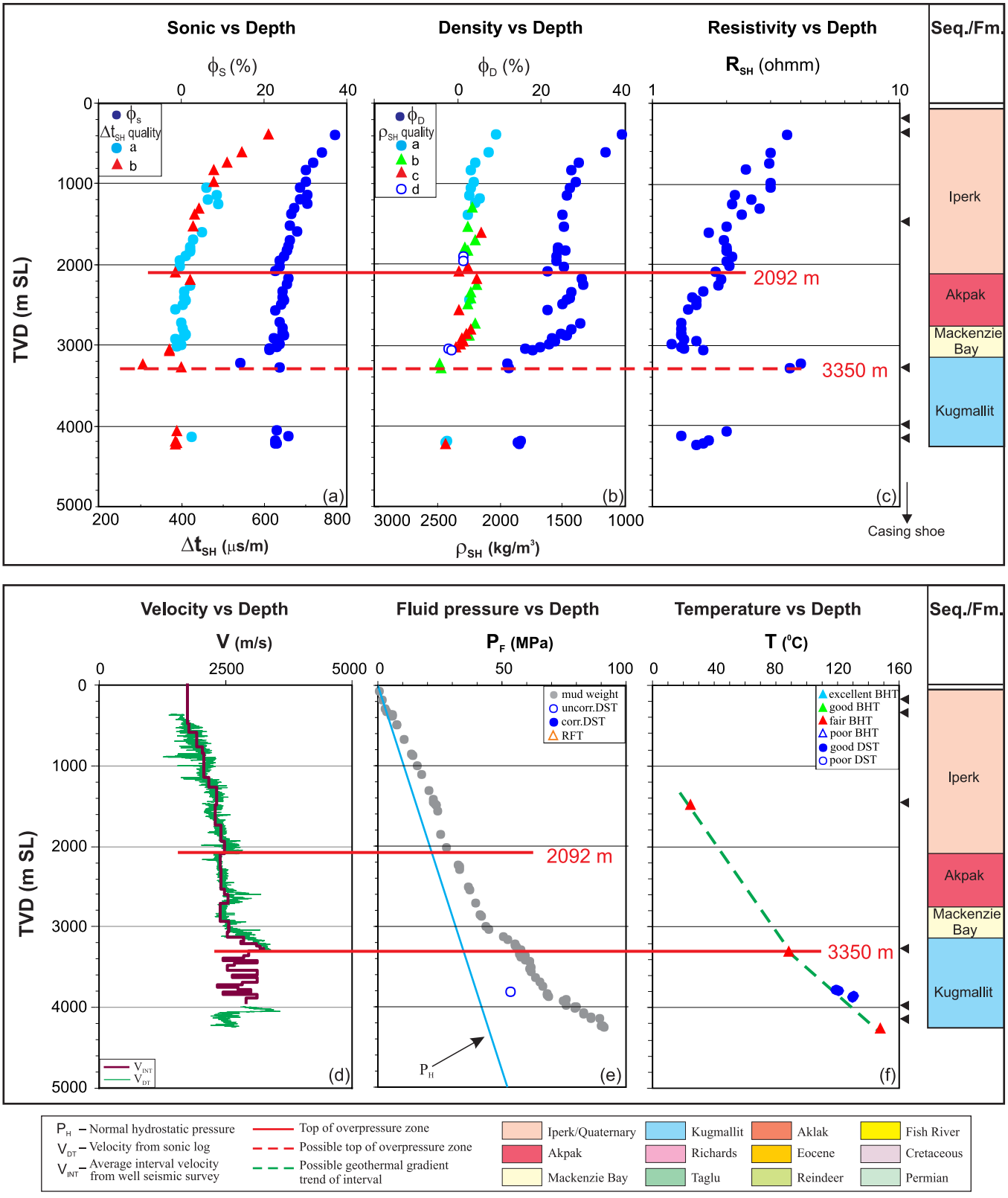

Figure B-7. Overpressure zones are detected with a top of OPZ of 2092 m (quality "b") and 3350 m (quality "b") for the Arluk E-90 well in the Beaufort-Mackenzie Basin by using the integrated analysis. (a) shale sonic transit time (Δt_{SH}) and sonic porosity (ϕ_S) vs. depth; (b) shale bulk density (ρ_{SH}) and density porosity (ϕ_D) vs depth; (c) shale deep resistivity (R_{SH}) vs. depth; (d) continuous sonic velocity (V_{DT}) and average interval seismic velocity (V_{INT}) vs. depth; (e) fluid pressure (P_F) from well test and drilling mud weight vs. depth; and (f) borehole temperature vs. depth.

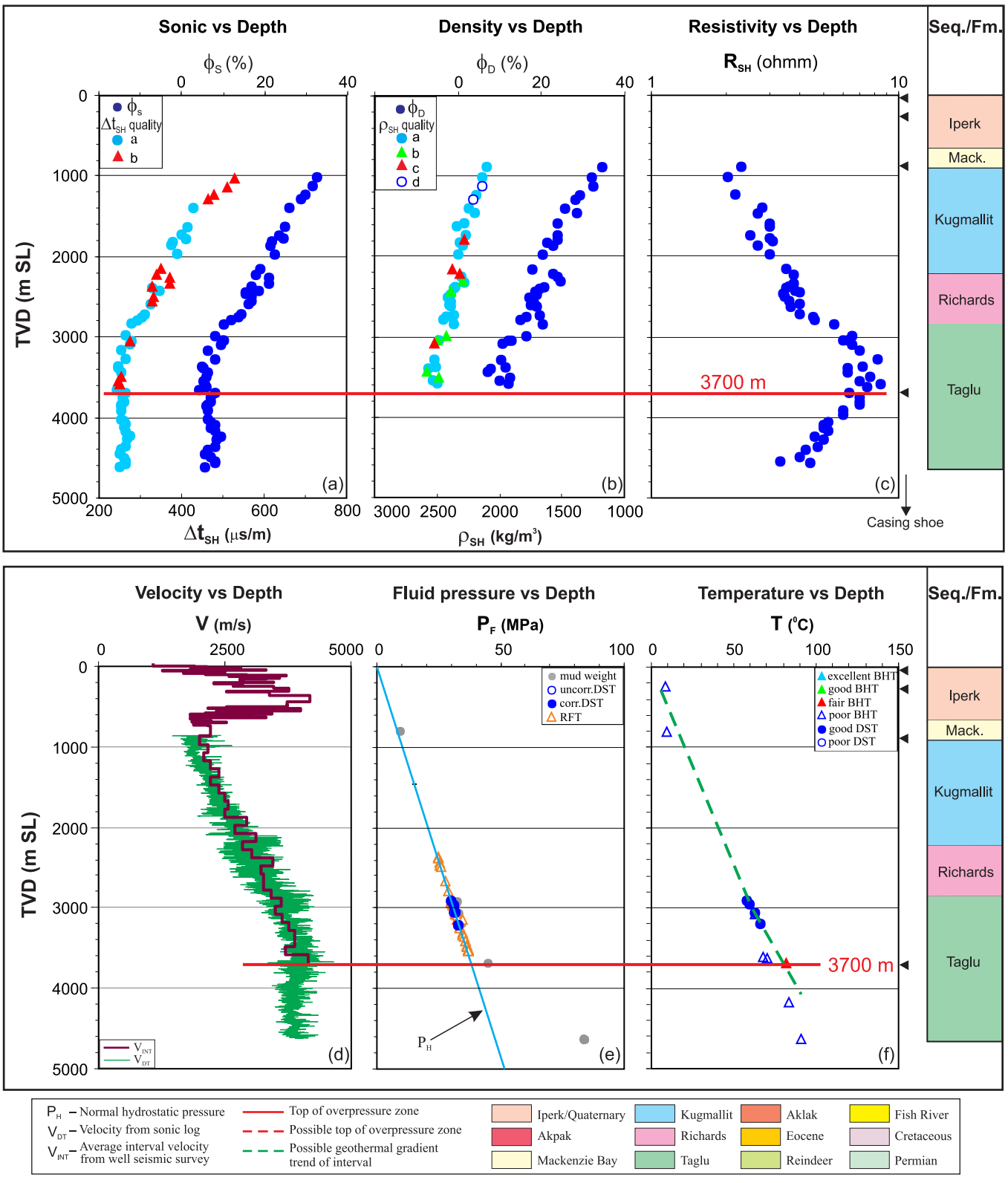

Figure B-8. Top of overpressure is detected at 3700 m with quality "b" by using the integrated analysis for the Arnak K-06 well in the Beaufort-Mackenzie Basin. (a) shale sonic transit time (Δt_{SH}) and sonic porosity (ϕ_S) vs. depth; (b) shale bulk density (ρ_{SH}) and density porosity (ϕ_D) vs depth; (c) shale deep resistivity (R_{SH}) vs. depth; (d) continuous sonic velocity (V_{DT}) and average interval seismic velocity (V_{INT}) vs. depth; (e) fluid pressure (P_F) from well test and drilling mud weight vs. depth; and (f) borehole temperature vs. depth. Mack. - Mackenzie Bay.

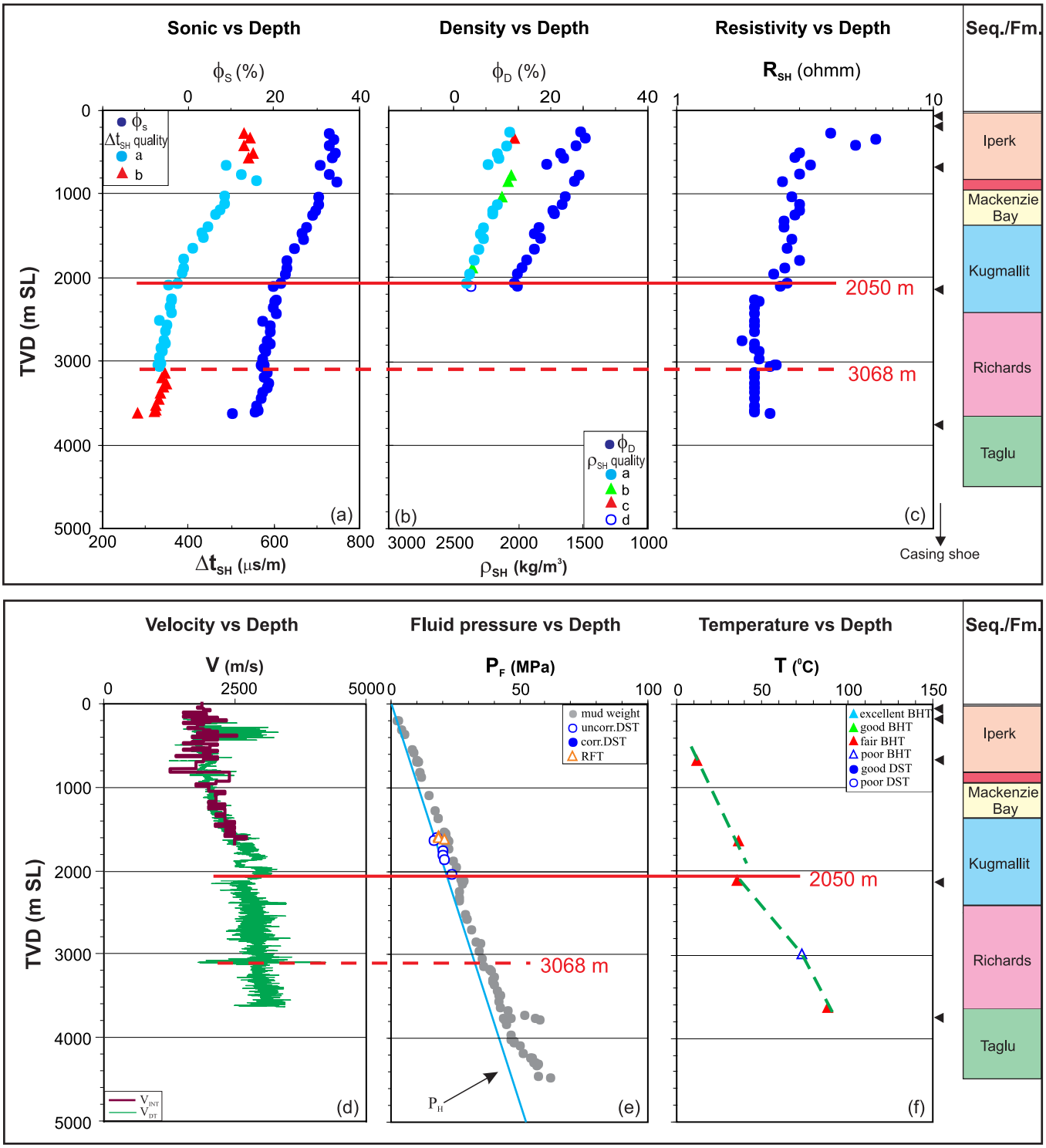

Figure B-9. Overpressure zones are detected by using the integrated analysis with a top of 2050 m and quality "b", and a top of 3068 m and quality "c" for the East Tarsiut N-44 well in the Beaufort-Mackenzie Basin. (a) shale sonic transit time (Δt_{SH}) and sonic porosity (ϕ_S) vs. depth; (b) shale bulk density (ρ_{SH}) and density porosity (ϕ_D) vs depth; (c) shale deep resistivity (R_{SH}) vs. depth; (d) continuous sonic velocity (V_{DT}) and average interval seismic velocity (V_{INT}) vs. depth; (e) fluid pressure (P_F) from well test and drilling mud weight vs. depth; and (f) borehole temperature vs. depth.

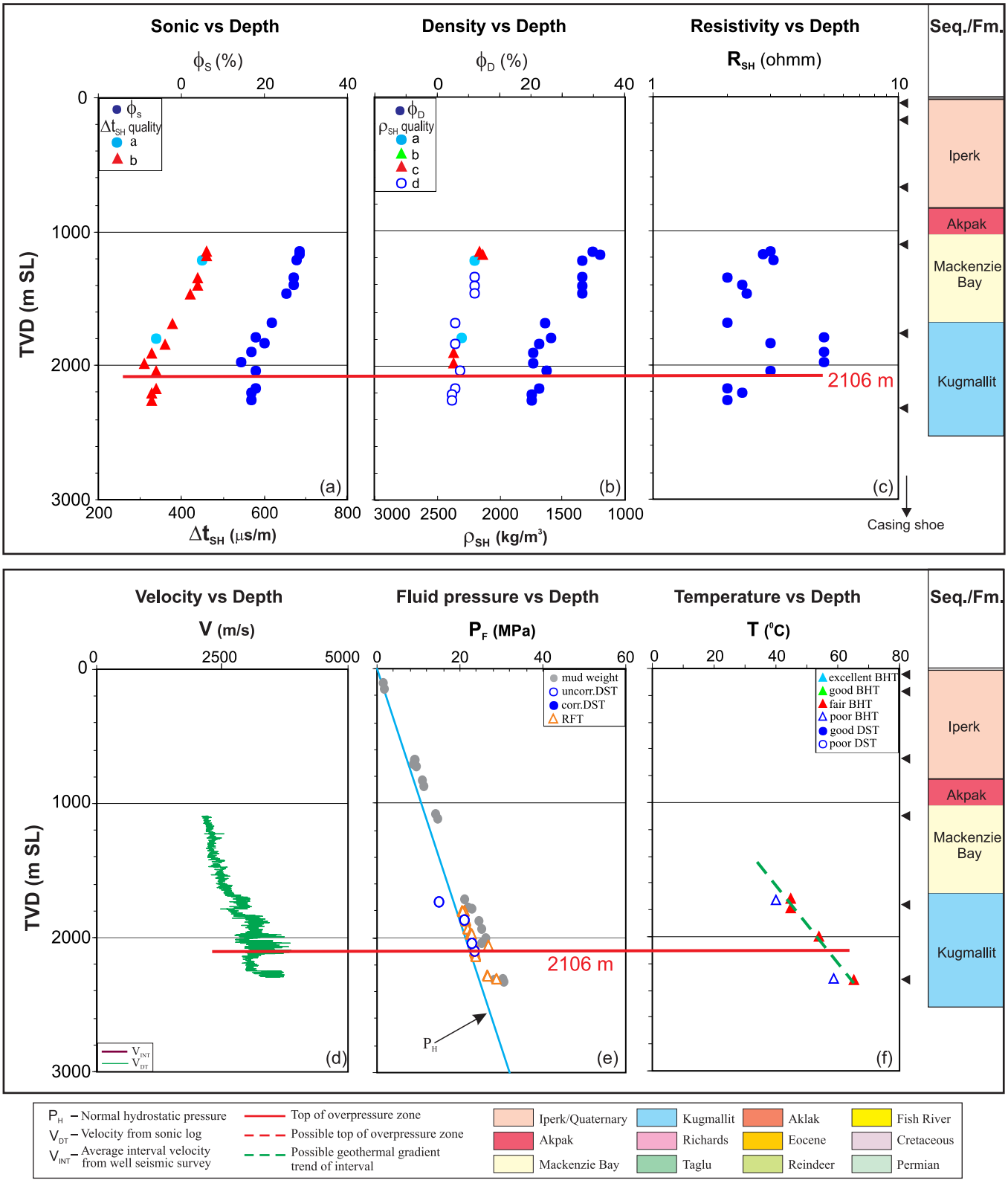

Figure B-10. Top of overpressure zone is detected at 2106 m with quality "b" by using the integrated analysis for the East Tarsiut N-44A well in the Beaufort-Mackenzie Basin. (a) shale sonic transit time (Δt_{SH}) and sonic porosity (ϕ_S) vs. depth; (b) shale bulk density (ρ_{SH}) and density porosity (ϕ_D) vs depth; (c) shale deep resistivity (R_{SH}) vs. depth; (d) continuous sonic velocity (V_{DT}) vs. depth; (e) fluid pressure (P_F) from well test and drilling mud weight vs. depth; and (f) borehole temperature vs. depth.

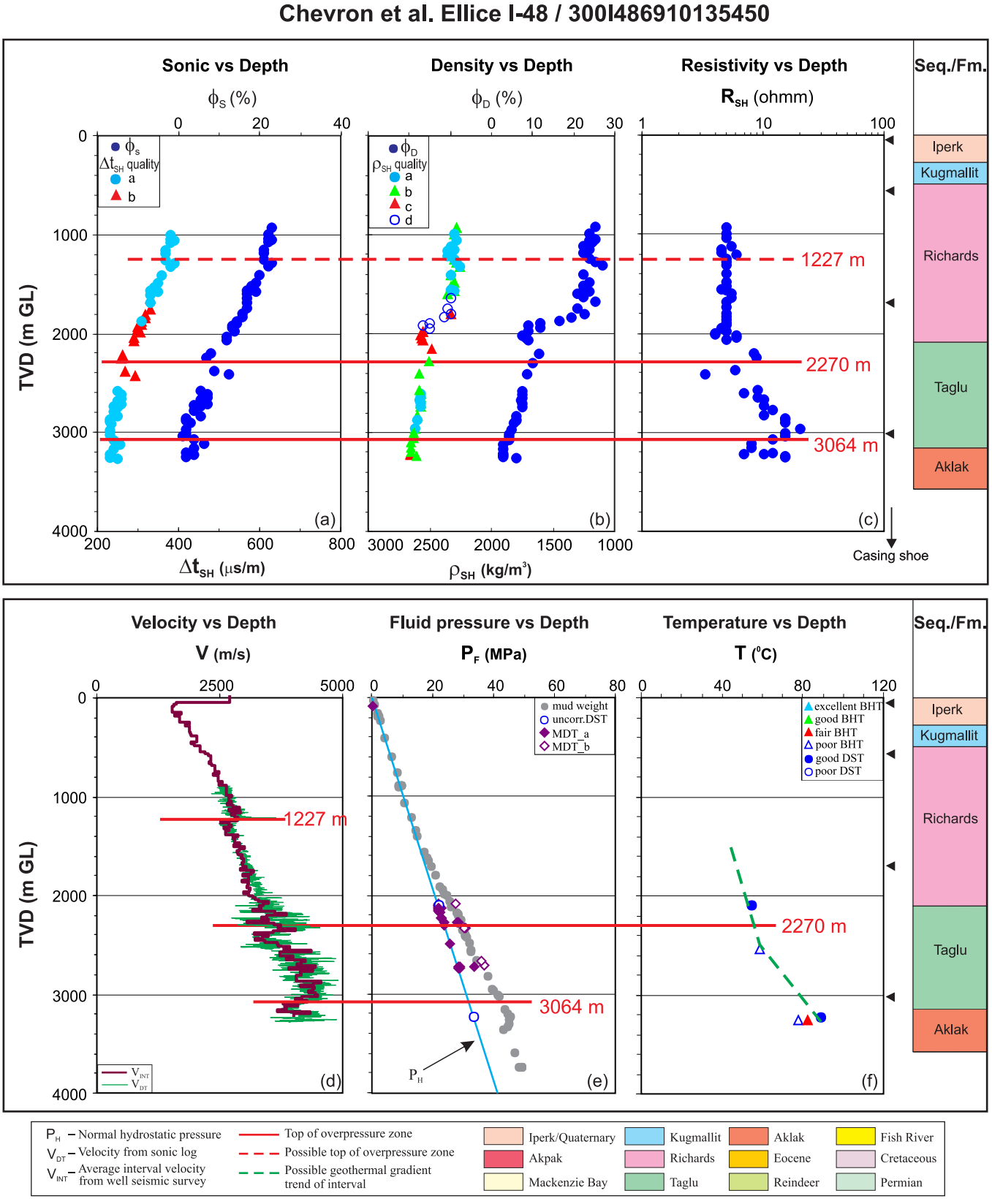

Figure B-11. Overpressure zones are detected by using the integrated analysis with quality "b" at 2270 m and 3064 m, and at 1227 m with quality "c" for the Ellice I-48 well in the Beaufort-Mackenzie Basin. (a) shale sonic transit time (Δt_{SH}) and sonic porosity (ϕ_S) vs. depth; (b) shale bulk density (ρ_{SH}) and density porosity (ϕ_D) vs depth; (c) shale deep resistivity (R_{SH}) vs. depth; (d) continuous sonic velocity (V_{DT}) and average interval seismic velocity (V_{INT}) vs. depth; (e) fluid pressure (P_F) from well test and drilling mud weight vs. depth; and (f) borehole temperature vs. depth.

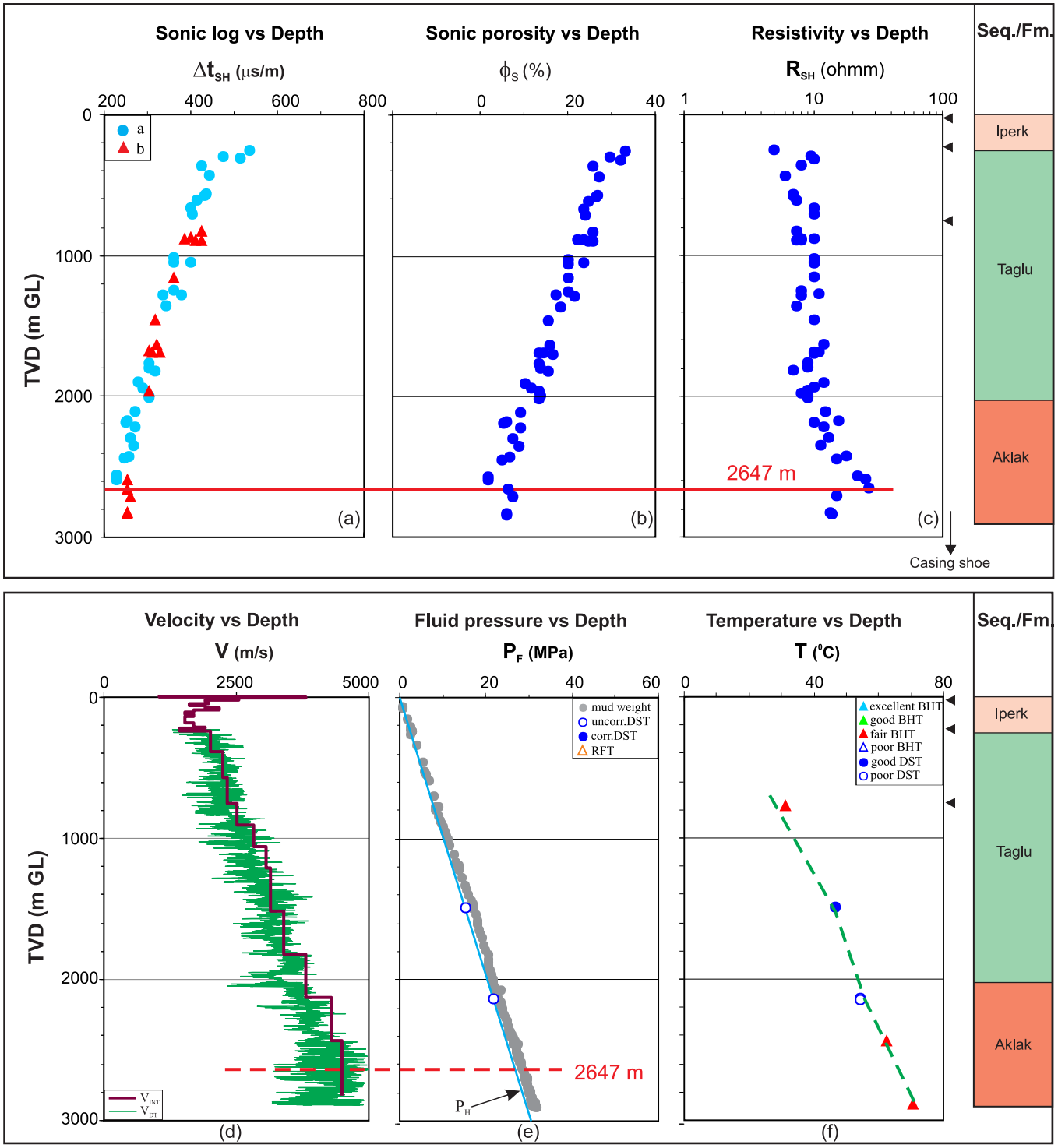

Figure B-12. Top of overpressure zone is detected at 2647 m with quality "b" by using the integrated analysis for the Ellice O-14 well in the Beaufort-Mackenzie Basin. (a) shale sonic transit time (Δt_{SH}) vs. depth; (b) shale sonic porosity (ϕ_S) vs. depth; (c) shale deep resistivity (R_{SH}) vs. depth; (d) continuous sonic velocity (V_{DT}) and average interval seismic velocity (V_{INT}) vs. depth; (e) fluid pressure (P_F) from well test and drilling mud weight vs. depth; and (f) borehole temperature vs. depth.

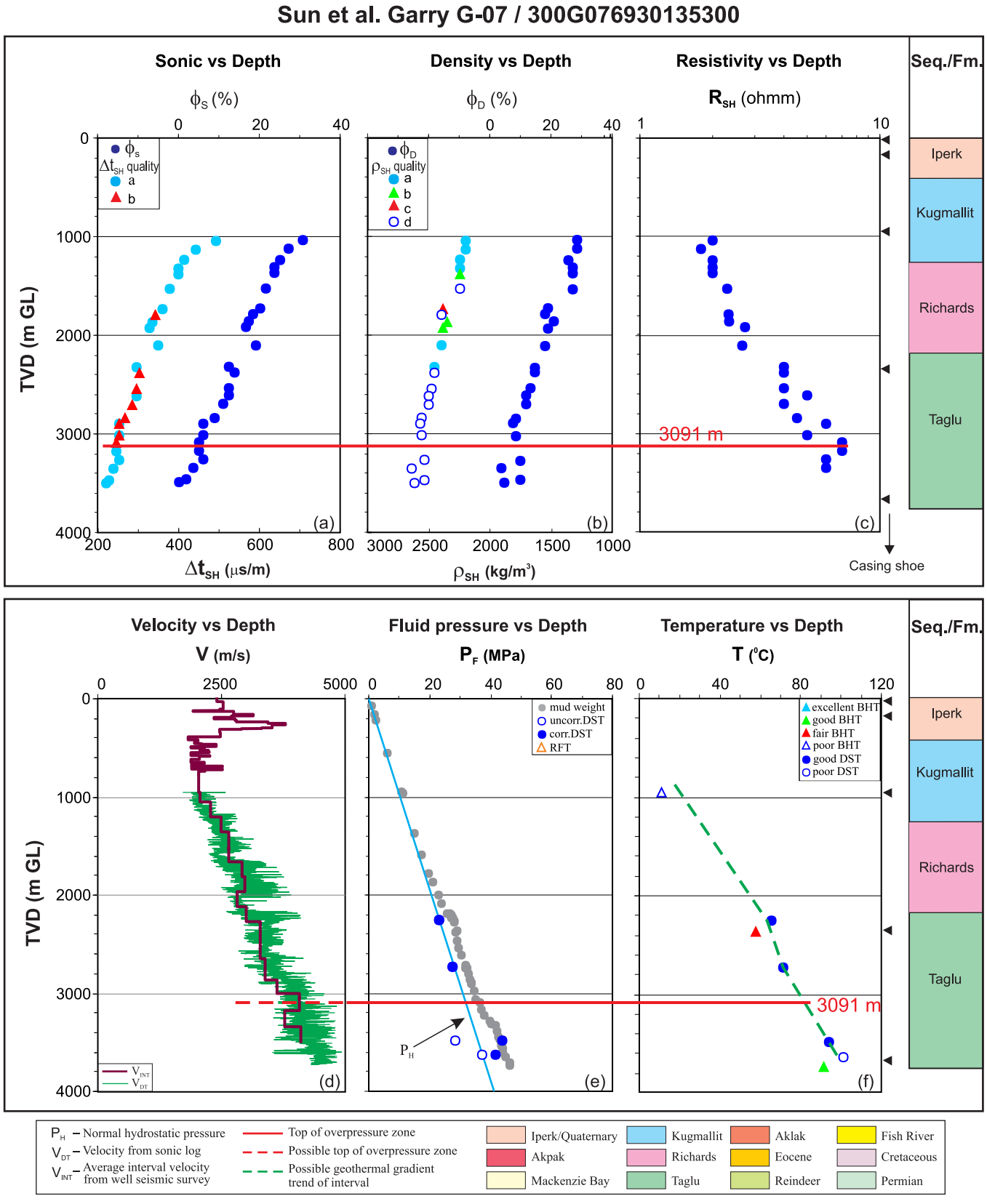

Figure B-13. Top of overpressure zone is detected at 3091 m with quality "b" by using the integrated analysis for the Garry G-07 well in the Beaufort-Mackenzie Basin. (a) shale sonic transit time (Δt_{SH}) and sonic porosity (ϕ_S) vs. depth; (b) shale bulk density (ρ_{SH}) and density porosity (ϕ_D) vs depth; (c) shale deep resistivity (R_{SH}) vs. depth; (d) continuous sonic velocity (V_{DT}) and average interval seismic velocity (V_{INT}) vs. depth; (e) fluid pressure (P_F) from well test and drilling mud weight vs. depth; and (f) borehole temperature vs. depth.

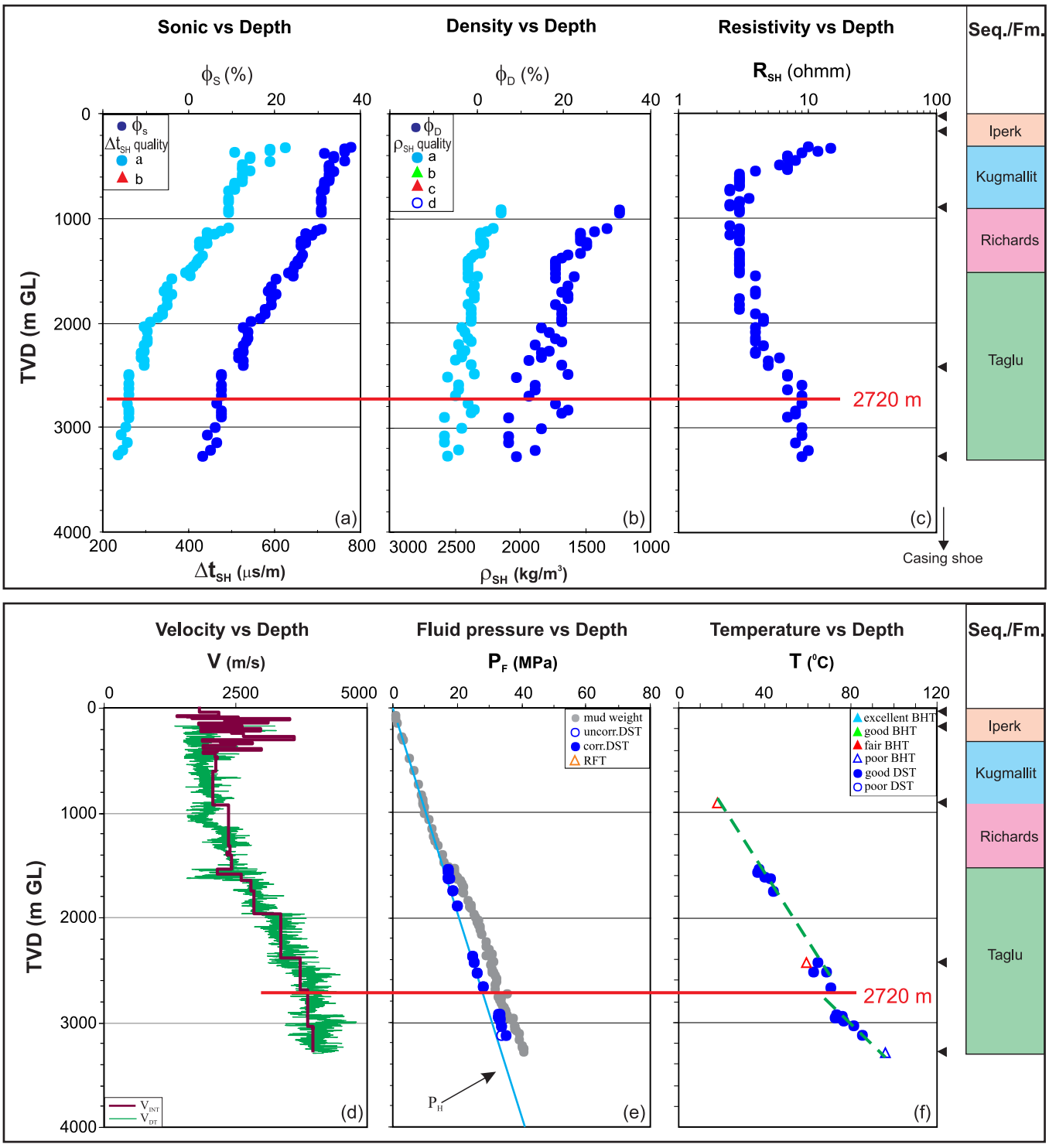

Figure B-14. Top of overpressure zone is detected at 2720 m with quality "b" by using the integrated analysis for the Garry P-04 well in the Beaufort-Mackenzie Basin. (a) shale sonic transit time (Δt_{SH}) and sonic porosity (ϕ_S) vs. depth; (b) shale bulk density (ρ_{SH}) and density porosity (ϕ_D) vs depth; (c) shale deep resistivity (R_{SH}) vs. depth; (d) continuous sonic velocity (V_{DT}) and average interval seismic velocity (V_{INT}) vs. depth; (e) fluid pressure (P_F) from well test and drilling mud weight vs. depth; and (f) borehole temperature vs. depth.

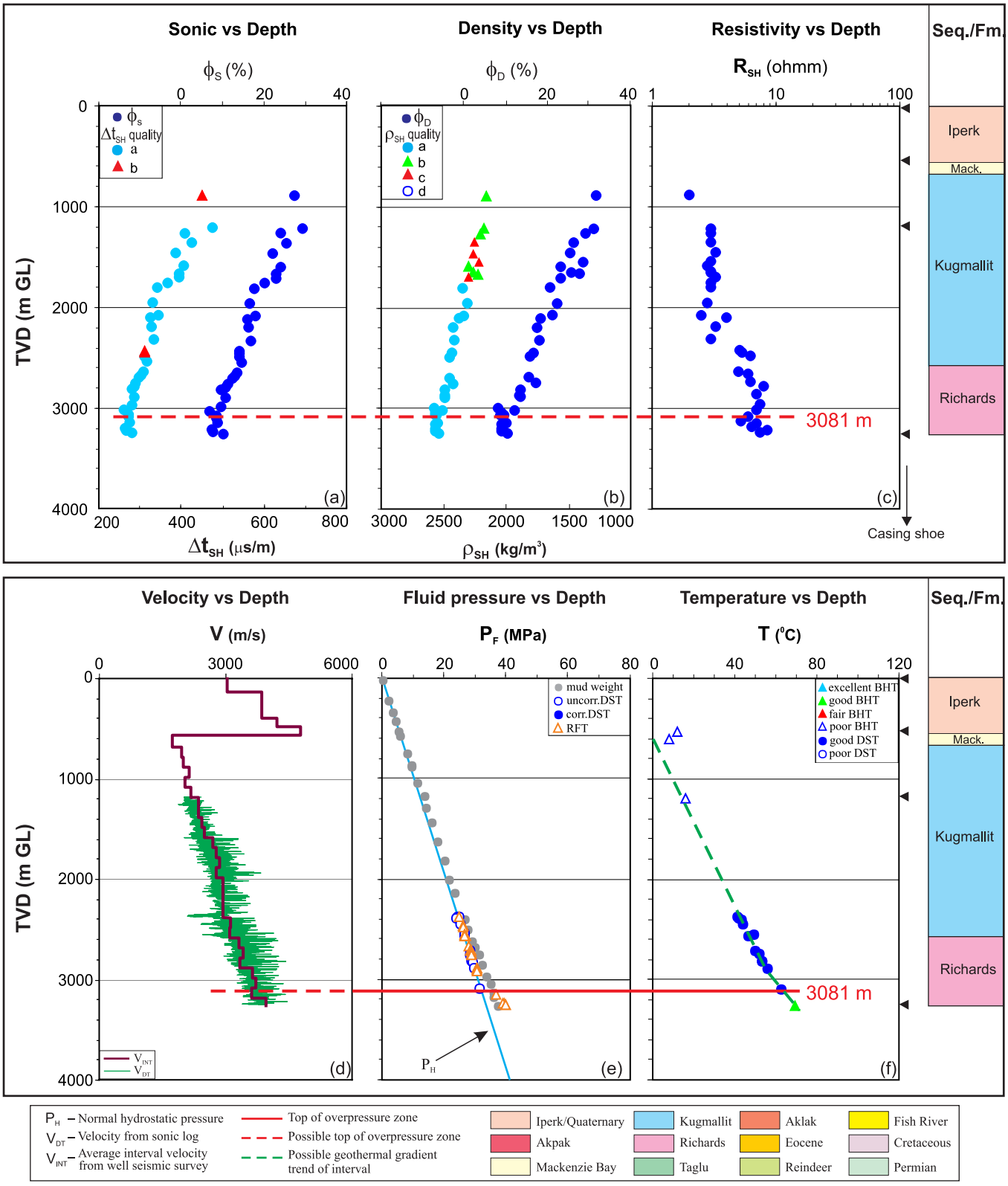

Figure B-15. Top of overpressure zone is detected at 3081 m with quality "b" by using the integrated analysis for the Hansen G-07 well in the Beaufort-Mackenzie Basin. (a) shale sonic transit time (Δt_{SH}) and sonic porosity (ϕ_S) vs. depth; (b) shale bulk density (ρ_{SH}) and density porosity (ϕ_D) vs depth; (c) shale deep resistivity (R_{SH}) vs. depth; (d) continuous sonic velocity (V_{DT}) and average interval seismic velocity (V_{INT}) vs. depth; (e) fluid pressure (P_F) from well test and drilling mud weight vs. depth; and (f) borehole temperature vs. depth. Mack. - Mackenzie Bay.

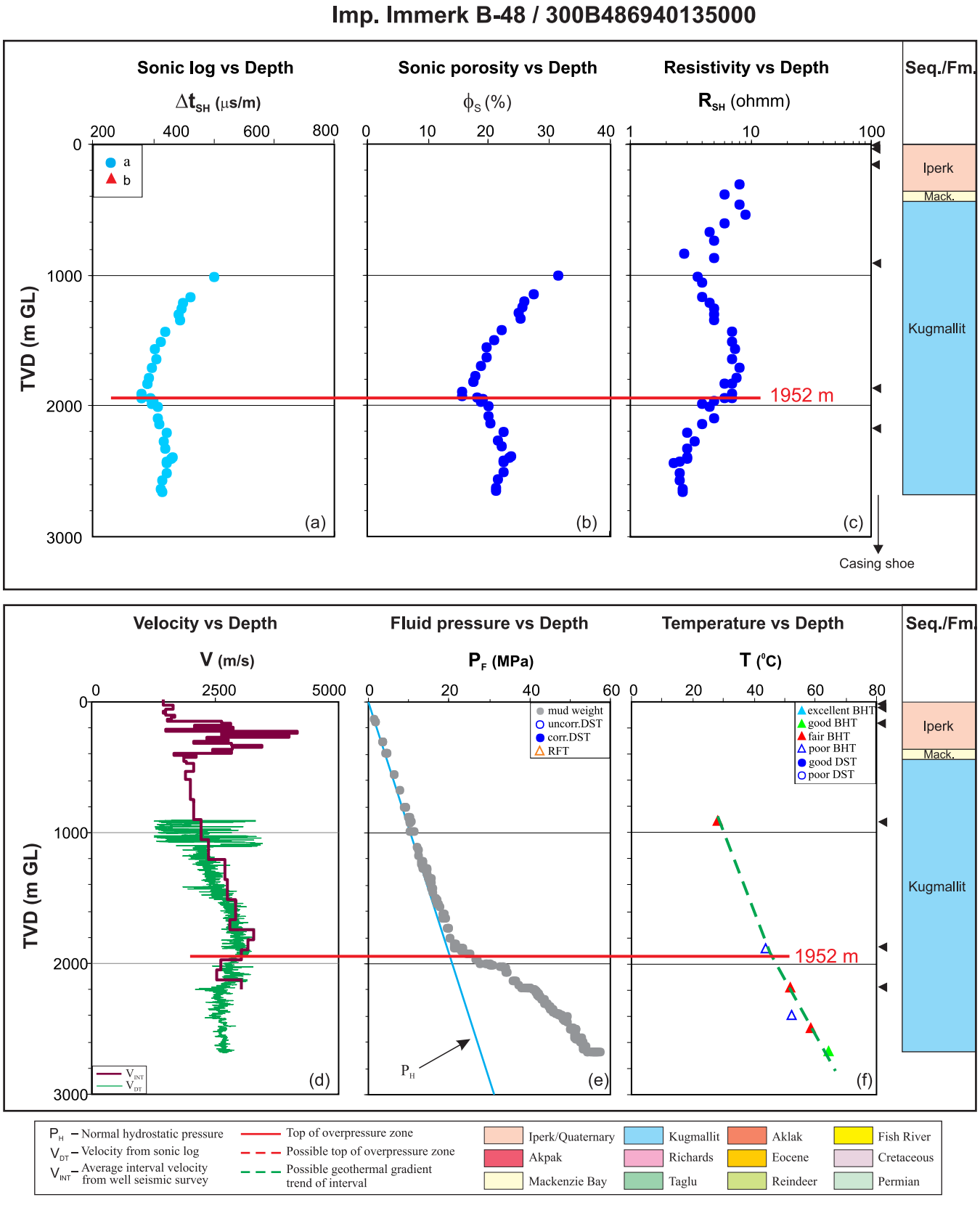

Figure B-16. Top of overpressure zone is detected at 1952 m with quality "b" by using the integrated analysis for the Immerk B-48 well in the Beaufort-Mackenzie Basin. (a) shale sonic transit time (Δt_{SH}) vs. depth; (b) shale sonic porosity (ϕ_S) vs depth; (c) shale deep resistivity (R_{SH}) vs. depth; (d) continuous sonic velocity (V_{DT}) and average interval seismic velocity (V_{INT}) vs. depth; (e) fluid pressure (P_F) from drilling mud weight vs. depth; and (f) borehole temperature vs. depth. Mack. - Mackenzie Bay.

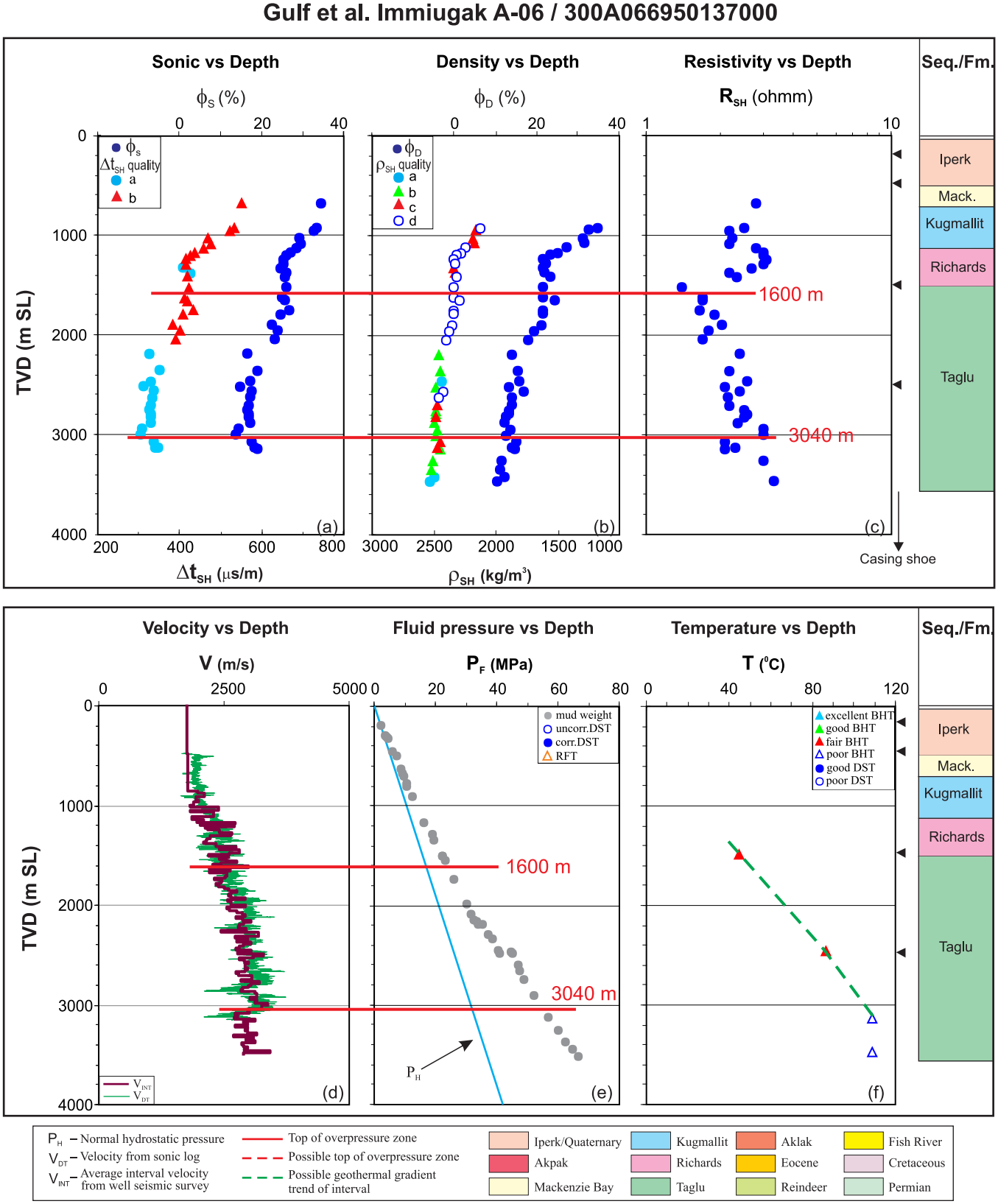

Figure B-17. Overpressure zones are detected with tops of OPZ at 1600 m (quality "c") and 3040 m (quality "b") by using the integrated analysis for the Immiugak A-06 well in the Beaufort-Mackenzie Basin. (a) shale sonic transit time (Δt_{SH}) and sonic porosity (ϕ_S) vs. depth; (b) shale bulk density (ρ_{SH}) and density porosity (ϕ_D) vs depth; (c) shale deep resistivity (R_{SH}) vs. depth; (d) continuous sonic velocity (V_{DT}) and average interval seismic velocity (V_{INT}) vs. depth; (e) fluid pressure (P_F) from well test and drilling mud weight vs. depth; and (f) borehole temperature vs. depth. Mack. - Mackenzie Bay.

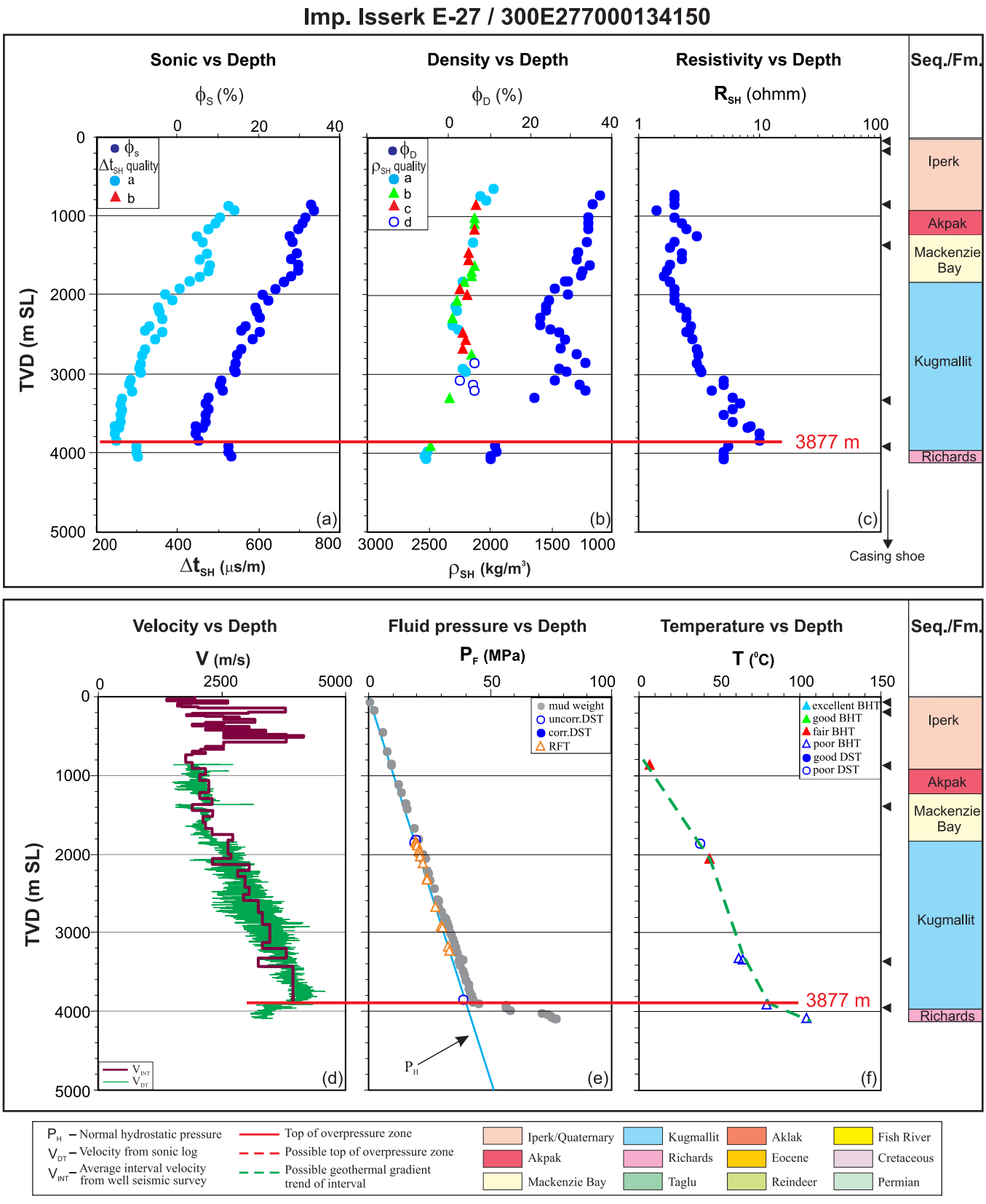

Figure B-18. Top of overpressure zone is detected at 3877 m with quality "b" by using the integrated analysis for the Isserk E-27 well in the Beaufort-Mackenzie Basin. (a) shale sonic transit time (Δt_{SH}) and sonic porosity (ϕ_S) vs. depth; (b) shale bulk density (ρ_{SH}) and density porosity (ϕ_D) vs depth; (c) shale deep resistivity (R_{SH}) vs. depth; (d) continuous sonic velocity (V_{DT}) and average interval seismic velocity (V_{INT}) vs. depth; (e) fluid pressure (P_F) from well test and drilling mud weight vs. depth; and (f) borehole temperature vs. depth.

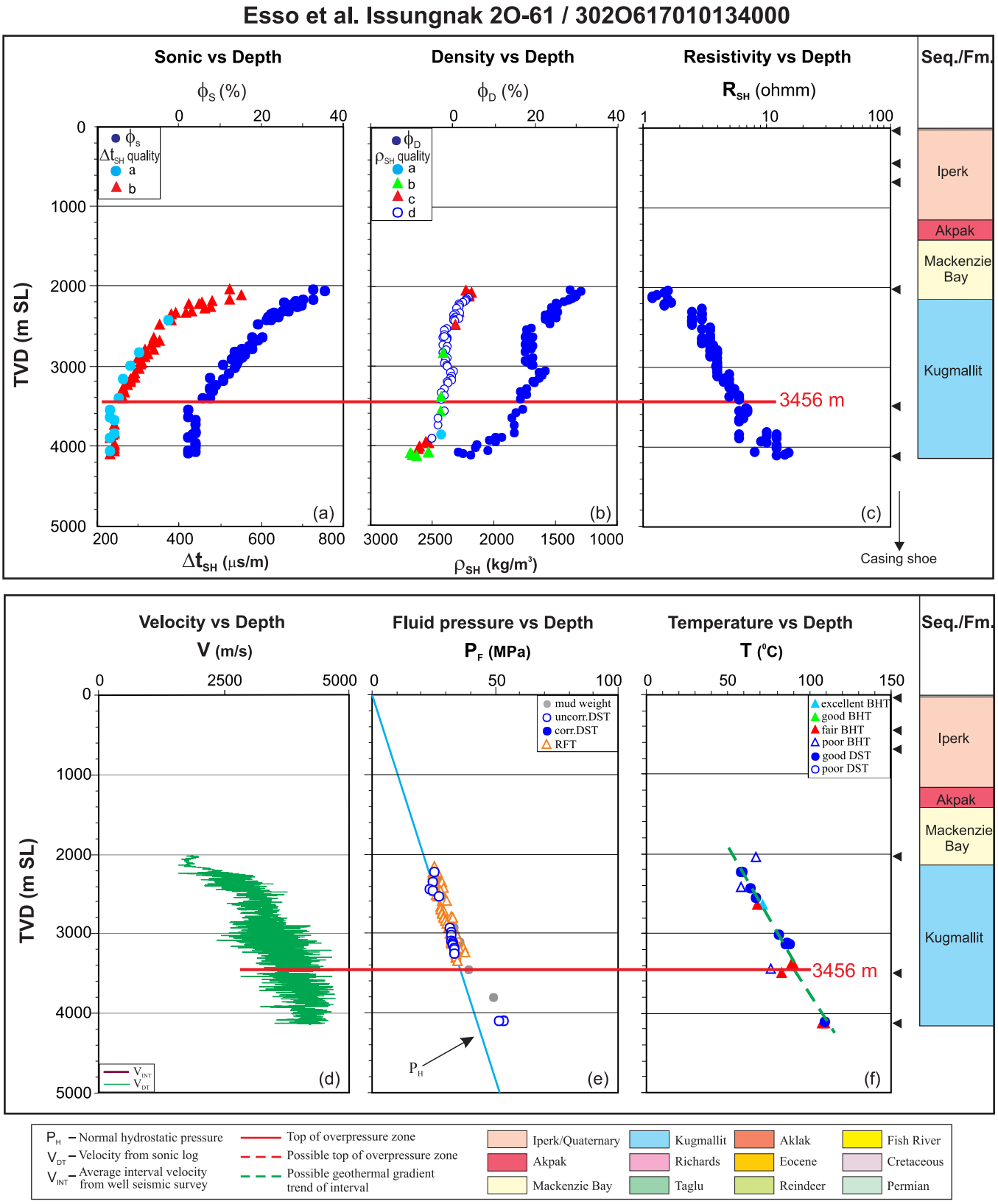

Figure B-19. Top of overpressure zone is detected at 3456 m with quality "b" by using the integrated analysis for the Issungnak 2O-61 well in the Beaufort-Mackenzie Basin. (a) shale sonic transit time (Δt_{SH}) and sonic porosity (ϕ_S) vs. depth; (b) shale bulk density (ρ_{SH}) and density porosity (ϕ_D) vs depth; (c) shale deep resistivity (R_{SH}) vs. depth; (d) continuous sonic velocity (V_{DT}) and average interval seismic velocity (V_{INT}) vs. depth; (e) fluid pressure (P_F) from well test and drilling mud weight vs. depth; and (f) borehole temperature vs. depth.

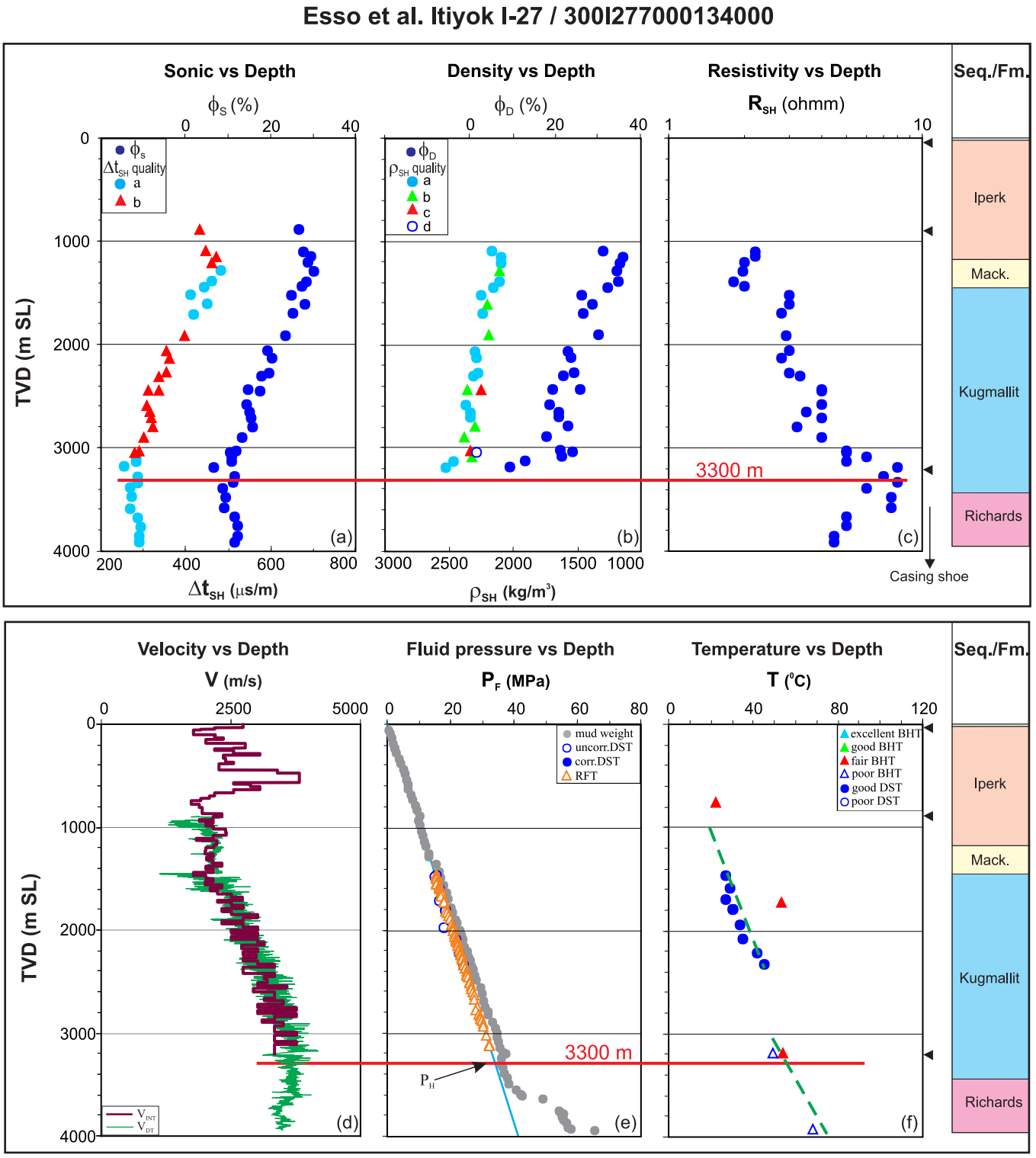

Figure B-20. Top of overpressure zone is detected at 3300 m with quality "b" by using the integrated analysis for the Itiyok I-27 well in the Beaufort-Mackenzie Basin. (a) shale sonic transit time (Δt_{SH}) and sonic porosity (ϕ_S) vs. depth; (b) shale bulk density (ρ_{SH}) and density porosity (ϕ_D) vs depth; (c) shale deep resistivity (R_{SH}) vs. depth; (d) continuous sonic velocity (V_{DT}) and average interval seismic velocity (V_{INT}) vs. depth; (e) fluid pressure (P_F) from well test and drilling mud weight vs. depth; and (f) borehole temperature vs. depth. Mack. - Mackenzie Bay.

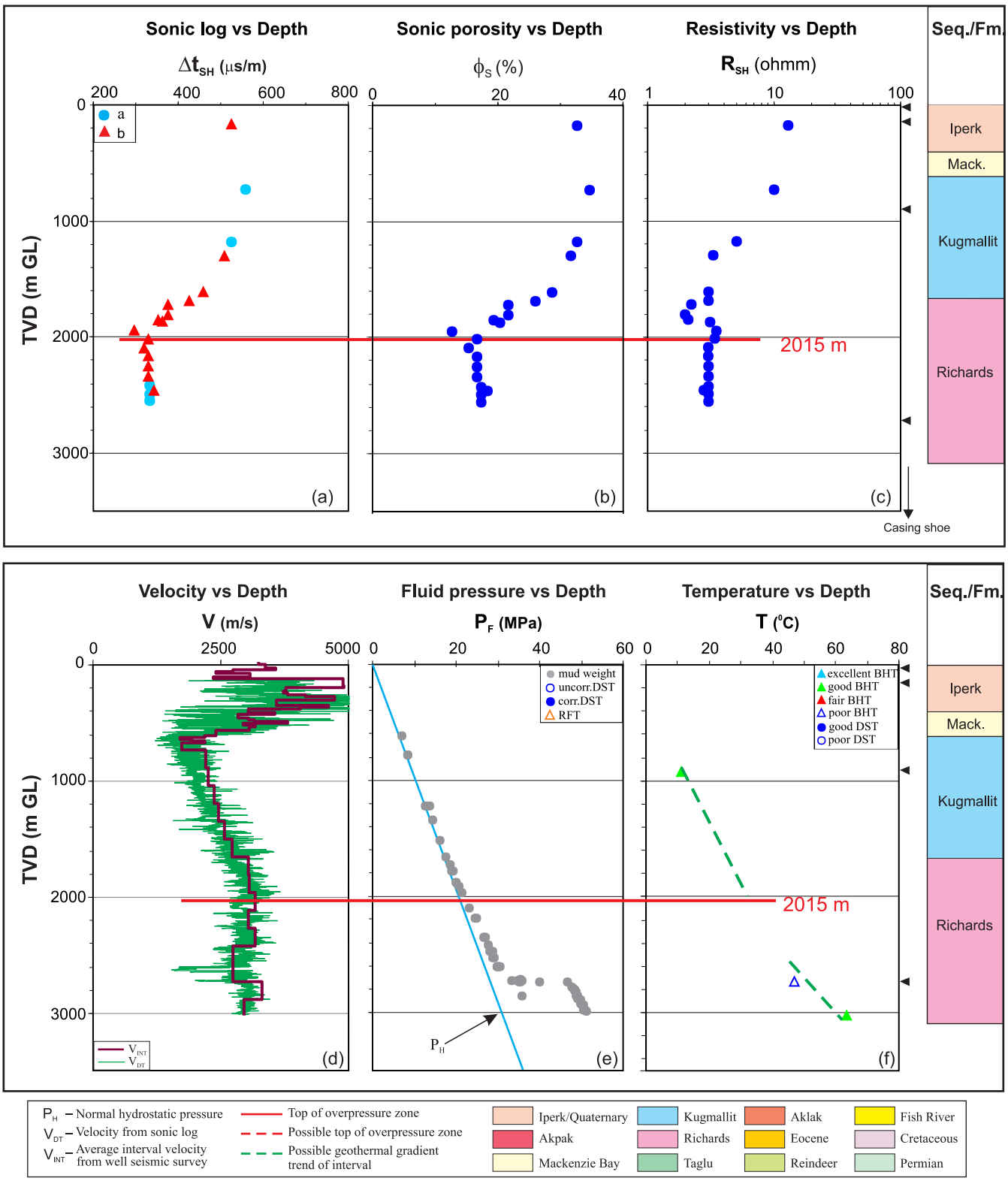

Figure B-21. Top of overpressure zone is detected at 2015 m with quality "b" by using the integrated analysis for the Ivik C-52 well in the Beaufort-Mackenzie Basin. (a) shale sonic transit time (Δt_{SH}) vs. depth; (b) shale sonic porosity (ϕ_S) vs. depth; (c) shale deep resistivity (R_{SH}) vs. depth; (d) continuous sonic velocity (V_{DT}) and average interval seismic velocity (V_{INT}) vs. depth; (e) fluid pressure (P_F) from drilling mud weight vs. depth; and (f) borehole temperature vs. depth. Mack. - Mackenzie Bay.

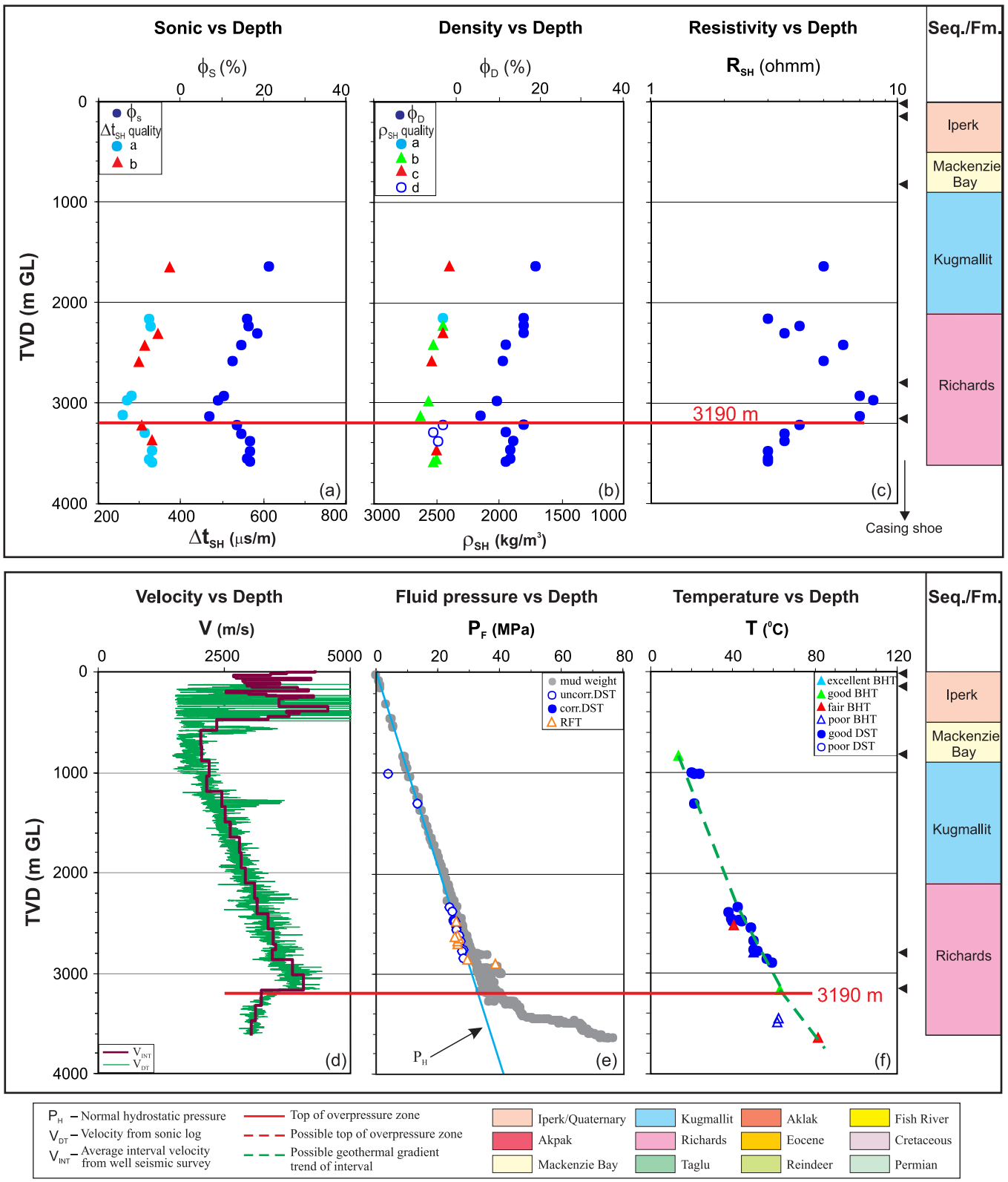

Figure B-22. Top of overpressure zone is detected at 3190 m with quality "b" by using the integrated analysis for the Ivik J-26 well in the Beaufort- Mackenzie Basin. (a) shale sonic transit time (Δt_{SH}) and sonic porosity (ϕ_S) vs. depth; (b) shale bulk density (ρ_{SH}) and density porosity (ϕ_D) vs depth; (c) shale deep resistivity (R_{SH}) vs. depth; (d) continuous sonic velocity (V_{DT}) and average interval seismic velocity (V_{INT}) vs. depth; (e) fluid pressure (P_F) from well test and drilling mud weight vs. depth; and (f) borehole temperature vs. depth.

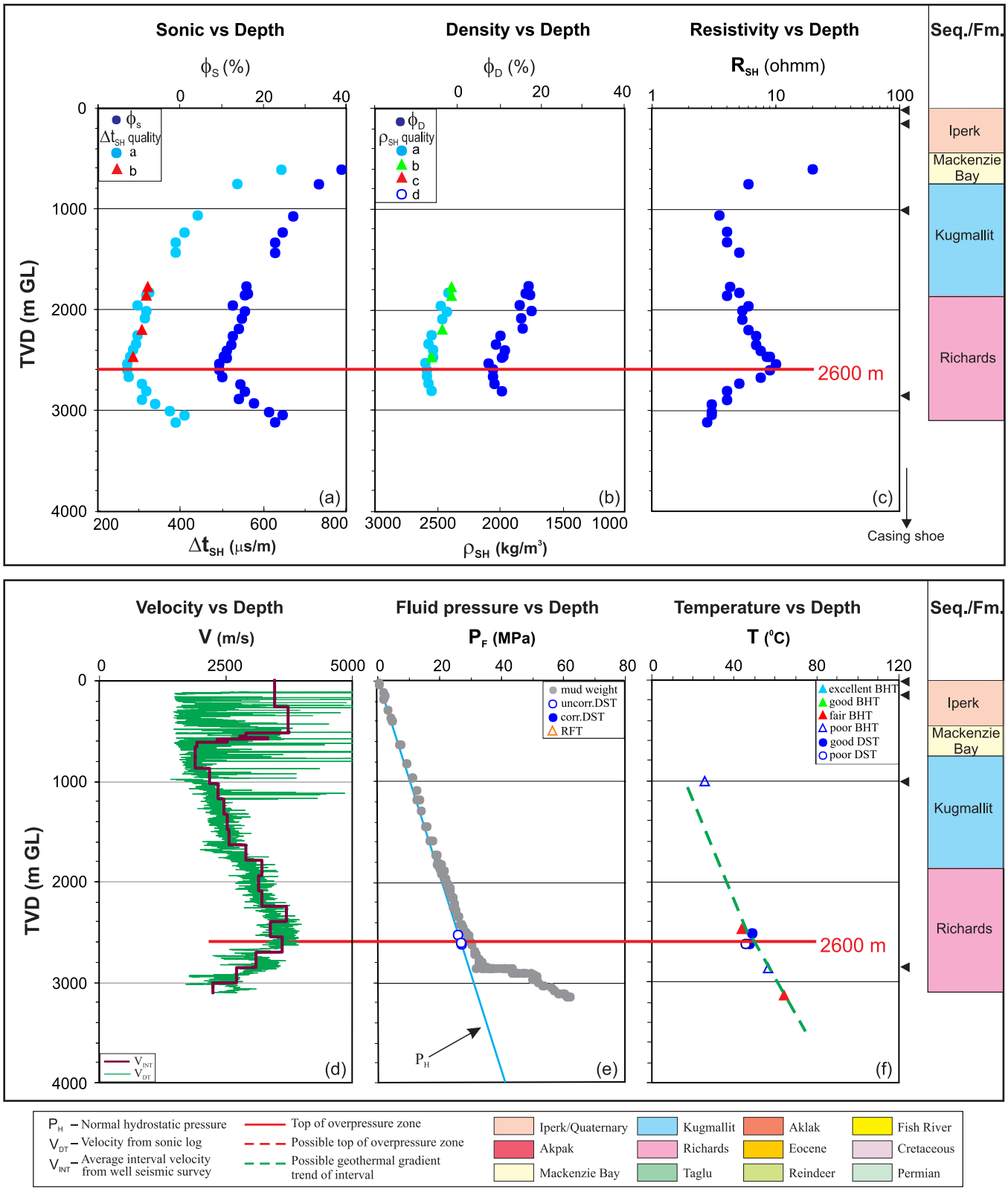

Figure B-23. Top of overpressure zone is detected at 2600 m with quality "b" by using the integrated analysis for the Ivik K-54 well in the Beaufort-Mackenzie Basin. (a) shale sonic transit time (Δt_{SH}) and sonic porosity (ϕ_S) vs. depth; (b) shale bulk density (ρ_{SH}) and density porosity (ϕ_D) vs depth; (c) shale deep resistivity (R_{SH}) vs. depth; (d) continuous sonic velocity (V_{DT}) and average interval seismic velocity (V_{INT}) vs. depth; (e) fluid pressure (P_F) from well test and drilling mud weight vs. depth; and (f) borehole temperature vs. depth.

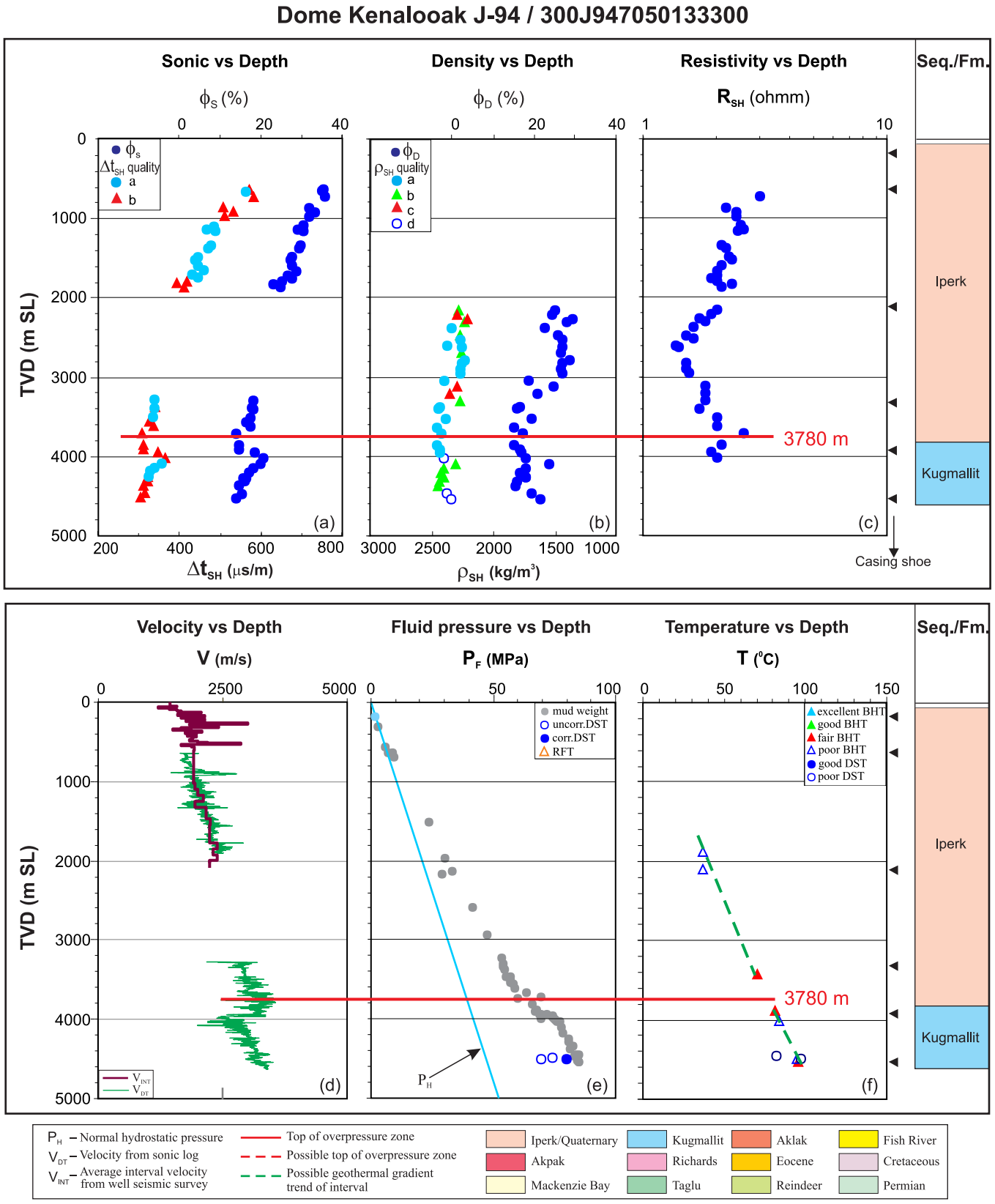

Figure B-24. Top of overpressure zone is detected at 3780 m with quality "b" by using the integrated analysis for the Kenalooak J-94 well in the Beaufort-Mackenzie Basin. (a) shale sonic transit time (Δt_{SH}) and sonic porosity (ϕ_S) vs. depth; (b) shale bulk density (ρ_{SH}) and density porosity (ϕ_D) vs depth; (c) shale deep resistivity (R_{SH}) vs. depth; (d) continuous sonic velocity (V_{DT}) and average interval seismic velocity (V_{INT}) vs. depth; (e) fluid pressure (P_F) from well test and drilling mud weight vs. depth; and (f) borehole temperature vs. depth.

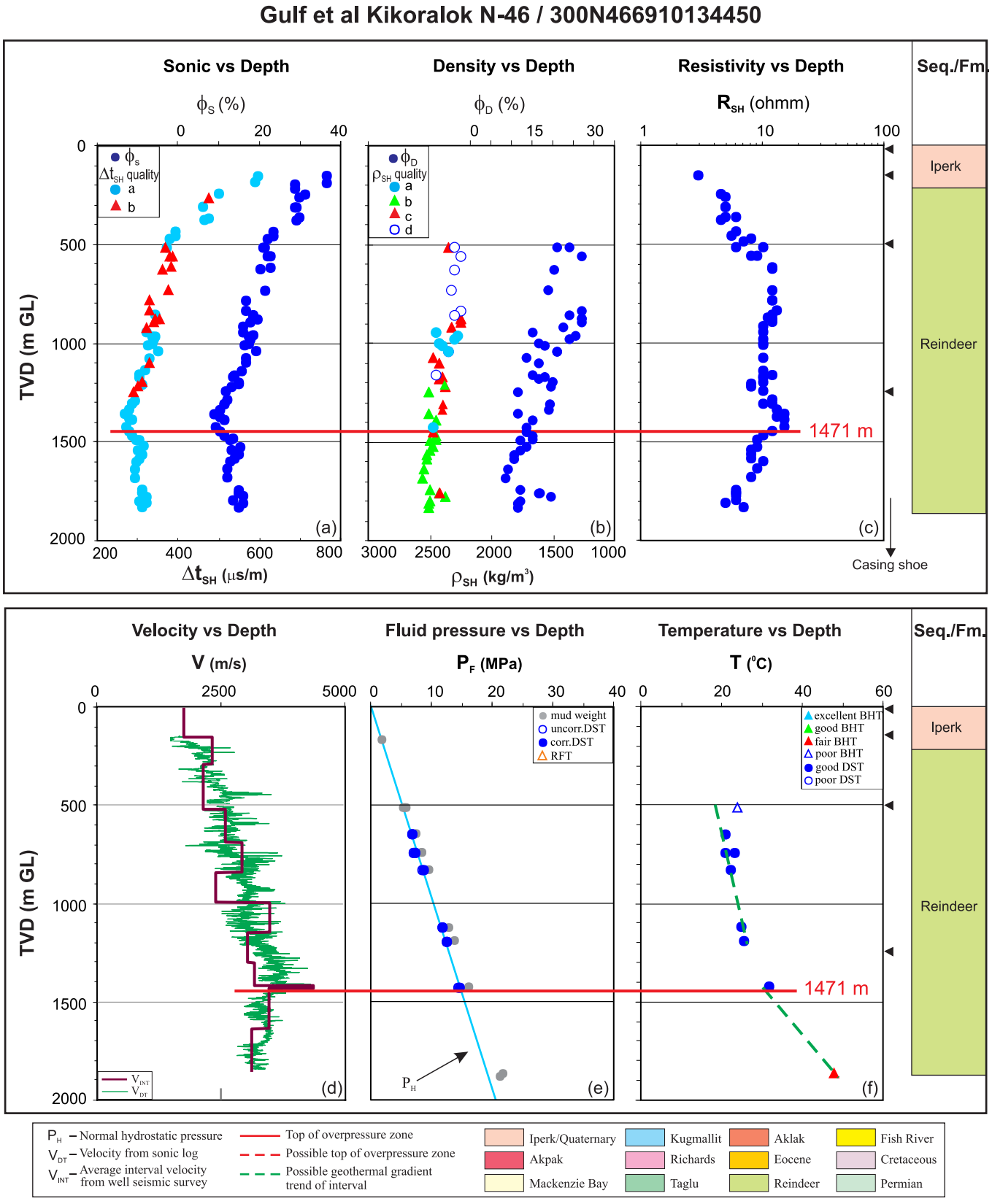

Figure B-25. Top of overpressure zone is detected at 1471 m with quality "b" by using the integrated analysis for the Kikoralok N-46 well in the Beaufort-Mackenzie Basin. (a) shale sonic transit time (Δt_{SH}) and sonic porosity (ϕ_S) vs. depth; (b) shale bulk density (ρ_{SH}) and density porosity (ϕ_D) vs depth; (c) shale deep resistivity (R_{SH}) vs. depth; (d) continuous sonic velocity (V_{DT}) and average interval seismic velocity (V_{INT}) vs. depth; (e) fluid pressure (P_F) from well test and drilling mud weight vs. depth; and (f) borehole temperature vs. depth.

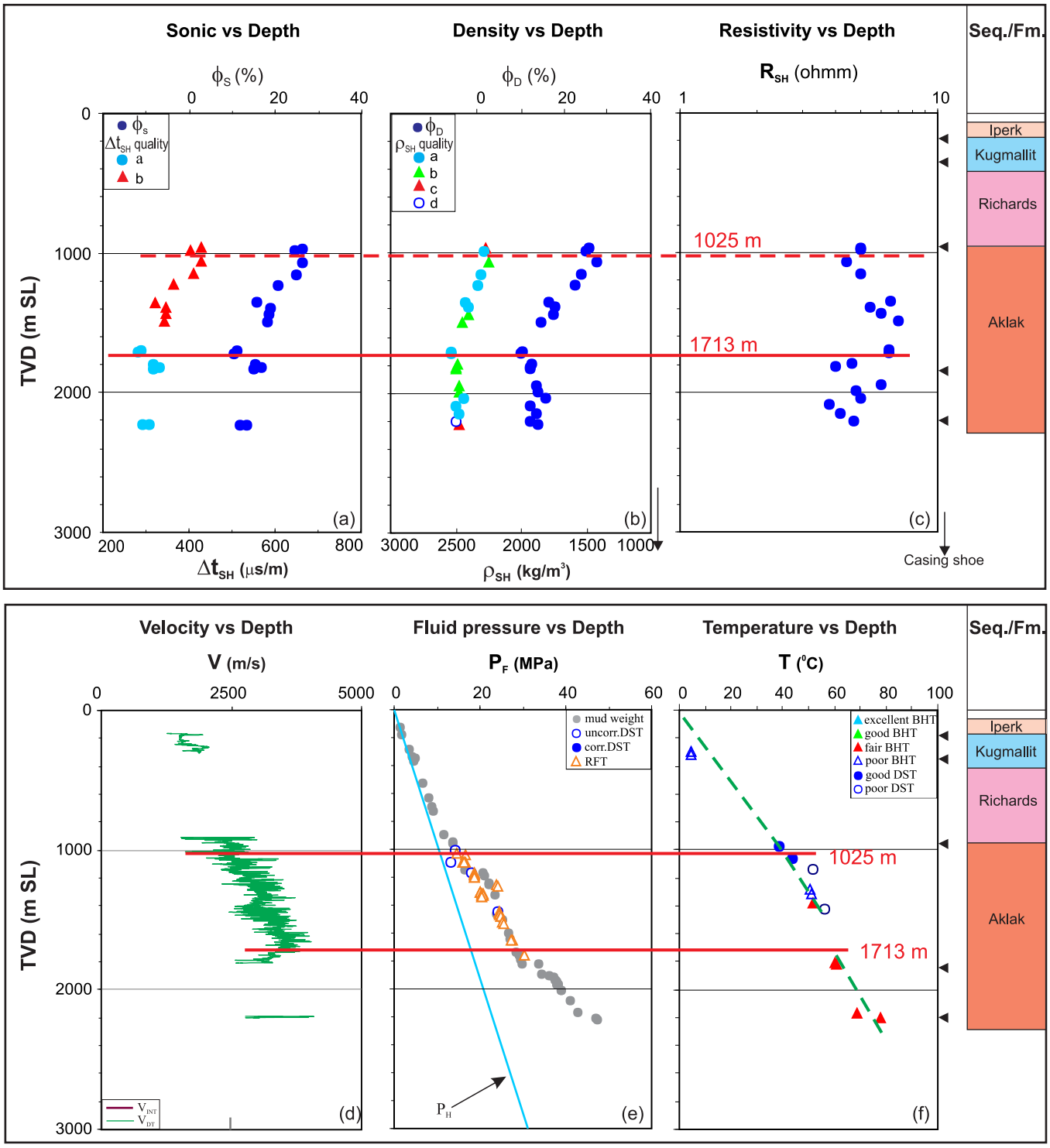

Figure B-26. Overpressure zones are detected with tops at 1025 m (quality "c") and 1713 m (quality "b") by using the integrated analysis for the Kingark J-54 well in the Beaufort-Mackenzie Basin. (a) shale sonic transit time (Δt_{SH}) and sonic porosity (ϕ_S) vs. depth; (b) shale bulk density (ρ_{SH}) and density porosity (ϕ_D) vs depth; (c) shale deep resistivity (R_{SH}) vs. depth; (d) continuous sonic velocity (V_{DT}) vs. depth; (e) fluid pressure (P_F) from well test and drilling mud weight vs. depth; and (f) borehole temperature vs. depth.

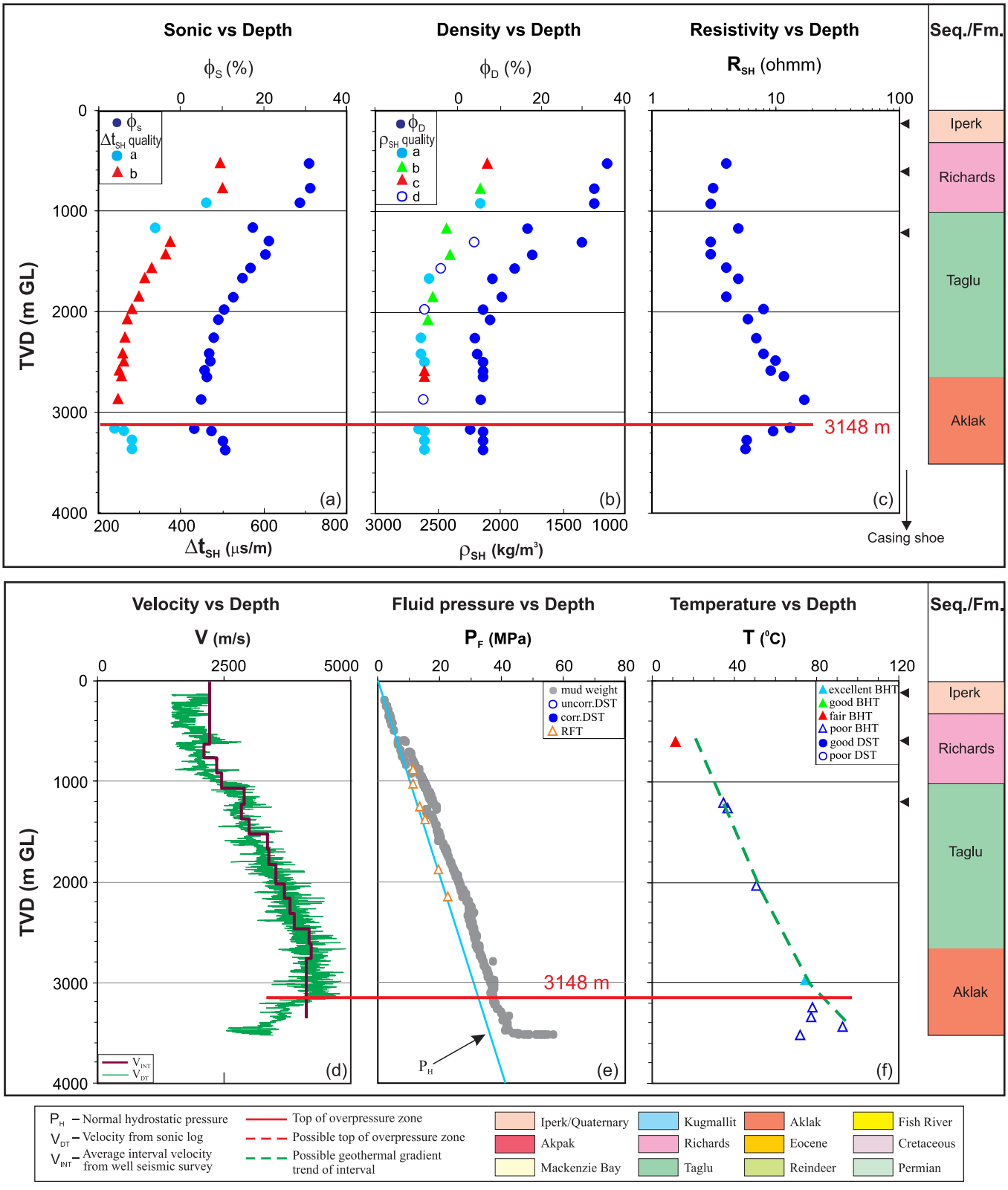

Figure B-27. Top of overpressure zone is detected at 3148 m with quality "b" by using the integrated analysis for the Kumak C-58 well in the Beaufort-Mackenzie Basin. (a) shale sonic transit time (Δt_{SH}) and sonic porosity (ϕ_S) vs. depth; (b) shale bulk density (ρ_{SH}) and density porosity (ϕ_D) vs depth; (c) shale deep resistivity (R_{SH}) vs. depth; (d) continuous sonic velocity (V_{DT}) and average interval seismic velocity (V_{INT}) vs. depth; (e) fluid pressure (P_F) from well test and drilling mud weight vs. depth; and (f) borehole temperature vs. depth.

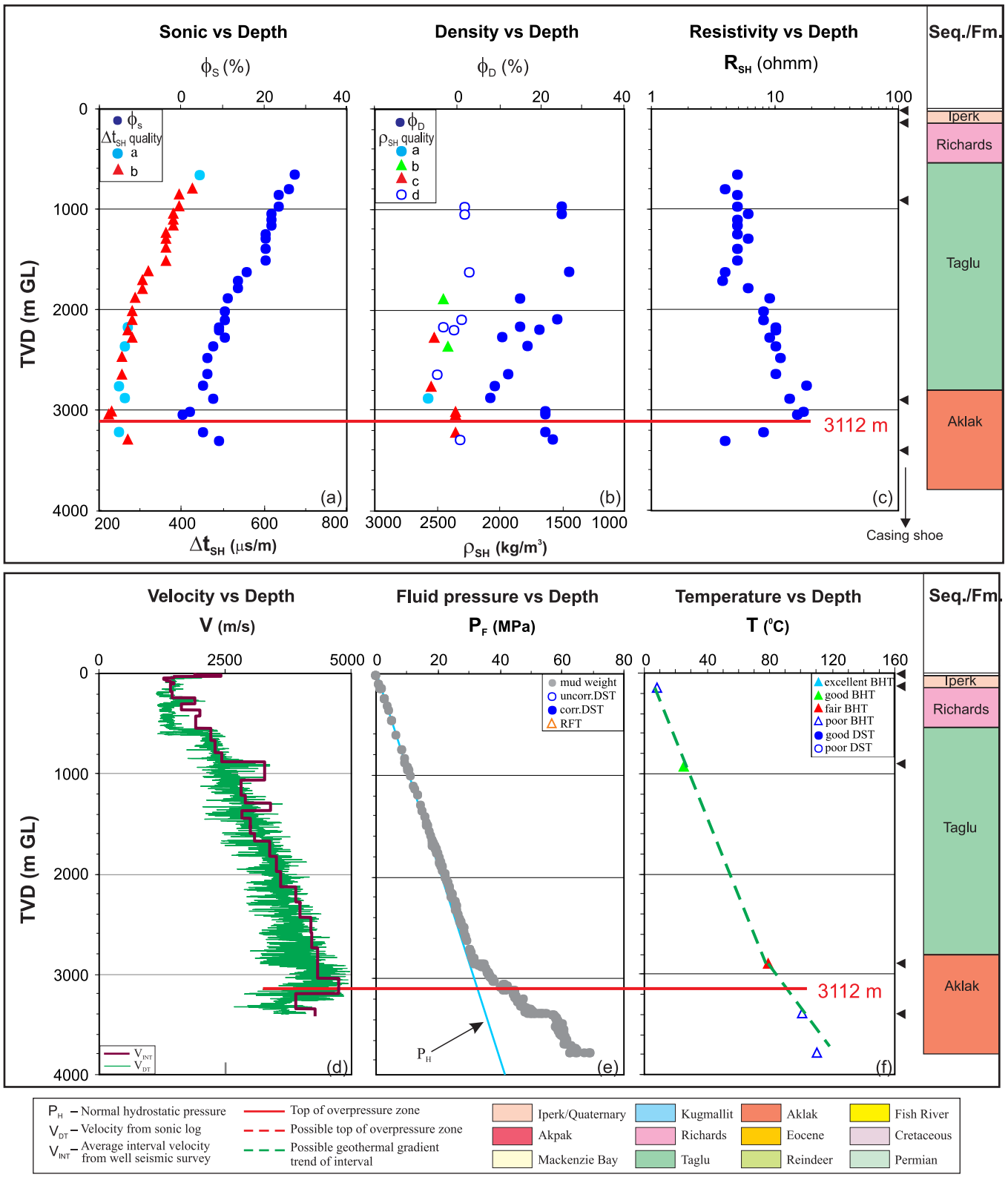

Figure B-28. Top of overpressure zone is detected at 3112 m with quality "b" by using the integrated analysis for the Langley E-29 well in the Beaufort-Mackenzie Basin. (a) shale sonic transit time (Δt_{SH}) and sonic porosity (ϕ_S) vs. depth; (b) shale bulk density (ρ_{SH}) and density porosity (ϕ_D) vs depth; (c) shale deep resistivity (R_{SH}) vs. depth; (d) continuous sonic velocity (V_{DT}) and average interval seismic velocity (V_{INT}) vs. depth; (e) fluid pressure (P_F) from well test and drilling mud weight vs. depth; and (f) borehole temperature vs. depth.

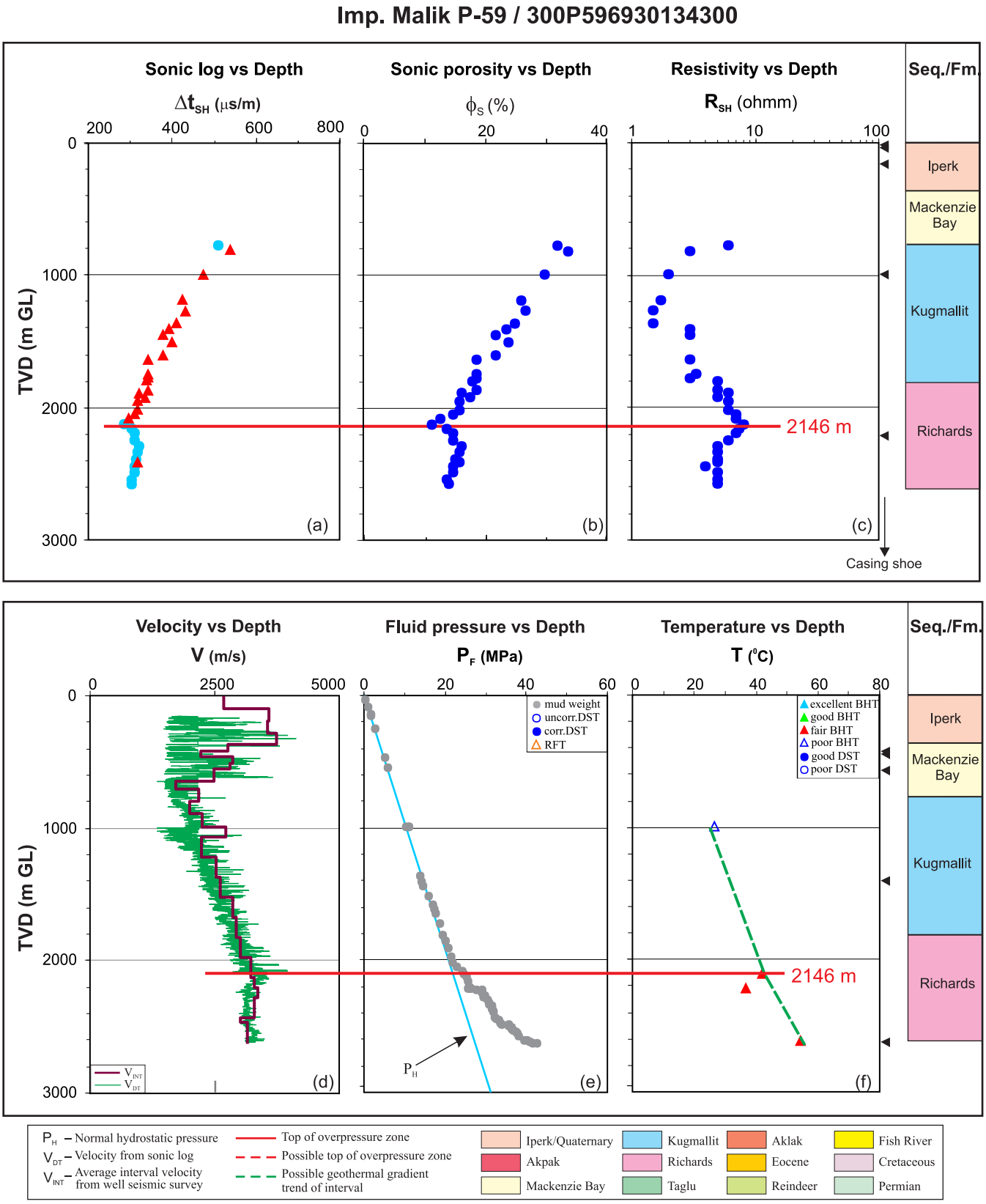

Figure B-29. Top of overpressure zone is detected at 2146 m with quality "b" by using the integrated analysis for the Mallik P-59 well in the Beaufort-Mackenzie Basin. (a) shale sonic transit time (Δt_{SH}) vs. depth; (b) shale sonic porosity (ϕ_S) vs. depth; (c) shale deep resistivity (R_{SH}) vs. depth; (d) continuous sonic velocity (V_{DT}) and average interval seismic velocity (V_{INT}) vs. depth; (e) fluid pressure (P_F) from well test and drilling mud weight vs. depth; and (f) borehole temperature vs. depth.

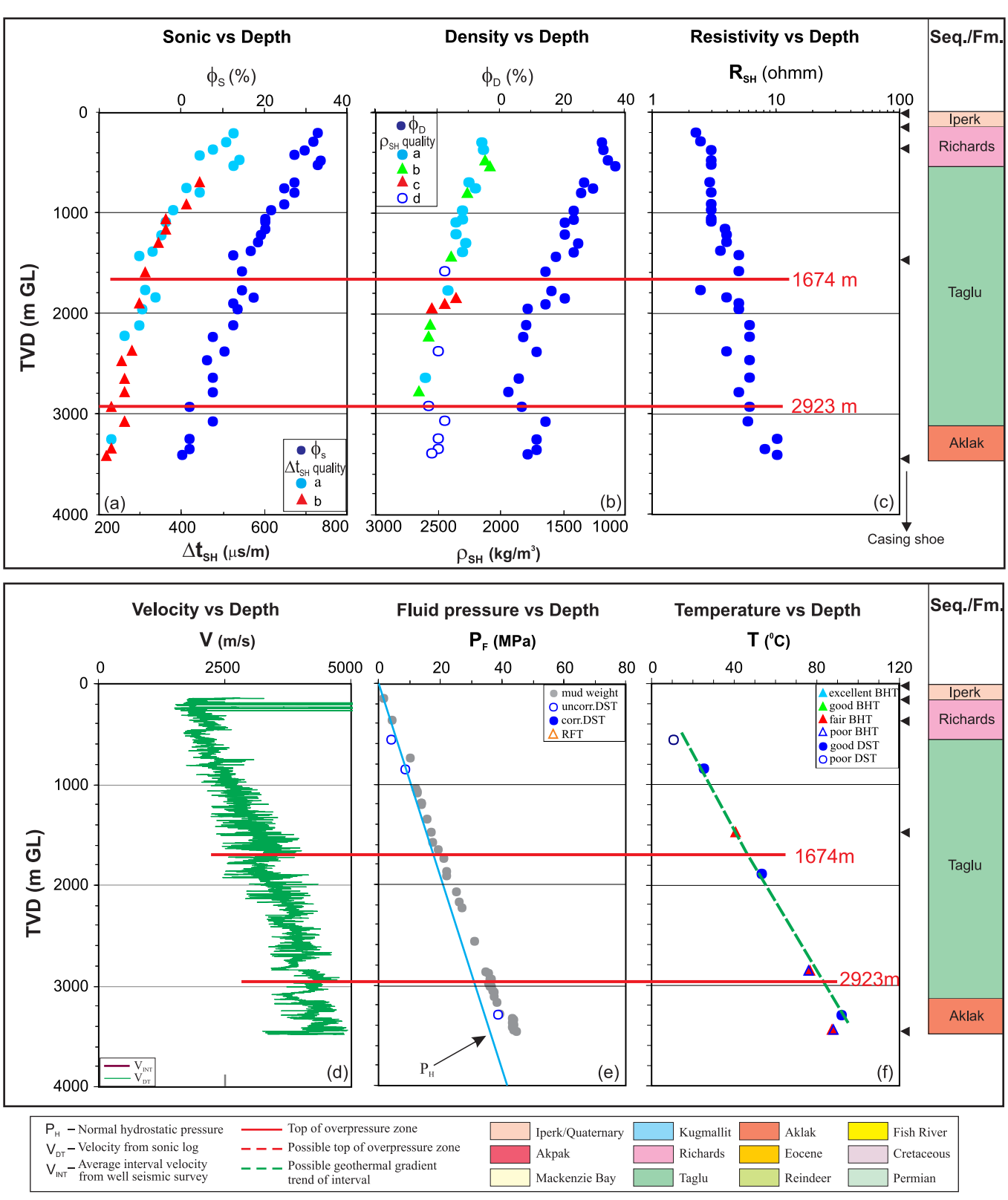

Figure B-30. Overpressure zones are detected with tops at 1674 m (quality "b") and 2923 m (quality "b") by using the integrated analysis for the North Ellice J-23 well in the Beaufort-Mackenzie Basin. (a) shale sonic transit time (Δt_{SH}) and sonic porosity (ϕ_S) vs. depth; (b) shale bulk density (ρ_{SH}) and density porosity (ϕ_D) vs depth; (c) shale deep resistivity (R_{SH}) vs. depth; (d) continuous sonic velocity (V_{DT}) and average interval seismic velocity (V_{INT}) vs. depth; (e) fluid pressure (P_F) from well test and drilling mud weight vs. depth; and (f) borehole temperature vs. depth.

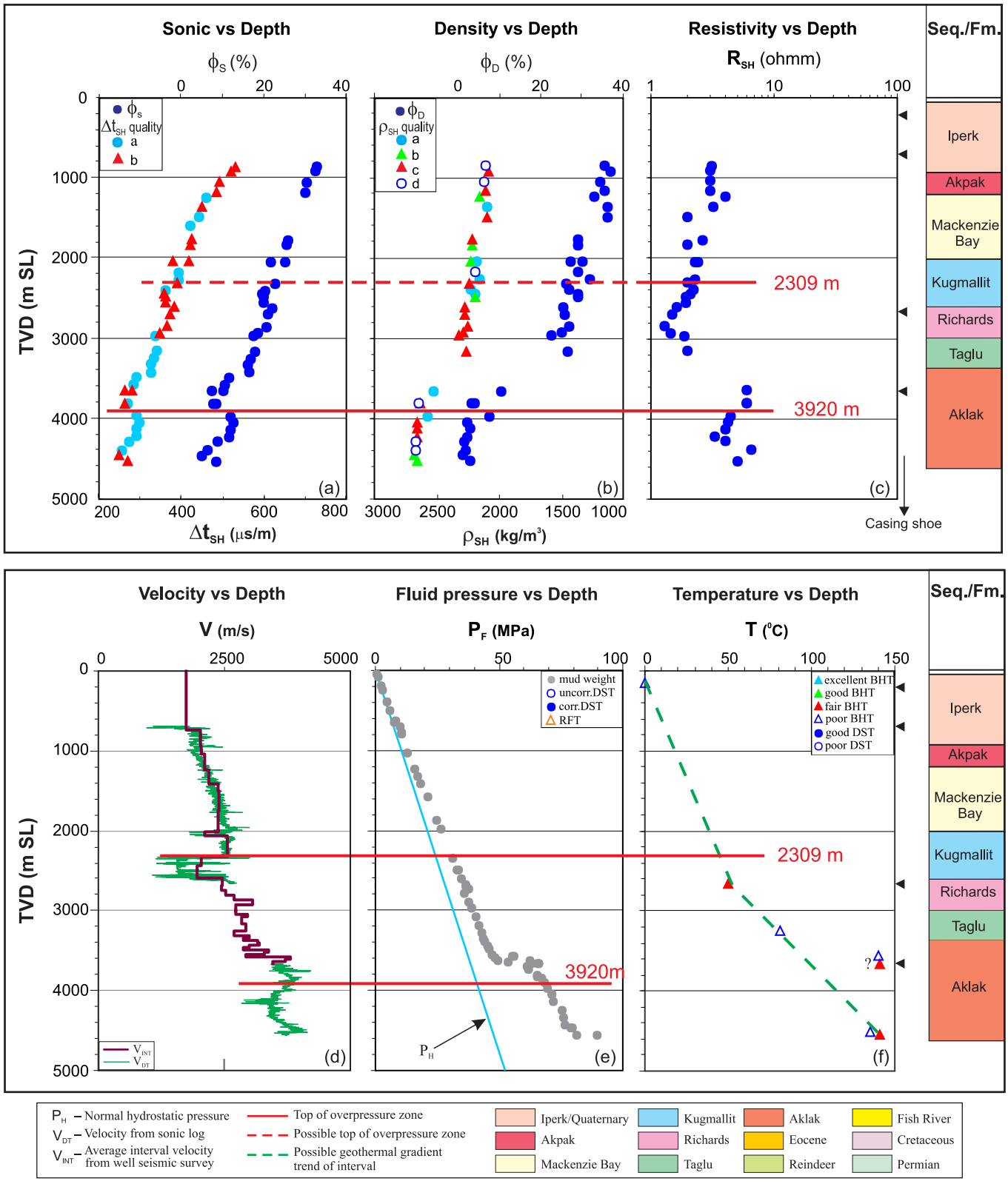

Figure B-31. Overpressure zones are detected with a top at 2309 m (quality "b") and 3920 m (quality "b") by using the integrated analysis for the Natiak O-44 well in the Beaufort-Mackenzie Basin. (a) shale sonic transit time (Δt_{SH}) and sonic porosity (ϕ_S) vs. depth; (b) shale bulk density (ρ_{SH}) and density porosity (ϕ_D) vs depth; (c) shale deep resistivity (R_{SH}) vs. depth; (d) continuous sonic velocity (V_{DT}) and average interval seismic velocity (V_{INT}) vs. depth; (e) fluid pressure (P_F) from well test and drilling mud weight vs. depth; and (f) borehole temperature vs. depth.

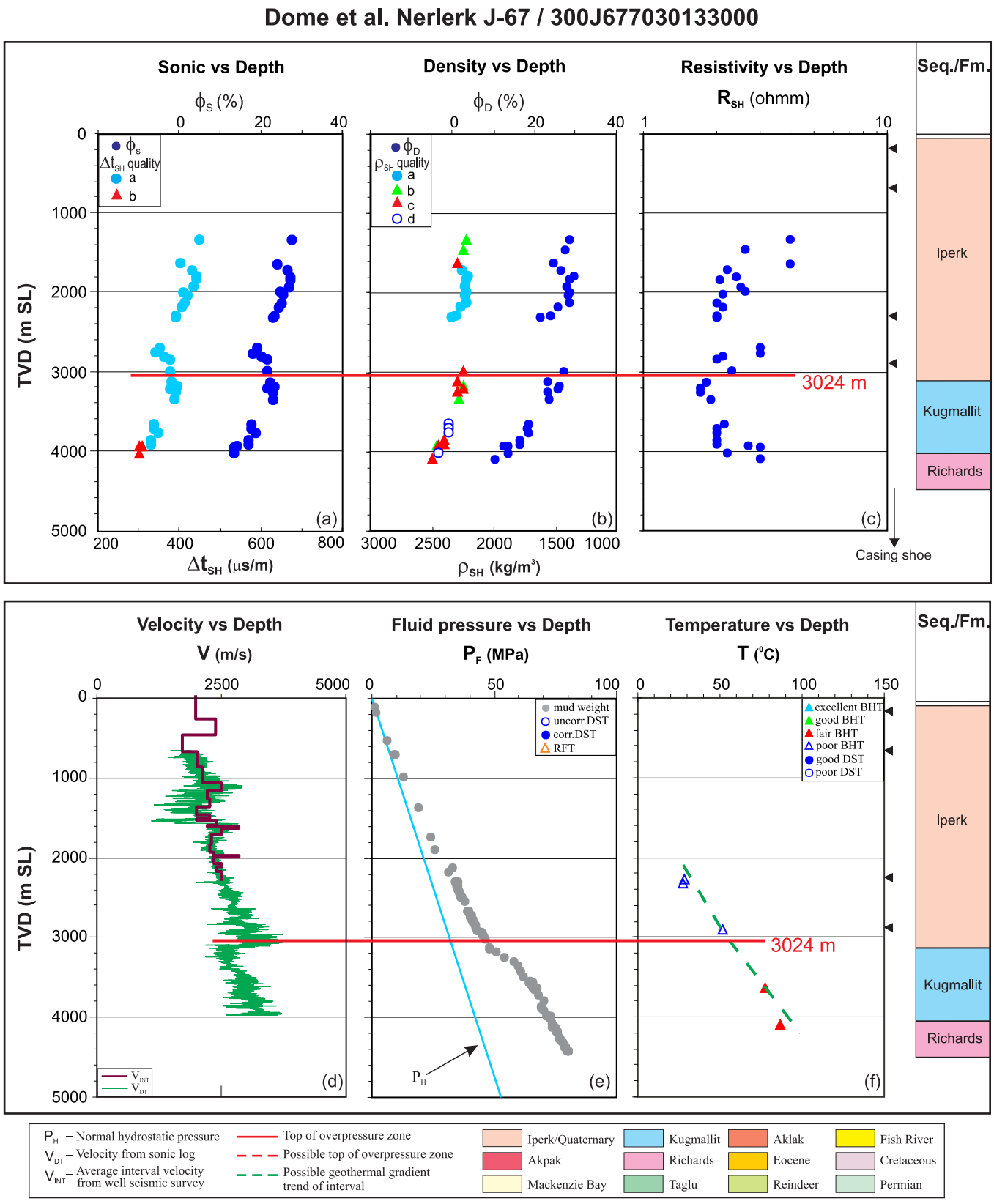

Figure B-32. Top of overpressure zone is detected at 3024 m with quality "b" by using the integrated analysis for the Nerlerk J-67 well in the Beaufort-Mackenzie Basin. (a) shale sonic transit time (Δt_{SH}) and sonic porosity (ϕ_S) vs. depth; (b) shale bulk density (ρ_{SH}) and density porosity (ϕ_D) vs depth; (c) shale deep resistivity (R_{SH}) vs. depth; (d) continuous sonic velocity (V_{DT}) and average interval seismic velocity (V_{INT}) vs. depth; (e) fluid pressure (P_F) from well test and drilling mud weight vs. depth; and (f) borehole temperature vs. depth.

Shell Niglintgak M-19 / 300M196920135150

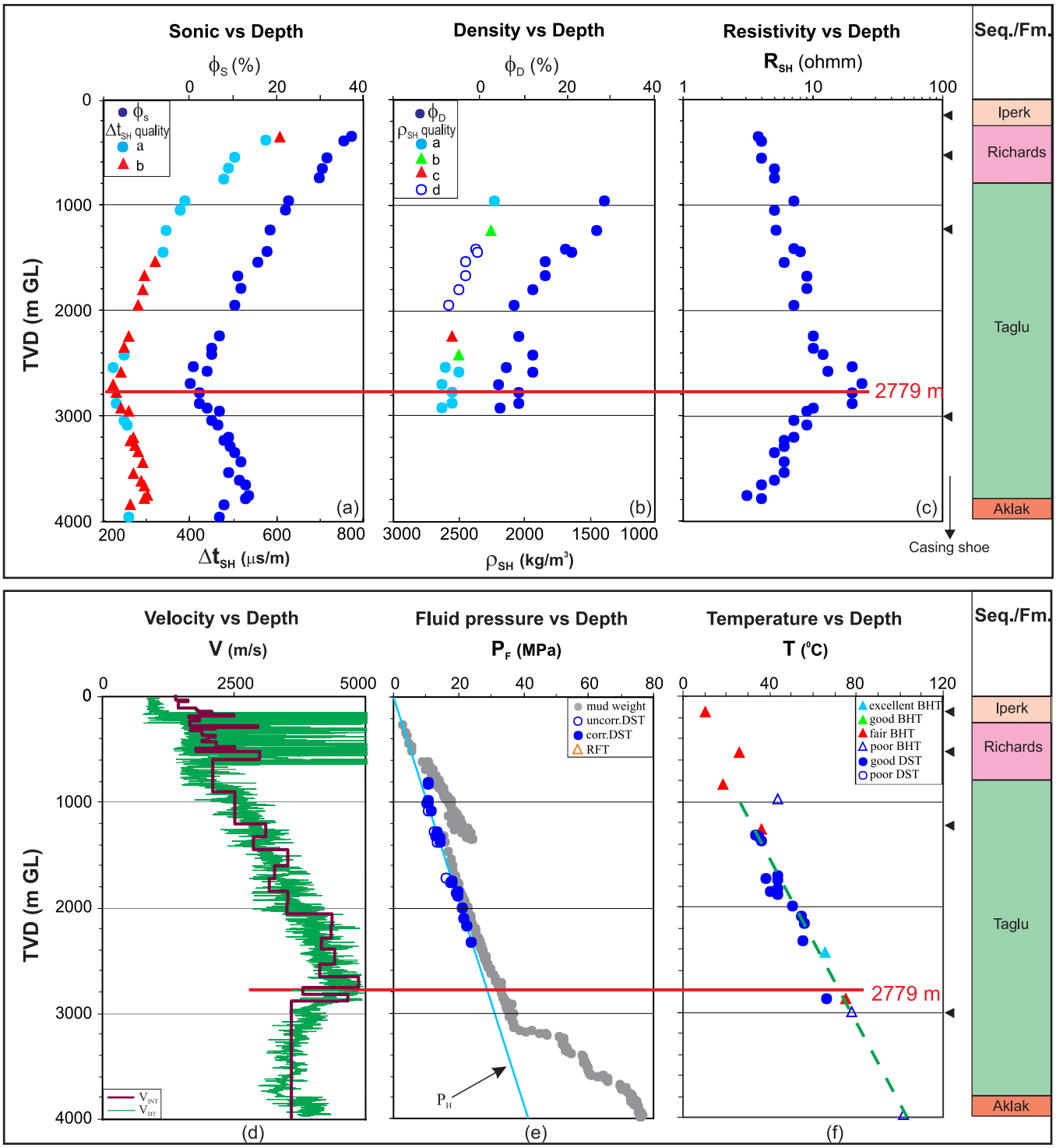

Figure B-33. Top of overpressure zone is detected at 2779 m with quality "b" by using the integrated analysis for the Niglintgak M-19 well in the Beaufort-Mackenzie Basin. (a) shale sonic transit time (Δt_{SH}) and sonic porosity (ϕ_S) vs. depth; (b) shale bulk density (ρ_{SH}) and density porosity (ϕ_D) vs depth; (c) shale deep resistivity (R_{SH}) vs. depth; (d) continuous sonic velocity (V_{DT}) and average interval seismic velocity (V_{INT}) vs. depth; (e) fluid pressure (P_F) from well test and drilling mud weight vs. depth; and (f) borehole temperature vs. depth.

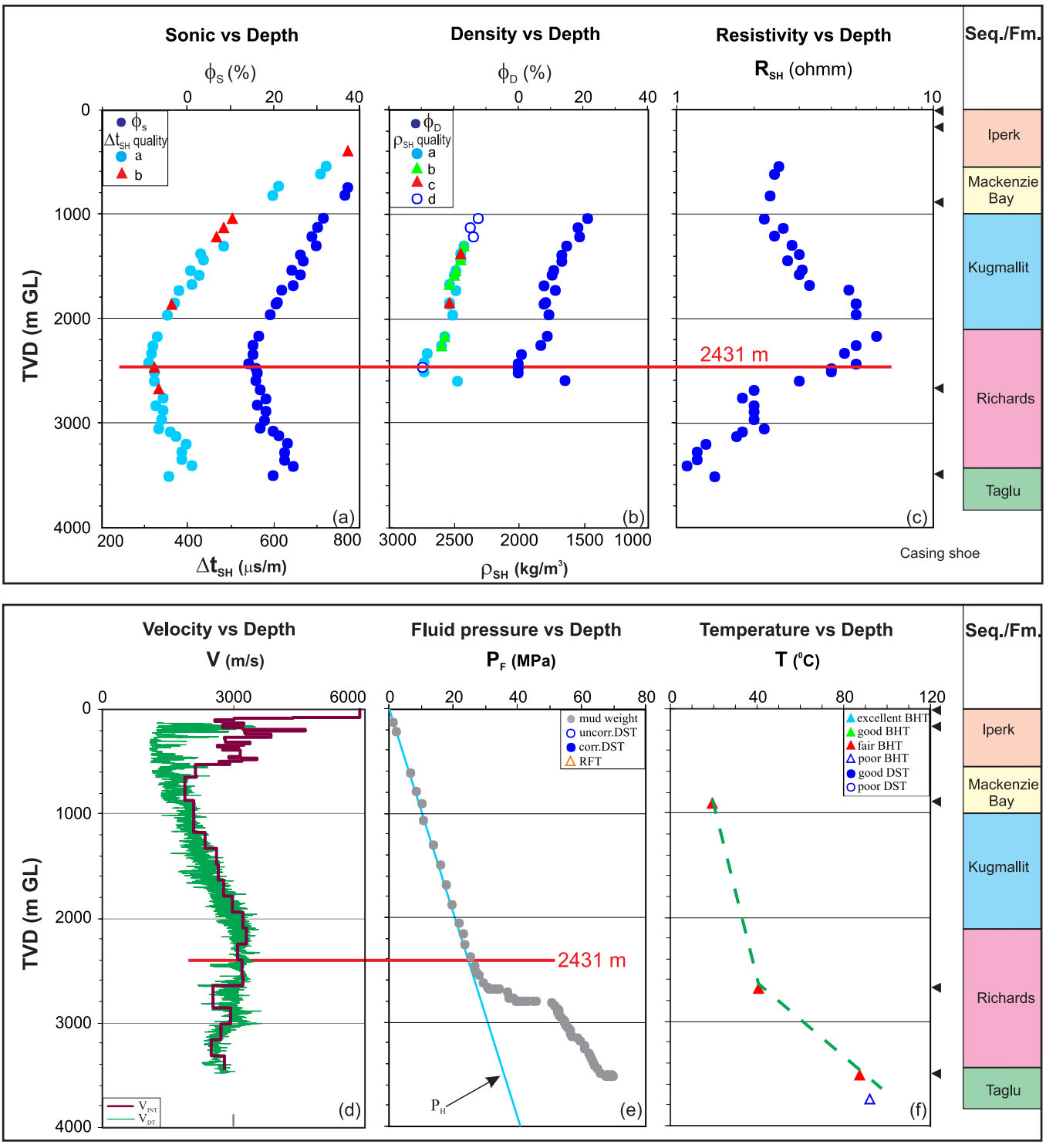

Figure B-34. Top of overpressure zone is detected at 2431 m with quality "b" by using the integrated analysis for the Nuktak C-22 well in the Beaufort-Mackenzie Basin. (a) shale sonic transit time (Δt_{SH}) and sonic porosity (ϕ_S) vs. depth; (b) shale bulk density (ρ_{SH}) and density porosity (ϕ_D) vs depth; (c) shale deep resistivity (R_{SH}) vs. depth; (d) continuous sonic velocity (V_{DT}) and average interval seismic velocity (V_{INT}) vs. depth; (e) fluid pressure (P_F) from well test and drilling mud weight vs. depth; and (f) borehole temperature vs. depth.

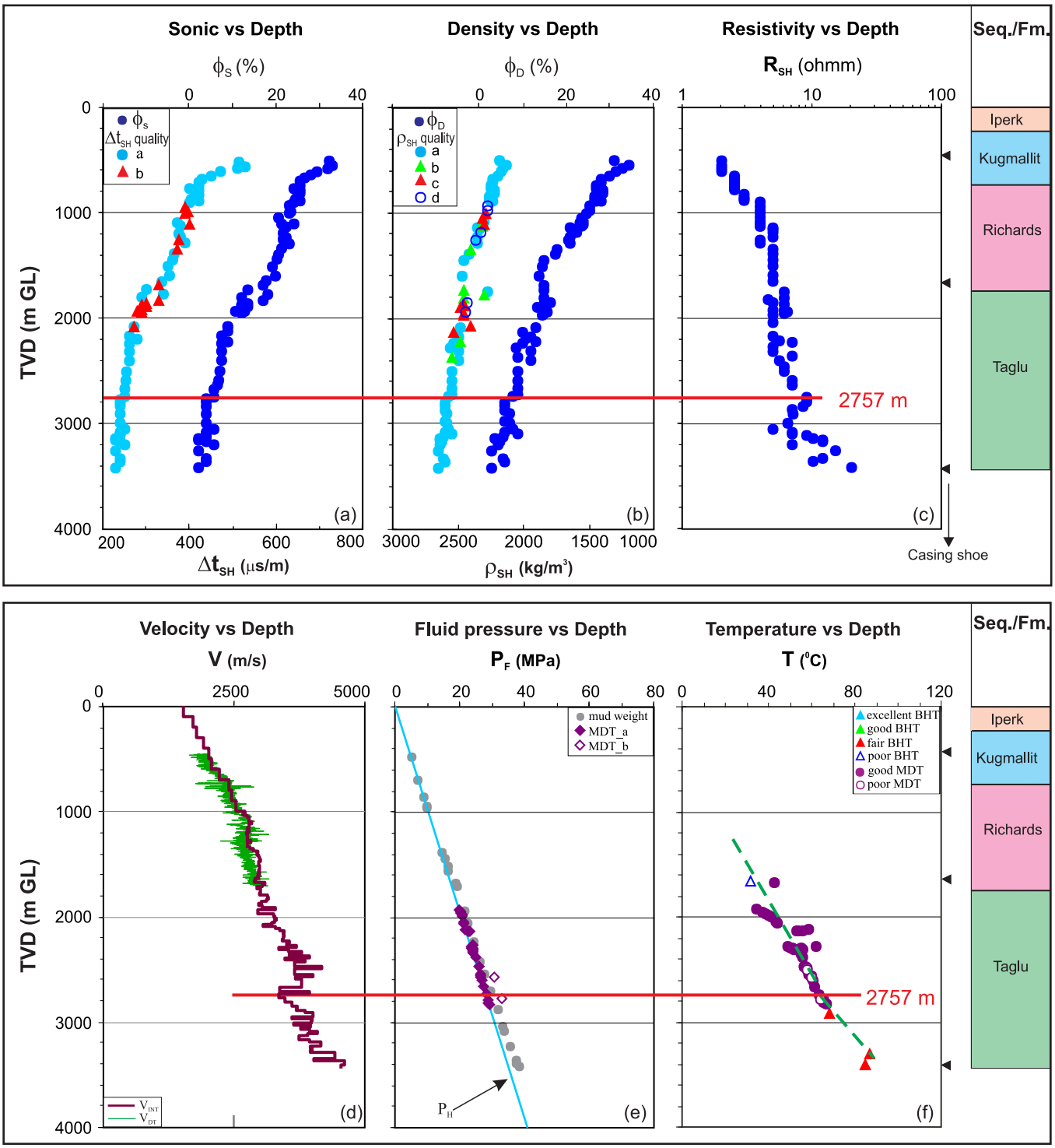

Figure B-35. Top of overpressure zone is detected at 2757 m with quality "b" by using the integrated analysis for the Olivier H-01 well in the Beaufort-Mackenzie Basin. (a) shale sonic transit time (Δt_{SH}) and sonic porosity (ϕ_S) vs. depth; (b) shale bulk density (ρ_{SH}) and density porosity (ϕ_D) vs depth; (c) shale deep resistivity (R_{SH}) vs. depth; (d) continuous sonic velocity (V_{DT}) and average interval seismic velocity (V_{INT}) vs. depth; (e) fluid pressure (P_F) from well test and drilling mud weight vs. depth; and (f) borehole temperature vs. depth.

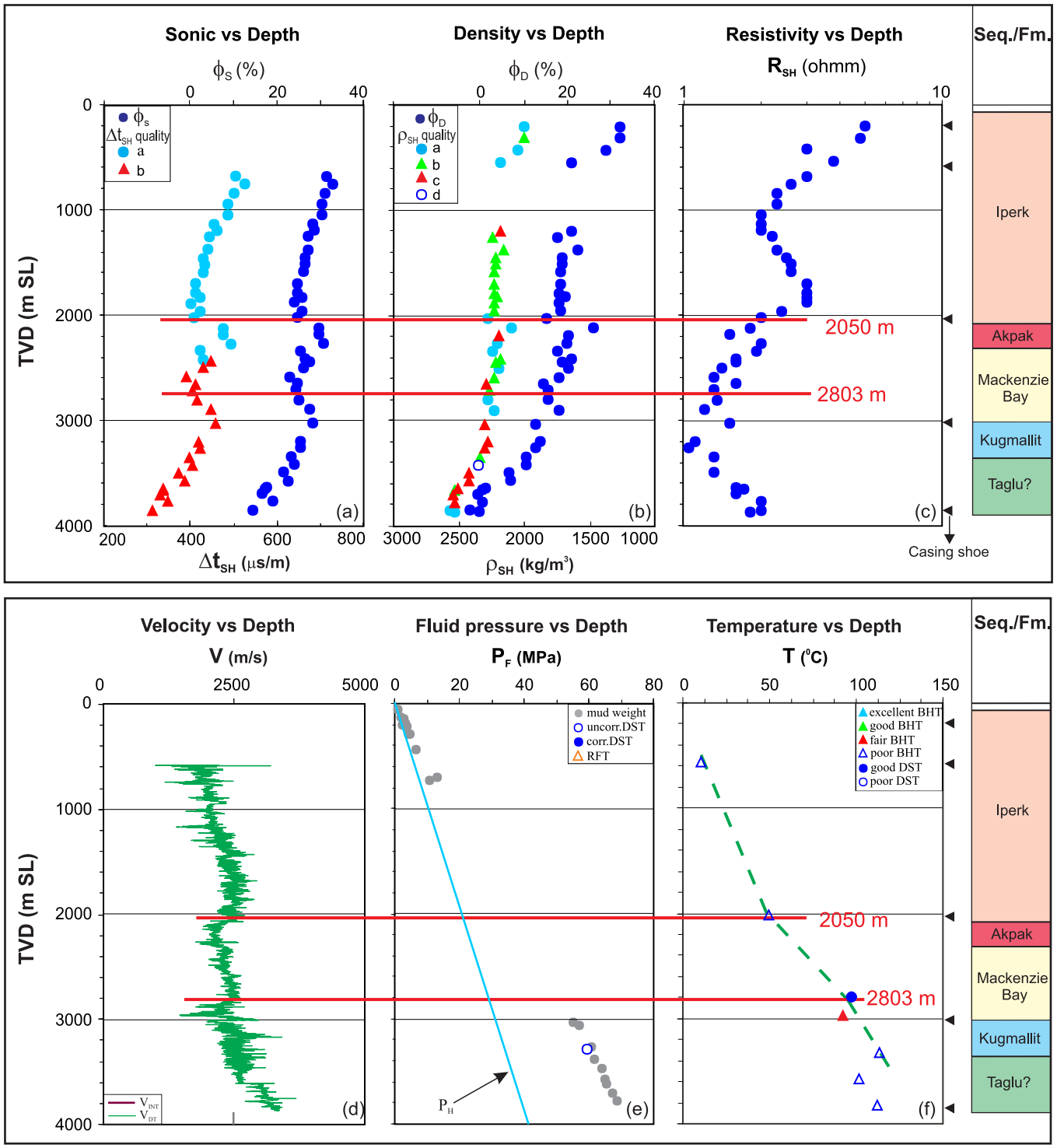

Figure B-36. Top of overpressure zones are detected at 2050 m and 2803 m with quality "b" by using the integrated analysis for the Orvilruk O-03 well in the Beaufort-Mackenzie Basin. (a) shale sonic transit time (Δt_{SH}) and sonic porosity (ϕ_S) vs. depth; (b) shale bulk density (ρ_{SH}) and density porosity (ϕ_D) vs depth; (c) shale deep resistivity (R_{SH}) vs. depth; (d) continuous sonic velocity (V_{DT}) vs. depth; (e) fluid pressure (P_F) from well test and drilling mud weight vs. depth; and (f) borehole temperature vs. depth.

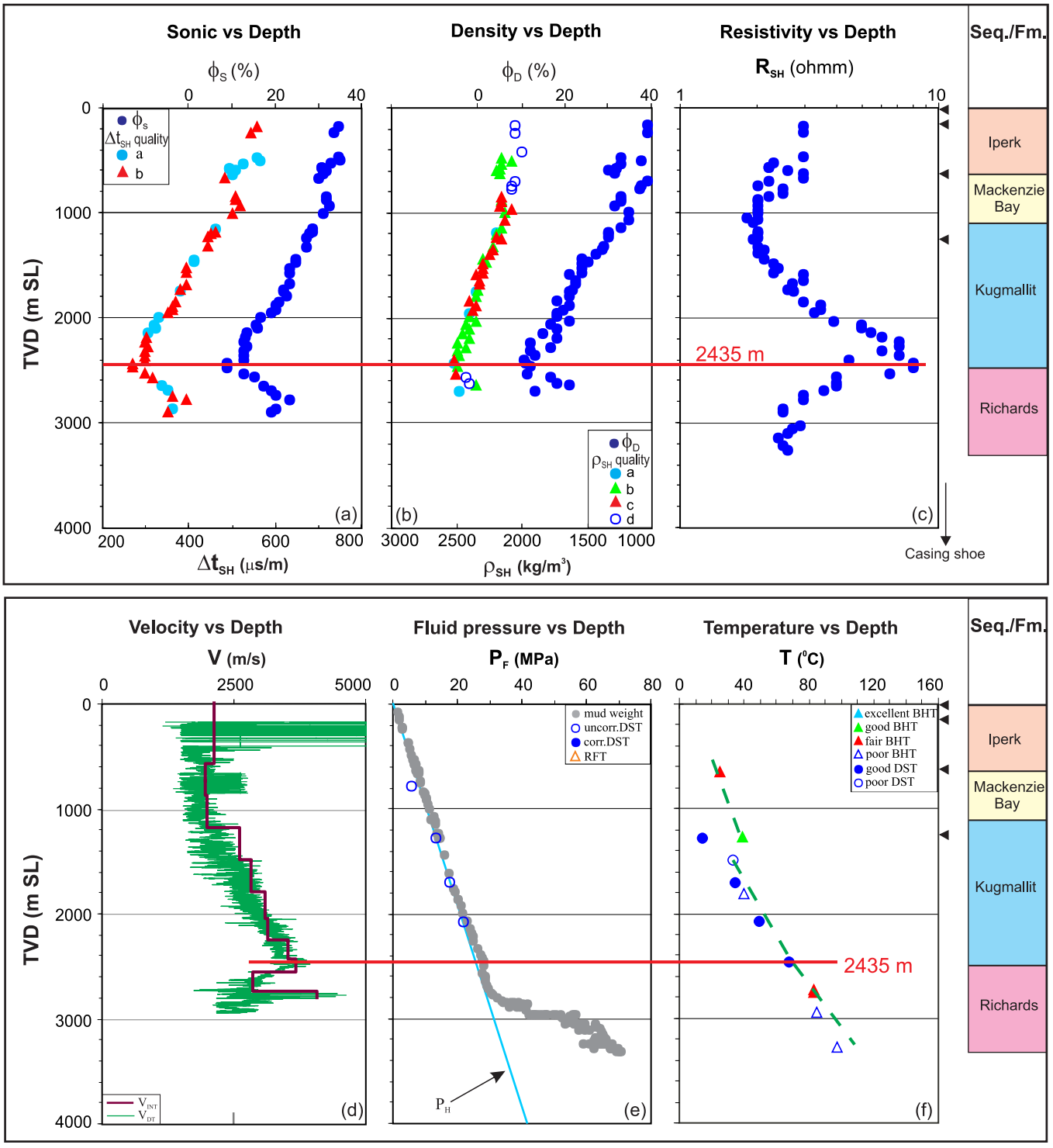

Figure B-37. Top of overpressure zone is detected at 2435 m with quality "b" by using the integrated analysis for the Pelly B-35 well in the Beaufort-Mackenzie Basin. (a) shale sonic transit time (Δt_{SH}) and sonic porosity (ϕ_S) vs. depth; (b) shale bulk density (ρ_{SH}) and density porosity (ϕ_D) vs depth; (c) shale deep resistivity (R_{SH}) vs. depth; (d) continuous sonic velocity (V_{DT}) and average interval seismic velocity (V_{INT}) vs. depth; (e) fluid pressure (P_F) from well test and drilling mud weight vs. depth; and (f) borehole temperature vs. depth.

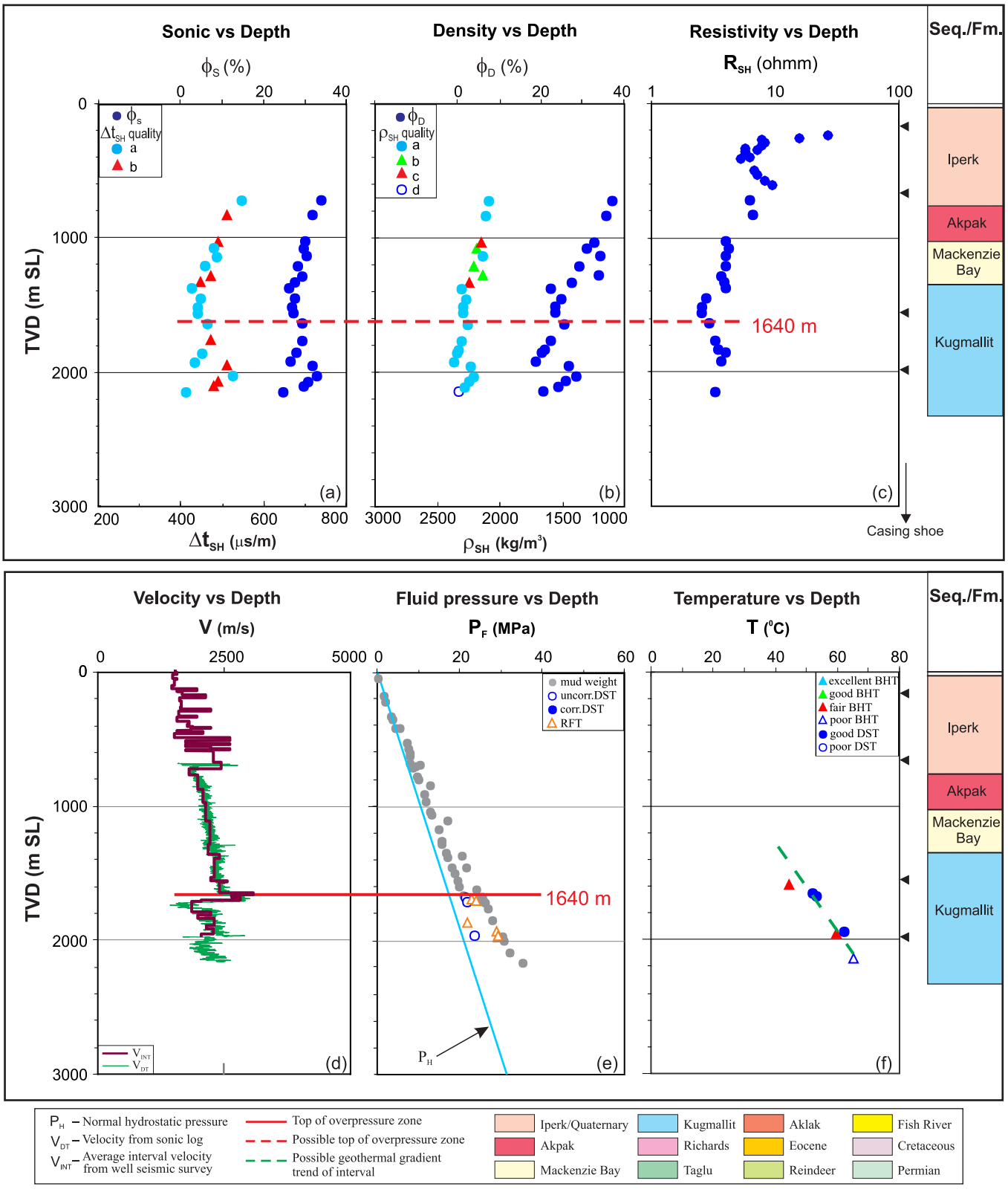

Figure B-38. Top of overpressure zone is detected at 1640 m with quality "b" by using the integrated analysis for the Pitsiulak A-05 well in the Beaufort-Mackenzie Basin. (a) shale sonic transit time (Δt_{SH}) and sonic porosity (ϕ_S) vs. depth; (b) shale bulk density (ρ_{SH}) and density porosity (ϕ_D) vs depth; (c) shale deep resistivity (R_{SH}) vs. depth; (d) continuous sonic velocity (V_{DT}) and average interval seismic velocity (V_{INT}) vs. depth; (e) fluid pressure (P_F) from well test and drilling mud weight vs. depth; and (f) borehole temperature vs. depth.

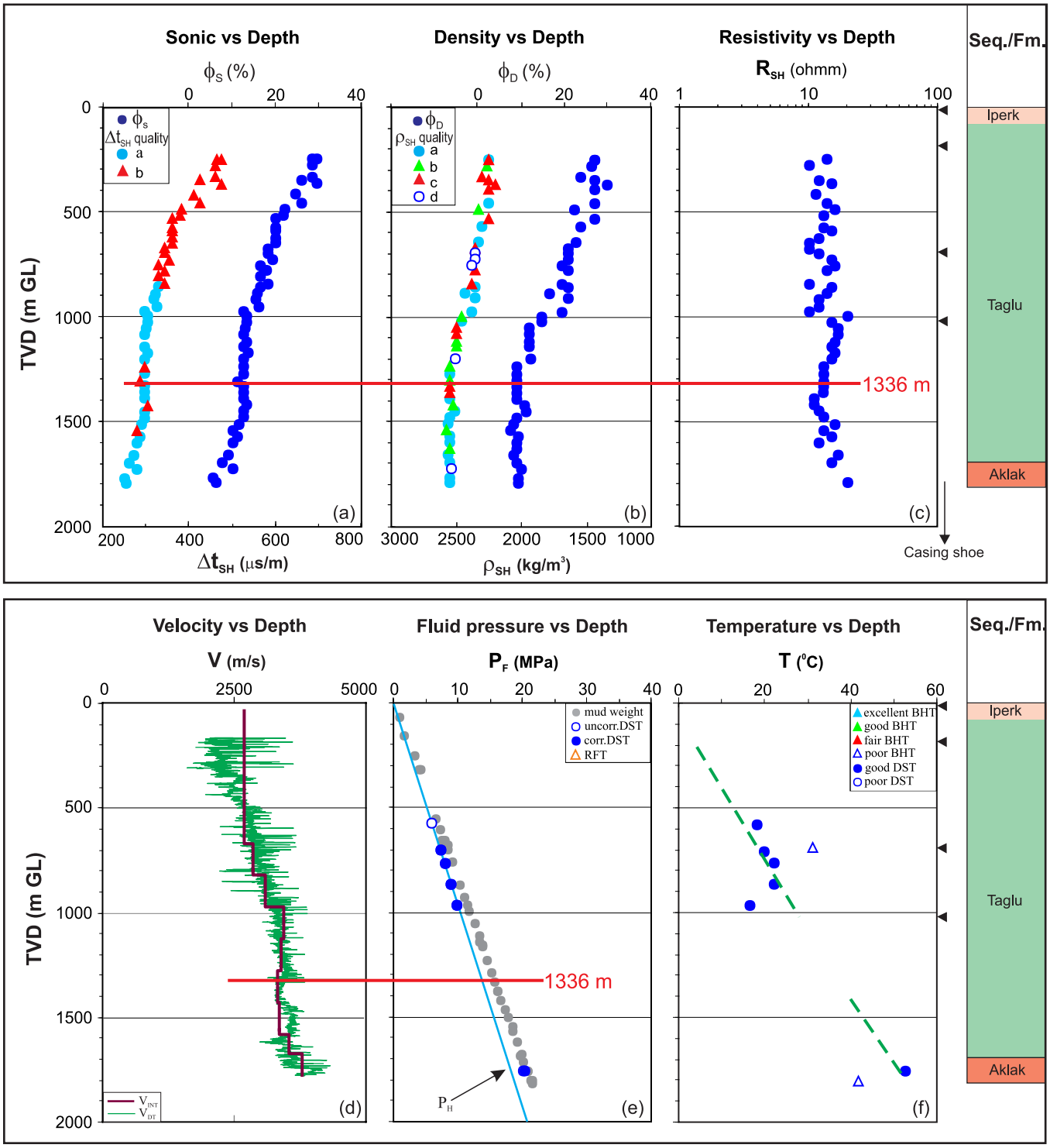

Figure B-39. Top of overpressure zone is detected at 1336 m with quality "b" by using the integrated analysis for the Reindeer A-41 well in the Beaufort-Mackenzie Basin. (a) shale sonic transit time (Δt_{SH}) and sonic porosity (ϕ_S) vs. depth; (b) shale bulk density (ρ_{SH}) and density porosity (ϕ_D) vs depth; (c) shale deep resistivity (R_{SH}) vs. depth; (d) continuous sonic velocity (V_{DT}) and average interval seismic velocity (V_{INT}) vs. depth; (e) fluid pressure (P_F) from well test and drilling mud weight vs. depth; and (f) borehole temperature vs. depth.

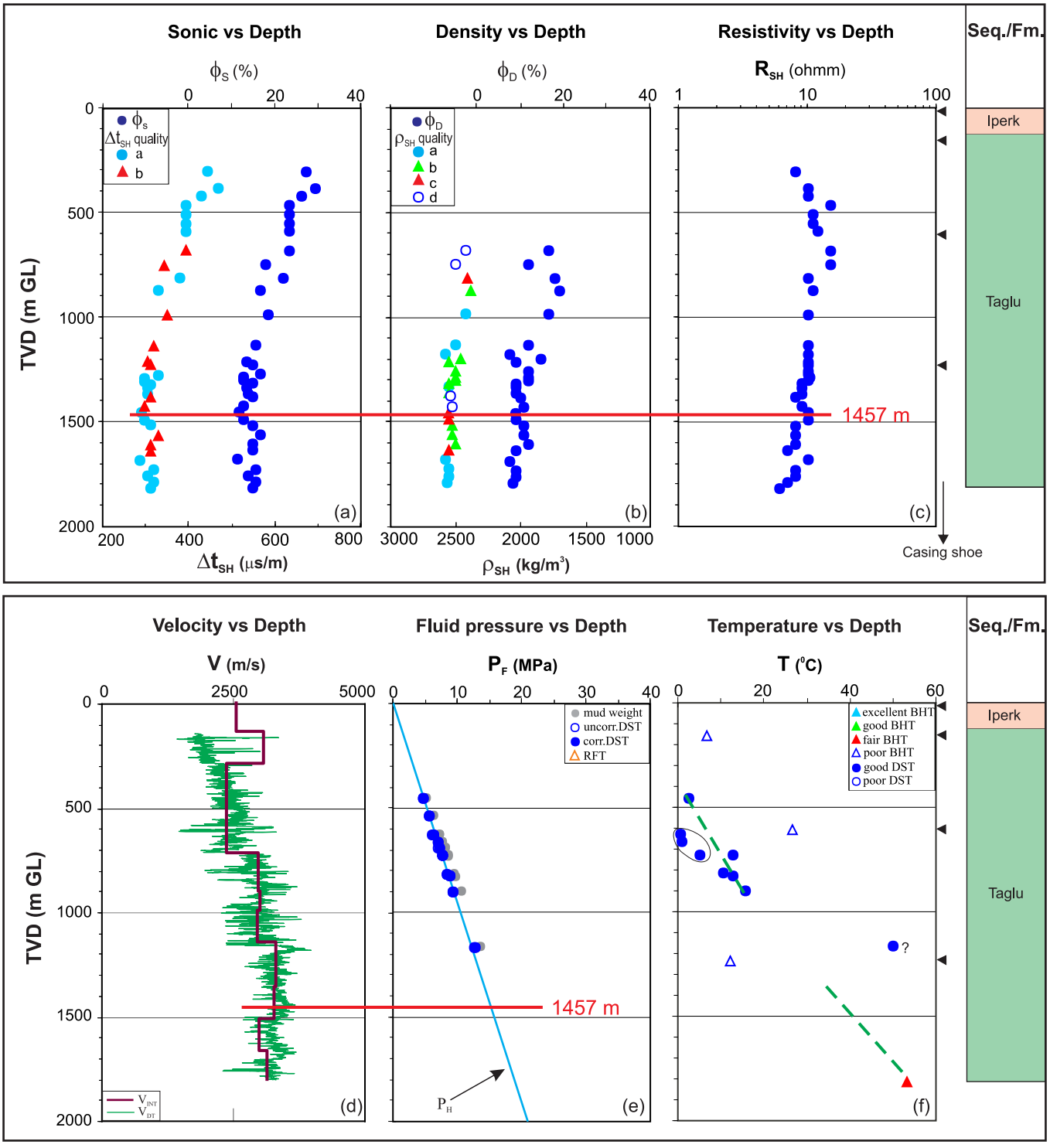

Figure B-40. Top of overpressure zone is detected at 1457 m with quality "b" by using the integrated analysis for the Reindeer F-36 well in the Beaufort-Mackenzie Basin. (a) shale sonic transit time (Δt_{SH}) and sonic porosity (ϕ_S) vs. depth; (b) shale bulk density (ρ_{SH}) and density porosity (ϕ_D) vs depth; (c) shale deep resistivity (R_{SH}) vs. depth; (d) continuous sonic velocity (V_{DT}) and average interval seismic velocity (V_{INT}) vs. depth; (e) fluid pressure (P_F) from well test and drilling mud weight vs. depth; and (f) borehole temperature vs. depth.

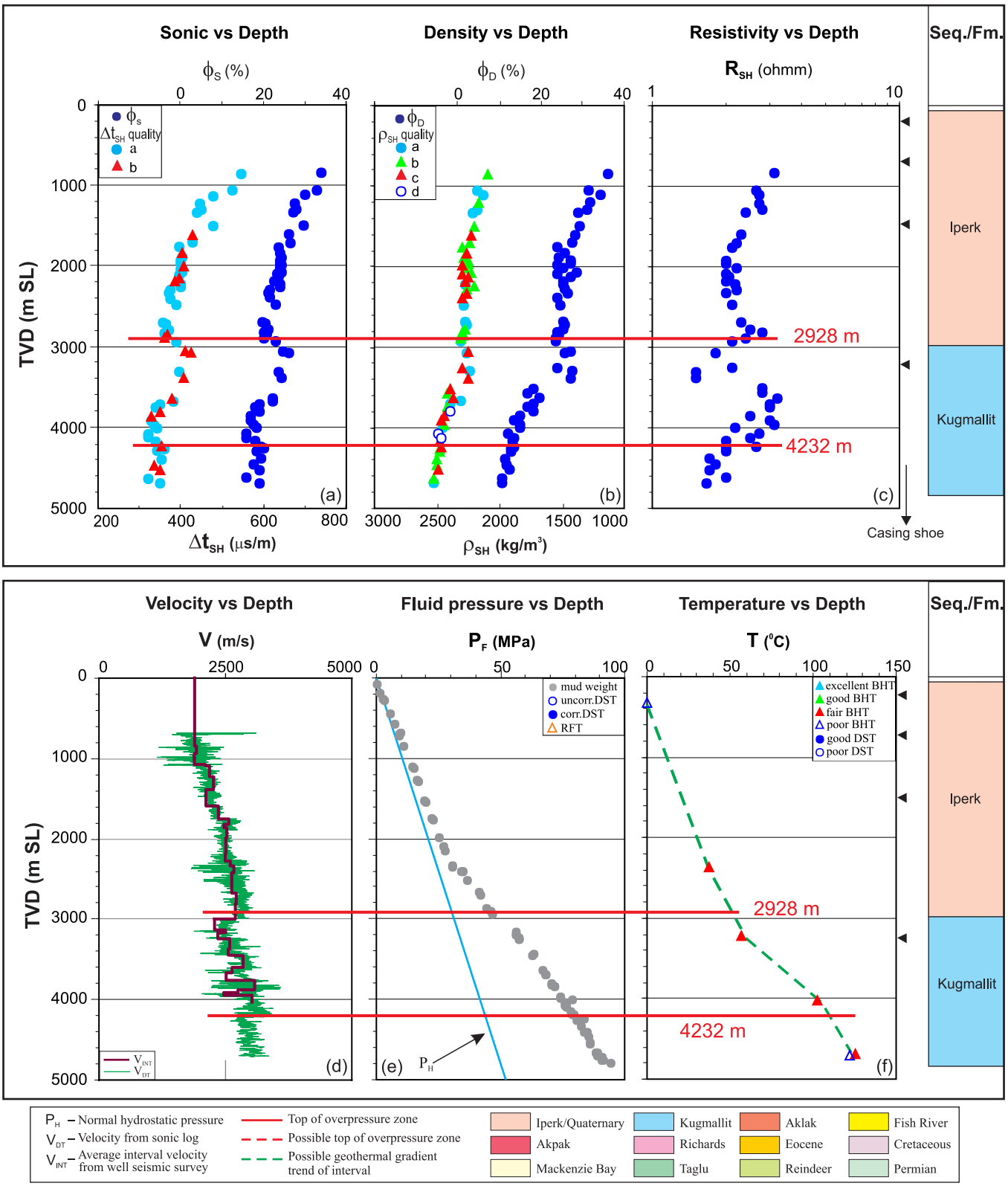

Figure B-41. Overpressure zones are detected with tops of 2928 m (quality "b") and 4232 m (quality "b") by using the integrated analysis for the Siulik I-05 well in the Beaufort-Mackenzie Basin. (a) shale sonic transit time (Δt_{SH}) and sonic porosity (ϕ_S) vs. depth; (b) shale bulk density (ρ_{SH}) and density porosity (ϕ_D) vs depth; (c) shale deep resistivity (R_{SH}) vs. depth; (d) continuous sonic velocity (V_{DT}) and average interval seismic velocity (V_{INT}) vs. depth; (e) fluid pressure (P_F) from well test and drilling mud weight vs. depth; and (f) borehole temperature vs. depth.

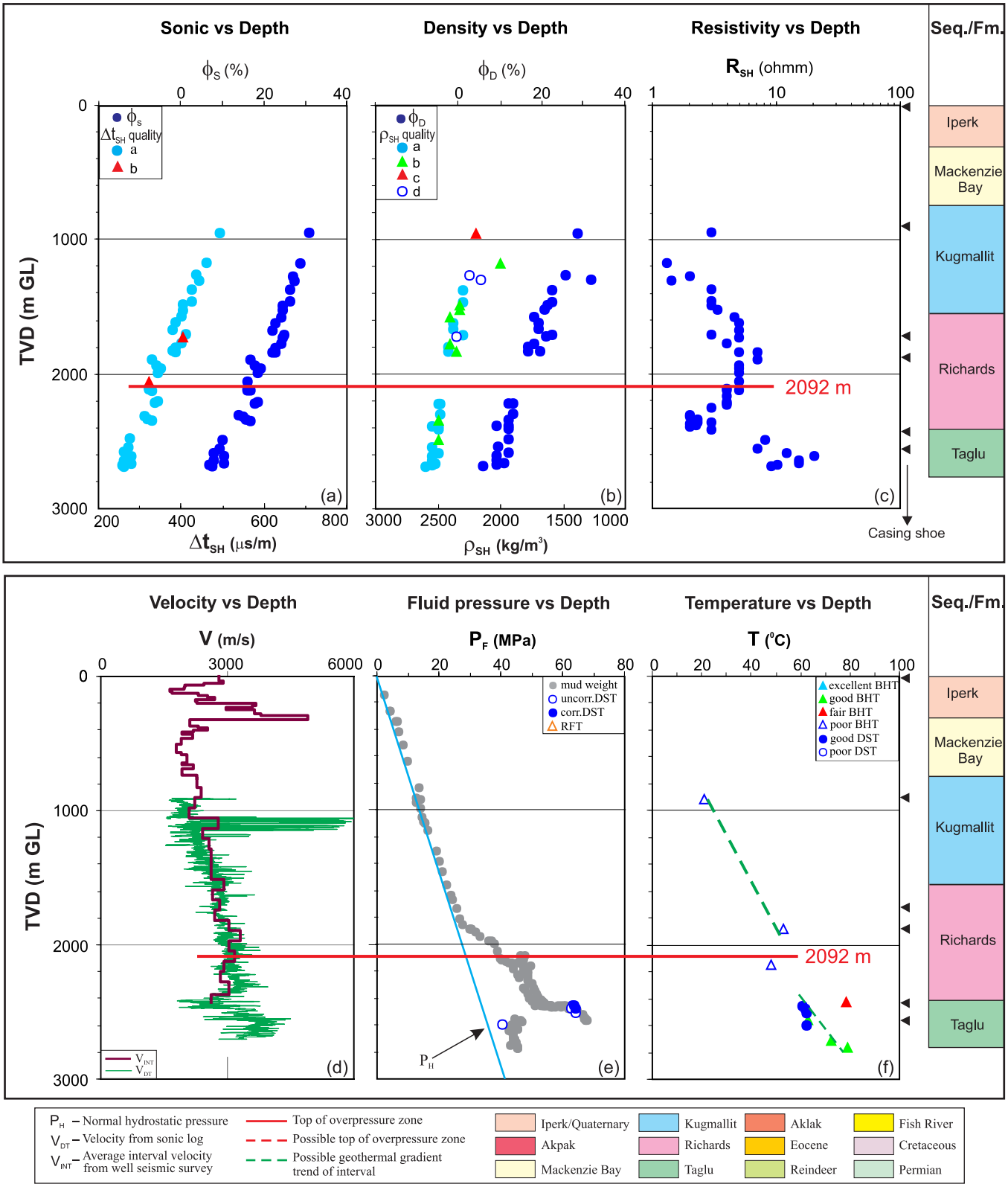

Figure B-42. Top of overpressure zone is detected at 2092 m with quality "b" by using the integrated analysis for the Taglu H-54 well in the Beaufort-Mackenzie Basin. (a) shale sonic transit time (Δt_{SH}) and sonic porosity (ϕ_S) vs. depth; (b) shale bulk density (ρ_{SH}) and density porosity (ϕ_D) vs depth; (c) shale deep resistivity (R_{SH}) vs. depth; (d) continuous sonic velocity (V_{DT}) and average interval seismic velocity (V_{INT}) vs. depth; (e) fluid pressure (P_F) from well test and drilling mud weight vs. depth; and (f) borehole temperature vs. depth.

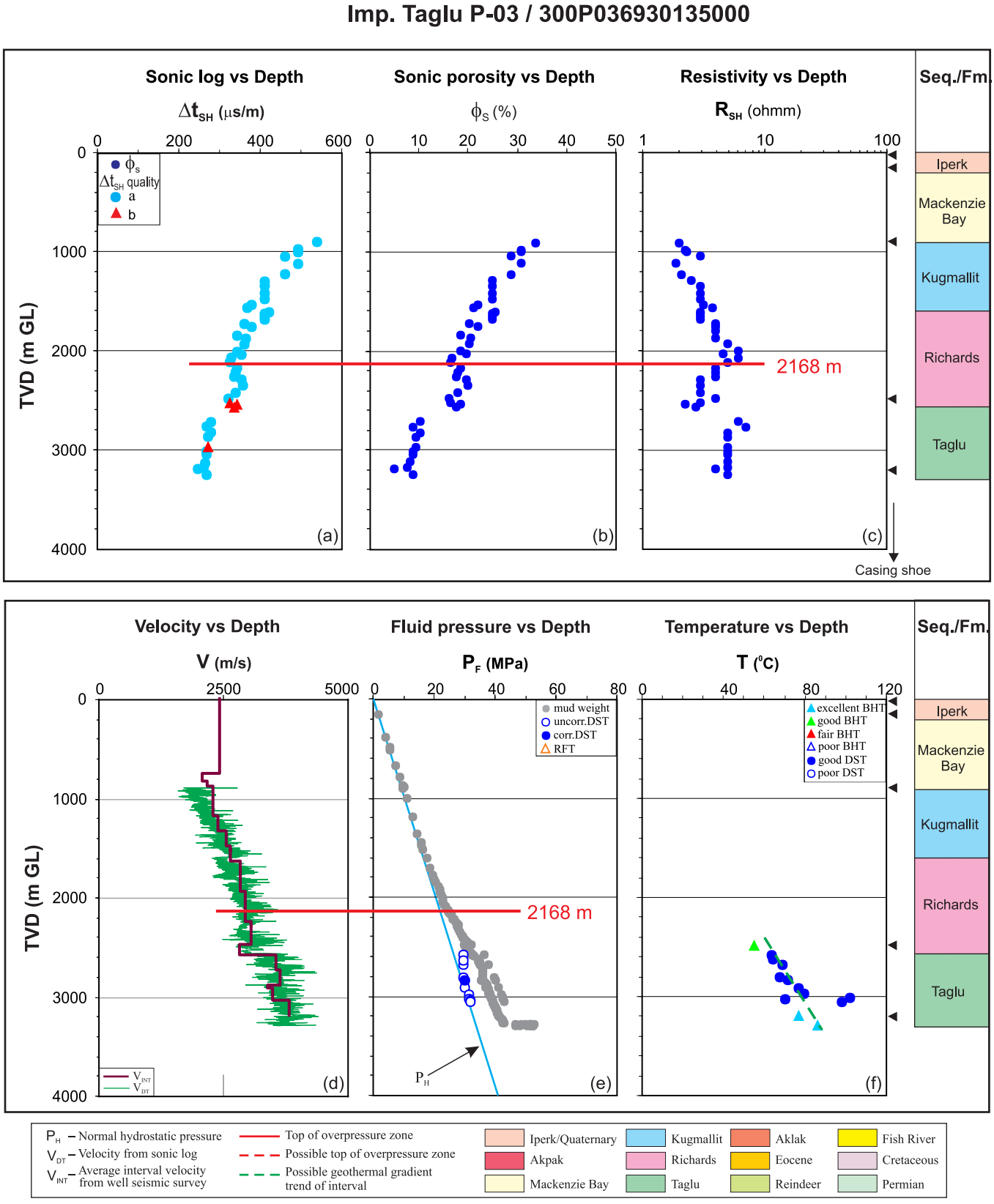

Figure B-43. Top of overpressure zone is detected at 2168 m with quality "b" by using the integrated analysis for the Taglu P-03 well in the Beaufort-Mackenzie Basin. (a) shale sonic transit time (Δt_{SH}) and sonic porosity (ϕ_S) vs. depth; (b) shale bulk density (ρ_{SH}) and density porosity (ϕ_D) vs depth; (c) shale deep resistivity (R_{SH}) vs. depth; (d) continuous sonic velocity (V_{DT}) and average interval seismic velocity (V_{INT}) vs. depth; (e) fluid pressure (P_F) from well test and drilling mud weight vs. depth; and (f) borehole temperature vs. depth.

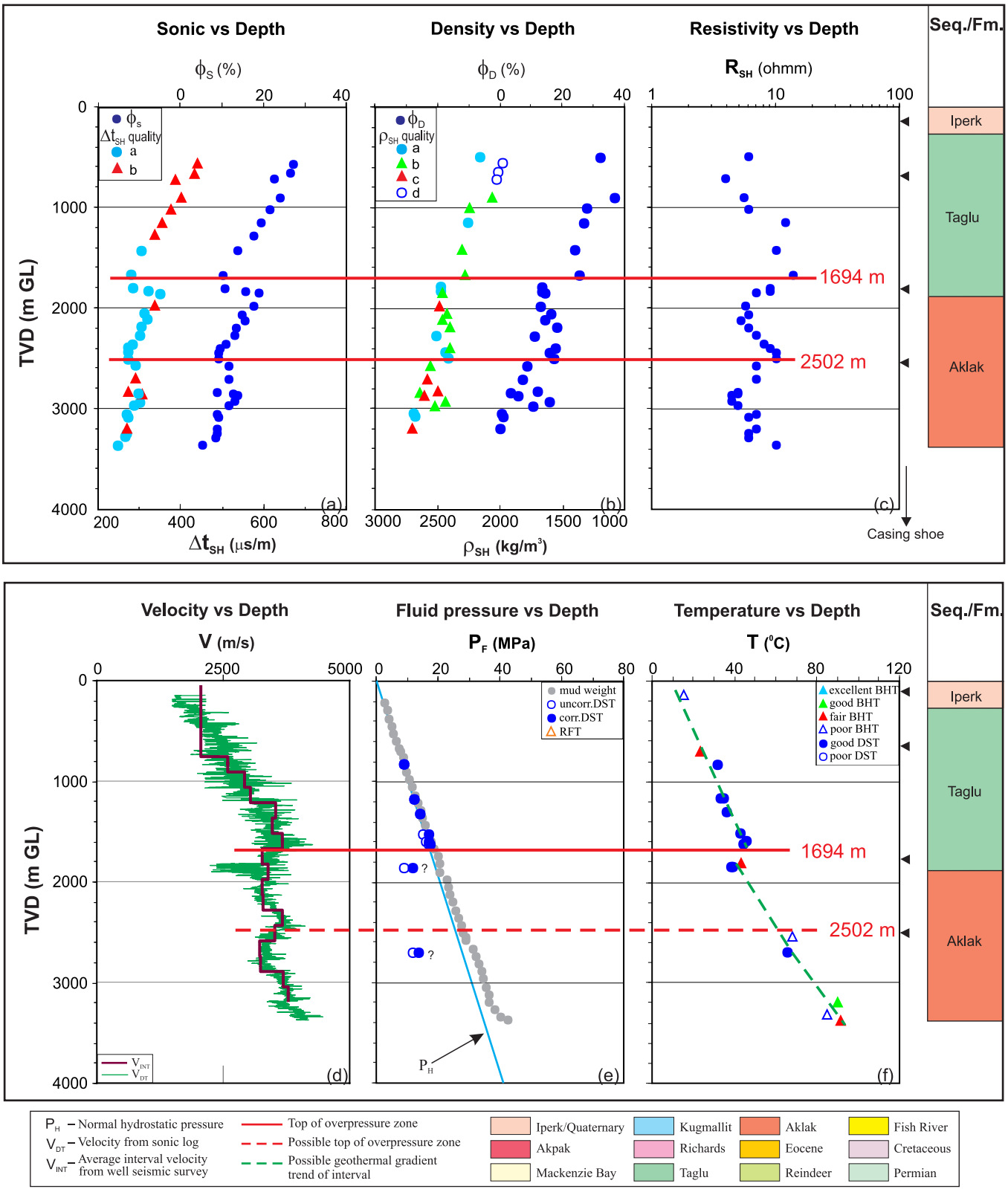

Figure B-44. Overpressure zones are detected with tops of OPZ at 1694 m and 2502 m with quality "b" by using the integrated analysis for the Titalik O-15 well in the Beaufort-Mackenzie Basin. (a) shale sonic transit time (Δt_{SH}) and sonic porosity (ϕ_S) vs. depth; (b) shale bulk density (ρ_{SH}) and density porosity (ϕ_D) vs depth; (c) shale deep resistivity (R_{SH}) vs. depth; (d) continuous sonic velocity (V_{DT}) and average interval seismic velocity (V_{INT}) vs. depth; (e) fluid pressure (P_F) from well test and drilling mud weight vs. depth; and (f) borehole temperature vs. depth.

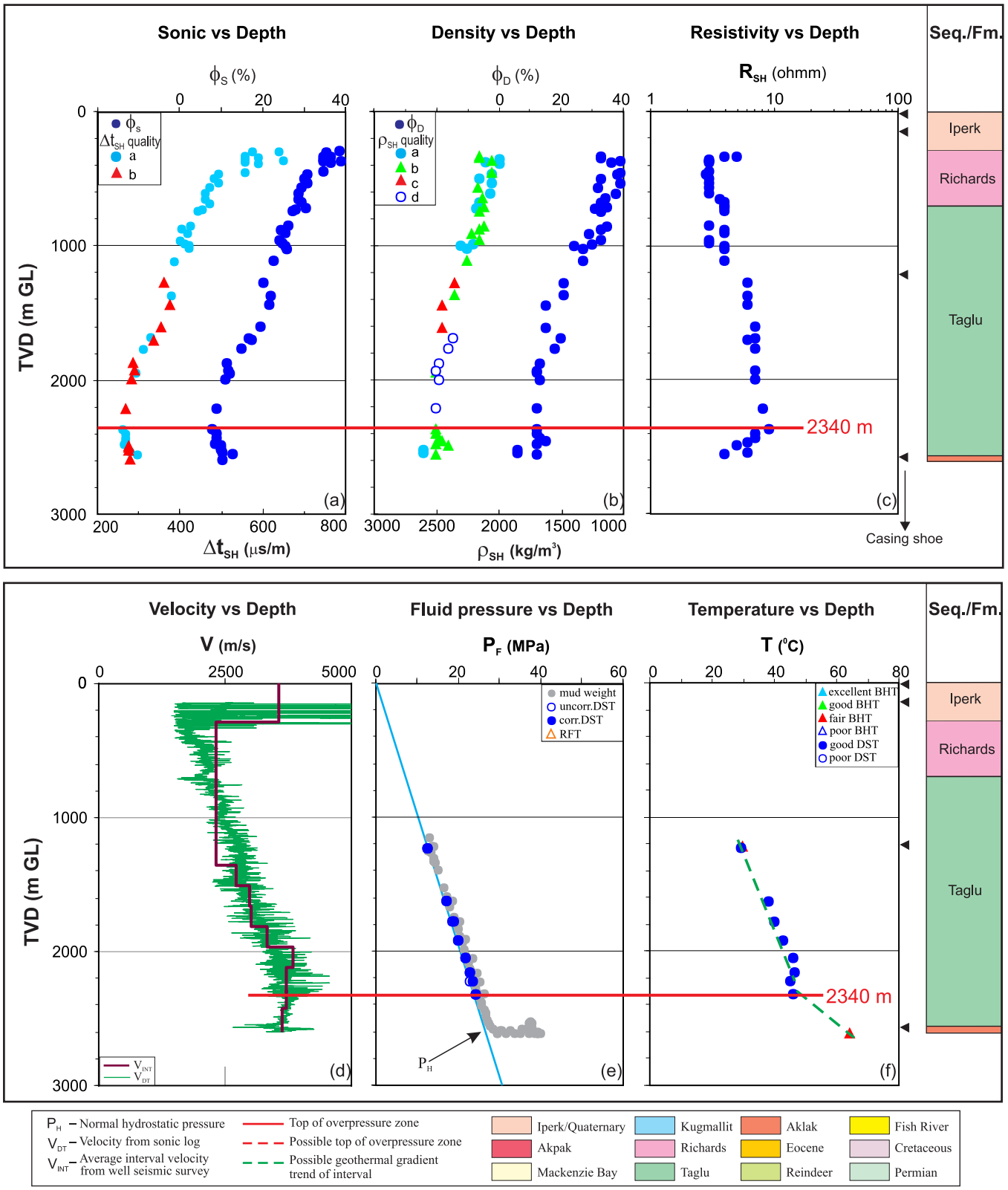

Figure B-45. Top of overpressure zone is detected at 2340 m with quality "b" by using the integrated analysis for the Toapolok H-24 well in the Beaufort-Mackenzie Basin. (a) shale sonic transit time (Δt_{SH}) and sonic porosity (ϕ_S) vs. depth; (b) shale bulk density (ρ_{SH}) and density porosity (ϕ_D) vs depth; (c) shale deep resistivity (R_{SH}) vs. depth; (d) continuous sonic velocity (V_{DT}) and average interval seismic velocity (V_{INT}) vs. depth; (e) fluid pressure (P_F) from well test and drilling mud weight vs. depth; and (f) borehole temperature vs. depth.

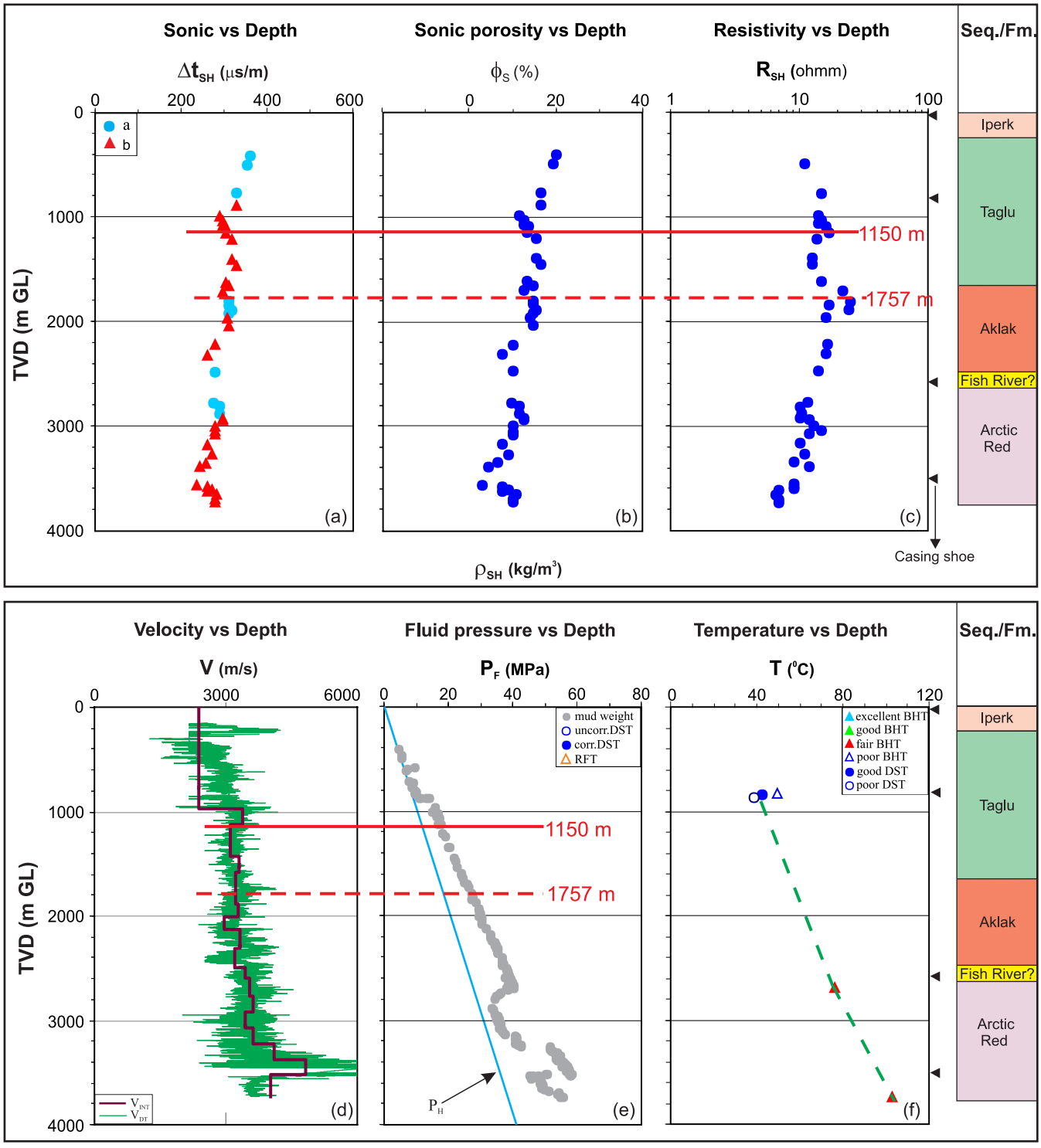

Figure B-46. Overpressure zones are detected with a top of 1150 m (quality "b") and a top of 1757 m (quality "c") by using the integrated analysis for the Tununuk K-10 well in the Beaufort-Mackenzie Basin. (a) shale sonic transit time (Δt_{SH}) vs. depth; (b) shale sonic porosity (ϕ_S) vs. depth; (c) shale deep resistivity (R_{SH}) vs. depth; (d) continuous sonic velocity (V_{DT}) and average interval seismic velocity (V_{INT}) vs. depth; (e) fluid pressure (P_F) from well test and drilling mud weight vs. depth; and (f) borehole temperature vs. depth.

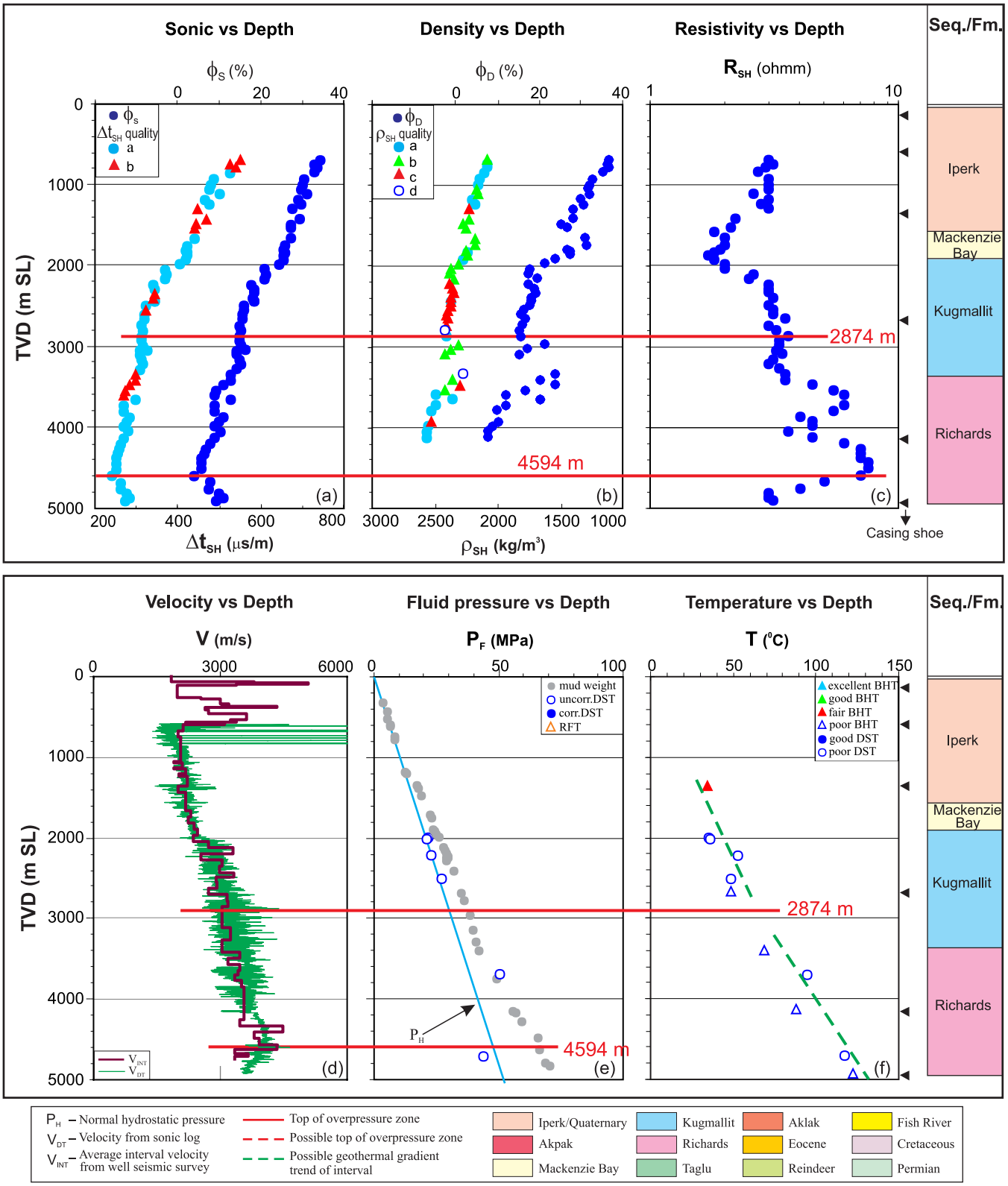

Figure B-47. Overpressure zones are detected with tops of OPZ at 2874 m and 4594 m with quality "b" by using the integrated analysis for the Ukalerk 2C-50 well in the Beaufort-Mackenzie Basin. (a) shale sonic transit time (Δt_{SH}) and sonic porosity (ϕ_S) vs. depth; (b) shale bulk density (ρ_{SH}) and density porosity (ϕ_D) vs depth; (c) shale deep resistivity (R_{SH}) vs. depth; (d) continuous sonic velocity (V_{DT}) and average interval seismic velocity (V_{INT}) vs. depth; (e) fluid pressure (P_F) from well test and drilling mud weight vs. depth; and (f) borehole temperature vs. depth.

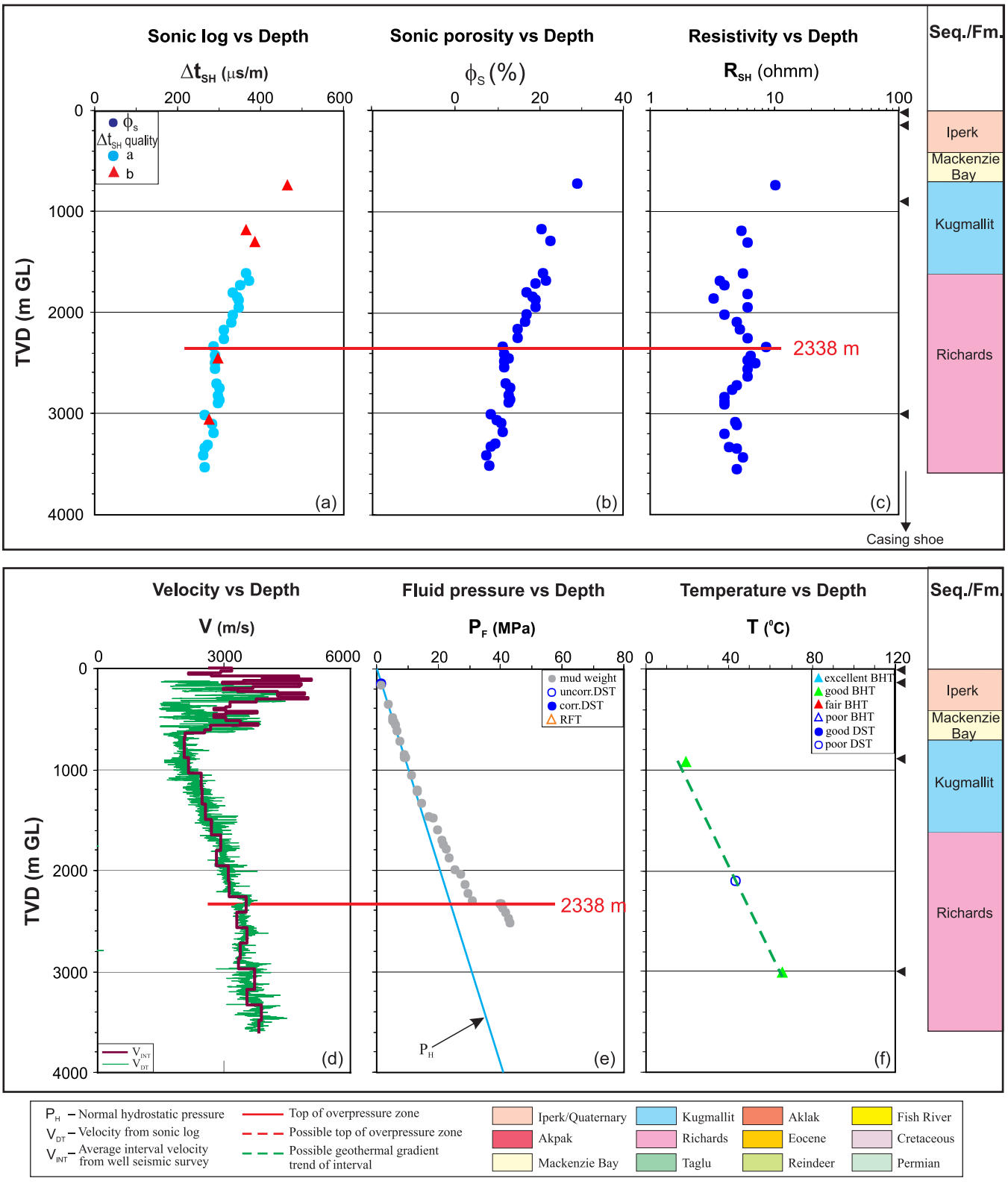

Figure B-48. Top of overpressure zone is detected at 2338 m with quality "b" by using the integrated analysis for the Umiak J-37 well in the Beaufort-Mackenzie Basin. (a) shale sonic transit time (Δt_{SH}) vs. depth; (b) shale sonic porosity (ϕ_S) vs. depth; (c) shale deep resistivity (R_{SH}) vs. depth; (d) continuous sonic velocity (V_{DT}) and average interval seismic velocity (V_{INT}) vs. depth; (e) fluid pressure (P_F) from well test and drilling mud weight vs. depth; and (f) borehole temperature vs. depth.

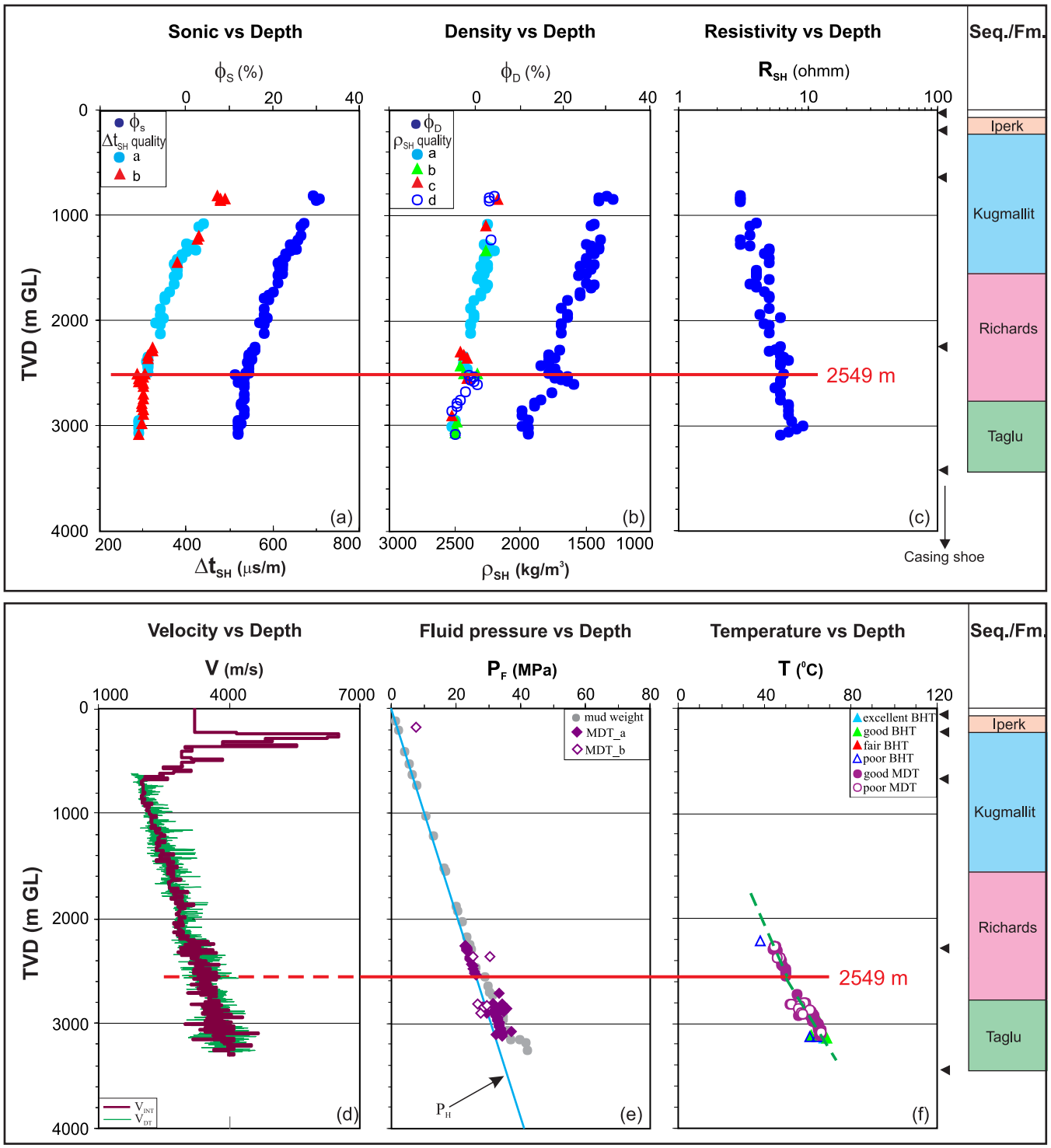

Figure B-49. Top of overpressure zone is detected at 2549 m with quality "b" by using the integrated analysis for the Umiak N-05 well in the Beaufort-Mackenzie Basin. (a) shale sonic transit time (Δt_{SH}) and sonic porosity (ϕ_S) vs. depth; (b) shale bulk density (ρ_{SH}) and density porosity (ϕ_D) vs depth; (c) shale deep resistivity (R_{SH}) vs. depth; (d) continuous sonic velocity (V_{DT}) and average interval seismic velocity (V_{INT}) vs. depth; (e) fluid pressure (P_F) from well test and drilling mud weight vs. depth; and (f) borehole temperature vs. depth.

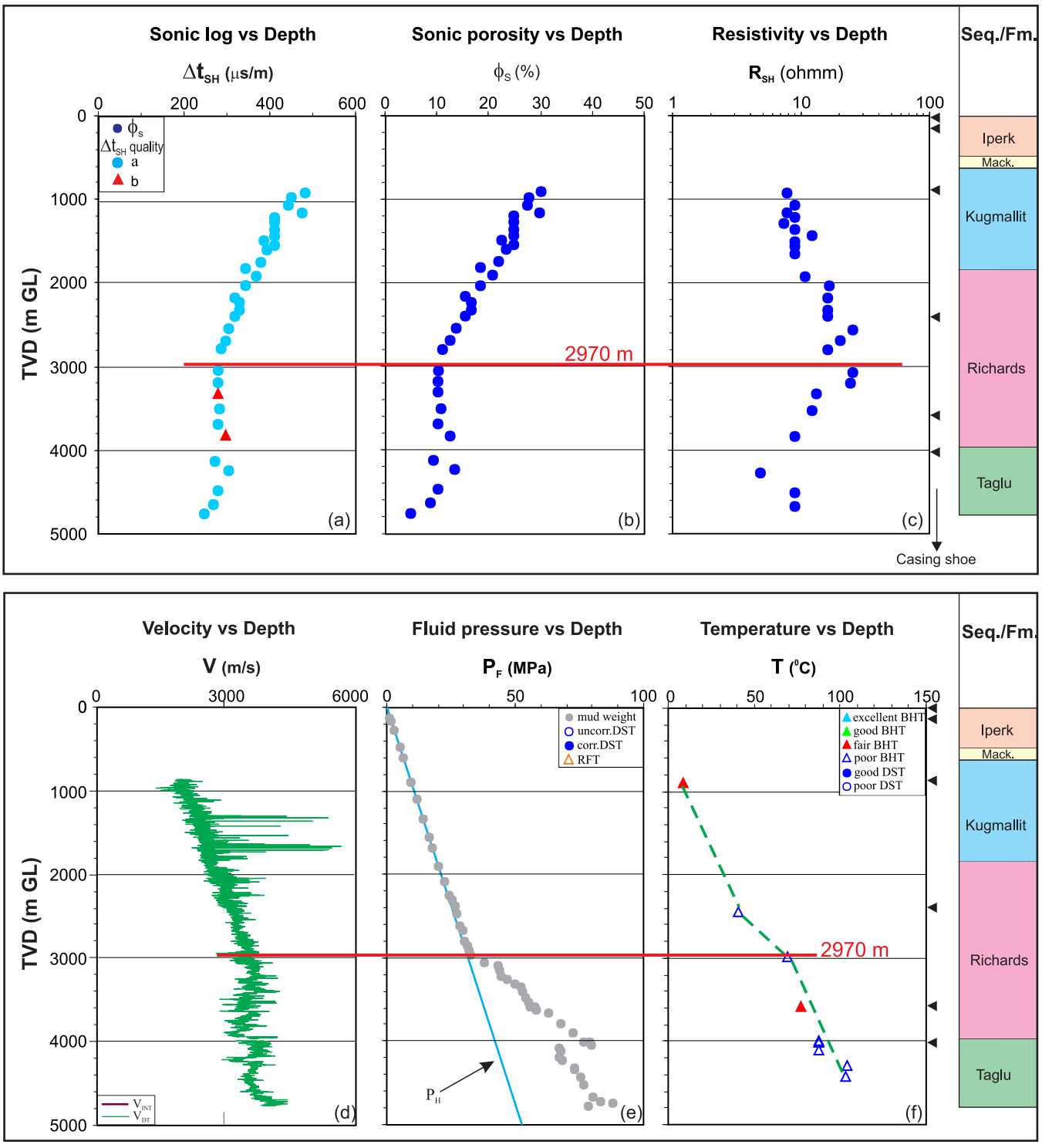

Figure B-50. Top of overpressure zone is detected at 2970 m with quality “b” by using the integrated analysis for the Umiak N-10 well in the Beaufort-Mackenzie Basin. (a) shale sonic transit time (Δt_{SH}) vs. depth; (b) shale sonic porosity (ϕ_S) vs. depth; (c) shale deep resistivity (R_{SH}) vs. depth; (d) continuous sonic velocity (V_{DT}) and average interval seismic velocity (V_{INT}) vs. depth; (e) fluid pressure (P_F) from well test and drilling mud weight vs. depth; and (f) borehole temperature vs. depth. Mack. - Mackenzie Bay.

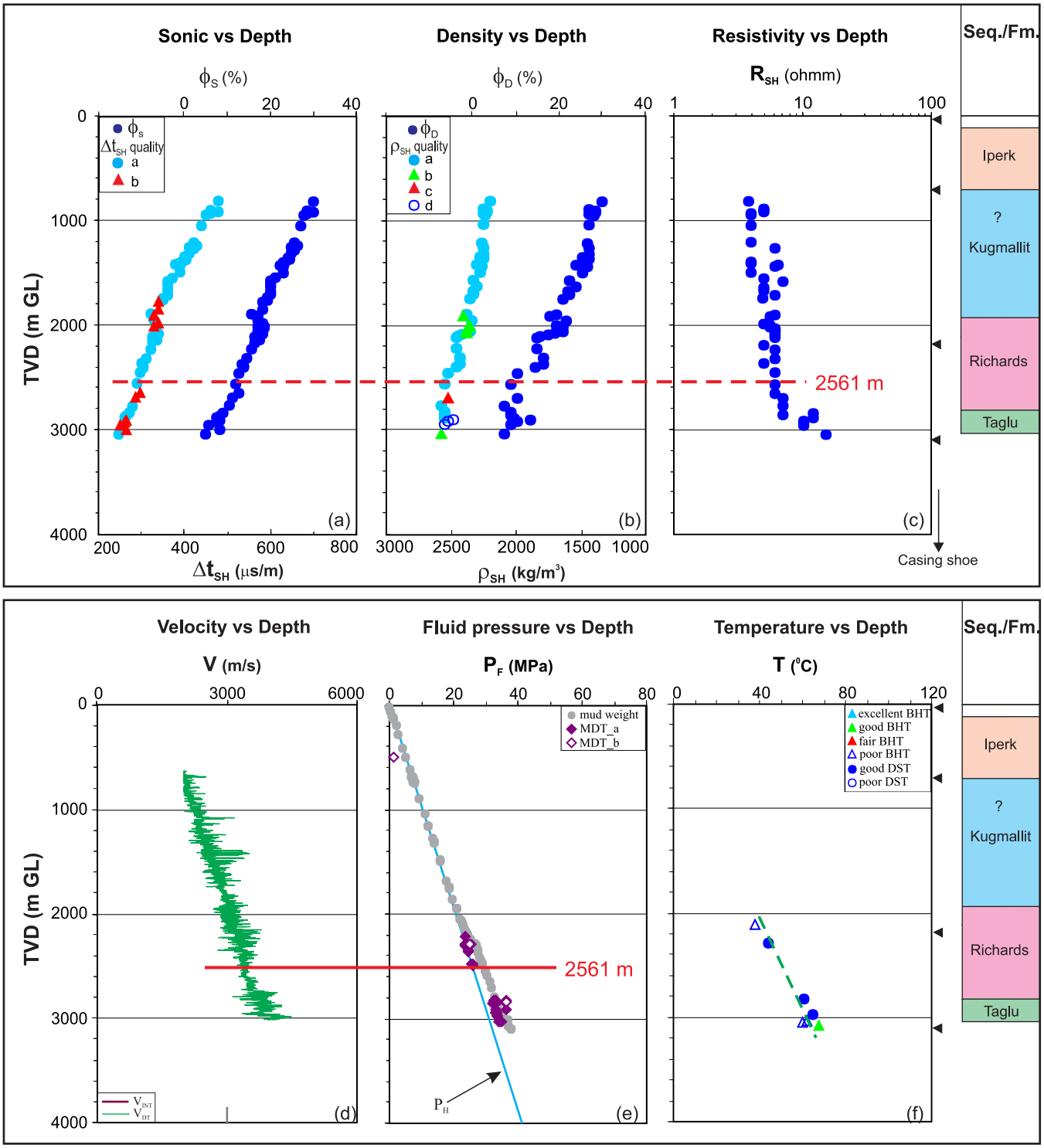

Figure B-51. Top of overpressure zone is detected at 2561 m with quality "b" by using the integrated analysis for the Umaik N-16 well in the Beaufort-Mackenzie Basin. (a) shale sonic transit time (Δt_{SH}) and sonic porosity (ϕ_S) vs. depth; (b) shale bulk density (ρ_{SH}) and density porosity (ϕ_D) vs depth; (c) shale deep resistivity (R_{SH}) vs. depth; (d) continuous sonic velocity (V_{DT}) vs. depth; (e) fluid pressure (P_F) from well test and drilling mud weight vs. depth; and (f) borehole temperature vs. depth.

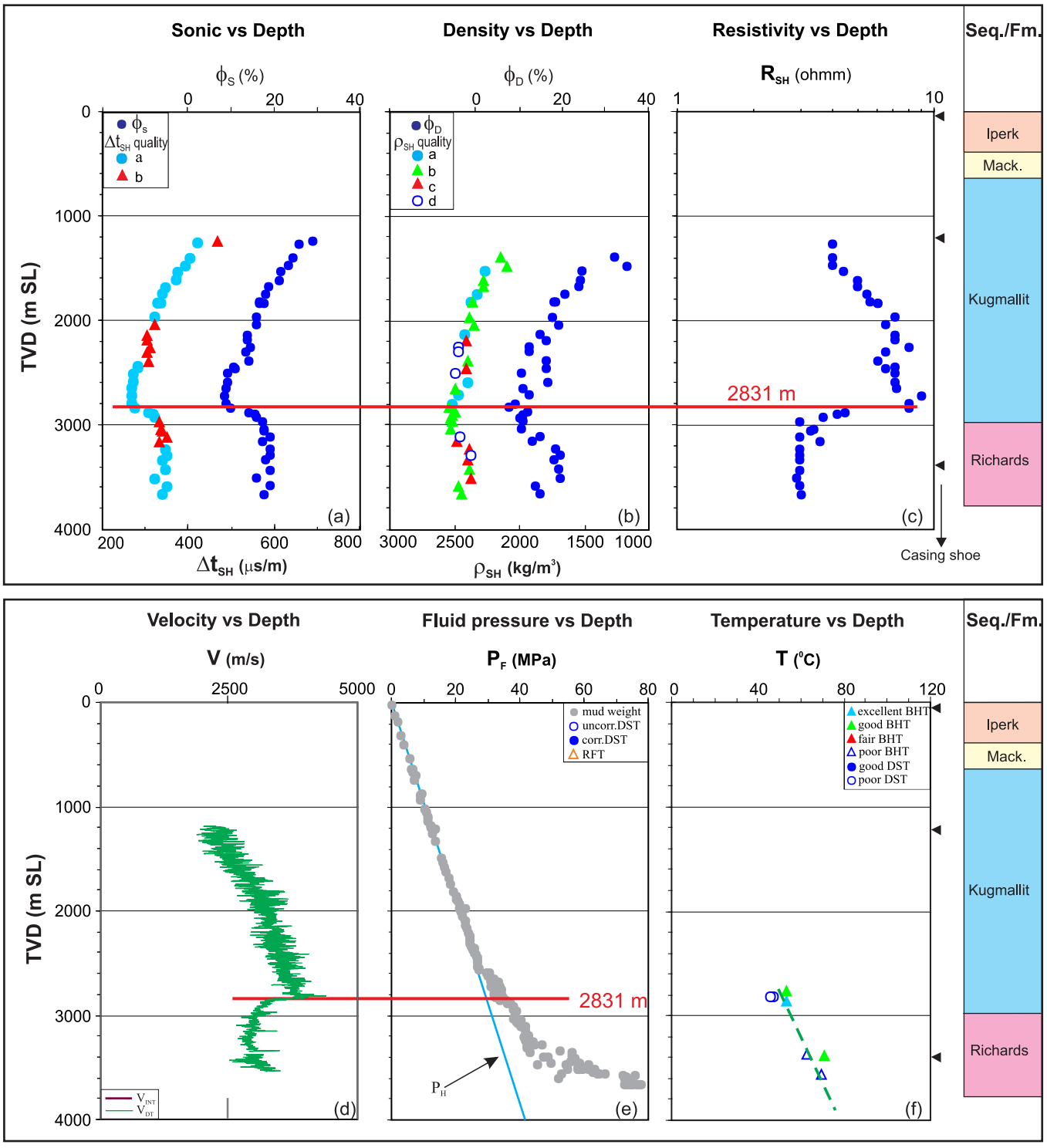

Figure B-52. Top of overpressure zone is detected at 2831 m with quality "b" by using the integrated analysis for the Unark L-24A well in the Beaufort-Mackenzie Basin. (a) shale sonic transit time (Δt_{SH}) and sonic porosity (ϕ_S) vs. depth; (b) shale bulk density (ρ_{SH}) and density porosity (ϕ_D) vs depth; (c) shale deep resistivity (R_{SH}) vs. depth; (d) continuous sonic velocity (V_{DT}) vs. depth; (e) fluid pressure (P_F) from well test and drilling mud weight vs. depth; and (f) borehole temperature vs. depth. Mack. - Mackenzie Bay.

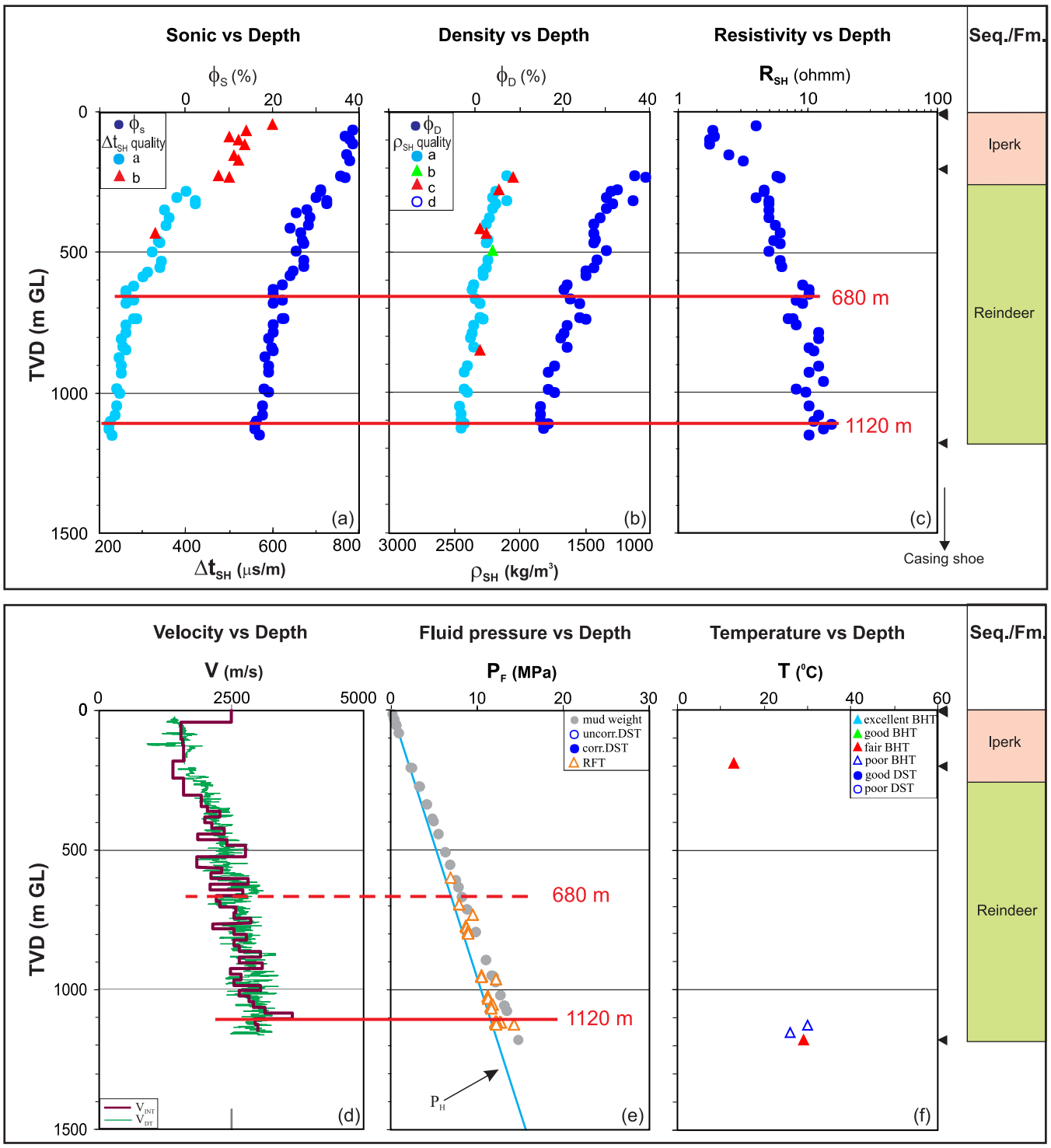

Figure B-53. Overpressure zones are detected with tops at 680 m (quality "c") and 1120 m (quality "b") by using the integrated analysis for the well Unipkat B-12 in the Beaufort Mackenzie Basin. (a) shale sonic transit time (Δt_{SH}) and sonic porosity (ϕ_S) vs. depth; (b) shale bulk density (ρ_{SH}) and density porosity (ϕ_D) vs depth; (c) shale deep resistivity (R_{SH}) vs. depth; (d) continuous sonic velocity (V_{DT}) and average interval seismic velocity (V_{INT}) vs. depth; (e) fluid pressure (P_F) from well test and drilling mud weight vs. depth; and (f) borehole temperature vs. depth.

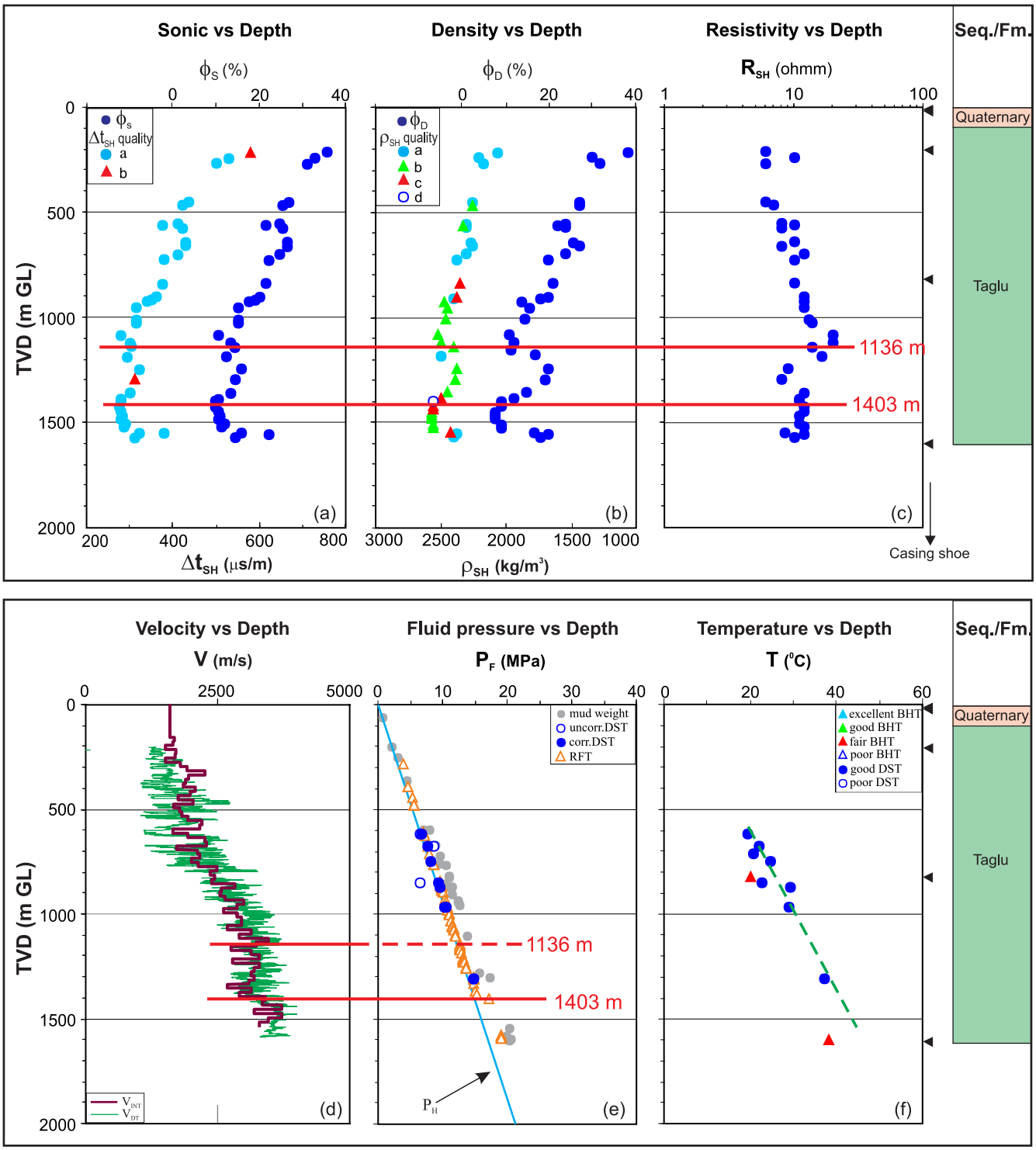

Figure B-54. Overpressure zones are detected with tops of OPZ at 1136 m and 1403 m with quality "b" by using the integrated analysis for the well Unipkat N-12 in the Beaufort Mackenzie Basin. (a) shale sonic transit time (Δt_{SH}) and sonic porosity (ϕ_S) vs. depth; (b) shale bulk density (ρ_{SH}) and density porosity (ϕ_D) vs depth; (c) shale deep resistivity (R_{SH}) vs. depth; (d) continuous sonic velocity (V_{DT}) and average interval seismic velocity (V_{INT}) vs. depth; (e) fluid pressure (P_F) from well test and drilling mud weight vs. depth; and (f) borehole temperature vs. depth.

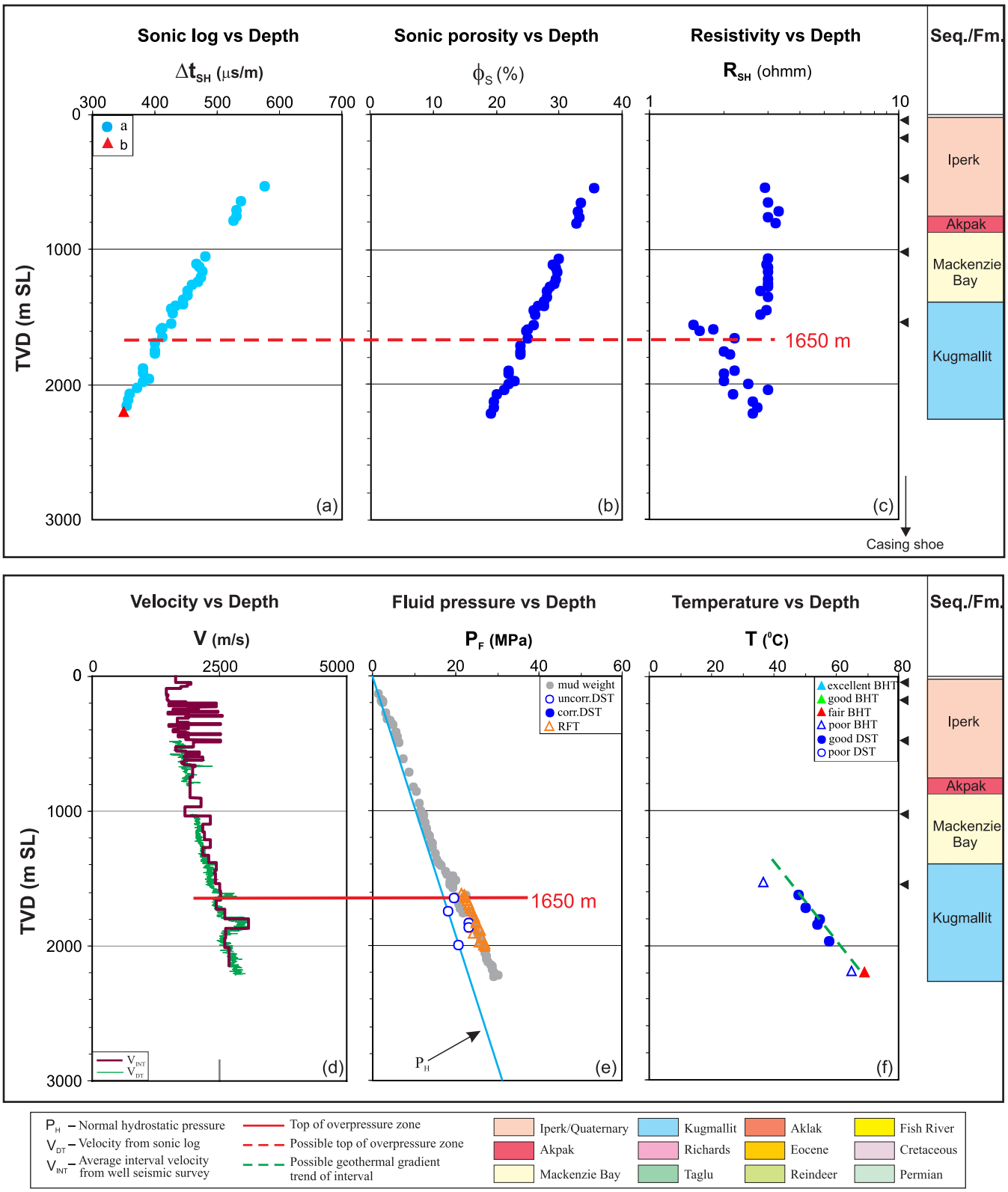

Figure B-55. Top of overpressure zone is detected at 1650 m with quality "b" by using the integrated analysis for the well West Tarsiut P-45 in the Beaufort Mackenzie Basin. (a) shale sonic transit time (Δt_{SH}) vs. depth; (b) shale sonic porosity (ϕ_S) vs depth; (c) shale deep resistivity (R_{SH}) vs. depth; (d) continuous sonic velocity (V_{DT}) and average interval seismic velocity (V_{INT}) vs. depth; (e) fluid pressure (P_F) from well test and drilling mud weight vs. depth; and (f) borehole temperature vs. depth.

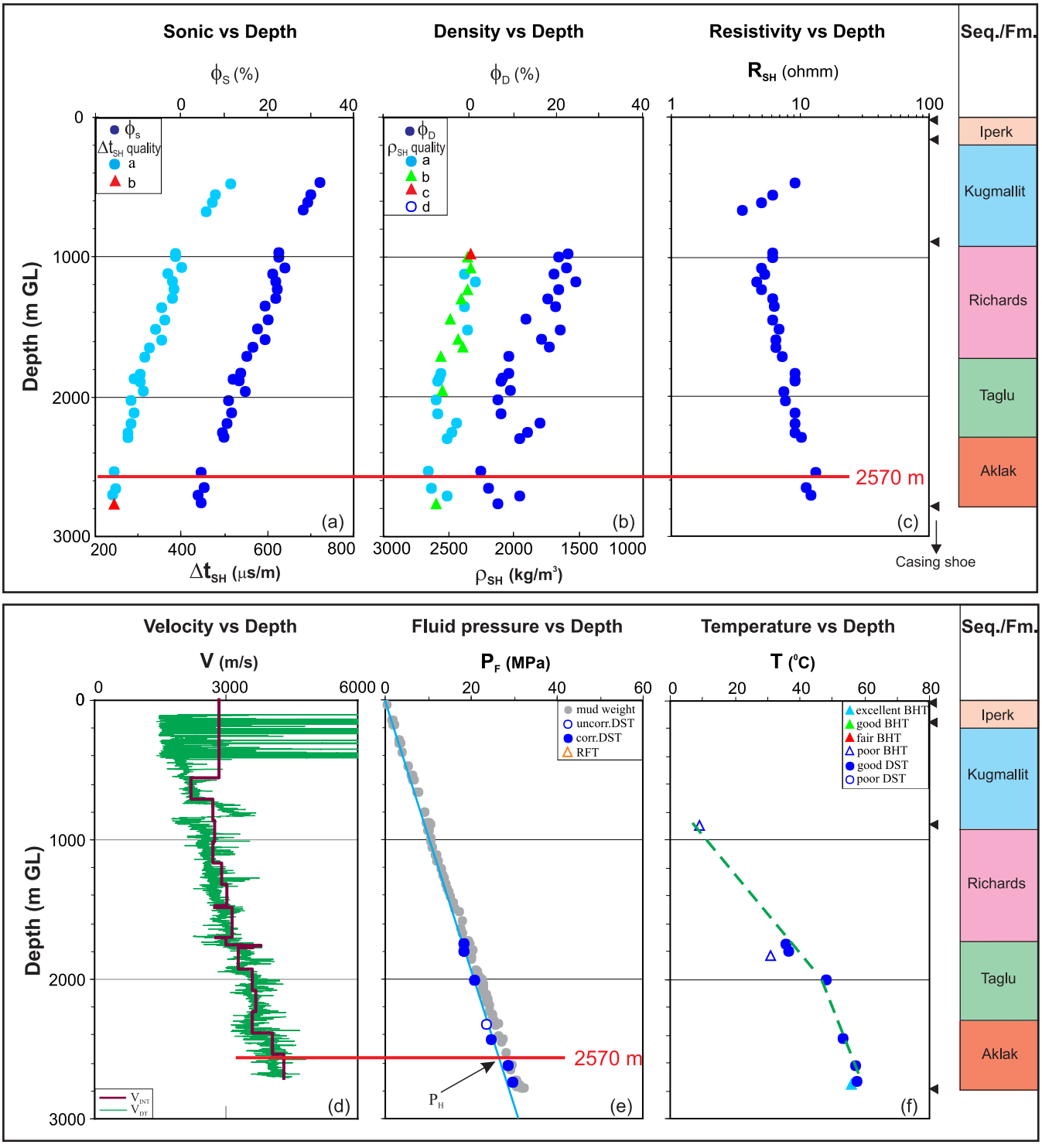

Figure B-56. Top of overpressure zone is detected at 2570 m with quality "b" by using the integrated analysis for the well Ya Ya M-33 in the Beaufort Mackenzie Basin. (a) shale sonic transit time (Δt_{SH}) and sonic porosity (ϕ_S) vs. depth; (b) shale bulk density (ρ_{SH}) and density porosity (ϕ_D) vs depth; (c) shale deep resistivity (R_{SH}) vs. depth; (d) continuous sonic velocity (V_{DT}) and average interval seismic velocity (V_{INT}) vs. depth; (e) fluid pressure (P_F) from well test and drilling mud weight vs. depth; and (f) borehole temperature vs. depth.

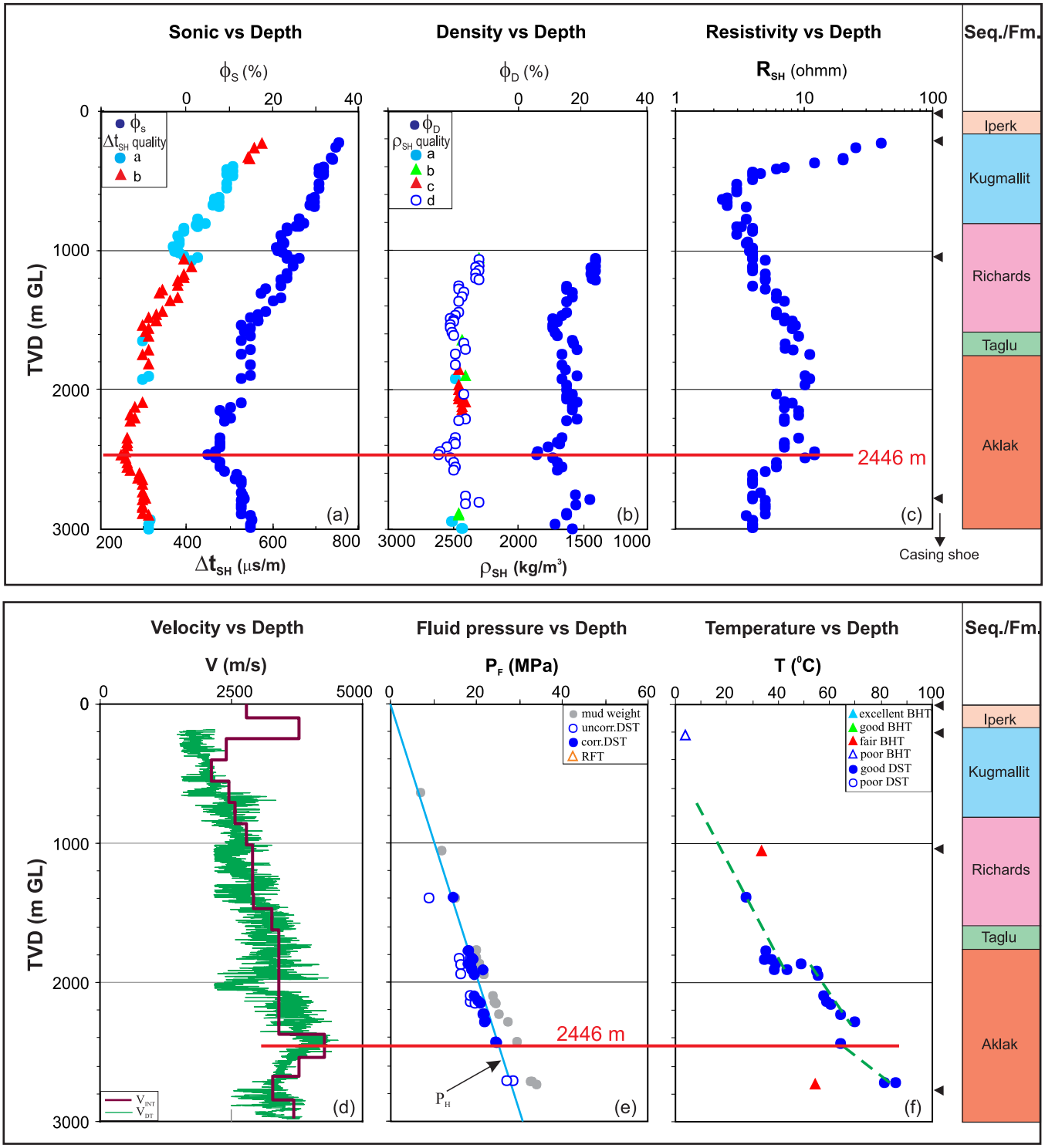

Figure B-57. Top of overpressure zone is detected at 2446 m with quality "b" by using the integrated analysis for the well Ya Ya P-53 in the Beaufort Mackenzie Basin. (a) shale sonic transit time (Δt_{SH}) and sonic porosity (ϕ_S) vs. depth; (b) shale bulk density (ρ_{SH}) and density porosity (ϕ_D) vs depth; (c) shale deep resistivity (R_{SH}) vs. depth; (d) continuous sonic velocity (V_{DT}) and average interval seismic velocity (V_{INT}) vs. depth; (e) fluid pressure (P_F) from well test and drilling mud weight vs. depth; and (f) borehole temperature vs. depth.

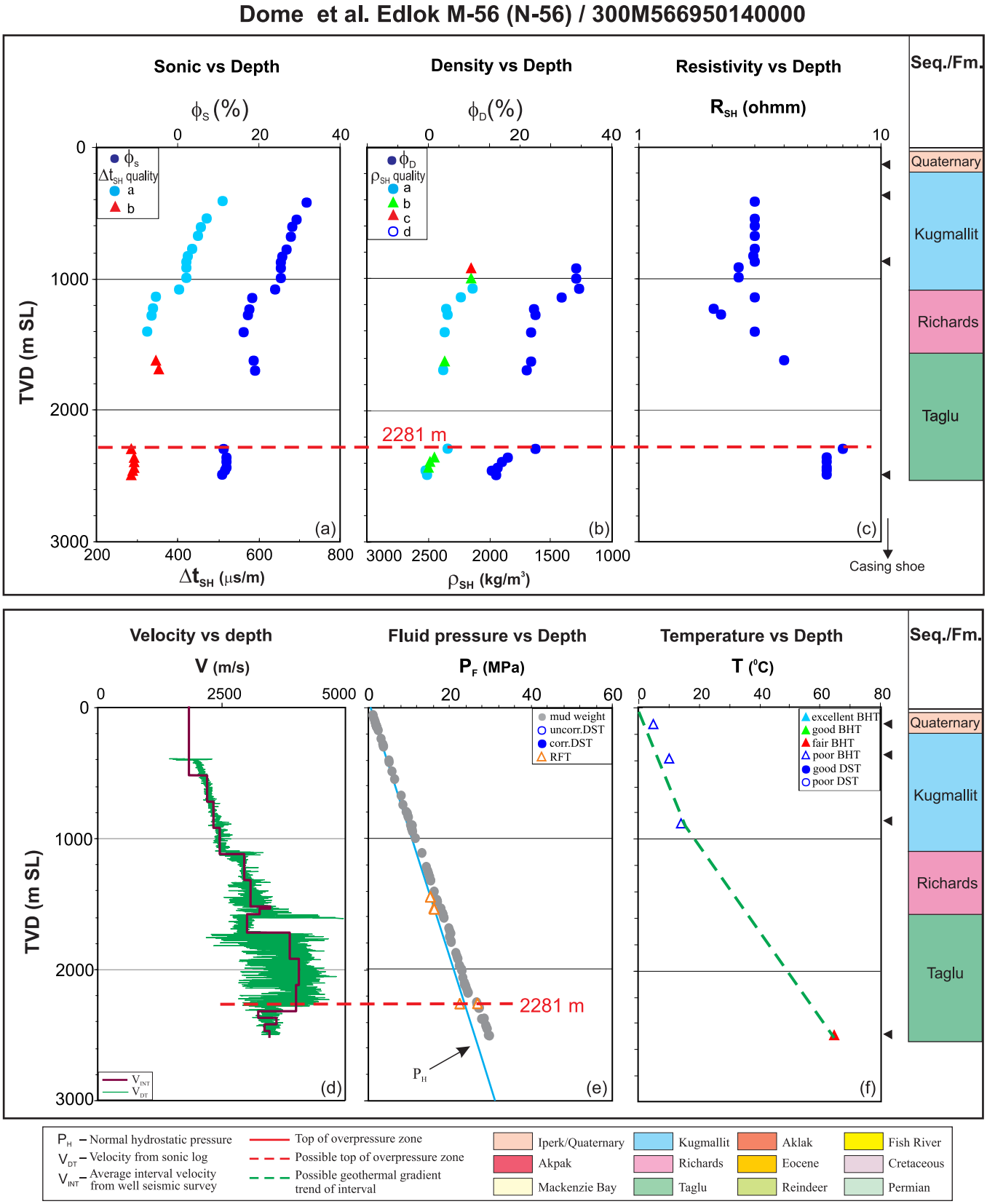

Figure C-1. A possible overpressure zone is indicated by an integrated analysis with quality "c" for the well Edlok M-56 in the Beaufort-Mackenzie Basin. (a) Shale sonic transit time (Δt_{SH}) and sonic porosity (ϕ_S) vs. depth; (b) shale bulk density (ρ_{SH}) and density porosity (ϕ_D) vs. depth; (c) shale deep resistivity (R_{SH}) vs. depth; (d) continuous sonic velocity (V_{DT}) and average interval seismic velocity (V_{INT}) vs. depth; (e) pore fluid pressure (P_F) from well test and drilling mud weight vs. depth; and (f) borehole temperature vs. depth.

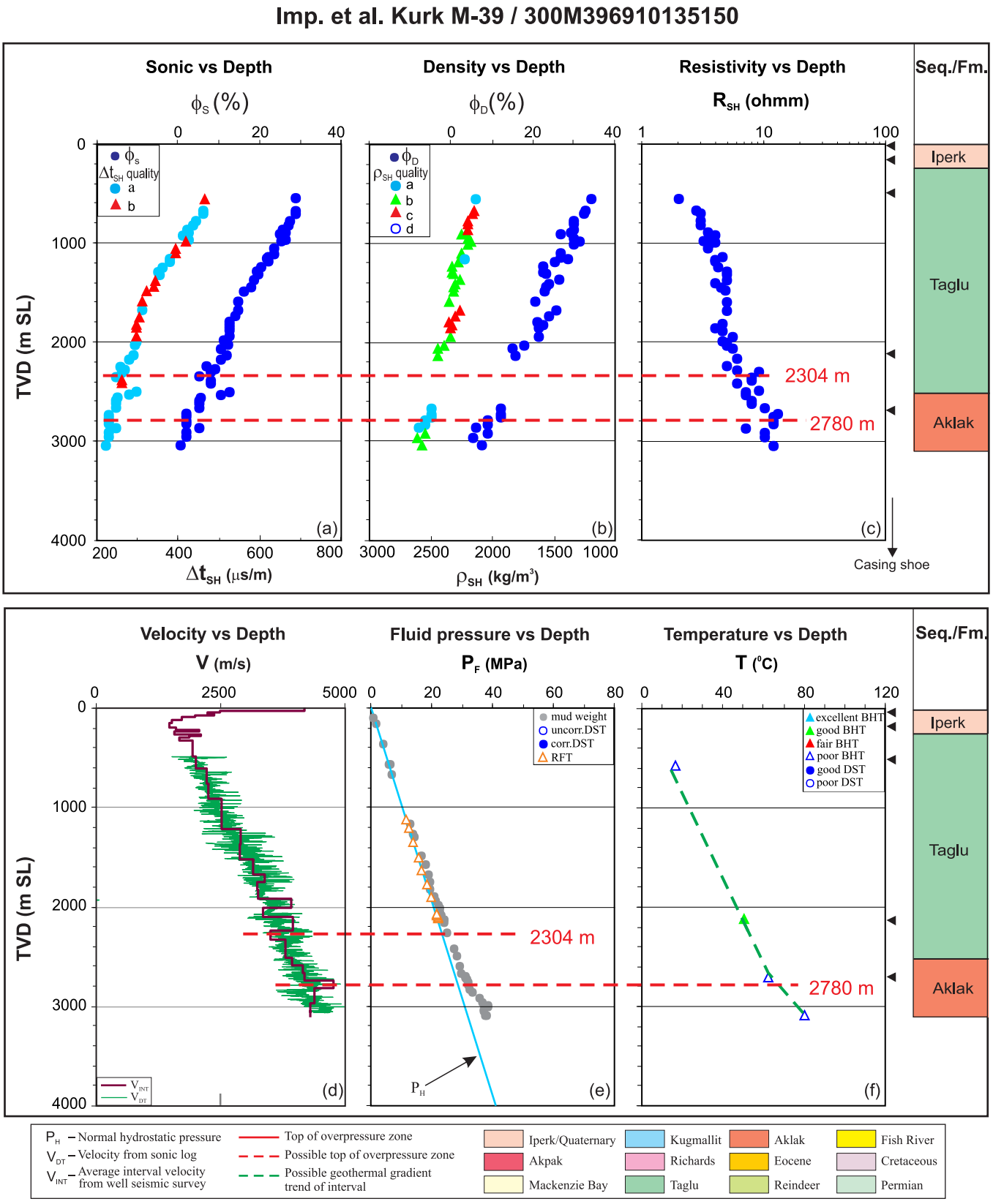

Figure C-2. Possible overpressure zones are indicated by an integrated analysis with quality "c" for the well Kurk M-39 in the Beaufort-Mackenzie Basin. (a) shale sonic transit time (Δt_{SH}) and sonic porosity (ϕ_S) vs. depth; (b) shale bulk density (ρ_{SH}) and density porosity (ϕ_D) vs. depth; (c) shale deep resistivity (R_{SH}) vs. depth; (d) continuous sonic velocity (V_{DT}) and average interval seismic velocity (V_{INT}) vs. depth; (e) pore fluid pressure (P_F) from well test and drilling mud weight vs. depth; and (f) borehole temperature vs. depth.

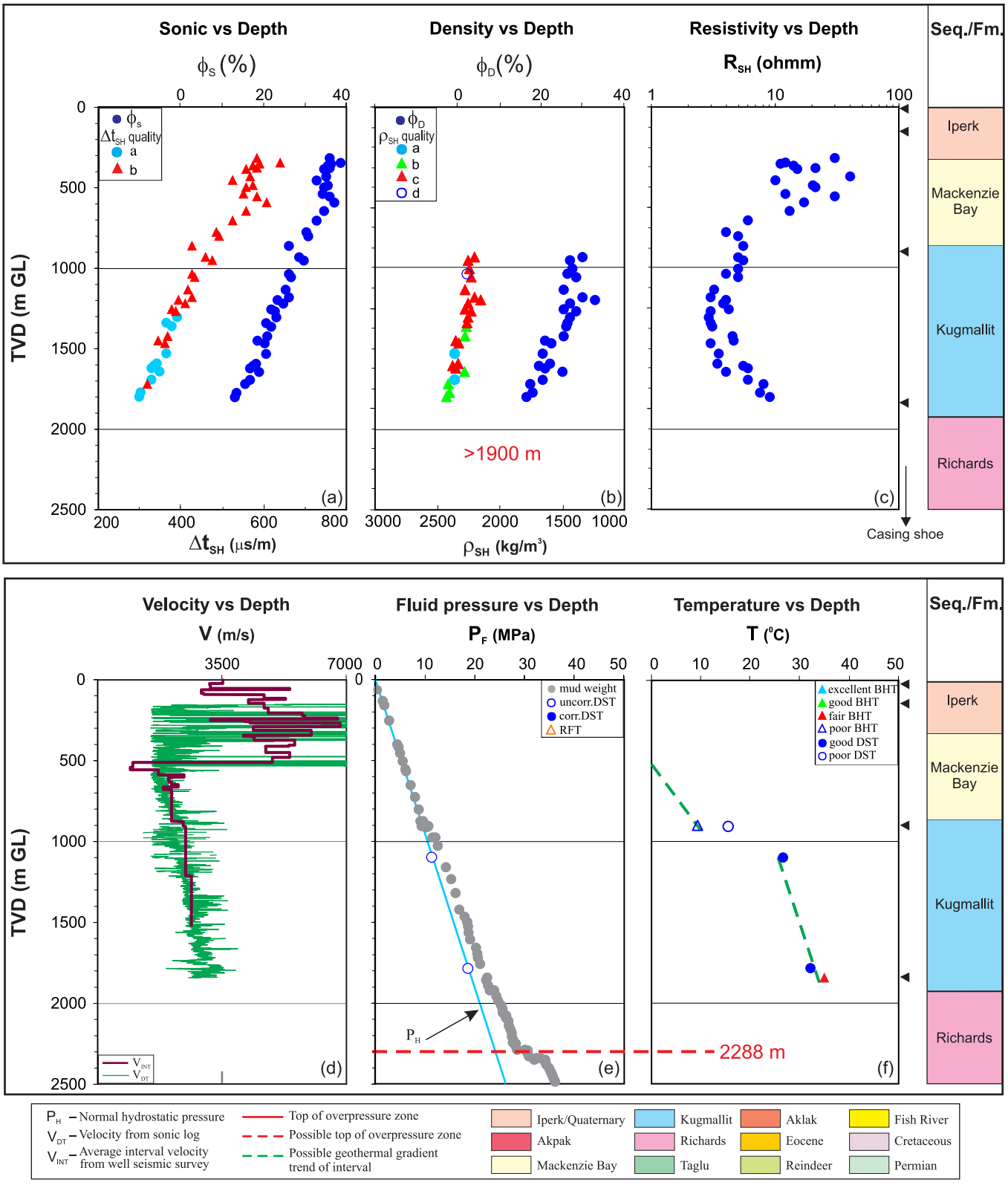

Figure C-3. A possible overpressure zone is marked by drilling mud weight (quality "c") for the well Mallik L-38 in the Beaufort-Mackenzie Basin. (a) shale sonic transit time (Δt_{SH}) and sonic porosity (ϕ_S) vs. depth; (b) shale bulk density (ρ_{SH}) and density porosity (ϕ_D) vs. depth; (c) shale deep resistivity (R_{SH}) vs. depth; (d) continuous sonic velocity (V_{DT}) and average interval seismic velocity (V_{INT}) vs. depth; (e) pore fluid pressure (P_F) from well test and drilling mud weight vs. depth; and (f) borehole temperature vs. depth.

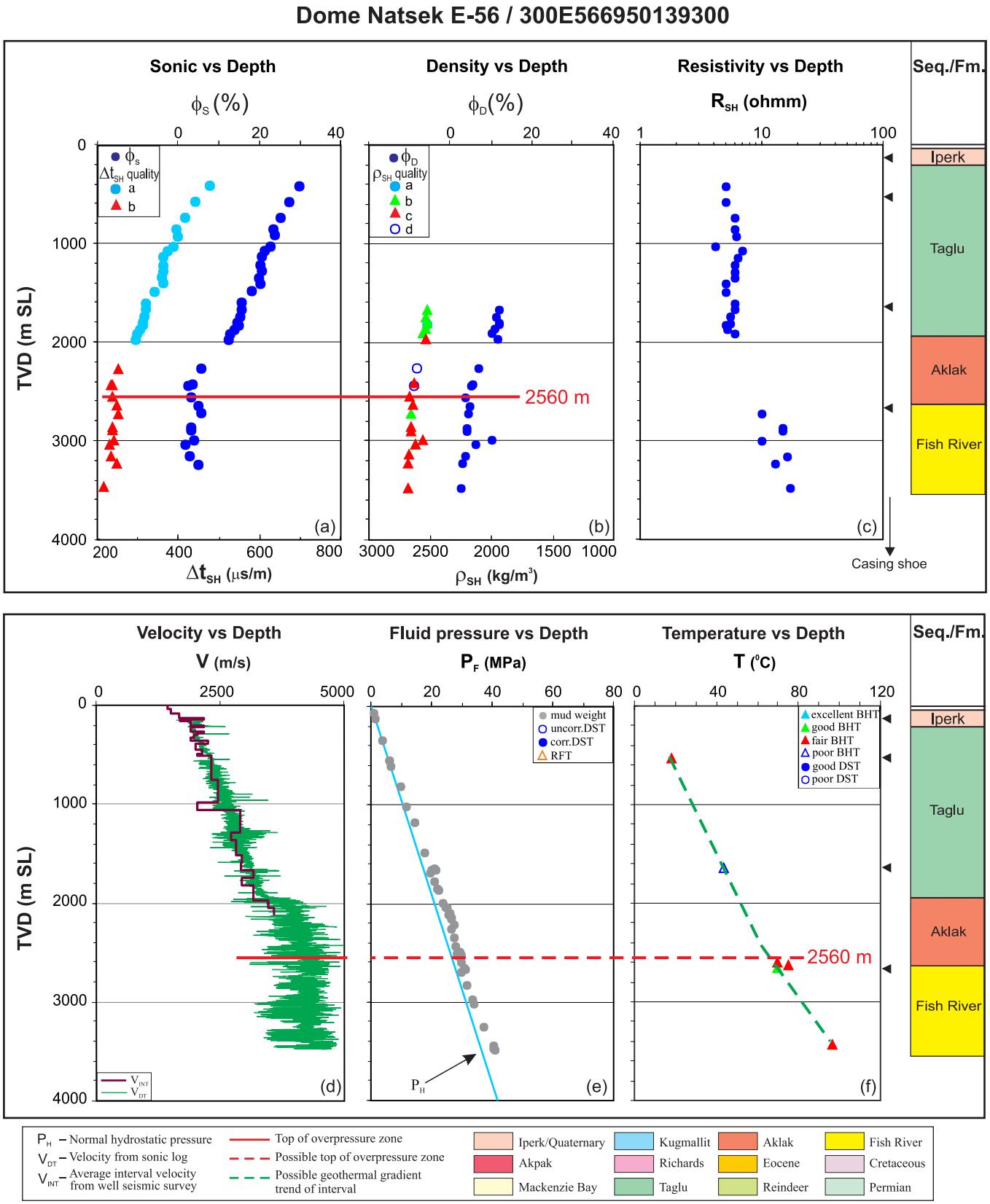

Figure C-4. A possible overpressure zone is indicated by an integrated analysis with quality "c" for the well Natsek E-56 in the Beaufort-Mackenzie Basin. (a) Shale sonic transit time (Δt_{SH}) and sonic porosity (ϕ_S) vs. depth; (b) shale bulk density (ρ_{SH}) and density porosity (ϕ_D) vs. depth; (c) shale deep resistivity (R_{SH}) vs. depth; (d) continuous sonic velocity (V_{DT}) and average interval seismic velocity (V_{INT}) vs. depth; (e) pore fluid pressure (P_F) from drilling mud weight vs. depth; and (f) borehole temperature vs. depth.

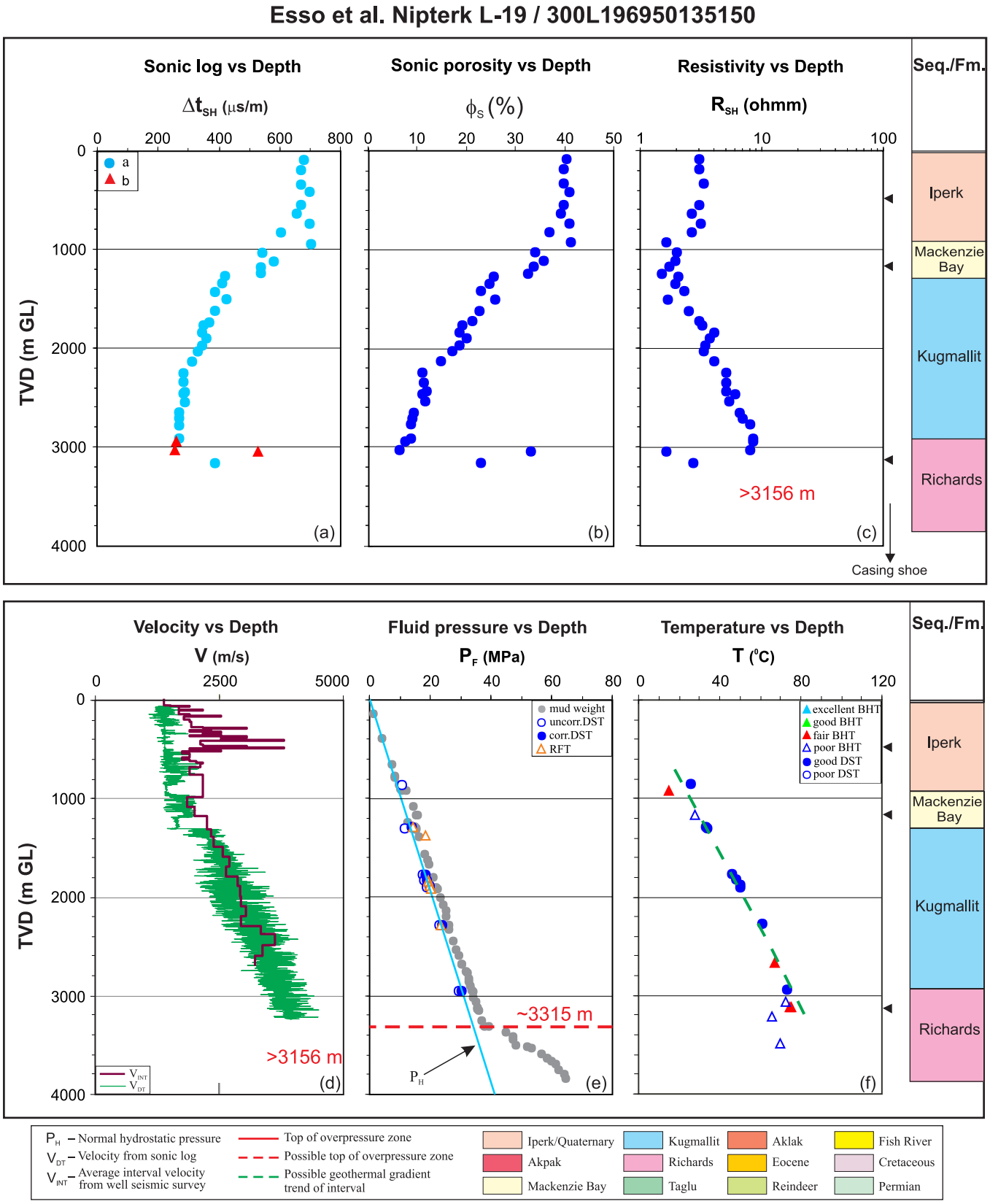

Figure C-5. An overpressure zone is indicated by drilling mud weight method only with quality "c" for the well Nipterk L-19 in the Beaufort-Mackenzie Basin although other data are not available for the depth range. (a) Shale sonic transit time (Δt_{SH}) vs. depth; (b) shale sonic porosity (ϕ_S) vs. depth; (c) shale deep resistivity (R_{SH}) vs. depth; (d) continuous sonic velocity (V_{DT}) and average interval seismic velocity (V_{INT}) vs. depth; (e) pore fluid pressure (P_F) from well test and drilling mud weight vs. depth; and (f) borehole temperature vs. depth.

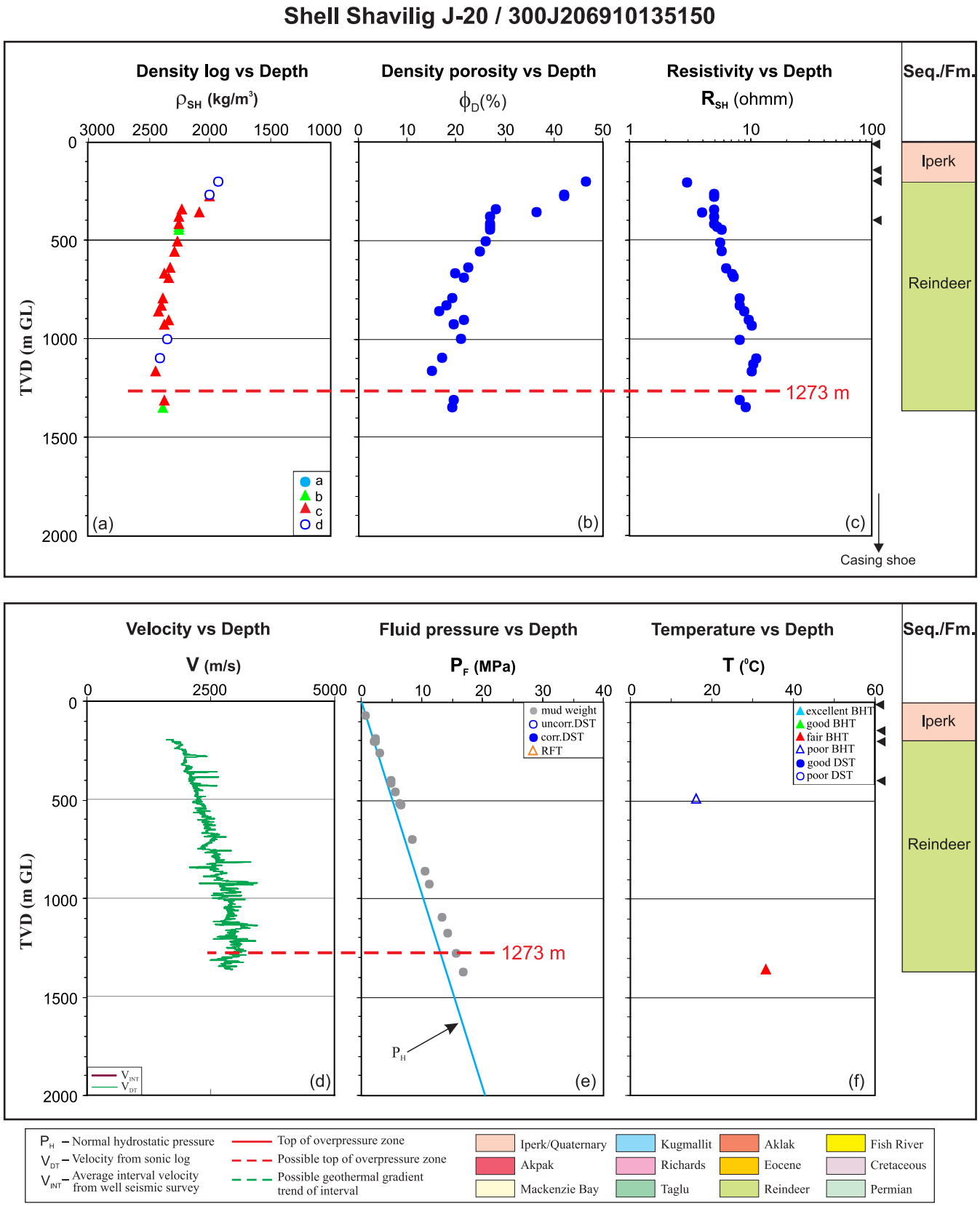

Figure C-6. A possible top of overpressure zone is indicated by geophysical methods with quality "c", appearing at near the bottom of the well Shavilig J-20 in the Beaufort-Mackenzie Basin. (a) Shale bulk density (ρ_{SH}) versus depth; (b) shale density porosity (ϕ_D) versus depth; (c) shale deep resistivity (R_{SH}) versus depth; (d) continuous sonic velocity (V_{DT}) versus depth; (e) estimated fluid pressure (P_F) from drilling mud weight versus depth; and (f) borehole temperature versus depth.

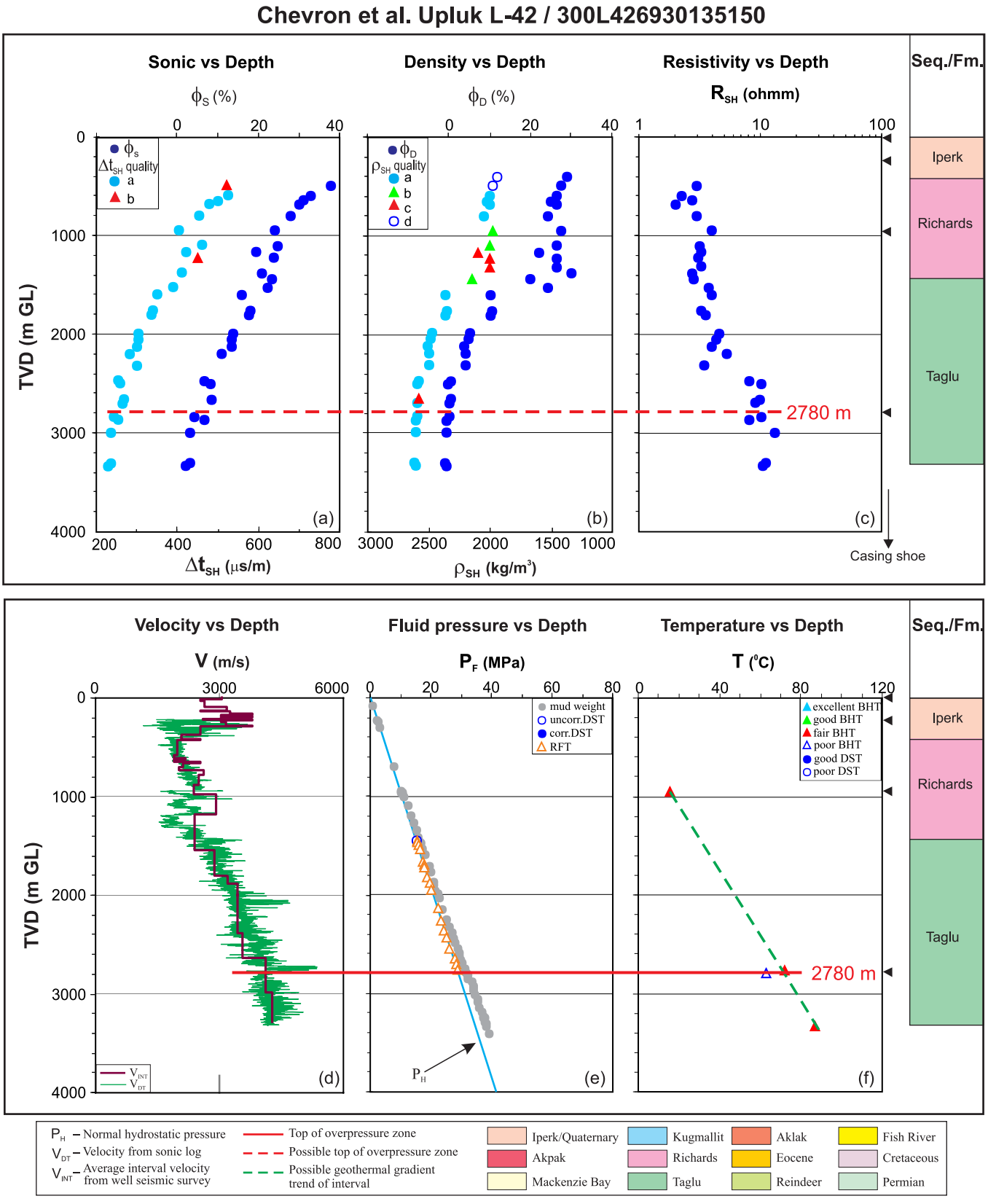

Figure C-7. A possible overpressure zone is indicated by an integrated analysis with quality "c" for the well Upluk L-42 in the Beaufort-Mackenzie Basin. (a) shale sonic transit time (Δt_{SH}) and sonic porosity (ϕ_S) vs. depth; (b) shale bulk density (ρ_{SH}) and density porosity (ϕ_D) vs. depth; (c) shale deep resistivity (R_{SH}) vs. depth; (d) continuous sonic velocity (V_{DT}) and average interval seismic velocity (V_{INT}) vs. depth; (e) pore fluid pressure (P_F) from well test and drilling mud weight vs. depth; and (f) borehole temperature vs. depth.